Development of a Microfluidic Based Analytical System for Copper Monitoring in Environmental Water Samples

By

Éadaoin Tyrrell B.Sc. (Hons)

A thesis submitted to Dublin City University in part fulfilment for the degree of

DOCTOR OF PHILOSOPHY

Dublin City University.

School of Chemical Sciences.

Supervisor: Dr. Brett Paull.

August 2005

AUTHORS DECLARATION

I hereby certify that this material, which I now submit for assessment on the programme of study leading to the award of Doctor of Philosophy is entirely my own work and has not been taken from the work of others' save and to the extent that such work has been cited and acknowledged within the text of my work.

Signed: Éadaoin Tyrrell

I.D. No: 97341720

Date: 23/11/05

ACKNOWLEDGEMENTS

I would like to express my thanks to the following people, without whom this would not have been possible:

To my supervisor Dr. Brett Paull for all his advice, guidance and support throughout this Ph.D. research.

To all the technical staff, in particular Maurice for all his assistance and help throughout this work.

To all the members of the research group in S205D, in particular Edel, Colmán, Danielle, Johnny and Leon. I really appreciate all the help and support.

To Orla, Susan and all of the other postgrads (past and present – way too many to mention!) for everything over the past four years.

Finally, to my family, Mam, Dad, Lorcan, Breid and Irene for the encouragement, support and tolerance especially over the last twelve months.

Sincere thanks to you all.

TABLE OF CONTENTS

3. MICROFLUIDIC STUDIES WITH CHEMILUMINESCENCE DETECTION

5. APPLICATION OF CONVECTIVE-INTERACTION MEDIA® DISK MONOLITHIC COLUMNS

ABSTRACT

A microfluidic-based system has been developed for copper (II) monitoring in water samples with sensitive and selective detection, based on the measurement of light emitted from the copper (II) catalysed oxidation of 1,10-phenanthroline by hydrogen peroxide. Work initially focussed on the development of a flow injection analysis (FIA) system with micellar enhanced chemiluminescence (CL) detection. Sufficient selectivity was achieved by removing interfering metal ions using an on-line itaconic acid modified microcolumn, allowing copper (II) to be easily determined at concentrations as low as 1 $\mu g\ L^{-1}$ from high concentrations of calcium (II) and magnesium (II).

The FIA-CL system was further developed and scaled-down to create a microfluidic-based system. A number of different microflow devices, of various designs and dimensions, were manufactured from polymethylmethacrylate (PMMA). A range of in-house micro-fabrication techniques were investigated for the fabrication of the microfluidic devices including hot embossing, laser ablation and direct micro-milling. A complete miniaturised flow system was developed incorporating miniaturised peristaltic pumps, a microfluidic plastic manifold and a compact photomultiplier tube for CL detection. Experimental conditions including reagent concentrations and flow rates were optimised and the system was found to produce linear results for copper (II) over the concentration range 0 to 150 $\mu g\ L^{-1}$.

Selectivity of the microfluidic-based CL system was further enhanced by incorporating an on-line separation step into the microflow manifold. A number of different solid phases were compared and contrasted for the on-line separation of copper (II) from complex sample matrices. These included incorporating a stationary phase e.g. monolithic and chelating resin micro-columns into the plastic microflow device and the use of on-line modified Convective-Interaction Media® (CIM®) disk monolithic columns. Finally the optimised system was successfully used for trace copper (II) determinations in a standard reference freshwater sample (SRM 1640) and in real water samples.

PUBLICATIONS

"Retention of alkali, alkaline earth and transition metals on an itaconic acid cation-exchange column. Eluent pH, ionic strength and temperature effects upon selectivity" Wasim Bashir, Éadaoin Tyrrell, Orlagh Feeney, Brett Paull, ***Journal of Chromatography A***, 2002 **964** 113

"Design of a micro-fluidic sensor for high sensitivity copper (II) sensing applications" Ceri Gibson, Patrick Byrne, David Gray, Brian MacCraith, Brett Paull, Éadaoin Tyrrell, ***Proceedings of SPIE***, 2003 **4876** 615

"Development of a micro-fluidic manifold for copper monitoring utilising chemiluminescence detection" Éadaoin Tyrrell, Ceri Gibson, Brian MacCraith, David Gray, Nigel Kent, Brett Paull, ***Lab on a Chip***, 2004 **4(4)** 384

POSTER PRESENTATIONS

Posters were presented at the following conferences:

2nd Biennial Conference on Analytical Science in Ireland,
Tallaght Insitute of Technology, 4th-5th April 2002

Analytical Research Forum Incorporating Research and Development 2002,
Kingston University, London, U.K. 15th-17th July 2002

Analytical Research Forum Incorporating Research and Development 2003,
University of Sunderland, Sunderland, U.K. 21st-23rd July 2003

Analytical Research Forum Incorporating Research and Development 2004,
University of Central Lanchashire, Preston, U.K. 19th-21st July 2004

7th Asian Conference on Analytical Sciences,
Hong Kong Baptist University, Hong Kong. 28th-31st July 2004

3rd Biennial Conference on Analytical Sciences in Ireland,
University College Cork, Co. Cork. 9th-10th September 2004.

Analytical Research Forum Incorporating Research and Development 2005,
University of Plymouth, Plymouth, U.K. 18th-20th July 2005.

List of Abbreviations

μTAS	Micro-Total Analysis System
1,10-phen	1,10-Phenanthroline
8-HQ	8-Hydroxyquinoline
8-HQS	8-Hydroxyquinoline 5-Sulphonic acid
AAS	Atomic Absorption Spectroscopy
AIBN	Azobisisobutyronitrile
ASV	Anodic Stripping Voltammetry
BSF	Brilliant Sulfoflavin
CAD	Computer Aided Design
CEDAB	Cetylethyldimethylammonium Bromide
CIM®	Convective-Interaction Media®
CL	Chemiluminescence
CO-APDC	Cobalt Ammonium 1-Pyrrolidinedithiocarbamate
CTAB	Cetyltrimethylammonium Bromide
DCF	Dichlorofluorescein
DDAB	Didodecyldimethylammonium Bromide
EDTA	Ethylenediaminetetraacetic Acid
EPA	Environmental Protection Agency
EtOH	Ethanol
FAAS	Flame Atomic Absorption Spectroscopy
FIA	Flow Injection Analysis
GFAAS	Graphite Furnace Atomic Absorption Spectroscopy
HPLC	High Performance Liquid Chromatography
ICP-AES	Inductively Coupled Plasma Atomic Emission Spectroscopy
I.D.	Internal Diameter
IDA	Iminodiacetic acid
IPA	Isopropyl Alcohol
IR	Infrared
LC	Liquid Chromatography
LOD	Limit of Detection
MeOH	Methanol

MEMS	Microelectromechanical Systems
MST	Microsystems Technology
NIST	National Institute of Standards and Technology
o-CPC	*o*-Cresolphthalein Complexone
OD	Outer Diameter
PC	Polycarbonate
PCR	Post Column Reagent
PD	Photodiode
PDMS	Polydimethylsiloxane
PE	Polyethylene
PEEK	Poly(ether ether ketone)
PET	Polyethyleneterephtalate
PMMA	Polymethylmethacrylate
PMT	Photomultiplier Tube
PRP	Polymer Reversed Phase
PS	Polystyrene
PS-DVB	Polystyrene Divinylbenzene
PVC	Polyvinyl Chloride
RDA	Recommended Daily Allowance
R_e	Reynolds Number
RSD	Relative Standard Deviation
S/N	Signal/Noise
SDS	Sodium Dodecyl Sulphate
SPE	Solid Phase Extraction
SRM	Standard Reference Material
TAS	Total Analysis System
TCNQ	7,7,8,8-Tetracyanoquinodimethane
TEPA	Tetraethylenepentamine
TFA	Trifluoroacetic Acid
T_g	Glass Transition Temperature
UV	Ultraviolet
UV-VIS	Ultraviolet-Visible
WHO	World Health Organisation

LIST OF FIGURES

LIST OF TABLES

CHAPTER ONE

INTRODUCTION TO MICROFLUIDICS AND CHEMILUMINESCENCE

The aim of this literature review is to provide a general overview of both microfluidics and chemiluminescence. The first section deals with the idea of a microflow system and includes discussion on the concept of miniaturisation, flow within miniaturised devices, and instrumentation employed for the fabrication of microfluidic devices. The second focus of the review is on the use of chemiluminescence as a detection tool for metal determinations and the combination of microflow systems with chemiluminescence detection. This section also introduces the concept of preconcentration for trace metal determinations and focuses in particular on chelation ion chromatography for preconcentration or separation purposes.

1.1 Total Analysis System

The accurate determination and real time measurement of results is an important issue in environmental and chemical analyses. Typical analytical procedures involve a number of different steps that must be carried out in an automated and rapid fashion as shown in Figure 1.1 [1,2].

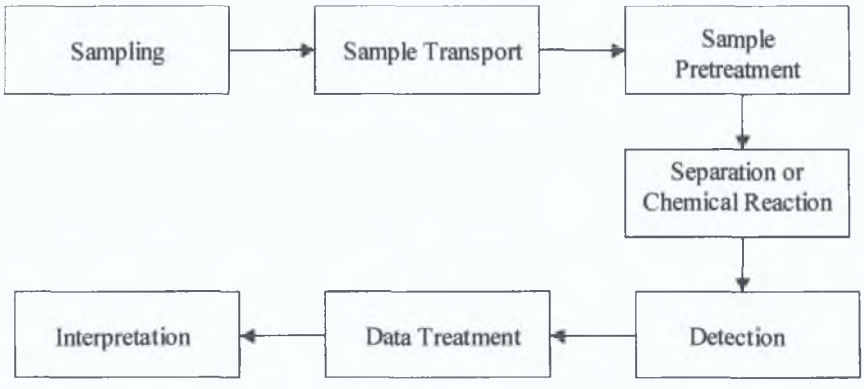

Figure 1.1: Scheme of a chemical analysis [1,2].

By following these steps, more accurate and reproducible results can be achieved, but the process can be very labour intensive and time consuming. The term 'total analysis system' (TAS) is used to describe the automation of all the steps of a chemical analysis using conventional laboratory equipment. Automation speeds up analytical procedures, limits human involvement and is achieved by the optimisation

of the systems design, leading to a more efficient sample analysis. Although reliable, the conventional laboratory equipment used in initial TAS approaches was big and bulky.

To miniaturise common laboratory devices, techniques and approaches, the TAS concept has been modified by scaling down and integrating multiple steps, such as injection, reaction, separation and detection, onto a single device. The result is a system termed 'micro-total analysis system' (μTAS), with fast response time, low sample consumption, on-site operation and high stability.

1.2 Micro-Total Analysis System (μTAS)

The term and concept of a μTAS for chemical analyses was first introduced by Manz, Widmer and colleagues at the analytical laboratories of Ciba-Geigy in Basel, Switzerland in the late 1980s [3]. Their original plan was to develop miniaturised devices whereby all the necessary components needed to perform a chemical analysis were integrated onto one device. Beyond the mere shrinking down of traditional bench top techniques this approach required research in the area of many fields, such as chemistry, biology, optics, materials, fluid mechanics and micro-fabrication. New devices for chemical sensing were developed to replace sensors that were not performing adequately in terms of selectivity and general lifetime. These devices evolved as a consequence of the development of electronic circuits, which had started in the 1950's whereby circuits had been miniaturised and integrated in large numbers onto silicon wafers. Knowledge from the microelectronics area was later used in the development and fabrication of microsystems for chemical sensing and the benefits of this micro-instrumentation were similar to those of the microelectronics, such as low cost, compact size and high speed.

A typical μTAS involves the miniaturisation of all the functions of an analytical method including pumps, valves, mixing and reaction chambers, separation columns, detectors and electronics. The first miniaturised devices consisted of a manifold, whereby only parts of the system were integrated, while all of the connections were

made using conventional tubing. The ultimate goal of miniaturisation is to combine and integrate all of the necessary steps required for an analytical investigation in one single automated system. The main challenge of a μTAS is to obtain a system with a flow manifold in which the volumes are small enough to achieve short analysis times, but which can incorporate all of the elements for the analysis of multi-component samples.

In order to give a clearer picture, a μTAS is defined here in relation to a TAS and a chemical sensor (see Figure 1.2). An ideal chemical sensor is specific in that it simply transforms the chemical information of one species selectively into electrical information [3,4]. It gives reproducible results and has a short response time. The advantage of this type of sensor is that it can also be immersed directly into the sample. The classic example of an (almost) ideal sensor is the pH electrode, which can be used on-line by immersion directly into the sample solution. A TAS system integrates a number of different techniques in order to obtain a satisfactory result. In this case the sample must be brought to the TAS in order to be analysed. A μTAS system performs all of the TAS steps in close proximity to the point of detection.

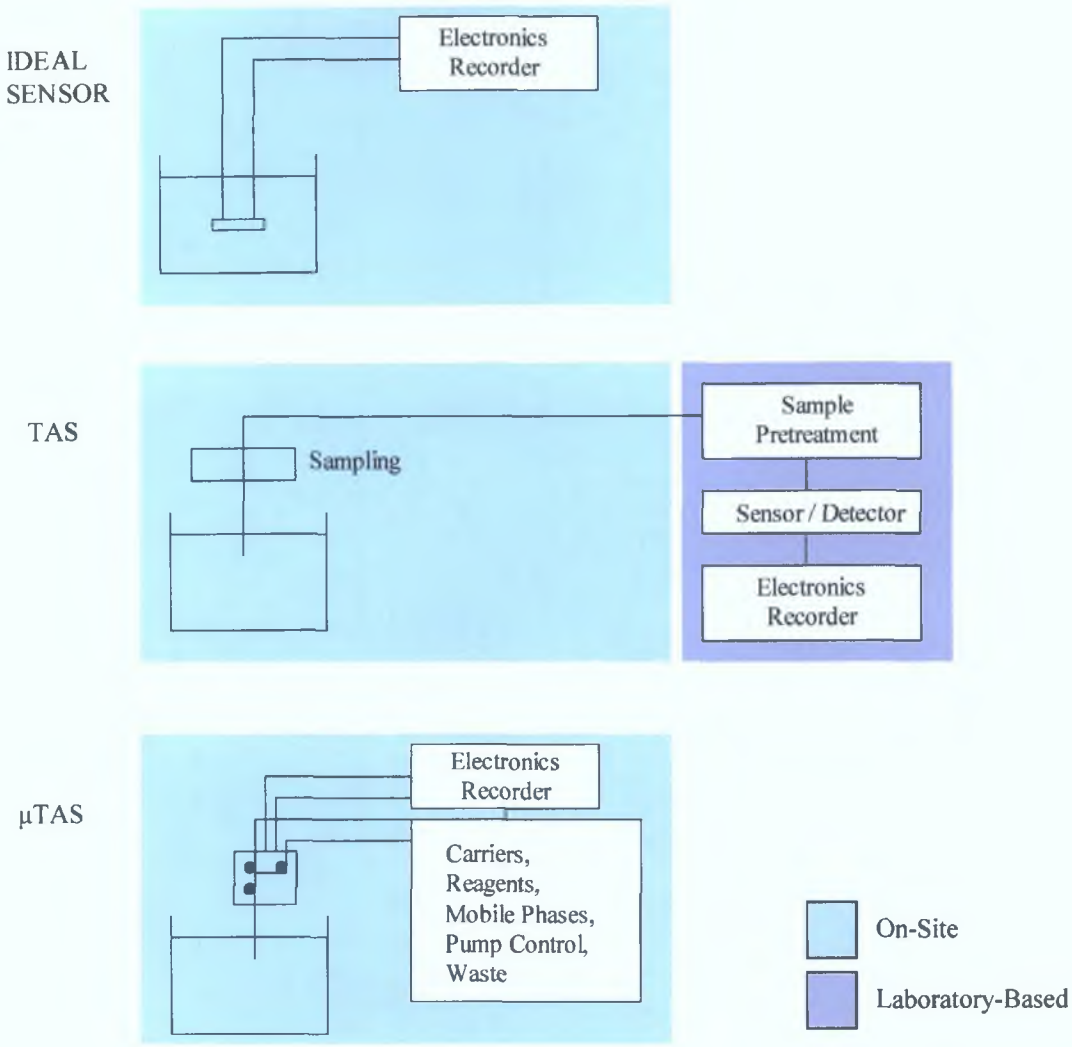

Figure 1.2: A schematic diagram of an ideal chemical sensor, a total analysis system (TAS) and a miniaturised TAS (μTAS) [3,4].

In many ways the μTAS is a combination of both a TAS and an ideal chemical sensor, by incorporating the reliability of a TAS with the size of a sensor. The μTAS differs from the TAS in terms of the distance the sample has to travel before it is detected, while an ideal sensor selectively detects the sample without any interference from other species. It should be noted that the outer dimensions of a μTAS do not need to be very small unless size is critical [5]. The concepts of performance, integration and automation are far more important than size. In practice a μTAS will normally be connected to fluid reservoirs and electrical power sources.

1.3 MINIATURISATION

The concept of analytical miniaturisation can be termed in a number of ways including micro total analysis systems (μTAS), microsystems technology (MST), Lab-on-a-chip and microelectromechanical systems (MEMS). There is no absolute nomenclature to include all the aspects of miniaturisation. Generally, the term μTAS is used in Europe, while in America, MEMS is used because the technology originates from the fabrication of semi-conductor micro devices made from silicon.

Miniaturised systems, in general, hold a number of advantages over conventional large-scale analysis systems [1,6-7]. Some of these are listed as follows;

- A decrease in size results in a decrease in the amount of sample and reagent consumption, therefore making the process a lot more economical, safer (as less amounts of hazardous substances or special materials are used), and more environmentally friendly due to a decrease in the amount of waste generated.
- A decrease in the volume and distances involved in the analysis results in faster operation and analysis or response time. It also allows an increased number of analyses to take place in a certain length of time.
- Miniaturisation can also lead to new techniques, which may not be available on larger scale devices.
- An integrated device, which incorporates all the components of a chemical analysis, removes the need for a conventional laboratory and therefore means it is portable, can be used directly at the point of sampling and can be used for on-site analysis. This also reduces the errors in the process by reducing the amount of sample handling.
- All of the above lead to a more cost efficient analysis.

However, it should be noted that a miniaturised system can also have certain drawbacks;

- Gas bubbles or particles can easily result in blockages within the device.

- Smaller sample volumes can lead to increased limits of detection i.e. less signal for detection.
- Fluids flow through channels with little or no turbulence and as a result mixing is by diffusion only.
- Small devices can sometimes be difficult to handle.
- Due to the lack of commercial components, the need for in-house fabrication and machining may be required.

1.4 Basic Flow Injection Analysis Concept

Flow injection analysis (FIA) is based on the introduction of a liquid sample into an un-segmented, flowing, non-reactive carrier stream of liquid, whereby the sample undergoes well-defined and controllable dispersion [8]. The carrier stream may be a pH or ionic strength buffer or it may simply be water. Once the liquid sample is introduced into the carrier stream, the analyte can be moved, concentrated, diluted, reacted, purified and delivered to a detector without any intervention from an operator. Three key features lead to the rapid acceptance of FIA systems [9]. Firstly, the fundamental principles were easy to understand and implement. Secondly, the instrumentation could readily be assembled from simple, inexpensive, off-the-shelf components, and finally, it provided a simple means of automating many manual wet chemical analytical procedures.

Some of the earlier flow analysis systems were based on a system whereby a continuous flowing stream used air bubbles to segment the samples and the samples were allowed to react with the reagent near completion (termed 'segmented flow analysis'). The need for air segmentation meant that the manifold was elaborate and difficult to miniaturise, and the flow stream tended to pulsate due to the air bubbles required for segmentation. The non-segmented approach removed these problems by removing the air bubbles from the system. As a result, FIA is now a small, simple and inexpensive procedure to operate.

A sample injection valve is a simple method that can be used for sample introduction, as it is capable of injecting a fixed, precise volume of sample into the

carrier stream. This allows the sample to be injected with high precision so that the volume and length of the sample zone at the point of injection is reproducible. A manual rotary injection valve is simple to incorporate into a FIA system for the introduction of a well-defined sample plug volume. The unit has two operating positions: (a) the loading of the sample loop, and (b) the eluting of the sample plug from the loop into the carrier stream (Figure 1.3). Rotary injection valves are compact, rapidly operated, simple to use and robust.

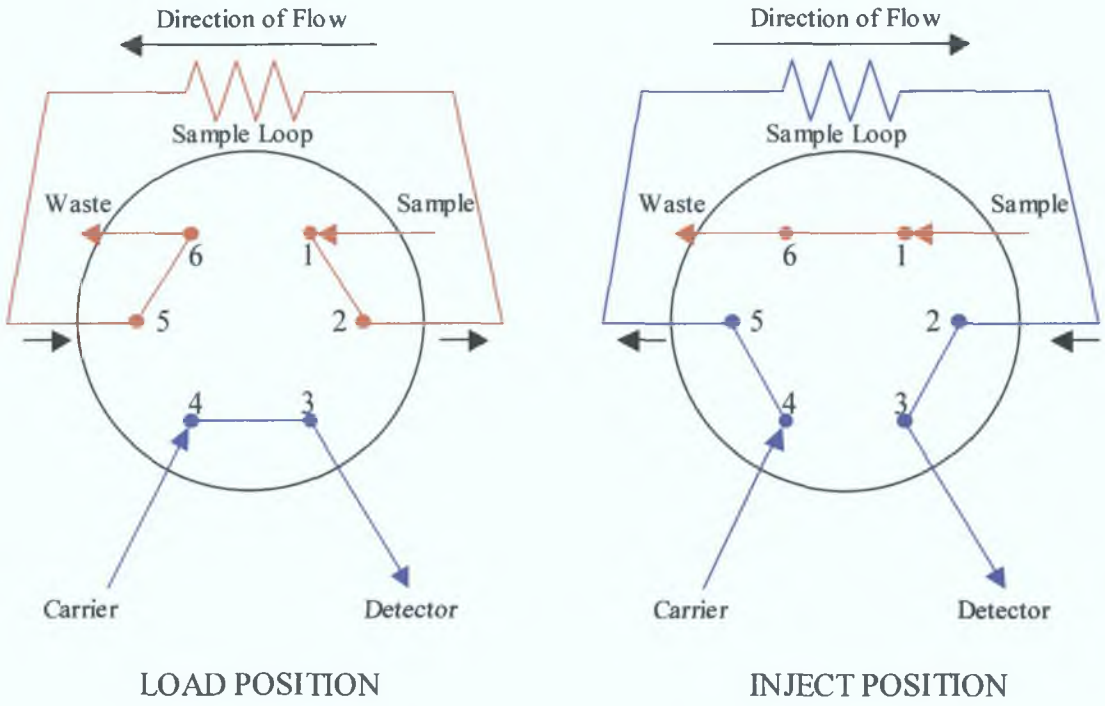

Figure 1.3: The 6-way rotary injection valve used for sample introduction in a FIA system.

Following injection of the sample, the sample zone undergoes physical dispersion as it is pumped through the system. The degree of dispersion can be controlled by adjusting the operating parameters such as flow rate, injection volume and tubing length or diameter. Růžička and Hansen [10] defined dispersion as the ratio of the original analyte concentration (C_0) to the concentration of analyte at the peak maximum (C_{max}) after time, t, as shown in Equation 1.1;

$$\text{Dispersion after time t } (D_t) = C_0/C_{max} \qquad \text{(Equation 1.1)}$$

There are three categories of dispersion;

- Limited dispersion, where, $D_t = 1 - 3$
- Medium dispersion, where, $D_t = 3 - 10$
- Large dispersion, where, $D_t > 10$

In a limited system, FIA is used for sample measuring and transport, and very little mixing takes place. In medium dispersion, it is necessary for the sample and reagents to mix together and time must be allowed for some product to form, so some dispersion occurs. Large dispersion occurs when sample dilution needs to be obtained.

Sample volume can be used to control dispersion. If a large sample volume is introduced, the sample zone will be long and the centre of the zone will be unaffected. Dispersion will only occur at either end of the zone and in this case $D_t = 1$. As the sample volume is decreased, the sample zone becomes shorter so that more of the carrier solution can disperse to the centre of the sample zone, resulting in $D_t > 1$. Increasing the tubing length and increasing the flow rate can also increase dispersion within the system. Therefore, if a longer residence time is required to allow more time for a reaction to take place, the flow rate should be reduced rather than increasing the length of tubing. If the flow is stopped, dispersion also stops and sample spreading only occurs as a result of diffusion. If a long residence time is required, it can be advantageous to stop the flow during the analysis.

1.5 Microfluidic Systems

Microfluidic systems have the potential for a wide range of applications, which can be categorised into four main areas of development [11];

1. Miniaturised analytical systems e.g. clinical analyses, environmental testing.
2. Biomedical devices e.g. implantable devices.
3. Tools for chemistry/biochemistry e.g. small-scale organic synthesis.

4. Systems for fundamental research e.g. study of fluid flow, trace analysis studies.

All the basic functions in a μTAS device – sampling, mixing, reacting, separating, detecting and transporting waste – involve fluid handling. Microfluidics is the behaviour of fluids in small sized channels and is an important factor in the design of a miniaturised system [12]. Although microfluidic devices are often described as miniature versions of their large-scale counterparts, the control of flows in microchannel systems raises very specific problems compared to its larger scale versions, as many areas do not simply scale linearly from large-scale to small-scale systems. For example, as a result of the micron-sized dimensions of the microfluidic devices, small volumes are used and there is less analyte present. The conservation of the analyte in a micro-device is therefore important and can only be achieved through good sample handling and minimal dispersion of all processes that take place on-chip [13].

The effects of miniaturisation are shown in Table 1.1, which shows a number of device characteristics as a function of a typical channel length, d [5]. One of the important factors is the maximum number of devices that can be arranged on a surface (1 cm^2). Typically, this number increases with $1/d^2$. Therefore, at a length of 10 μm, 250,000 devices can be made per cm^2.

Table 1.1: Effects of miniaturisation demonstrating a number of device characteristics as a function of a typical length, d [5].

Typical Channel Length	**1 mm**	**100 μm**	**10 μm**
Volume	10^{-6} L	10^{-9} L	10^{-12} L
No. of molecules at 1μmol L^{-1}	6×10^{11}	6×10^{8}	6×10^{5}
Diffusion Time (for molecule with diffusion coefficient of 10^{-9} m^2 s^{-1})	1000 s	10 s	100 ms
Arrangement (per cm^2)	25 devices/cm^2	2500 devices/cm^2	2.5×10^5 devices/cm^2

The downsizing of a system has an affect on some of the processes that take place on a miniaturised device including mixing, separation and detection. As mentioned earlier, in some cases the characteristics of microsystems are different from those in larger-scale systems. In microfluidic systems one of the most dramatic effects on

device performance, that is a direct result of the small channel dimensions, is that fluid flow is strictly laminar, limiting the ability to accomplish efficient and effective mixing [14]. In conventional chemistry, mixing usually occurs by turbulence, whereby the flow becomes unstable and randomly mixes. In microsystems, however, where size is reduced, the same mechanism cannot be used and laminar flow occurs, where a series of parallel layers are moving at different velocities. Figure 1.4 shows a section of the flow profiles associated with pressure driven laminar and turbulent flow. In laminar flow, the parallel arrows indicate well-defined streamlines of the flow and the profile is parabolic as shown in (a), while in turbulent flow, the flow randomly mixes and mini-vortices can begin to occur. The flow profile is less parabolic as shown in (b) due to the turbulence occurring.

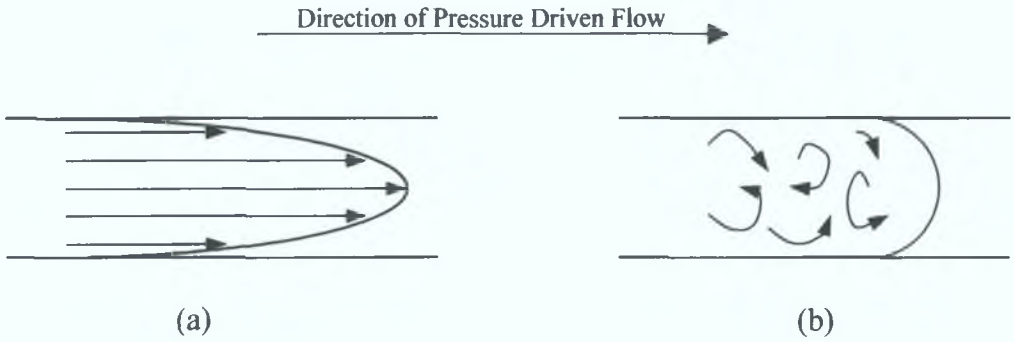

Figure 1.4: Flow profiles associated with pressure driven (a) laminar flow, where parallel streams occur and (b) turbulent flow, where mini-vortices occur.

In small devices, the Reynolds numbers (*Re*) are so low that turbulence cannot be produced [1,15]. The Reynolds number is a dimensionless number that is associated with how smooth the flow of a fluid is. As the flow rate increases in a system, the flow becomes turbulent which results in eddy currents and vortices [16]. The Reynolds number was originally proposed by Osborne Reynolds in 1883 and is basically the ratio of the momentum of the fluid to the friction force imparted by the channel walls. The Reynolds number of a fluid can be calculated using the following equation:

$$Re = \frac{\rho v d}{\eta} \qquad \text{(Equation 1.2)}$$

Where, ρ is the fluid density (kg m^{-3}),

v is the average flow rate or fluid velocity (m s^{-1}),

d is the tube or channel diameter (m) and

η is the viscosity (kg m^{-1} s^{-1}).

A low Reynolds number describes a flow that is laminar, whereby the flow of the fluid occurs in parallel to each other, while a high Reynolds number describes turbulent flow. Turbulence only typically occurs when $Re > 2{,}000$, with the exception of slit type openings where turbulence occurs at $Re > 15$, and with coiled tubes where turbulence occurs at $Re > 2{,}300$ [17]. As a result mixing in the microstructures is only by diffusion of molecules.

Diffusion is the process whereby matter is transported from one part of a system to another as a result of random motions of its atoms, molecules or ions [18]. It occurs as a result of intermolecular collisions rather than as a result of turbulence. A reduction by a factor of 10 of the original size reduces the related time variables (transport time and response time of a detector) by a factor of 100.

1.5.1 Pumping System

Fully integrated microsystems need micropumps for fluid handling. There are two types of pumping that can be used, non-mechanical and mechanical pumping [19]. Both of these have been successfully employed in microfluidic systems. The general requirements of a pumping system for use in a μTAS are:

- Low pressure generation
- Pulse free
- Corrosion resistant components
- High flow control and reproducibility

Some of the earlier miniaturised systems found electroosmotic pumping (non-mechanical pumping) as an attractive and feasible way to flow liquids through the interconnected channels in a micro-device, particularly where separation was needed [3]. Electroosmotic pumps are characterised by the absence of mechanically moving parts, producing an even flow through the system, but external voltage fields, can result in poor flow control reproducibility [13].

More recently peristaltic pumps (mechanical pumping) have been used [20]. Peristalsis occurs when travelling contractile waves in the walls of tubing induces a flow. Peristaltic pumps consist of a number of moving rollers arranged in a circular configuration on a revolving drum compressing flexible tubing against a bridge to produce a constant pulsing flow. As the rotor turns, the rollers move in relation to the tubing thus pushing solution through the tubing. A schematic diagram of a peristaltic pump is shown in Figure 1.5.

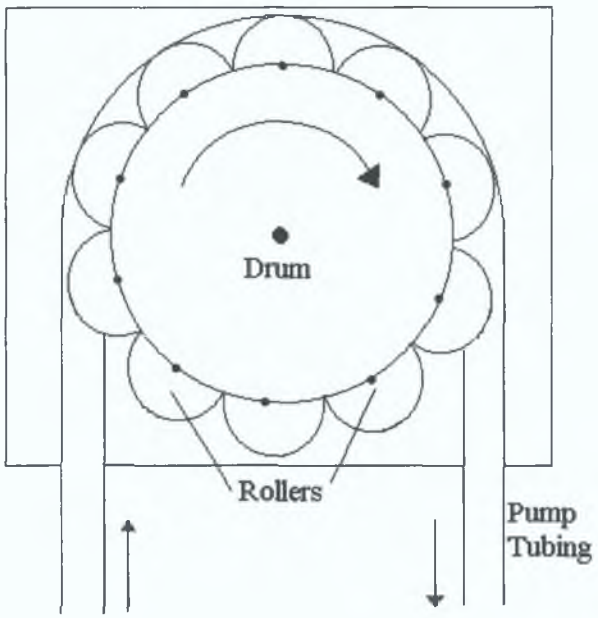

Figure 1.5: Schematic diagram of peristaltic pump containing 10 rollers.

These pumps are simple and reliable to use, as well as being robust and relatively inexpensive to operate. However, the noise generated by the flow pulsing effect of the pump is disadvantageous. The number of rollers and the rate of rotation can determine the magnitude and the frequency of the pulsing. Modern peristaltic pumps have 8 to 10 rollers, and half of them will squeeze the tubing at any one time, leading to a controlled flow rate that minimises the pulsing motion of flow.

1.6 Concept of a Miniaturised Manifold

Concepts, similar to the development of computer chips have been applied to the design of miniaturised chemical microfluidic manifolds, whereby liquids are manipulated in a microchannel system in a similar way to electrons, which are

manipulated in microcircuits [6]. The technology developed for the micro-fabrication of electronics can be applied to silicon, plastic and glass substrates, producing channel networks in two dimensions for sample transport, mixing, separation and detection systems on-chip [1]. However, fluid flow differs from electron flow and therefore bends, orifices and surface topography are important along with the need to minimise flow resistance and potential fluid traps. In terms of size, 'chemical chips' are bigger than microelectronic chips because molecules need much more space than electrons. Typical analytical micro-fabricated manifolds range in overall size from mm to cm scale, with the channels in the μm-scale.

1.7 Materials for a Micro-Fabricated Device

There are a number of different materials that can be used for the production of micro-fabricated devices e.g. silicon, glass, metals, plastics and ceramics [6-7]. Conventionally, glass and silicon were the main materials used. A silicon wafer can be used but is quite expensive to produce. Silicon is also not transparent in the wavelengths typically used for optical detection. Silicon manifolds with channels made in either glass or plastic can be used instead. These are also much cheaper to produce than a silicon wafer but they can be costly to develop. More recently, much investigation has taken place on the use of polymers, which can be mass-produced inexpensively. Silicon and glass devices are usually fabricated using photolithographic methods (developed for microelectronics), while polymer-based manifolds can be made from a much wider range of micro-structuring technologies including hot embossing, injection moulding and laser ablation.

1.7.1 Polymers

It was only recently that interest in microsystems fabricated from plastic materials has grown [21]. Their material properties, versatility and low cost make them a desirable alternative to silicon and glass. The word polymer comes from the Greek words "poly" meaning many and "mers" meaning parts. Basically, polymers are macromolecular substances with a high molecular mass. They are formed as a result of polymerisation reactions where monomers react forming linear chains or three

dimensional polymer chains [18]. Because the polymer is a saturated molecule, it is usually unreactive and therefore gives the polymer a useful range of physical and mechanical properties.

Polymers can be classified into three main categories depending on their moulding behaviour [18,22].

1. Thermoplastic polymers: unlinked or weakly linked chain molecules, which at temperatures above their *glass transition temperature, T_g, become plastic and can be moulded into shapes which are retained after cooling below their T_g. The most common thermoplastics are polyethylene (PE), polyvinyl chloride (PVC) and polystyrene (PS).
2. Duroplastic polymers or thermosets: consist of highly cross-linked chains and therefore are usually rigid and brittle. These must be given their shape before their final chemical structure is produced, which can only be altered mechanically. Some examples of these include epoxy and polyester.
3. Elastic polymers: also very weakly cross-linked polymer chains. If an external force is applied, the chains stretch but relax to their original state when the force is removed.

* Glass transition temperature, T_g, is the temperature range where the polymer substrate changes from a rigid glassy material to a soft (not melted) material, and is usually measured in terms of stiffness or modulus [23].

All of these polymers have different, application-dependable properties. They are cheaper, easier to work with and are more rugged than glass or silicon. In addition, more complex structures can be made with polymers than in glass and a wide range of replication technologies can make these devices disposable or semi-disposable.

To date, polymethylmethacrylate (PMMA), polydimethylsiloxane (PDMS) and polycarbonate (PC) are the most popular polymer materials for micro-fabrication by hot embossing and injection moulding. PMMA is commonly known as Perspex or Plexiglas [22]. It is a hard, amorphous, non-porous, transparent and colourless thermoplastic. It has good optical transparency and abrasion resistance, but it has

poor low temperature and solvent resistances. The T_g of PMMA is 105°C. It has the added advantages of being low cost and has excellent mechanical properties [24]. PDMS is an elastomer that is known as silicone rubber. It is optically transparent down to 280 nm, can seal reversibly on itself, and other materials and its surface chemistry can be controlled by a number of well-developed techniques [11]. Its unique flexibility is due to the fact that it has one of the lowest T_g values of any polymer (T_g of –123 °C) [25]. PC is known as Makrolon and has a T_g of 150 °C [22]. Although PC is a tough polymer, it only has fair chemical resistance and is degraded by many organic solvents [26].

1.8 Fabrication

The design and use of a micro-fabricated device is dependent on the availability of technology to fabricate them, modify their surfaces and interface them with a variety of detection modes [19]. There are a number of different methods available for the fabrication of polymeric devices, that can be separated into two main categories, direct fabrication and replication methods [27]. Direct methods include laser ablation, ion etching and mechanical milling whereby individual polymer surfaces are structured to form system features. These are not very economical as each device must be fabricated separately. On the other hand, replication methods such as injection moulding, hot embossing, and soft lithography, all use a template or master from which the desired polymer microstructures can be made. Polymer microstructures can be repeatedly replicated with the template. These type of technologies are economical when mass production of the microfluidic devices is required.

1.8.1 Direct Fabrication Methods

Direct techniques micromachine each single device individually. This allows the rapid fabrication of single devices, but the fabrication throughput is limited by the fabrication time of each individual device.

Laser ablation uses a high-powered laser to break the chemical bonds in the polymer chain and then remove the fragments from the surface (using laser induced shock

waves). The process relies on the absorption of laser photons by the sample material. Two of the most common lasers used include KrF (which deliver light pulses at 248 nm, typical pulse frequency 10-100 Hz) and ArF (193 nm, several kHz). They are both effective depending on the absorption spectra of the polymer. Polymers that have significant absorption at the emission wavelength of the laser are the most effectively ablated [23].

There are two ways by which ablation can take place, by direct writing and by mask projection [28]. In direct writing, a laser beam generates the structure directly but it should be noted that this method limits the range of shapes or patterns that can be ablated. In the mask projection technique, a mask is used to define the ablated region and the pattern is made by moving the substrate on an x-y stage under the mask. This technique is more flexible than direct writing and can produce more complex structures.

Ion etching is similar to laser ablation, except that gaseous plasmas are used rather than radiation to alter the polymer surface [22]. Oxygen and Argon plasmas are often used for this purpose.

1.8.2 Replication Methods

The underlying principle of replication methods involves the use of a micro-fabricated mould tool, which contains the pattern of the desired polymer structure. These templates are made mainly from four materials: photocurable epoxy, thermoplastic, silicon and metal [24]. A photocurable epoxy can be produced rapidly using a photolithographic process to produce a template, but its insufficient hardness limits its lifetime and run production. The use of a thermoplastic can also result in the simple and fast production of a template, where the dimensions of the microstructures can be easily controlled. However, the template is soft and can easily be deformed, and the widths of the microchannels can only be controlled down to 250 μm. Silicon templates can be used for the fabrication of polymer microchanneled manifolds, but are not the best templates to use as they can easily disintegrate. Also, they are expensive for single use particularly in the area of

research and development where several iterations may be necessary before the development of the final design. The hardness of the metal template makes it more robust and allows many replications of designed patterns in polymer substrates.

The main advantage of replication methods over direct methods is that the expensive micro-fabrication step is only necessary once for the fabrication of the master, which can then be replicated many times into the polymeric structure [22]. This enables cheap and efficient mass production of a micro-device. As well as the cost advantages, this also allows the freedom of design and the master can be produced with a large number of different micro-fabrication technologies, which can result in various geometries.

There are some restrictions involved however with these replication techniques. Undercuts (structures in the polymer with overhanging edges) cannot be fabricated, as the master has to be removed from the moulded device. The lifetime and quality of the moulded structure depends on the surface quality of the moulded tool. Evidence suggests the advantages of replication outweigh the disadvantages.

Injection moulding is a standard process that can form almost any geometry and dimensions from a large variety of thermoplastic materials. With injection moulding, the T_g, melting temperature and thermal expansion coefficient are the most critical parameters for successful fabrication [23]. In this process, the polymer is melted down and injected under high pressure into an evacuated cavity containing a master mould [27]. This is then kept at a temperature close to the melting point of the polymer for a specific length of time after which it is finally cooled. The micro-fabricated device is dependent on the quality of the master template.

Imprinting or hot embossing are accepted as efficient in the production of micro-fabricated devices with embossing being the most widely used replication process for fabricating channel structures in microfluidic structures. As with injection moulding the T_g, melting temperature and thermal expansion coefficient are the three most important factors for good fabrication. In room temperature imprinting, hardness is an important parameter.

There are two ways in which imprinting and embossing can be done. The simplest method uses wires of micron diameter, which are pressed into the substrate material and heated to a temperature slightly above the T_g of the polymer [29]. A controlled force is also applied and the device is cooled. The wires are then removed when the process is finished. However, it has been found that this method is not very reproducible for multiple fabrications. The second method is an improvement on the first approach which involves the manufacture of a machined negative master template of the desired channel layout, which is then pressed into the polymer material instead of using the wires [22]. The rest of the process is the same as for the imprinting method.

Hot embossing has a number of advantages over the injection moulding techniques. During the embossing process very fine structures can be formed without deformations occurring. Also, internal stresses on the plastic are minimised when the hot embossing technique is used compared to the injection moulding because the whole process takes place close to the thermal equilibrium as the tool and plastic are heated to a similar temperature prior to moulding.

Soft lithography methods involve the moulding of elastomeric polymers using a master template. For moulding by this method, elasticity/ability to hold original shape after deformation and shelf life are two important parameters to consider. A positive master is fabricated and the elastomer and a curing agent are poured into it [29]. After curing, the device is then peeled away from the template and placed on a planar surface e.g. a glass slide to form closed channels.

In brief, replication technologies have the potential for mass generated production and can allow μTAS to become disposable devices (see Table 1.2 for properties of processes).

Table 1.2: Summary of different replication techniques [22].

Process	Materials	Tool Cost	Processing Time	Temperature	Automation	Geometry
Injection moulding	Thermo-plastics Duro-plastics	High	Short-med. (0.3-3 min)	High Above melting (150-400°C)	Yes	Bulk, spherical
Hot embossing	Thermo-plastics Duro-plastics	Low-med.	Med-long (3-10 min)	High Around T_g (100-200°C)	Little	Planar (wafers, plates)
Soft lithography	Elastomers Epoxies	Low	Long (min-hr)	Room temp-80°C	Little	Planar

1.8.3 Additional Technology for Complete Devices

Several other steps are required in order to complete a microfluidic device, including the closing of microchannels to form capillaries (bonding), dicing and hole fabrication [22]. Generally, bonding of polymer microchannels is much simpler than with silicon or glass channels [23]. There are a number of methods that can be used for bonding such as lamination, gluing, welding or the application of heat and pressure. In the lamination process, a thin polyethyleneterephtalate (PET) layer is rolled onto the structure with a heated roller. This technique has been used successfully in macrostructures but with small channels, the channel can become blocked. Similar problems can occur when gluing. Heat and pressure can also be used but care must be taken not to damage the structures. Dicing of the devices usually uses a rotating saw or lasers. The method depends on the material used and the accuracy required.

1.9 Detection

One of the main consequences of the reduction in size of a microfluidic device is the resulting demand on the detection system [5,30]. The problem is illustrated in Table 1.1, which shows that sensitive detection in microfluidic analytical devices is a challenge due the extremely low detection volumes available. For example, this table shows the number of molecules that are present in different volumes at a

typical concentration of 1 μM. When the detector is a cube and measures 1 x 1 x 1 mm, its volume is 1 μL and 600 billion molecules are present. However, when the detector measures 10 x 10 x 10 μm, 600,000 molecules are present in the detection area at any one time.

The idea of integrating techniques together is the basic concept of a total analysis system, but only a few techniques can be miniaturised sufficiently for use with a μTAS. A number of techniques have been introduced for detection purposes in μTAS manifolds [31] and are subject to their own advantages and disadvantages. The high cost and large size of some instrumental setups for detection purposes can sometimes make them incompatible with the concept of μTAS. For example, UV-VIS spectrometry can be used for detecting a wide range of analytes and is commonly used as a detection source in larger scale analysis. However, according to Beers Law, the path length is directly proportional to the signal output as:

$$A = \varepsilon c l \qquad \text{(Equation 1.3)}$$

Where, A is the absorbance,

ε is the molar absorptivity (M^{-1} cm^{-1})

c is the concentration of sample (mol L^{-1} or M)

l is the pathlength (cm)

In smaller devices, considering the small size of the sample introduced, it can be difficult to achieve a large path length, which is required for sensitive detection. The detection method chosen for use within a μTAS manifold should therefore be easily incorporated resulting in a small and portable total system.

1.10 Luminescence

Luminescence (from the Latin *lumen* and *essentia*; meaning made of light) can be defined as the emission of ultraviolet, visible or near-infrared radiation from a molecule or an atom resulting from the transition of an electronically excited state to a lower energy state (usually the ground state) [32]. Generally, atoms emit photons

of electromagnetic energy when they decay to the ground state after being in the excited state. Luminescence in living organisms (bioluminescence) has been reported as far back as 1500 BC in Chinese literature with the example of the emission of light from fireflies and glow-worms [33]. The first report of artificial luminescence (chemiluminescence) was in 1669 by the German physician, Hennig Brand. In this work, it was observed that phosphorate ($NaNH_4HPO_4$) present in urine, reacted with carbon during calcinations to yield phosphorus, which was then oxidised to phosphorous pentaoxide giving an emission of light. Since then, the number of known luminescent reactions has increased and is now no longer a curiosity but a powerful method of analysis. Today, analysis by application of luminescence techniques is becoming one of the fastest growing topics in analytical chemistry finding widespread use in many diverse scientific areas.

Three processes are commonly used to generate an atom into the electronically excited state [34]:

1. Bond cleavage: either inter- or intra-molecular.
2. Bond formation: either intramolecular or via the collision and interaction of ions, atoms or molecules. This can involve ion pair formation, molecular collisions and intermolecular forces, such as those occurring in crystal formation.
3. Energy transfer: either from a primary energy source, which can be radiative or non-radiative or from an atom or molecule already in an excited state, to another without direct transfer of a photon. Radiative methods can include heat through conduction or electromagnetic radiation through infrared, visible light or ultraviolet light. Non-radiative methods include dipole-dipole interactions and electron transfer.

Luminescence measurements are more sensitive and selective than absorption measurements [32]. The sensitivity of a luminescence experiment can be increased by increasing the incident power, as shown in Equation 1.4;

$$I = kP_0c \qquad \text{(Equation 1.4)}$$

Where, I is the emission intensity,

k is the extinction coefficient,

P_0 is the radiant power of incident light and

c is the concentration of the emitting species.

There are a number of different types of luminescence, outlined in Table 1.3, which are classified on the basis of the kind of energy source responsible for the excitation that eventually results in the light emission [34]. Elegant instrumentation allows the use of luminescence to be applied to the most intricate analytical problems.

Table 1.3: Classification of luminescence [34].

Type	Basis of light emission
Associated with heating	
Candoluminescence	Luminescence of incandescent solids emitting shorter λ than expected
Pyroluminescence	Luminescence of metal atoms in flames
Thermoluminescence	Luminescence of solids and crystals on mild heating
Associated with prior irradiation	
Photoluminescence	Irradiation by UV or VIS light
Cathodoluminescence	Irradiation by β particles (electrons)
Anodoluminescence	Irradiation by α particles (the nuclei)
Radioluminescence	Irradiation by γ or X-rays
Associated with electrical phenomena	
Electroluminescence & piezoluminescence	Luminescence associated with electric discharges and fields
Galvanoluminescence	Luminescence during electrolysis
Sonoluminescence	Luminescence from intense sound waves in solution
Associated with structural rearrangements in solids	
Triboluminescence	Luminescence on shaking, rubbing or crushing of crystals (material stressed to point of fraction)
Crystalloluminescence	Luminescence on crystallisation
Lyoluminescence	Luminescence on dissolving of crystals
Associated with chemical reactions	
Chemiluminescence (oxyluminescence)	Chemical reaction
Bioluminescence (organoluminescence)	Luminous organisms

Luminescence is a general term applied to the emission of electromagnetic radiation by an atomic or molecular species, originating from the decay of that species from a higher to a lower energy state. Figure 1.6 shows an electronic state diagram (Jablonski diagram), which shows the pathways that can take place for a photon-absorbing molecule excited between the ground state and electronically excited states and illustrates the processes of absorption, fluorescence (relatively fast),

phosphorescence (relatively slow), internal conversion and intersystem crossing. Compounds in the ground state, known as the singlet ground state (S_0), generally have a pair of electrons with opposing spins. The absorption of UV or visible radiation can raise an electron to an excited singlet state, which can follow either a non-radiative (internal conversion or intersystem crossing) or a radiative (fluorescence or phosphorescence) pathway back to the ground state.

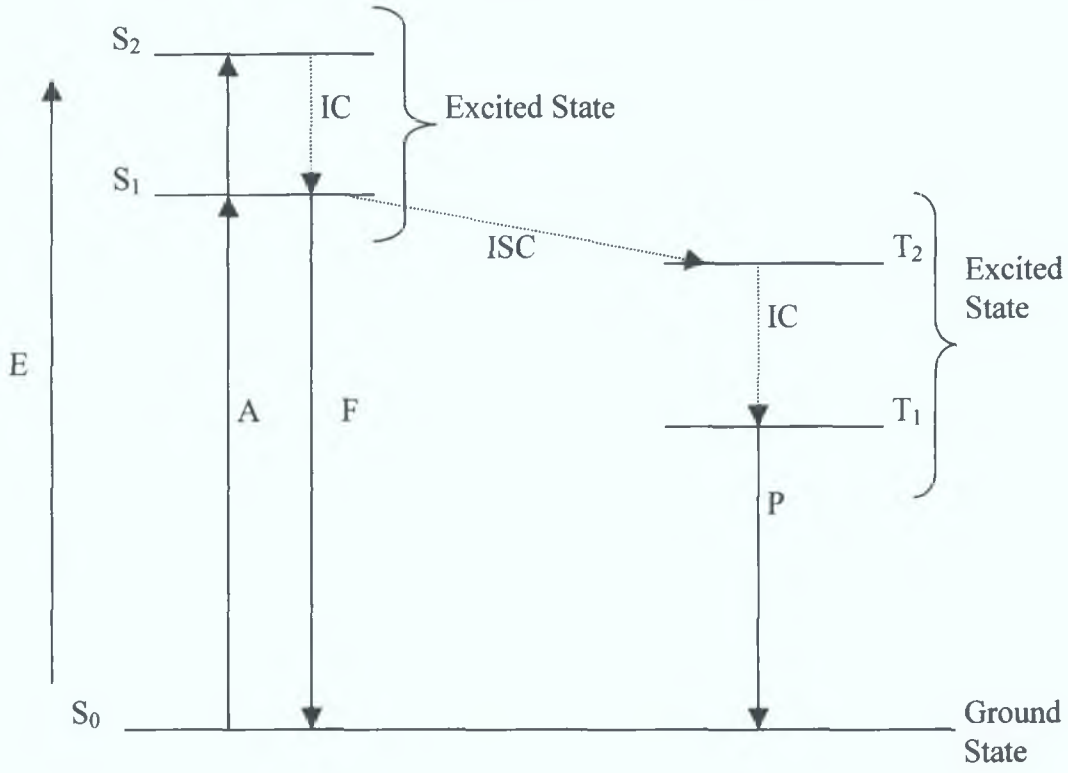

Figure 1.6: *Energy diagram for a photoluminescent system illustrating molecular excitement due to the absorption of a photon and the various pathways for returning to the ground state. A, photon absorption; F, fluorescence; P, phosphorescence; IC, internal conversion; ISC, intersystem crossing; E, energy; S, singlet state; T, triplet state [34].*

To explain the above energy diagram, the Pauli Exclusion Principle should be understood, whereby electrons exist in one of two quantised spin states. The rotation of the electron around its axis generates a small magnetic field and the direction of the rotation and the associated magnetic fields are opposite but equal magnitude for the two spin states. A pair of electrons with opposite spin in one molecule is known as a singlet spin state. An excited molecule is normally a singlet, where all the electron spins are paired and the emission is equivalent to fluorescence. Sometimes, the excited electron can realign parallel to the electron left behind, and the electrons

are termed unpaired and the excited molecule formed is known as an excited triplet state. This emission process is termed phosphorescence. Intersystem crossing is a change in electron spin to form an excited triplet state. Triplet states are generally less energetic than corresponding singlet states and the emission will be considerably slower from a singlet to triplet spin state than the emission of a singlet-to-singlet transition.

1.11 Chemiluminescence

'Das bei chemischen processen auftretende leuchten würde chemiluminescenz...' or translated 'Light emission occurring as a result of chemical processes would then be referred to as chemiluminescence'

Eilhard Wiedemann, 1888

Chemiluminescence (CL) is a luminescent phenomenon, defined as the emission of electromagnetic radiation (ultraviolet, visible or infrared) produced during the course of a chemical reaction [35]. The observed emission results from the ejection of a photon from its excited state. In most cases, the amount of energy released in a chemical reaction is not large enough for chemiluminescence to be produced and the energy dissipates as heat. The process by which chemiluminescence is generated is similar to that of photoluminescence (fluorescence and phosphorescence) except that it does not require a source of irradiation [36]. In fluorescence and phosphorescence the electronically excited state is produced by absorption of ultraviolet or visible light.

The phenomenon of chemiluminescence was discovered in the middle of the nineteenth century. In 1877, Radziszewski reported green light emitted by a synthetic organic compound, lophine (2,4,5-triphenylimidazole) when reacting with oxygen in the presence of a strong base [37]. However, the term "chemiluminescence" was not introduced until 1888, when Wiedemann defined the term "luminescence" to distinguish between light emission from thermally excited substances and light emission from molecules excited by other mechanisms.

If a chemical reaction is to generate light there must be sufficient energy available from it to produce a photon or to transfer its energy to a molecule that can emit photons. Three main features are associated with chemiluminescence reactions;

1. The reaction must be exothermic in order to generate sufficient energy for the formation of an electronically excited state.
2. A pathway must exist for the formation of the electronically excited state. In the case of dark reactions that lead directly to ground state products, i.e. if the chemical energy is lost as heat, the reaction will not be chemiluminescent.
3. The excited state must be capable of losing its energy as a photon or be capable of energy transfer to a fluorophore.

An analyte can be determined by chemiluminescence only if it has one of the following three characteristics [38];

1. It chemiluminesces when mixed with a specific reagent.
2. It catalyses chemiluminescence between other reagents.
3. It suppresses chemiluminescence between other reagents.

Chemiluminescence reactions emit light of varying degrees of intensity and lifetime, with colours that span the visible spectrum. These reactions are observed in solid, liquid and gas-phase reactions. In solution chemiluminescence has many different applications in analytical chemistry for the determination of metal ions, inorganic anions, carcinogens and drugs in a variety of environmental and clinical matrices. The simplest type of reaction of compounds producing chemiluminescence can be illustrated as [39];

$$A + B \longrightarrow C^* + D$$
$$C^* \longrightarrow C + h\nu$$

Where, C* represents the excited state of the species C, produced from the chemical reaction when the two reagents A and B are mixed together. In this case, the luminescence spectrum is that of the reaction product C. Chemiluminescence reactions can last from less than a second to more than a day.

1.11.1 Characterisation of a Chemiluminescence Reaction

Essentially four principles characterise a particular chemiluminescence reaction;

1. The brightness of the light emission, especially whether or not it is visible to the naked eye. Some emissions can be very dim and are described as ultra weak chemiluminescence.
2. The state in which the chemiluminescence reaction occurs, particularly if the excited state emitter and the reaction producing it occur in a gas or liquid or at a gas-liquid, gas-solid, liquid-liquid, or liquid-solid interface.
3. Whether the chemiluminescence reaction i.e. the light emitting species, is organic (i.e. a compound of carbon) or inorganic.
4. The existence or requirement of an acceptor substance that takes the energy from the initial excited product of the chemiluminescence reaction and then becomes the actual light emitter. This process is known as an indirect reaction.

Chemiluminescence can be visible and bright, visible and dim, or invisible and ultra-weak.

1.11.2 Direct and Indirect Chemiluminescence Reactions

There are two basic mechanisms of chemiluminescence reactions that have been defined, either direct or indirect (also described as sensitised chemiluminescence or energy transfer chemiluminescence) [35].

In the case of direct chemiluminescence, two reagents, usually a substrate and an oxidant, possibly in the presence of some co-factors, react to form a product or intermediate, sometimes in the presence of a catalyst. Some fraction of the product or intermediate is formed in an electronically excited state, which subsequently relaxes to the ground state with the emission of a photon. The substrate is the chemiluminescence precursor, which is converted into the electronically excited molecule, responsible for light emission or acting as the energy transfer donor in indirect chemiluminescence. The catalyst (metal ion) reduces the activation energy.

Co-factors are sometimes necessary to convert one or more of the substrates into a form capable of reacting with the catalyst.

In contrast, in indirect chemiluminescence the excited product is not the light emitter, but instead transfers its energy to a fluorescent acceptor (sensitiser), which then emits light. This process makes it possible for those molecules that are unable to be directly involved in chemiluminescence reactions to transfer their excess energy to a fluorophore that in turn is excited. The actual spectrum may be entirely from the fluorophore or it may be a combination of the product and the fluorophore.

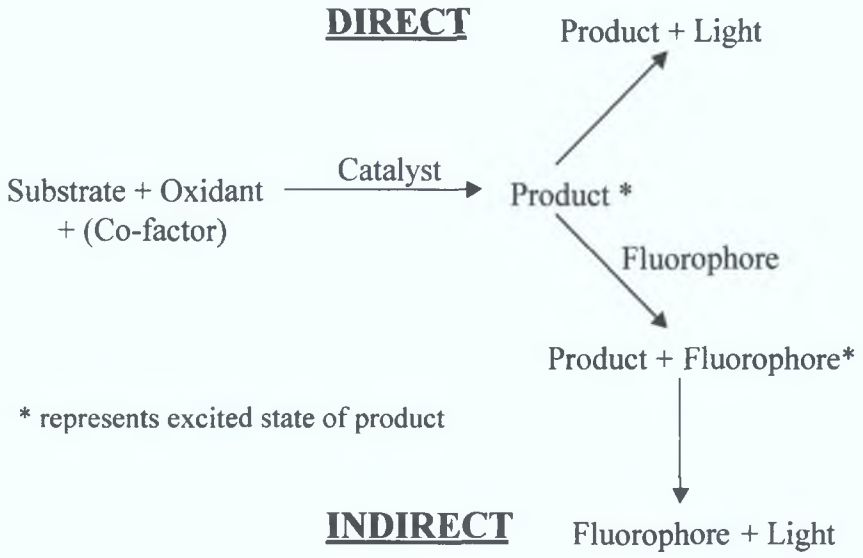

Figure 1.7: Classification of chemiluminescence reactions [35].

1.11.3 Efficient Chemiluminescence Reactions

An efficient chemiluminescence reaction requires up to five components [34];

1. The chemiluminescent substrate(s), which react to form the electronically excited state molecule, responsible for light emission in direct chemiluminescence or acting as the energy transfer donor in indirect chemiluminescence.
2. An electron acceptor, such as oxygen, if an oxidation reaction is involved.

3. A catalyst i.e. the metal ion. The catalyst has one or more of three functions;
   (a) to reduce the activation energy and therefore, initiate or speed up a reaction that would otherwise be very slow, or not occur at all,
   (b) to provide an environment for a high overall quantum yield,
   (c) to process an oxidant.
4. Cofactors which are necessary to convert one or more of the substrates into a form capable of reacting or interacting with the catalyst, or necessary to provide an efficient leaving group if bond cleavage is required to generate the excited emitter.
5. An energy or electron acceptor, if energy transfer chemiluminescence is involved (indirect chemiluminescence).

Whether the chemiluminescence reaction is direct or indirect, there are four main parameters that are characteristic of both types of chemiluminescence;

1. Intensity.
2. Colour.
3. Speed of onset and decay of light intensity.
4. Polarisation of light (if any).

These parameters are determined by the rate of the primary chemical reaction, and by the chemical structure and environment of the excited state product. The most useful of these parameters for analytical purposes is the light intensity [36] where;

$$I_{CL} = \Phi_{CL} (dP/dt) \qquad \text{(Equation 1.5)}$$

where, I_{CL} is the chemiluminescence intensity i.e. the number of photons emitted per second,

Φ_{CL} is the chemiluminescence quantum yield i.e. the number of photons emitted per reacting molecule,

dP/dt is the rate of the chemical reaction i.e. the number of molecules that react per unit time, in seconds.

The chemiluminescence quantum yield is expressed as a product of two efficiencies;

$$\emptyset_{CL} = \emptyset_{EX}\, \emptyset_{EM} \qquad \text{(Equation 1.6)}$$

where, $\emptyset_{EX}$ is the excitation quantum yield i.e. the number of excited states formed per reacting molecule,

$\emptyset_{EM}$ is the emission quantum yield i.e. the number of excited photons emitted per excited state.

When a chemiluminescence reaction occurs, it is desirable for the quantum yield ($\emptyset_{CL}$) of the chemiluminescence to be $\geq$ 0.20 ($\geq$ 20 %) by maintaining the appropriate reaction medium. Bioluminescence on the other hand frequently has a $\emptyset_{CL}$ approaching 1.0 (100 %). The efficiency of the emission has no effect on the wavelength of emission. The actual emission wavelength, λ, is determined by the energy as shown in the following equation;

$$E = \frac{hc}{\lambda} \qquad \text{(Equation 1.7)}$$

where, E is the energy required for the emission of photons of wavelength λ.

h is Planck's Constant (6.63×10^{-34} J.s. molecule^{-1}).

c is the velocity of light (3.0×10^{8} m s^{-1}).

λ is the wavelength of emission.

As mentioned earlier, chemiluminescence emission can be characterised by four variables: colour, intensity, rate of production and decay of intensity and polarisation of light, if any. The reaction time and duration of chemiluminescence vary from very fast and/or short lived (less than 1 second) to very slow and/or long lasting (more than 1 day). However, emission intensity has the most impact on the application of a chemiluminescence reaction, as it is the intensity that is measured over the lifetime of the emission and this is dependent on the rate of the reaction and the efficiency at generating molecules in an excited state. The overall efficiency of a chemiluminescence reaction can be described by the following equation [34];

$$\emptyset_{CL} = \emptyset_C * \emptyset_F * \emptyset_{EX} \qquad \text{(Equation 1.8)}$$

where, $\emptyset_{CL}$ is the chemiluminescence quantum yield i.e. a measure of the overall efficiency of the chemiluminescence reaction,

$\emptyset_C$ is the chemical yield i.e. the fraction of molecules that go through the chemiluminescent pathway,

$\emptyset_F$ is the excited state quantum yield i.e. the fraction of excited molecules that produce a photon and undergo fluorescence decay,

$\emptyset_{EX}$ is the yield of the excited molecules i.e. the fraction of molecules that are produced in the excited state.

In general, chemical events such as bond cleavage and formation are much slower than electronic events such as excitation or decay to new orbital or intramolecular vibrations. Therefore, the kinetics of a chemiluminescence reaction are determined by the activation energy, the concentration of the reagents and any catalyst involved and temperature. The brightness of the light emission at any point in time is dependent on the number of excited state emitters at that point. The use of chemiluminescence within an analytical methodology has several advantages such as;

1. No external light source is required which means it has a potentially lower limit of detection (LOD) than other emission techniques employing external energy sources since there is no scattered background light to reduce the signal to noise ratio (S/N).
2. The apparatus is simple, at most basic a light detector and a flow cell (with propulsion unit) is all that is required.
3. Many chemiluminescence reactions can be specific for one, or a small number of chemically similar analytes.

1.12 INSTRUMENTATION

The instrumentation for a chemiluminescence measurement is relatively simple and in some cases may consist of only the reaction vessel and a photomultiplier tube (PMT). Generally, no wavelength-restricting device is needed, because the only

source of radiation is the chemical reaction between the analyte and the reagent. The typical signal from chemiluminescence as a function of time rapidly rises to a maximum, as the reagent and analyte react, followed by an exponential decay of the signal.

Four principle methods have been used to detect and quantify changes in light intensity resulting from chemiluminescence. These can be seen in Table 1.4.

Table 1.4: Detectors of light from chemiluminescence reactions.

Method	Example
Biological	Human eye, photoreceptors from other organisms, photosynthetic and photosensitive pigments
Chemical	Photographic paper and film, photosensitive substances in solution
Thermal	Pneumatic device, bolometer, thermopile
Electrical	Photoelectric device (photomultiplier), photovoltaic device (light meter), photoconductor device (photodiode)

All of the original discoveries of chemiluminescence, in the early 1900's, involved initial observations by the naked eye. Today most modern detectors are transducers that convert radiant energy into an electrical signal that is amplified and recorded. It was the introduction of the highly sensitive PMT, which is capable of detecting just a few photons per second that led to the discovery of much weaker or ultra-weak chemiluminescence, not visible to the naked eye.

Sensitivity (signal to dark-current ratio) and spectral response are important considerations in choosing a light-detecting device. An ideal detector should have the following characteristics;

- High sensitivity, down to 1 photon s^{-1}, with low noise.
- Sensitivity range, at least six orders of magnitude, ideally linearly.
- Constant response at the appropriate wavelength.
- Produce an output signal that is directly proportional to the light intensity.
- Precise and reproducible.
- Stable and hardy.
- Cheap and available.

It would be advantageous if the detector could be incorporated into the miniaturised manifold, providing a small, portable and complete system. Integrating the detector into the system also eliminates the requirement of interfacing the miniaturised device with large bench top instruments. It has also been found that larger instruments require larger sample sizes and higher flow rates, which are not compatible in the smaller manifolds.

As mentioned, modern detectors for chemiluminescence are based on photon transducers (converting photons into electrical signal). These can be based on either solid-state devices or on vacuum tubes. The simplest solid-state device is a silicon diode, consisting of a reverse biased pn junction on a silicon manifold. Semiconductors can be doped by adding tiny amounts of impurities, which add extra non-bonding electrons (n-type) and positive holes (p-type) [40]. A diode is formed by manufacturing adjacent n- and p- type regions within a silicon crystal, called a pn junction. A reverse bias can create a depletion layer reducing the conductance of the n junction. When light hits the silicon device, positive holes and negative electrons are drawn in opposite directions to form a depletion layer and a current is produced. Photodiodes (PDs) consist of a number of silicon diodes linked in a circuit allowing measurement over a wide spectral range. These devices are small and can be used in a portable system, but they lack sensitivity and signal to noise ratio compared to PMTs.

A PMT is a photosensitive device which generates electrons at a photocathode, which are focussed and multiplied by an electrode chain, eventually being collected at the anode. The tube can be divided into four main parts [34,36]:

1. The glass envelope - which maintains a vacuum within it and has a transparent window through which photons can enter.
2. The photocathode - the light receiver and generator of the primary electrons.
3. The dynode chain - the electron focusing and multiplication device, which generates secondary electrons.
4. The anode - the electron collector.

The PMT receives a photon at the photocathode, which, because of the photoelectric effect, emits an electron. This is known as primary emission. The electron is then electrostatically accelerated, and focused so that it hits the first dynode (positive surface). This is made of a material different from that of the photocathode and emits several electrons (usually between 5 and 7 electrons) as a result of secondary emission. Each of these electrons is then accelerated and focussed to hit the second dynode (which is more positive than the first dynode), where a further multiplication of electrons occurs, which are then accelerated to a third dynode. This amplification may be repeated as many as 13 times, producing more than 10^6 electrons for each photon which struck the first surface, before the resulting electrons are collected as a pulse of charge at the anode. The anode then delivers the pulse, via a preamplifier, to the discriminator. This then decides whether it is big enough to be considered as a 'count'. A schematic of a photomultiplier tube is shown in Figure 1.8.

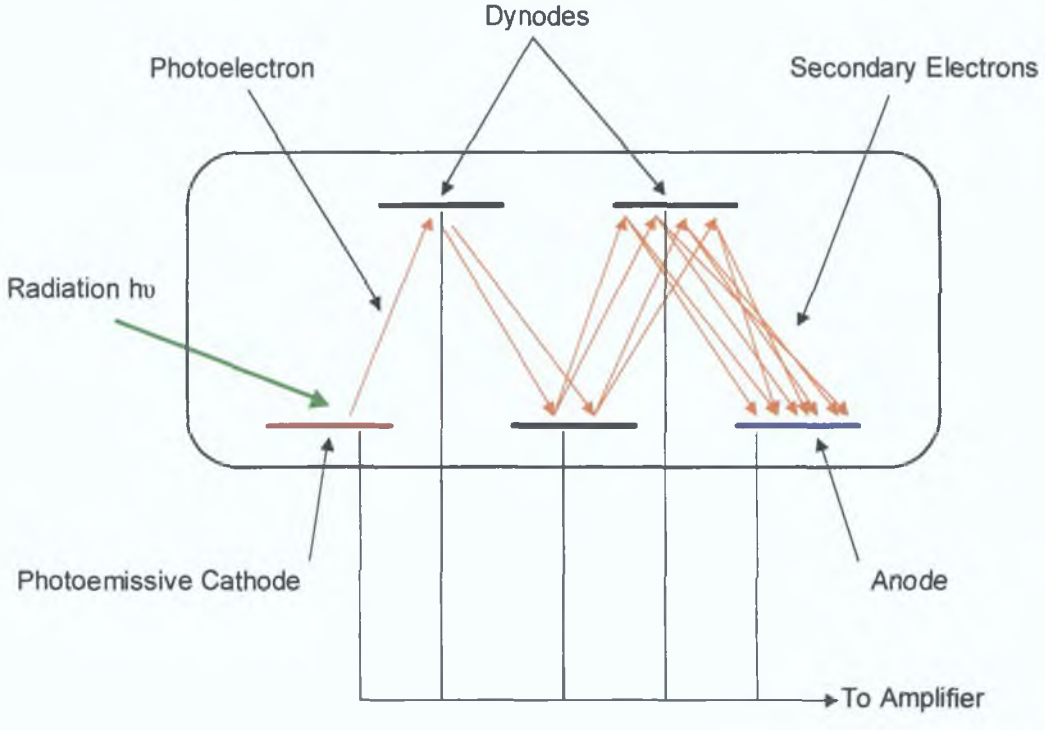

Figure 1.8: Schematic of photomultiplier tube (PMT).

Note: The above schematic is used to illustrate how a photomultiplier tube works and an actual photomultiplier tube contains more dynodes than represented in Figure 1.8.

Ultimately with a PMT, the main aim is to achieve the maximum output signal from the anode, but with minimum noise. There are many potential sources of noise in a PMT. These include ionisation of residual gases or those permeating through the glass envelope, light generated in the tube by ionisation, electrons hitting the glass (this can be minimised by a positive anode and an earthed photocathode), electron leakage at the output e.g. caused by dirt, fingerprints or moisture at the base of the tube and primary electron emission from the dynodes when at high potentials. As well as this, tubes may also 'burst', particularly if damaged or if near other apparatus causing sparks, radio signals or mains surges. The most common source of noise is thermal i.e. electrons emitted spontaneously from the photocathode and the dynodes.

There are a number of points to watch when using a PMT;

1. The tube should not be exposed to daylight with the high voltage on. This will burn the photocathode, with the result that the tube will never return to its original low dark current, and will probably 'burst'. Exposure to light even with the high voltage off should be avoided, because when the voltage is turned on it will take longer to stabilise to a low dark current compared to a dark-adapted tube. Care should also be taken to avoid bright chemiluminescent flashes for the same reason.
2. If the light intensity becomes too high e.g. at $10^7 - 10^8$ photons s^{-1}, the photon rate becomes greater than the rate of transit of the electrons down the tube. If the current between the photocathode and the first dynode becomes high there will be a voltage drop between them. To increase the light intensity when saturation occurs, the voltage of the first dynode must be decreased.
3. The following environmental factors should also be avoided: exposure of the tube to daylight, high temperature, magnetic fields, vibrations and helium, which can permeate the glass. It should also be noted the high voltage across a PMT is dangerous.

1.13 METAL DETERMINATIONS

The use of chemiluminescence for the determination of dissolved trace species has gained much attention in recent years, due to its relatively simple and inexpensive instrumentation for monitoring emission. It also offers high sensitivity for many species, because low light levels are readily monitored in the absence of noise, and is often linear over a wide dynamic range. In addition, chemiluminescence techniques are often selective for particular chemical forms and therefore, can be used for speciation studies. Chemiluminescence is often coupled with FIA as it gives improved limits of detection, higher precision and faster sample throughput as compared to manual methods of sample processing [41].

Table 1.5 summarises the potential impact of some metal ions caused by pollution, which can be found in samples such as tap water, natural waters, soil extracts and sediments [42].

Table 1.5: Summary of sources and potential impact of some common metal ions found in the environment [42].

Metal	Sources and Potential Impact
Aluminium	Almost always exists in +3 oxidation state, and all compounds are relatively insoluble. The increase is linked to the increasing amounts of acids released due to industrialisation and fossil fuels. Until recently, it was considered non-toxic, but it is being linked to neural diseases such as Alzheimer's Disease.
Cadmium	Present in industrial wastewaters and associated with zinc mining wastes. Extremely toxic and a long biological half-life in humans.
Chromium	Frequently present (as Cr (VI)) in industrial wastewaters; commonly used as a rust inhibitor. Poisonous but noncumulative.
Copper	Derived from many industrial processes. Toxic to fish, algae, bacteria; hence frequently used to control excessive algae blooms (eutrophication).
Iron	Objectionable primarily because of taste and colour in water and staining/deposition characteristics. Common derivatives of general corrosion, but the worst effects are frequently a by-product of acid mine drainage.
Lead	Major sources of environmental pollution are from fossil fuels, pesticides, fertilisers and the smelting industry.
Manganese	These compounds are more readily solubilised than those of iron i.e. a less reducing environment is required. Objections to discharges of this metal e.g. staining properties are similar to those of iron.
Nickel	Corrosion from stainless steels etc. Toxic to fish.
Zinc	Ubiquitous associate of industrialisation. Impact closely parallels that of copper.

1.13.1 Copper

Copper is the twenty-fifth most abundant crustal element (~ 0.01 %) and occurs in the lithosphere mixed with other metals. It occurs naturally in the environment in rocks, soil, water and air [43-44]. It is one of a relatively small group of metallic elements that are essential to human health. It is an important element for normal biochemical processes such as respiration, biosynthesis and metabolism, but as with many other metals, at high concentrations it is toxic. High levels can have adverse health effects including irritation of the nose, mouth and eyes, as well as nausea, vomiting and diarrhoea. Copper accumulation in the liver is a characteristic of Wilson's disease, producing neurological and psychiatric defects [45]. In some cases a large excess may cause liver and kidney damage and can even lead to death.

Copper has been used since the bronze age when it was first alloyed with tin to produce bronze. Due to its softness, copper forms more than one thousand different alloys, especially brasses and bronzes. Copper compounds are widely used in water treatment and in agriculture, as preservatives, fertilisers, fungicides and antifouling paints. They can be derived from mining and industrial processes and applications, as well as through the combustion of fossil fuels and wastes [44]. On a global basis, the atmospheric copper flux from anthropogenic sources are approximately 3 times higher than its flux from natural sources [46]. Global emissions of copper from natural sources include marine spray, volcanoes and forest fires, while anthropogenic sources are outlined above.

The World Health Organisation (WHO) and the European Water Quality Directive recommends the concentration of copper in drinking water should not exceed 2 mg/L (31 μM) [47] and the recommended daily allowance (RDA) for adults is 1.1 mg per day [48]. The concentration of copper in drinking water is highly variable due to hardness and pH and the types of pipes and taps. Concentrations can range from a few micrograms to more than 1 mg L^{-1}. As a result of this, a lot of work has been conducted to design methods capable of determining trace amounts of copper in environmental and biological samples.

1.13.1.1 Determination and Quantification of Copper in Complex Samples

Some of the earliest successful determinations of copper in seawater were carried out by solvent extraction [49] or co-precipitation using cobalt ammonium 1-pyrrolidinedithiocarbamate (Co-APDC) [50] with graphite furnace atomic absorption spectroscopy (GF-AAS) for the quantification of the copper [51]. Since then a number of different analytical techniques have been developed for the analysis of copper in different sample matrices including atomic absorption spectroscopy (AAS), inductively coupled plasma (ICP) and spectrophotometric techniques. Recently, a lot of work has taken place within the area of optical copper sensing which are based on absorbance, reflectance or luminescence measurements.

1.13.1.2 Chemiluminescence Detection of Copper

Perhaps the most common chemiluminescence reaction for the determination of copper is based on the formation of a complex between the copper and 1,10-phenanthroline, followed by the subsequent emission of light during the oxidation of the complex by hydrogen peroxide at an alkaline pH (ideally pH 9.8 to pH 10.1) [51-56]. Upon the initiation of the reaction, the copper (II) ion complexes with one or two of the 1,10-phenanthroline molecules as shown in Figure 1.9. Each of the 1,10-phenanthroline molecules has a pair of nitrogen atoms with unpaired electrons that form covalent bonds with the copper (II) ion.

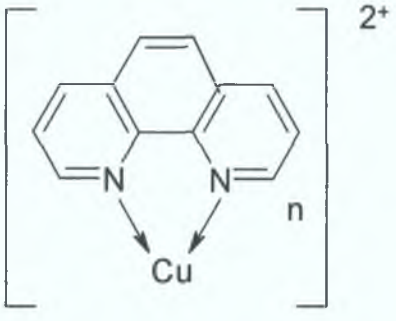

Figure 1.9: Structure of copper 1,10-phenanthroline structure where n = 1 or 2.

The chelated copper (II) then catalyses the decomposition of the hydrogen peroxide to produce superoxide anion radicals, although only a small fraction of them act as oxidants, the majority of them causing the catalytic decomposition of the hydrogen peroxide [54-55]. The superoxide radicals oxidise the 1,10-phenanthroline to the excited chemiluminescence emitter 3,3'-diformyl-2,2-dipyridyl (emission in the wavelength range 445 – 450 nm) and ultimately to 2,2'-dipyridyl-3,3'-dicarboxylic acid. The key steps in the mechanism of the reaction can be seen in Figure 1.10.

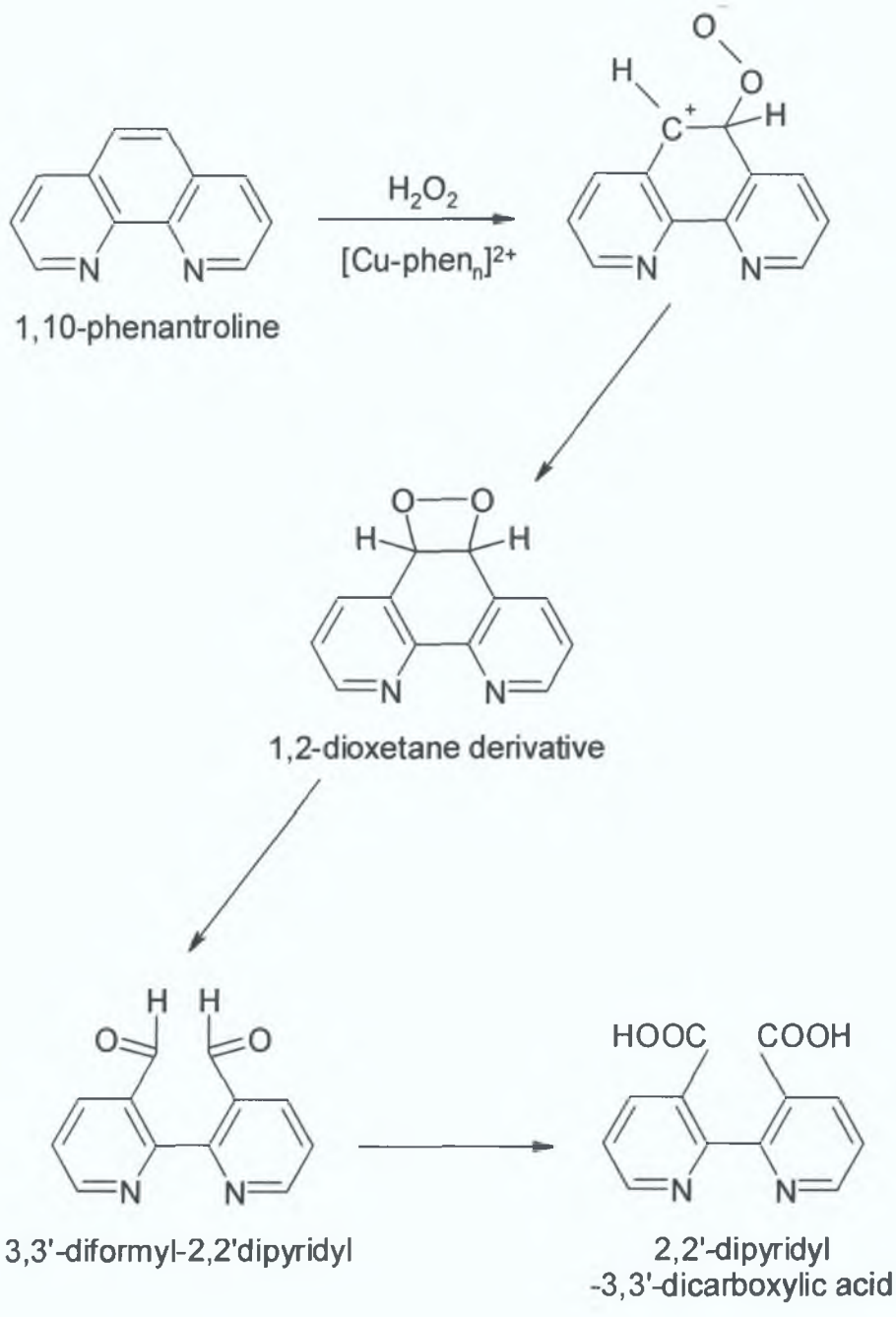

Figure 1.10: Proposed mechanism for oxidation of 1,10-phenanthroline by superoxide anion radical [54-55].

In a situation where the 1,10-phenanthroline and hydrogen peroxide are in excess over the copper (II), the amount of chemiluminescence is proportional to the amount of copper (II) present. The overall reaction is greatly enhanced by the addition of a cationic surfactant such as cetylethyldimethylammonium bromide (CEDAB), to the alkaline reaction medium, due to a surface catalytic effect, outlined in work by Yamada and Suzuki [52]. This arises because the O_2^- is attracted to the positively

charged micellar surface, forming an intermediate, which initiates the reaction with 1,10-phenanthroline. The background chemiluminescence can be reduced by the addition of tetraethylenepentamine (TEPA), which is a strong complexing agent for copper and is used to minimise the effects of copper impurities present in the reagents. This ligand binds strongly to copper, but does not interfere in the analysis of copper as the kinetics of its reaction with copper are very slow in comparison to the overall time of the chemiluminescence [56].

Yamada and Suzuki also carried out selectivity and interference studies [52]. The study found that lead, zinc, iron (II) and iron (III) all produced a slight interference in the system (the highest signal was 25 % of that for copper which was seen for lead), while chromium (III) and (VI), manganese, aluminium, nickel and cobalt did not produce any chemiluminescence signal. This system was deemed more selective than previous work by the same authors using a flavine mononucleotide chemiluminescence system [57].

In similar interference studies carried out by Coale *et al.* it was found that both calcium and magnesium showed strong interference effects on the system [51]. It was found that the high concentration of magnesium ions in seawater (0.05 M) caused a 100-fold reduction in the intensity of chemiluminescence when the seawater was injected directly. As a result, a preconcentration step was employed using a micro-column of immobilised 8-hydroxyquinoline (8-HQ) to preconcentrate and remove matrix interference. The analysis of samples containing less than 5 nM copper in undiluted seawater resulted in low detection limits (0.3 nM) being obtained when preconcentration was carried out. Other notable points to this work included the rapidity of sample processing (8 min per sample approx.), small sample volumes required (4 mL approx.) and minimal precautions for the prevention of contamination during processing.

Yamada and Suzuki [52] also investigated the use of different surfactant micelles to increase sensitivity and selectivity, when using 1,10-phenanthroline for ultra trace copper determinations (concentrations < 1 nM (20 μL sample injection)). Various surfactants were added to the 1,10-phenantroline solution in order to investigate the

effects on the chemiluminescence reaction. Increases in the chemiluminescence signal were observed in the presence of cationic surfactants, whereas anionic and non-ionic surfactants did not increase the chemiluminescence signal. It was found, in particular, that alkylammonium salt surfactants such as cetyltrimethylammonium bromide (CTAB), cetylethyldimethylammonium bromide (CEDAB) and didodecyldimethylammonium bromide (DDDAB) all greatly increased the chemiluminescence signal, depending on the hydrophobic group of the surfactant. CEDAB caused the highest enhancement of the signal. The use of surfactants were, however, found to increase the background signal as a result of impurities from the reagents used in the system. As a result, TEPA was added to mask copper as an impurity. The addition of TEPA also prevented copper from absorbing on the sample injector, which lead to decreased tailing of the signal peak and resulted in a slight increase in the signal.

Safavi and Baezzat [58] also used a chemiluminescence reaction for the determination of copper. However, this method was based on the quenching effect of copper on the chemiluminescence reaction of dichlorofluorescein (DCF) with hydrogen peroxide. For this particular reaction copper showed an inhibitory effect on the DCF and peroxide reaction. When trace amounts of copper were present the emission decreased, leading them to conclude that, the decrease in chemiluminescence intensity could be taken as an indication of the amount of copper present in the sample.

1.13.2 Summary of Other Metal Ion Chemiluminescence Determinations

There are a number of other metal ion species that can be determined using chemiluminescence detection. Table 1.6 gives a summary of some other common flow injection chemiluminescence reactions for the detection of different metal ion species.

Table 1.6: Summary of some common flow injection chemiluminescence reactions for detection of metal ion species.

CHEMILUMINESCENCE REACTION	METAL ION SPECIES	SAMPLE MATRICES	REFERENCE
Oxidation of metal-1,10-phenanthroline chelates by hydrogen peroxide at alkaline pH.	Cu (II)	Freshwater and seawater	51, 52, 53, 59
Reaction of luminol-hydrogen peroxide-metal complex.	Mn (II) Fe (III) Cu (II), Co (II), Fe (II) Cr (III), Cr (VI)	Seawater Seawater Synthetic NIST reference material, water, food samples	60, 61 62 63 64, 65
Luminol reaction with sodium chloride without hydrogen peroxide.	Mn (II)	Certified biological sample	66
Luminol oxidation by potassium periodate.	Fe (II), Mn (II) Mn (II), Co (II)	Natural water Fresh and polluted water, Vitamin B_{12}	67 68
Luminol oxidation with peroxodisulphate	Au (II)	Synthetic	69
Oxidation of gallic acid in alkaline hydrogen peroxide.	Co (II)	Seawater	41
Oxidation of pyrogallol in alkaline hydrogen peroxide.	Co (II), Fe (II), Fe (III)	Estuarine and coastal waters	70
Flavin mononucleotide-hydrogen peroxide-phosphate buffer system.	Cu (II)	Synthetic	57
Dichlorofluorescein and hydrogen peroxide at alkaline pH.	Cu (II)	Blood Sera	58
Oxidation of 7,7,8,8-tetracyanoquinodimethane (TCNQ) in alkaline solution.	Mn (II)	Seawater	71,72
Brilliant sulfoflavin and hydrogen peroxide.	Fe (II)	Seawater	73,74

1.14 Combination of Chemiluminescence Techniques with Microflow Systems

It has only been recently that chemiluminescence techniques have been employed for detection purposes while using microflow systems. A highly sensitive method of detection is required due to the low flow rates and the small sample sizes, which are characteristic of a microflow system. This is difficult to match with most other detection techniques making chemiluminescence a very suitable method for sample determinations when using a microflow system due to the sensitivity and selectivity of the reactions, especially when combined with a preconcentration or separation method (discussed in section 1.15).

A number of different μTAS systems with chemiluminescence detection have been developed by different groups for a range of different samples. Xu *et al.* [15] used a micromachined device for the quantitative detection of chromium (III) aqueous samples using chemiluminescence detection. In this case, a detection limit of approximately 10^{-7} M was achieved. Greenway *et al.* developed a micromachined flow-through device with chemiluminescence detection for the detection of codeine [75]. Greenwood *et al.* used chemiluminescence detection incorporated into a μTAS manifold for the determination of atropine and pethidine [76]. Lv *et al.* developed a chemiluminescence microfluidic system on-chip for the determination of glucose in hair serum [77], and more recently developed a method using a micro-device based on flow injection chemiluminescence for the determination of cyanide in whole blood [78].

In 1991, Manz *et al.* questioned the developments of μTAS as to whether it was a 'look into the next century's technology or just a fashionable craze' [4]. Although this is still a relatively new science, an examination of the literature shows that there has been a positive growth in research in this area, with different approaches being used to find the best solutions with regard to detection and fluid handling. Developments within the area show that the technique is forming a basis of future methodology applicable to a wide range of applications ranging

from measurement science to chemical synthesis. Chemiluminescence reactions have a wide range of applications for sensitive and selective detection, while microflow systems have the advantage of being portable, requiring low reagent consumption and can lead to new techniques, which may not be available on the larger scale. According to Greenway *et al.* [75] 'chemiluminescence is a promising method of detection for μTAS due to its sensitivity and the simplicity of the measurement technique'.

1.15 Preconcentration/Separation

Proper sample preparation and handling are essential for a successful assay. Very often the target analyte is present at a low concentration and can be in solution with a number of other constituents that can impair the analysis. As mentioned in section 1.13, certain metal ions can interfere during a chemiluminescence reaction. In the case of the copper-1,10-phenanthroline reaction, metal ions such as lead, zinc, iron (II) and (III), calcium and magnesium were all found to interfere in this chemiluminescence reaction [51,57]. Coale *et al.* used a preconcentration step to remove any negative matrix interference and were successfully able to determine trace amounts of copper (II) in complex sample matrices such as seawater [51]. The use of a preconcentration or separation technique can enhance an analysis by minimising interference effects, reducing and simplifying the sample matrix, reducing the sample and reagent consumption and improving the limit of detection. Performing this preconcentration step prior to detection minimises sample handling and time, thus increasing the efficiency of the overall analysis.

1.15.1 On-Line Versus Off-Line Preconcentration

There are typically two major methods of concentration (on-line and off-line preconcentration) [79]. In the off-line preconcentration process, the enrichment manifold is separated from the measurement instrument and all preconcentration is carried out independently of the detector. Alternatively, in on-line

preconcentration the enrichment manifold is connected to the detector and the preconcentration and measurement steps are performed on a single instrument.

Before the introduction of on-line column preconcentration, the preconcentration of trace elements by off-line batch procedures with columns or by static equilibration was used [80]. These methods were found to increase sensitivity and matrix separation, but were awkward to operate, especially when several litres of sample were required for each determination. However, the advent of on-line column preconcentration overcame this.

The use of on-line column preconcentration is more efficient than the conventional batch methods. The enrichment factors of on-line preconcentration are higher for a defined time interval and the sample consumption is reduced, usually 5-10 mL per determination for enrichment factors of 10-100 compared to several hundred millilitres for conventional batch methods. The use of a closed preconcentration system also reduces the risk of contamination for the laboratory environment. It should be noted however, that in some cases, there is only a tiny improvement in efficiency and sometimes interferences can be enhanced.

Andrew *et al.* [81] detail the necessary requirements of an on-line process (which can be achieved using FIA). These include;

- Rapid analysis and high sampling frequency.
- Robust construction in order to withstand harsh chemical matrices.
- A simple design for easy maintenance.
- Ability to perform automated analysis.
- Minimal operating costs.

1.15.2 Solid Phase Extraction Techniques

The use of solid phase extraction (SPE) techniques based on ion-exchange resins is most suited to trace metal analysis for preconcentration [82]. There are a number of advantages of SPE techniques over traditional methods. They are

simple to use, inexpensive, easily automated and very little toxic solvents are used. They can be classified into three main categories;

- Cation exchangers
- Anion exchangers
- Chelating polymeric resins

These categories can be further subdivided into: strong, weak or intermediate depending on their functional groups [83]. The use of chelating polymeric resins as the solid support is one of the most popular choices for preconcentration purposes.

1.15.3 The Chelation Exchange Sorption Mechanism

When considering ion exchange, the process is based upon the exchange of ions between two or more ionised species located in different phases, at least one of which is an ion exchanger, and no new bonds are formed [84]. However, in chelation exchange (or chelation ion exchange), a coordinate bond is formed during the exchange process, therefore a different type of sorption mechanism is involved. There are two important differences between ion exchange and chelation exchange that should be noted;

1. In ion exchange, the alkali metal ions, although having a weaker affinity for the ion exchange site than a polyvalent ion, will have a major competitive effect as the concentration of the alkali metal increases. In chelation exchange, the alkali metal ions form such weak coordinate bonds that they can be neglected in comparison to the polyvalent metal ion coordinate bond, resulting in the effect of the alkali metal concentration being small.
2. In ion exchange, competition from hydrogen ions is less significant than in chelation exchange, and does not become significant until the pH is quite low. However, in chelation exchange, the hydrogen ion concentration will have a major effect on the formation of the polyvalent

metal complex, because most chelating ligands are conjugate bases of weak acidic groups and therefore have a strong affinity for hydrogen ions.

Most chelating agents are weak acids that ionise in water (the ionisable proton is displaced by the metal ion when the chelate is formed). Chelating polymers usually contain polyfunctional groups. Functional groups containing oxygen are considered hard, sulphur groups are termed soft and nitrogen groups have an intermediate character. The insertion of suitable functional groups into the polymeric matrix makes it capable of reacting with metal ions or metal species under certain conditions to form chelate rings.

The chelating functional group (Lewis base) donates one or more electron pairs to the metal ion (Lewis acid) with the formation of a coordinate bond, which can be ionic or covalent, depending on the electron availability and charge of the ion and chelating agent [32]. When a ligand binds to a metal to form a complex through only one atom, it is termed a monodentate ligand, while a ligand which bonds through more than one atom is said to be a multidentate or chelate ligand (from the Greek *chēlē*, meaning claw). Retention of metal ions on chelating substrates is dependent upon the conditional stability constants of the metal ion and the immobilised ligand, which are governed by the nature of the immobilised ligand, namely the number position and type of coordinates sites. The chelating resin can work in one of three different ways [85];

1. Ion exchange due to free or protonated chelating groups.
2. Complexation reactions in the stationary phase.
3. Complexation in the eluent can occur (less common).

1.15.4 Chelation Exchange for Preconcentration Purposes

Chelating agents form complexes with the metal ions within certain pH ranges. The metal complexes are retained on the support material at certain pH values, separating them from the sample matrix; therefore impurities are not retained and pass through the column. A suitable eluent is then selected to remove the metal ions from the chelating sites on the resin. This can be achieved by varying the

pH. Selectivity can be controlled by the different complexes formed as a result of the different stabilities of individual metals, due to size, valence, oxidation state etc.

The process of chelation exchange is illustrated in the following example, whereby the exchange reaction of the M^{n+} metal ion on an nH^+ acid-type resin can be considered [42]. The selectivity coefficient is given by K_S.

$$M^{n+}_{(aq)} + nH^+_{(resin)} \leftrightarrow M^{n+}_{(resin)} + H^+_{(aq)}$$

$$K_S = \frac{[M^{n+}_{(resin)}][H^+_{(aq)}]}{[M^{n+}_{(aq)}][H^+_{(resin)}]^n} \qquad \text{(Equation 1.9)}$$

Some of the chelating resins used in the past for preconcentration or separation of metal ions were quite inefficient [86]. Effective resins are dependent on the following physiochemical properties;

- Particle size and physical structure of the resin (including porosity, swelling, mechanical resistance).
- Chelating capacity.
- Selectivity and kinetics of chelating groups.

Table 1.7 gives some examples of the commonly used chemically bonded resins for the separation of metal ions in samples

Table 1.7: Commonly used chemically bonded resins for separation of metal ions in samples.

Chemically Bonded Resins	**Metals of Interest**	**Eluent**	**Application**	**Ref**
Iminodiacetate based resins	Cd, Co, Cu, Mn, Pb	2M HNO_3	Seawater, river water	[87]
	Mg, Ca, Sr, Ba	3mM EDA, 4mM citric acid	Alkali/alkaline earth metal-rich matrices e.g. seawater	[88]
	Pb, Cu, Ca, Ni, U, Cr, Mn, Al, Co, Ga, In, Zn, V, Tl, Bi, Ag, Sn	1.5M HNO_3, 2M ammonium acetate	River, estuarine, seawater	[89]
			Tap water	[90]
	Cu, Cd, Ni, Ca	1M HCl		
Quinolin-8-ol based resins	Cu, Zn, Cd, Mn, Ni	0.1M HNO_3	Synthetic seawater	[91]
Dithiocarbamate based resins	Cu	1M HCl	Seawater, biological samples	[92]
	Ca, Cu, Pb	MeOH (EtOH + MIBK used for comparison)	Coal fly ash, calcareous loam soil, lake sediment, riverine, estuarine sediment	[93]
Aminophosphonic based resins	Cu, Mn, Co, Zn, Ni, Pb, Cd	1M KNO_3	Transition and heavy metal analysis in water samples	[94]
	Pb, Cu, Cd, Zn	0.1mM $HClO_4$		[95]
Other chelating resins:				
Synthetic zeolites	Cu	MIBK	Drinking water	[96]
Nitrilotriacetate	Co, Ni, Cu, Zn, No, Cd, Sb, Pb, U	0.5mM HNO_3	Seawater	[97]
2-mercaptoethylamine	Au, Pt, Ag, Pd, Hg, Fe, Cu, Zn, Cd, Ni, Co	0.5M KCl		[98]

1.16 References

1. A. Manz, J.C.T. Eijkel, *Pure Appl. Chem.*, 73 (10) (2001) 1555-1561.
2. N. Graber, H. Lüdi, H.M. Widmer, *Sens. Actuators B1* (1990) 239-243.
3. A. Manz, N. Graber, H.M. Widmer, *Sens. Actuators B1* (1990) 244-248.
4. A. Manz, J.C. Fettinger, E. Verpoorte, H. Lüdi, H.M. Widmer, D.J. Harrison, *TrAC Trends in Anal. Chem.* 10 (5) (1991) 144-149.
5. J.C.T. Eijkel, A.J. de Mello, A. Manz. "A miniaturised total chemical analysis system: μ-TAS", in *Organic Mesoscopic Chemistry*, IUPAC Monograph, H. Masuhara and F.C. Schryver (Eds.), pp. 185-219 (1999).
6. J.P. Kutter, *TrAC Trends in Anal. Chem.*, 19 (6) 2000, 352-363.
7. J. Kuncova, *Lab-on-a-chip* 2000, Tampere University of Technology, Finland, viewed 27 October 2003 <http://www.ad.tut.fi/aci/courses/76527/Seminars2000/Lab-on-a-chip.pdf>
8. J. Růžička, E.H. Hansen, Flow Injection Analysis, Chemical Analysis Volume 62, John Wiley & Sons, Inc., 1981.
9. *Global FIA /Tutorial 1* 2003, Global FIA Inc., PO Box 480, Fox Island, WA, 98333, viewed 03 February 2004 <http://www.globalfia.com/tutorial1.html>
10. J. Růžička, E.H. Hansen, *Anal. Chim. Acta*, 99 (1978) 37-76.
11. J. Cooper McDonald, D.C. Duffy, J.R. Anderson, D.T. Chiu, H. Wu, O.J.A. Schueller, G.M. Whitesides, *Electrophoresis*, 21 (2000) 27-40.
12. P.A. Greenwood, G.M. Greenway, *TrAC Trends in Anal. Chem.*, 21 (11) (2002) 726-740.
13. N.A. Polson, M.A. Hayes, *Anal. Chem.*, 73 (2001) 313A-319A.
14. L.E. Locascio, *Anal. Bioanal. Chem.*, 379 (2004) 325-327.
15. Y. Xu, F.G. Bessoth, J.C.T. Eijkel, A. Manz, *Analyst*, 125 (2000) 677-683.
16. *Reynolds Number on Encyclopedia.com* 2005, Colombia Encyclopedia Sixth Edition, viewed 15 October 2003 <http://www.encyclopedia.com/html/r/rynldsnum.asp>
17. R. Tijssen, *Anal. Chim. Acta*, 114 (1980) 71-89.

18. Oxford Dictionary of Chemistry New Edition, Oxford University Press 1996.
19. D.R. Reyes, D. Iossifidis, P.A. Auroux, A. Manz, *Anal. Chem.*, 74 (2002) 2626-2636.
20. J.M. Berg, R. Anderson, M. Anaya, B. Lahlouh, M. Holtz, T. Dallas, *Sens. Actuators A*, 104 (2003) 6-10.
21. B. Graß, G. Weber, A. Neyer, M. Schilling, R. Hergenröder, *Spectrochim. Acta Part B.* 57 (2002) 1575-1583.
22. H. Becker, C. Gārtner, *Electrophoresis*, 21 (2000) 12-26.
23. H. Becker, L.E. Locascio, *Talanta*, 56 (2002) 267-287.
24. Z. Chen, Y. Gao, R. Su, C. Li, J. Lin, *Electrophoresis*, 24 (2003) 3246-3252.
25. J.C. Lötters, W. Olthuis, P.H. Veltink, P. Bergveld, *J. Micromech. Microeng.* 7 (1997) 145-147.
26. *A Guide to Polycarbonate in General* 2005, PTSLLC, 2315 Southpark Drive, Murfreesboro, TN 37128, viewed 27 May 2005 <http://www.ptsllc.com/polcarb_intro.htm>
27. A. De Mello, *Lab on a chip*, 2 (2002) 31N-36N.
28. M.A. Roberts, J.S. Rossier, P. Bercier, H. Girault, *Anal. Chem.*, 69 (1997) 2035-2042.
29. L. Martynova, L. Locascio, M. Gaitan, G.W. Kramer, R.G. Christensen, W.A. MacCrehan, *Anal. Chem.*, 69 (1997) 4783-4789.
30. K. Uchiyama, H. Nakajima, T. Hobo, *Anal. Bioanal. Chem.*, 379 (2004) 375-382.
31. M.A. Schwarz, P.C. Hauser, *Lab on a chip*, 1 (2001) 1-6.
32. D. Harris, Quantitative Chemical Analysis, Freeman, 5th Edition.
33. R. Carlson, S.W. Lewis, K.F. Lim, *Chemeda: Aust. J. Chem. Ed.,* 14 (1999) 51-53.
34. A.K. Campbell, Chemiluminescence: Principles and Applications in Biology and Medicine, Ellis Horwood Ltd.
35. K. Robards, P. J. Worsfold, *Anal. Chim. Acta*, 266 (1992) 147-173.
36. Y. Fuster Mestre, L. Lahuerta Zamora, J. Martinez Calatayud, *Luminescence*, 16 (2001) 213-235.

37. A.M. García-Campaña, W.R.G. Baeyens, L. Cuadros-Rodríguez, F. Alés Barrero, J.M. Bosque-Sendra, L. Gámiz-Gracia, *Current Organic Chemistry*, 6 (2002) 1-20.
38. *Liquid Phase Chemiluminescence* 2002, Sam Houston State University, Huntsville, Texas, viewed 11 March 2002 <http://www.shsu.edu/~chm_tgc/chemilumdir/liquid.html>
39. D. Skoog, J. Leary, Principles of Instrumental Analysis, Saunders College Publishing, 4th Edition.
40. E. Seale, *Diode* 2003, viewed 14 March 2005 <http://encyclobeamia.solarbotics.net/articles/diode.html>
41. C.M. Sakamoto-Arnold, K.S. Johnson, *Anal. Chem.*, 59 (1987) 1789-1794.
42. D. Burrell, Atomic Spectrometric analysis of heavy metal pollutants in water (4th Edition) 1980 Ann Arbour Science Publishers Inc.
43. *ATSDR – ToxFAQs: Copper* 2003, ATSDR, Division of Toxicity, 1600 Clifton Road NE, Atlanta, GA 30333, viewed 03 May 2003 <http://www.atsdr.cdc.gov/tfacts132.html>
44. *EPA Ground Water & Drinking Water > Consumer Factsheet on: Copper* 2002, Environmental Protection Agency, Ariel Rios Building 1200 Pennsylvania Avenue, N.W. Washington, DC 20460, viewed 28 July 2003 <http://www.epa.gov/safewater/dwh/c-ioc/copper.html>
45. *Galzin - Introduction* 2004, Wilson's Disease Association, 4 Navaho Drive, Brookfield, CT 06804, viewed 15 November 2004 <http://www.gatepharma.com/Galzin/physiciansguide.html>
46. *Copper* 2005, Spectrum Laboratories INC., Ft. Lauderdale, FL, Babson Park, FL & Savannah, GA USA, viewed 11 February 2005 <http://www.speclab.com/elements/copper.htm>
47. *Europa – Environment – Water quality in the EU – Drinking Water* 2003, Gateway to the European Union, Jacques Delors European Information Centre, 1400-026 Lisbon, Portugal, viewed 18 November 2004 http://europa.eu.int/comm/environment/water/water-drink/index_en.html>
48. *Food Safety Authority of Ireland - RDAs for Ireland* 2003, Food Safety Authority Ireland, Dublin, Ireland, viewed 11 May 2003

<http://193.120.54.7/publications/reports/recommended_dietary_allowances_Ireland_1999.pdf>

49. K.W.Bruland, R.P. Franks, G.A. Knauer, J.H. Martin, *Anal. Chim. Acta*, 105 (1979) 233-245.
50. E.A. Boyle, J.M. Edmond, *Anal. Chim. Acta*, 91 (1977) 189-197.
51. K.H. Coale, K.S. Johnson, P.M. Stout, C.M. Sakamoto, *Anal. Chim. Acta*, 266 (1992) 345-351.
52. M. Yamada, S. Suzuki, *Anal. Lett.*, 17 (1984) 251-263.
53. H. Zamzow, K.H. Coale, K.S. Johnson, C.M. Sakamoto, *Anal. Chim. Acta*, 377 (1998) 133-144.
54. O.S. Fedorova, S.E. Olkin, V.M. Berdnikov, *Zeit. Phys. Chemie (Leipzig)*, 263 (1982) 529-549.
55. M. Ishii, M. Yamada, S. Suzuki, *Bunseki Kagaku*, 35 (1986) 373-378.
56. W. Sunda, S. Huntsman, *Mar. Chem.*, 36 (1991) 137-163.
57. M. Yamada, S. Suzuki, *Chem. Lett.*, (1982) 1747-1748.
58. A. Safavi, M.R. Baezzat, *Anal. Lett.*, 33 (2000) 667-675.
59. E.P. Achterberg, C.B. Braungardt, R.C. Sandford, P.J. Worsfold, *Anal. Chim. Acta*, 440 (2001) 27-36.
60. E. Nakayama, K. Isshiki, Y. Sohrin, H. Karatani, *Anal. Chem.*, 61 (1989) 1392-1396.
61. K. Okamura, T. Gamo, H. Obata, E. Nakayama, H. Karatani, Y. Nozaki, *Anal. Chim. Acta*, 377 (1998) 125-131.
62. H. Obata, H. Karatani, E. Nakayama, *Anal. Chem.*, 65 (1993) 1524-1528.
63. B. Yan, P.J. Worsfold, *Anal. Chim. Acta*, 236 (1990) 287-292.
64. B. Gammelgaard, Y. Liao, O. Jøns, *Anal. Chim. Acta*, 354 (1997) 107-113.
65. R. Escobar, Q. Lin, A. Guiraúm, F.F. de la Rosa, *Analyst*, 118 (1993) 643-647.
66. A. Gaikwad, M. Silva, D. Pérez-Bendito, *Anal. Chim. Acta*, 302 (1995) 275-282.
67. Y. Zhou, G. Zhu, *Talanta*, 44 (1997) 2041-2049.
68. Q. Lin, A. Guiraúm, R. Escobar, F.F. de la Rosa, *Anal. Chim. Acta*, 283 (1993) 379-385.
69. P. Jones, H.G. Beere, *Anal. Pro. Inc. Anal.*, 32 (1995) 169-171.

70. V. Cannizzaro, A. R. Bowie, A. Sax, E.P. Achterberg, P.J. Worsfold, *Analyst*, 125 (2000) 51-57.
71. M. Yamada, S. Kamiyama, S. Suzuki, *Chem. Lett.*, (1985) 1597-1600.
72. T.P. Chapin, K.S. Johnson, K.H. Coale, *Anal. Chim. Acta*, 249 (1991) 469-478.
73. V.A. Elrod, K.S. Johnson, K.H. Coale, *Anal. Chem.*, 63 (1991) 893-898.
74. S. Hirata, H. Yoshihara, M. Aihara, *Talanta*, 49 (1999) 1059-1067.
75. G.M. Greenway, L.J. Nelstrop, S.N. Port, *Anal. Chim. Acta*, 405 (2000) 43-50.
76. P.A. Greenwood, C. Merrin, T. McCreedy, G.M. Greenway, *Talanta*, 56 (2002) 539-545.
77. Y. Lv, Z. Zhang, F. Chen, *Talanta*, 59 (2003) 571-576.
78. J. Lv, Z. Zang, J. Li, L. Luo, *Forensic Science International*, 148 (2005) 15-19.
79. V. Porta, C. Sarzanini, O. Abollino, E. Mentasti, E. Carlini, *JAAS*, 7 (1992) 19-22.
80. Z. Fang, S. Xu, S. Zhang, *Anal. Chim. Acta,* 200 (1987) 35-49.
81. K.N. Andrew, N.J. Blundell, D. Price, P.J. Worsfold, *Anal. Chem.*, 66 (18) (1994) 917A-921A.
82. B.S. Garg, R.K. Sharma, N. Bhojak, S. Mittal, *Microchem. Journal*, 61 (1999) 94-114.
83. C. Kantipuly, S. Katragadda, A. Chow, H.D. Gesser, *Talanta*, 37 (1990) 491-517.
84. O. Keil, J. Dahmen, D. Volmer, *Fresenius J. Anal. Chem*, 364 (1999) 694-699.
85. C. Sarzanini, E. Mentasti, *J. Chrom. A*, 789 (1997) 301-321.
86. J.S. Fritz, R.C. Freeze, M.J. Thornton, D.T. Gjerde, *J. Chrom. A.*, 739 (1996) 57-61.
87. R.A. Nickson, S.J. Hill, P.J. Worsfold, *Anal. Chim. Acta*, 351 (1997) 311-317.
88. G. Bonn, S. Reiffenstuhl, P. Jandik, *J. Chromatogr.*, 499 (1990) 669-676.
89. M. Nicolaï, C. Rosin, N. Tousset, Y. Nicolai, *Talanta*, 50 (1999) 433-444.
90. P. Hashemi, Å. Olin, *Talanta*, 44 (1997) 1037-1053.

91. G.M. Greenway, S.M. Nelms, I. Skhosana, S.J.L. Dolman, *Spectrochim. Acta B.*, 51 (1996) 1909-1915.
92. S.L.C. Ferreira, V.A. Lemos, B.C. Moreira, A.C. Spinola Costa, R.E. Santelli, *Anal. Chim. Acta*, 403 (2000) 259-264.
93. R. Ma, W. Van Mol, F. Adams, *Anal. Chim. Acta*, 285 (1994) 33-43.
94. P.N. Nesterenko, M.J. Shaw, S.J. Hill, P. Jones, *Microchemical Journal*, 62 (1999) 58-69.
95. P.N. Nesterenko, O.S. Zhukova, O.A. Shpigun, P. Jones, *J. Chrom. A*, 813 (1998) 47-53.
96. Y. Petit de Peña, W. López, J. Burguera, M. Burguera, M. Gallignani, R. Brunetto, P. Carrero, C. Rondon, F. Imbert, *Anal. Chim. Acta,* 403 (2000) 249-258.
97. H. Kumagai, M. Yamanaka, T. Sakai, T. Yokoyama, T.M. Suzuki, T. Suzuki, *JAAS*, 13 (1998) 579-582.
98. M.J. Chen, C.Y. Liu, *J. Chin. Chem. Soc.*, 46 (1999) 833-840.

CHAPTER TWO

FLOW INJECTION ANALYSIS WITH CHEMILUMINESCENCE DETECTION FOR DETERMINATION OF COPPER (II)

2.1 INTRODUCTION

Copper (II) is an important element for the metabolism of many living organisms, but, as with many other metals, at high concentrations it can be toxic. Copper (II) compounds are commonly used in agriculture, for preservatives and for water treatment. The World Health Organisation (WHO) and the European Water Quality Directive have specified that drinking water should not contain more than 2.0 mg L^{-1} of copper (II) [1], with levels above this producing astringent tastes.

The use of chemiluminescence reactions for the determination of dissolved trace metals has become a popular choice over recent years, requiring only simple and inexpensive instrumentation for detection purposes. Chemiluminescence detection can offer high sensitivity for many target species, as low light levels can be easily monitored with little background noise. The type of chemiluminescence reaction and the design of the different components of the detector instrumentation both significantly influence the sensitivity of a chemiluminescence method. Highly sensitive chemiluminescence reactions can also be selective for particular species, and are often used in a flow system where they can result in low limits of detection, high precision and fast sample throughput [2]. The low limits of detection result from the fact that no light source is required within the system, which reduces or suppresses Raman and Rayleigh scattering and other sources of background light [3].

Copper (II) can be determined sensitively using chemiluminescence detection. As discussed in the introduction in chapter 1, a number of different chemiluminescent methods have been proposed for the determination of copper (II) in different sample matrices. Yamada and Suzuki determined trace amounts of copper (II) using a chemiluminescence reaction based on a flavin mononucleotide-hydrogen peroxide-phosphate buffer system [4]. A second method developed by Yan and Worsfold determined copper (II) by its catalytic effect upon the reaction between luminol (5-amino-2,3-dihydrophtalazine-1,4-dione) and hydrogen peroxide [5]. More recently, a method based on the quenching effect of copper (II) on the chemiluminescence reaction of dichlorofluorescein with hydrogen peroxide was developed by Safavi and Baezzat, and subsequently used for the determination of copper (II) in blood samples [6]. Some other copper (II) determinations have included an additional pre-treatment

step prior to detection to improve selectivity. One such example, described by Coale and co-workers, used a micro-column of immobilised 8-hydroxyquinoline (8-HQ) for analyte preconcentration and for the removal of matrix interferences in seawater samples [7].

One well-known chemiluminescence reaction is based on the formation of a complex between copper (II) and 1,10-phenanthroline [7-9]. This reaction is popular due to its sensitivity and selectivity for copper (II). The chemiluminescence reaction, which emits between 445 – 450 nm, involves the reaction of copper (II) in the sample with 1,10-phenanthroline, and the subsequent release of photons from the oxidative destruction of the copper-1,10-phenanthroline complex by hydrogen peroxide at an alkaline pH. This reaction is highly pH dependant and requires a strongly alkaline environment for maximum sensitivity. The optimal reaction pH has been determined to be between 9.8 and 10.1 [7]. The excited products of the reaction decay to their ground state, emitting light, which is then detected by a photomultiplier tube (PMT) in order to quantify the amount of copper (II) present in the sample as previously discussed in chapter 1.

In the following chapter, a flow system developed for the monitoring of copper (II) in water samples, which was adapted from the procedure used by Yamada and Suzuki [9], is discussed. A flow injection analysis system coupled with chemiluminescence detection (FIA-CL) is presented here to determine ultra trace amounts of copper (II) by means of the 1,10-phenanthroline-hydrogen peroxide-sodium hydroxide system containing a cationic surfactant, cetyltrimethylammonium bromide (CTAB). This reaction is noteworthy for its high sensitivity and small sample volumes required for analysis.

In the method presented in this chapter, the use of a copper (II) selective itaconic acid (methylenesuccinic acid) modified polymeric micro-column in combination with the 1,10-phenanthroline reaction allowed the determination of copper (II) even more selectively than the 1,10-phenanthroline chemiluminescence reaction on its own. The unique selectivity of the itaconic acid mini-column allowed the separation of copper (II) from high concentrations of alkali and alkaline earth metals and resulted in a sensitive and selective analytical technique. Experimental conditions

including reagent concentrations have been optimised and the system has been applied to trace copper (II) determinations in a complex sample matrix.

2.2 EXPERIMENTAL

2.2.1 Flow Injection Analysis System

Initial work in this study took place using standard flow injection analysis instrumentation in order to optimise the chemistry of the system. The copper (II) catalysed oxidation of 1,10-phenanthroline was carried out using the reaction manifold configuration illustrated schematically in Figure 2.1. A variable speed, 10 roller model peristaltic pump (Gilson Minipuls 312, Villiers, France) was employed to deliver the sample and the reagents through 0.8 mm I.D. poly(ether ether ketone) (PEEK) tubing, from Alltech Associates Applied Science Ltd. (Lancashire, England) at a combined total flow rate of 2.1 mL min^{-1} (each individual line was 0.7 mL min^{-1}). The actual peristaltic tubing was standard PVC tubing, which was suitable for all the reagents. The pump was regularly calibrated to ensure accurate and reproducible flow rates. Care was taken not to over tighten the pump tubing, which would reduce its lifetime. The peristaltic tubing was directly attached to the PEEK manifold tubing. Chemically inert PEEK tubing and fittings were used throughout the rest of the system minimising metal contamination and resisting acid degradation. The tubing was non-transparent, thus reducing the amount of stray light entering the system, as transparent tubing can act as a light guide.

A six-port manual rotary injection valve, Rheodyne model 7125, (Rheodyne, Cotati, CA, USA) fitted with a 120 μL PEEK injection loop was used for the introduction of a well-defined sample plug volume and a 8.0 x 3.0 mm polymer PRP-X800 itaconic acid micro-column (particle size 12-20 μm) (Hamilton Company, Reno, Nevada, USA) was incorporated into the manifold to allow the separation of ultra trace amounts of copper (II) from high concentrations of alkali and alkaline earth metals which may be present in the sample matrix. The light intensity was continuously measured by a photomultiplier tube (PMT), which was obtained from Hamamatsu photonics (HC135-01 series with R1924 bi-alkali tube, measuring over the range 300

nm to 650 nm). The PMT was approximately 135 mm in height and the window of the detector was 25.4 mm inner diameter, with an effective area of 21 mm. The warm up time was approximately 180 seconds. This PMT used a + 5 volt power supply, which was connected to the detector and a cable connected the PMT directly to the PC, through the serial port. The PMT operated in photon counting mode and was used to process the PMT signal. Signals were then recorded on a computer and the data was processed using Microsoft Excel.

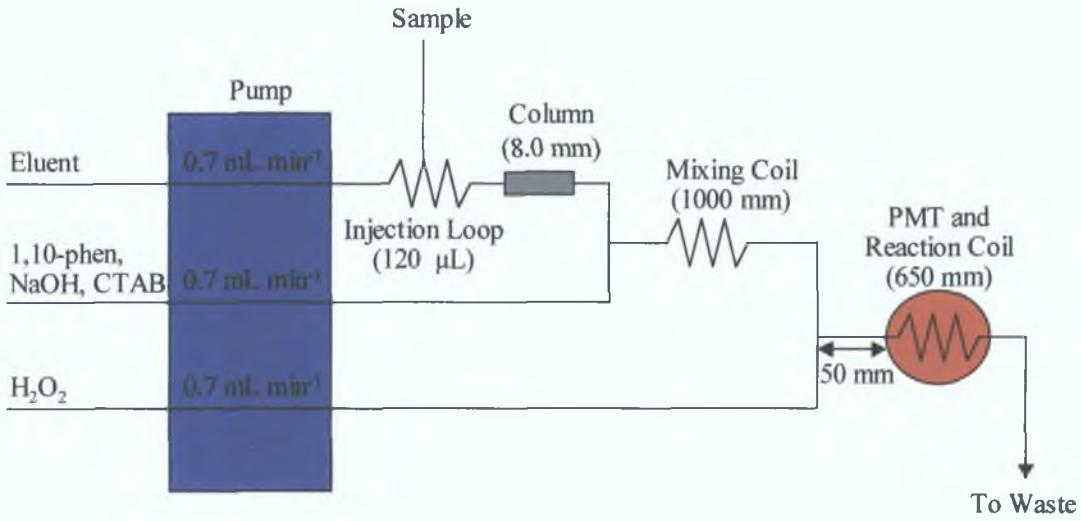

Figure 2.1: Schematic diagram of the reaction manifold used for the determination of copper (II) by flow injection analysis. This manifold employed the use of a 120 µL injection loop, a total flow rate of 2.1 mL min^{-1} and a 0.8 mm itaconic acid micro column of itaconic acid as described in the text.

A 120 µL sample volume was injected into the flowing carrier stream and merged with the 1,10-phenanthroline solution at a T-piece merging connection. Following this, the sample and 1,10-phenanthroline were mixed together in a 1,000 mm mixing coil of PEEK tubing prior to meeting with the hydrogen peroxide solution through a second T-piece connector. All of the flow rates were kept identical to ensure reproducible mixing at the T-piece connector.

The length of tubing between the second T-piece, where the sample and reagent streams merge, and the flow cell, where the chemiluminescence emission occurs, was kept as short as physically possible (approximately 50 mm, 0.72 s residence time) to ensure a rapid passage of solutions into the reaction cell, as the

chemiluminescence reaction occurred almost instantaneously. It was also kept short in order to minimise sample dispersion. The flow cell itself consisted of 650 mm x 0.6 mm I.D. transparent, flexible polyethylene (PE) tubing which was tightly spiralled in a coil to a diameter of 25.4 mm on the adhesive surface of a piece of adhesive tape. The total volume of this cell was 184 μL. Here, the mixed sample and reagents flowed from the centre of the flow cell to the outside. This cell was secured to the front of the PMT using strong black plastic insulating tape, so that the spiral flow cell faced the PMT window. The insulating tape also helped to keep ambient light away from the end window of the PMT. The PMT and detection cell were enclosed in a light tight box, in order to exclude all ambient light. They were also wrapped several times in aluminium foil to further reduce the dark count rate. Due to the nature of the analytical method, it was imperative to ensure high precision and accuracy, therefore the flow manifold was regularly acid cleaned with 10 % nitric acid solution and rinsed with Milli-Q water to minimise any sample carry over and contamination within the system.

2.2.2 Itaconic Acid Micro-Column

Itaconic acid (methylene succinic acid) is a dicarboxylic acid capable of acting as a weak cation exchanger and/or a strong chelating ion exchanger. The unique selectivity of itaconic acid allows the separation of copper (II) from high concentrations of alkali and alkaline earth metals [10]. A polystyrene divinylbenzene (PS-DVB) support functionalised with itaconic acid was used for the separation of copper (II) from complex sample matrices. The structure of the itaconic acid resin is shown here in Figure 2.2, where R is the polymer to which the itaconic acid is attached.

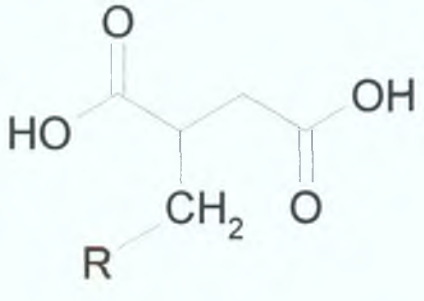

Figure 2.2: Structure of itaconic acid resin, where R is the polymer to which itaconic acid is attached.

The 8.0 x 3.0 mm PRP-X800 itaconic acid functionalised resin micro column (particle size 12-20 μm) used in the system is shown here in Figure 2.3. The column itself was housed inside the barrel along with a ceramic porous frit. The barrel material was PEEK with dimensions 11.2 mm in length by 6.3 mm O.D. The backpressure from the column was sufficiently low so it did not affect the performance of the peristaltic pumps used.

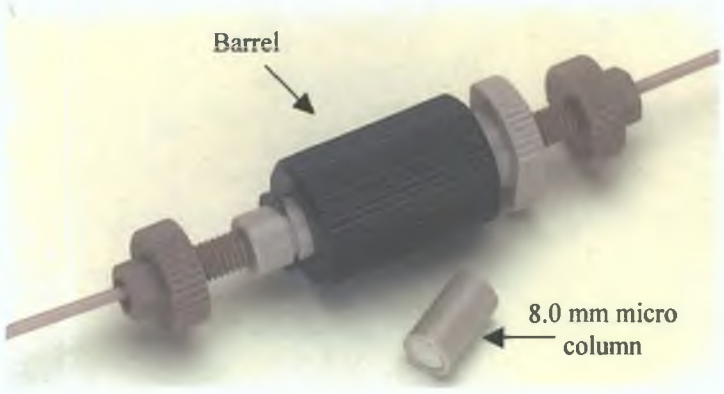

Figure 2.3: 8.0 x 3.0 mm PRP-X800 itaconic acid micro-column used in the FIA-CL system for separation purposes.

2.2.3 Reagent / Sample Preparation

In this study, all reagents were of analytical reagent grade and were used as is unless stated otherwise. All solutions were prepared with ultrapure 18 MΩ water obtained from a Milli-Q Plus system (Millipore, Milford, MA). All the solutions were degassed using sonication to ensure reagent dissolution and homogeneity. They were also all filtered through a 0.45 μm nylon membrane filter from Gelman Laboratories (Michigan, USA) prior to use. Normal precautions for trace metal analysis were taken including acid washing of all glassware and plastic containers to remove contamination.

The reagent conditions used in this work were similar to that used by Yamada and Suzuki for the determination of copper (II) in samples using the 1,10-phenanthroline chemiluminescence reaction [9]. The following reagents were prepared:

Reagent 1: An eluent of 100 mM nitric acid solution (69 % w/v, BDH Laboratory Supplies, Poole, England) was prepared and used as the sample carrier solution.

Reagent 2: A chemiluminescence reagent containing 0.06 mM 1,10-phenanthroline (BDH Laboratory Supplies, Poole, England) made from a 12 mM stock solution, 0.10 mM surfactant cetyltrimethylammonium bromide (CTAB) (obtained from BDH Laboratory Supplies, Poole, England) and 0.075 M sodium hydroxide (Sigma Aldrich Ltd., Dublin, Ireland). This solution was prepared using Milli-Q water and was made up fresh each day. The 12 mM stock solution of 1,10-phenanthroline was found to be stable for several days and was initially purified, prior to use, by recrystalisation using nitric acid (69 % w/v, BDH Laboratory Supplies, Poole, England). Two other surfactants used in a surfactant study in place of the CTAB in the 1,10-phenanthroline solution were Triton X-100 (Sigma Aldrich Ltd., Dublin, Ireland) and sodium dodecyl sulphate (SDS), (Sigma Aldrich Ltd., Dublin, Ireland).

Reagent 3: An oxidising agent of 5 % w/v hydrogen peroxide solution was made up from a 27.5 % w/v hydrogen peroxide solution in Milli-Q water (Sigma Aldrich Ltd., Dublin, Ireland). This was prepared freshly each day as the reagent was unstable over time which would lead to a decrease in the overall sensitivity of the analysis.

A 1 mg L^{-1} secondary copper (II) standard was made up daily in Milli-Q from a 1,000 mg L^{-1} copper atomic absorption spectroscopy standard solution stored in 1 % nitric acid (Sigma Aldrich Ltd., Dublin, Ireland). All copper (II) standard solutions were prepared freshly each day from the secondary stock solutions. Calcium chloride (obtained from Sigma Aldrich Ltd., Dublin, Ireland) and magnesium chloride (Sigma Aldrich Ltd., Dublin, Ireland) were used to make up a complex sample matrix to investigate the selectivity. Other metals used for interference studies included zinc (II), manganese (II), lead (II), nickel (II), cadmium (II) and cobalt (II). All of these were atomic absorption spectroscopy standard solutions stored in 1 % nitric acid and were obtained from Sigma Aldrich Ltd., Dublin, Ireland.

To ensure high accuracy and precision in the preparation and delivery of the reagents and samples, high precision variable volume micropipettes (Transferpette, 10 – 50 μL and 100 – 1000 μL) with plastic pipette tips were used throughout the work. They were regularly recalibrated using an analytical balance (Sartorius CP124S). Fresh pipette tips were used for each analysis, with each tip being kept exclusively for each solution. All pH measurements were performed with a Thermo Orion pH meter, Model 420, calibrated in the pH 4 – 7 or pH 7 – 10 ranges using standard buffer solutions (Sigma Aldrich Ltd., Dublin, Ireland) as required.

2.3 Results and Discussion

2.3.1 Design of a Detection Flow Cell and Mixing System

One of the most important components of a chemiluminescence system is the reaction cell/detection cell, as this regulates the amount of light that reaches the detector as well as the duration and the magnitude of the signal. It serves to retain the solution in view of the detector whilst it is emitting light most intensely, consequently care should be taken to ensure that the cell maximises the amount of emission that will be detected. In a small cell the number of emitted photons is small, but in a large cell a dilution effect can be produced.

A number of workers have investigated different assemblies and detection cells, in order to improve overall sensitivity of a chemiluminescence method. Work by Chung *et al.* proposed to mix the reagents in the same detection cell when a quick reaction was being studied [11]. A different method by De Jong *et al.* proposed the use of an integrating sphere in which the detection cell was placed. The internal reflective surface of the sphere directed radiation to the detector, which was attached to the sphere through a hole in the side [12]. Whichever flow cell is decided upon, it is important to note that poor resulting signals when using a flow injection analysis system can occur due to non-ideal connections between the injector and detector, as well as poor T-piece connections, abrupt changes in internal diameters or slowness of injection, detection or recording, making care in the design of the flow manifold critical [13].

2.3.2 Optimisation Studies

Using the flow manifold described previously in section 2.2.1, the reaction conditions were optimised and the interference effects of a complex sample matrix was also investigated. It is important in any analysis that the element of interest is measured under the best conditions. If this does not take place, it can result in unnecessarily poor measurement precision and can also result in reduced sensitivity. High reagent concentrations can increase the chemiluminescence emission, but can also cause an increase in the background emission. Also, self-quenching of light may occur at higher reagent concentrations. As a result, a series of experiments were carried out to determine the influence of reaction variables affecting the chemiluminescence signal for copper (II) and the following three reaction variables were optimised;

1. The concentration of hydrogen peroxide.
2. The concentration of 1,10-phenanthroline.
3. The concentration of surfactant.

The starting point for this optimisation was taken from the previously reported manifold by Yamada and Suzuki, for the determination of copper (II) in samples using the 1,10-phenanthroline chemiluminescence reaction [9]. For all of the optimisation studies in this section a 250 $\mu g\ L^{-1}$ copper (II) standard was used and the concentration of sodium hydroxide was kept constant at 0.075 M, to control the alkaline pH to between pH 9.8 and 10.1, which was required for efficient chemiluminescence to occur. Direct injection (without the use of the itaconic acid column) was used for this optimisation in order to keep the procedure as simple as possible. The flow rates used for each line was 0.7 mL min^{-1} resulting in a total flow rate of 2.1 mL min^{-1} using the flow system described in the previous section (section 2.2.1). The monitored parameter was the chemiluminescence peak height, which was recorded by the PMT as a function of time, and the emission intensity was proportional to the copper (II) concentration in the sample.

Each of the variables were individually optimised to investigate its effect on the system. In order to do this, a single variable was varied while the other parameters were all kept constant. Generally, the concentrations of the reagents were kept to a minimum to reduce the background chemiluminescence, while still maintaining adequate sensitivity and stability. To further simplify the system, and hence the subsequent optimisation of the system, the use of a complexing agent such as tetraethylenepentamine (TEPA) was not included [14]. In similar work by Sunda *et al.*, the heating of the reagents to 40 ^{o}C was reported, to accelerate the production of the superoxide radical from the hydrogen peroxide solution and to increase the activity of the mixed reagents. However, to simplify the system in this chapter, this was not carried out. Instead the 1,000 mm mixing coil was deemed satisfactory for mixing the reagents.

2.3.2.1 Effect of Hydrogen Peroxide Concentration

The concentrations of 1,10-phenanthroline, surfactant CTAB and sodium hydroxide were kept constant at 0.06 mM, 0.10 mM and 0.075 M respectively, while the concentration of hydrogen peroxide was varied. A 5 % hydrogen peroxide solution resulted in a higher analytical signal for a 250 μg L^{-1} copper (II) standard than a 10 % hydrogen peroxide solution, with little difference in background noise, even though in some of the literature a 10 % hydrogen peroxide solution was deemed to be more suitable [8]. The actual signal to noise ratio for the 5 % hydrogen peroxide was 13.2 compared to 8.4 for the 10 % peroxide solution (see Figure 2.4). The hydrogen peroxide solution was prepared daily to avoid a decrease in sensitivity that resulted from reagent instability over time. There were no significant reductions in detector response when using a single hydrogen peroxide solution for a period of 12 hours. The optimal reaction pH was determined by Coale and co-workers to be between pH 9.8 and pH 10.1 [7]. In this work, the reaction pH for copper (II) analysis was sometimes as high as 10.3, but this did not affect the overall sensitivity of the analysis.

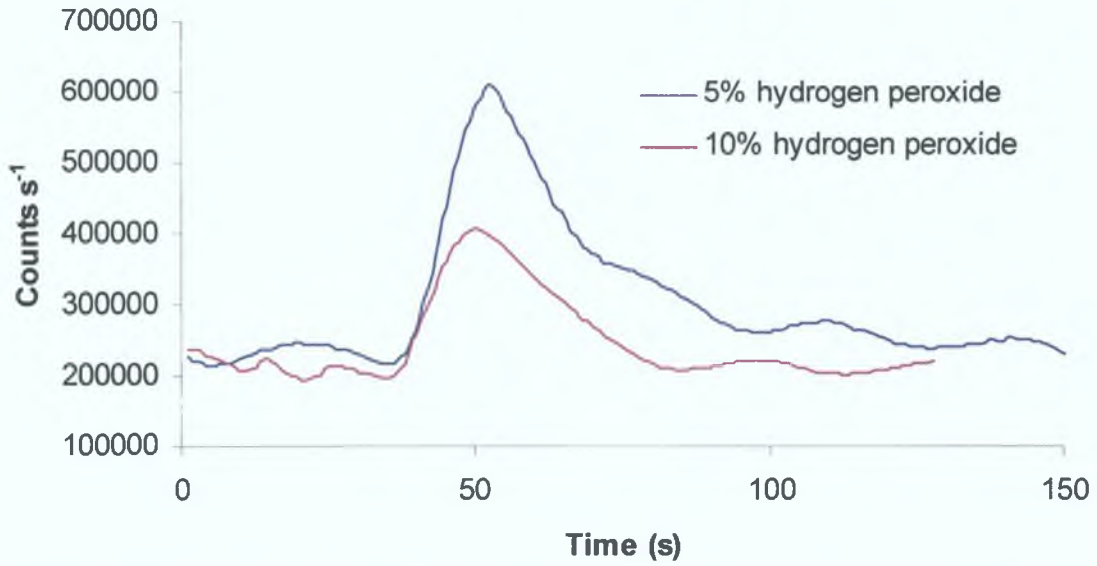

Figure 2.4: Comparison of signals produced for a 5 % and 10 % hydrogen peroxide solution using a 250 μg L^{-1} copper (II) standard. Reagent conditions: 0.06 mM 1,10-phenanthroline, 0.1 mM CTAB, 0.075 M NaOH.

2.3.2.2 Effect of 1,10-Phenanthroline Concentration

Work by Federova *et al.* [15] reported that the concentration of the 2,2'-dipyridyl-3,3'-dicarboxylic acid at the end of the reaction was the same as the concentration of 1,10-phenanthroline at the start of the reaction. They found that the chemiluminescence emission was proportional to the concentration of the 1,10-phenanthroline and the chemiluminescence intensity corresponded to the rate of decay of 1,10-phenanthroline. Therefore, the concentration of 1,10-phenanthroline determines the overall intensity of the chemiluminescence emission with respect to time, showing its important role in the chemiluminescence reaction.

Using the optimised peroxide concentration of 5 % hydrogen peroxide, the concentration of 1,10-phenanthroline (non-purified) was optimised. The concentrations of CTAB and sodium hydroxide again remained constant at 0.10 mM and 0.075 M respectively and a 250 μg L^{-1} copper (II) standard was used. It was found that high 1,10-phenanthroline concentrations increased the chemiluminescence emission, but also caused an increase in the background emission. The 0.03 mM 1,10-phenanthroline solution significantly reduced the background noise from approximately 200,000 counts s^{-1} to 30,000 counts s^{-1} as can be seen in Figure 2.5.

The signal to noise ratio for the 0.03 mM 1,10-phenanthroline solution was 27.6 compared to 8.9 for the 0.06 mM 1,10-phenanthroline solution.

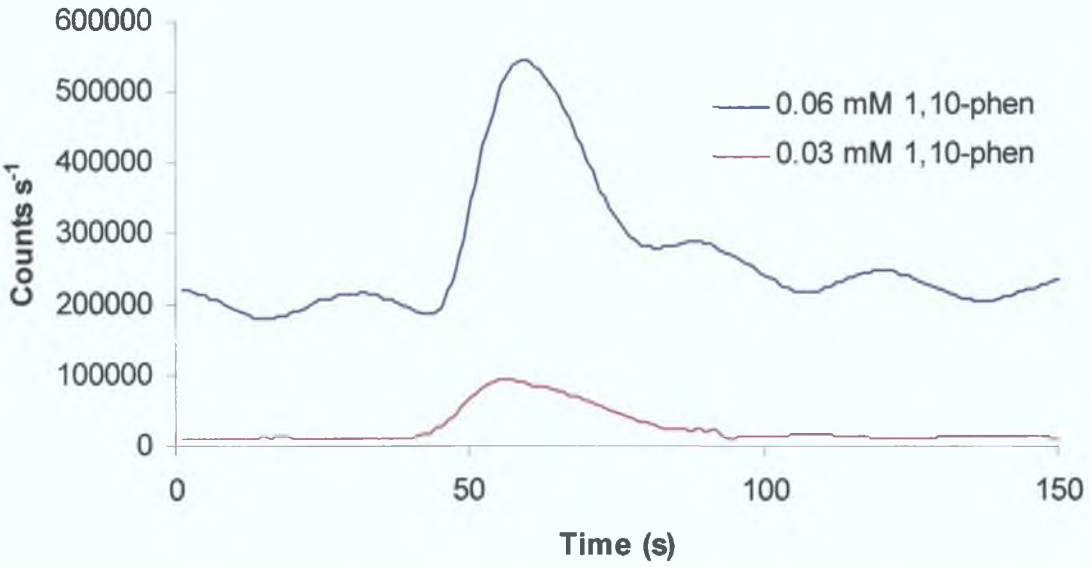

Figure 2.5: Comparison of 1,10-phenanthroline concentration using a 250 μg L^{-1} copper (II) standard. Reagent conditions: 0.1 mM CTAB, 0.075 M NaOH, 5 % H_2O_2.

A comparison of 'purified' 1,10-phenanthroline (purified by re-crystallisation with nitric acid) and 'non-purified' 1,10-phenanthroline is shown in Figure 2.6. The concentrations of 1,10-phenanthroline, CTAB and sodium hydroxide all remained constant at 0.03 mM, 0.1 mM and 0.075 M respectively. In this work a 20 μL sample loop (instead of the 120 μL loop used previously) was used for the introduction of a 1 mg L^{-1} copper (II) standard. A stopped-flow system, rather than a continuous flow system was used in this study. It can be seen that the copper (II) signal was enhanced considerably when the purified 1,10-phenanathroline was used. It was decided to use the purified 1,10-phenanthroline in all the future work.

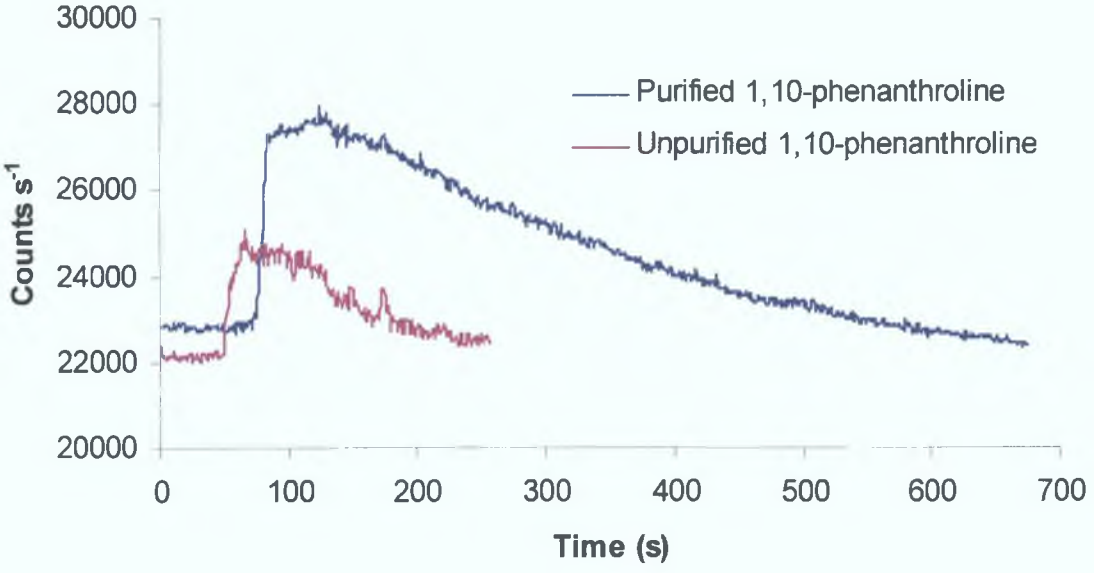

Figure 2.6: Comparison of purified and non-purified 1,10-phenanthroline using a stopped flow system for 1 mg L^{-1} copper (II) standard. Reagent conditions: 0.03 mM 1,10-phenanthroline, 0.1 mM CTAB, 0.075 M NaOH and 5 % H_2O_2.

2.3.2.3 Effect of Surfactant Nature and Concentration

Previous work by Yamada and Suzuki [4] investigated the effect of different surfactants on the chemiluminescence reaction of copper (II) and 1,10-phenanthroline. Micelles, which are formed as a result of the addition of a surfactant, often change the luminescent characteristics and result in a greatly improved analytical performance by enhancing the chemiluminescence quantum yields and can also result in an increase in the sensitivity and/or selectivity. Investigations of chemiluminescence reactions in surfactant media have shown that the enhanced chemiluminescence could arise due to the following [16-17]:

1. Solubilisation: the reactants and excited intermediates, which may be insoluble, become more soluble in a micellar medium.
2. Electrostatic effect: the electrostatic effect of the surfactant helps to concentrate the counter ion reactant.
3. Altering the environment of the chemiluminescence reaction: the cage structure of the micelle is helpful for stabilising the excited state and prevents it from quenching.

4. Altering the pH of the environment: as mentioned previously the pH is an important parameter for most chemiluminescence reactions.

These properties are advantageous in the analytical use of chemiluminescence because the possibility of enhancing quantum efficiency or energy transfer efficiency is increased. As well as this, the use of certain reagents, which may be insoluble in water can be permitted, and the overall selectivity of the reaction is improved.

In the 1,10-phenanthroline chemiluminescence reaction, the uncharged non-ionic species of 1,10-phenanthroline migrates to the micellar surface and the anionic superoxide radical is also attracted to the positively charged micellar surface and the active chemiluminescence species are brought close together [9,18]. The formation of dioxetane, the electronically excited chemiluminescence emitter is promoted, which enhances the efficiency of the chemiluminescence reaction. It was found by Yamada and Suzuki [9] that an increase in signal resulted from the addition of a cationic surfactant, while anionic and non-ionic surfactants had no significant effect.

In this section of work, three different surfactants were added to the 1,10-phenanthroline solution in order to investigate their effects on the overall efficiency of the chemiluminescence reaction. These surfactants included Triton X-100, sodium dodecylsulphate (SDS) and CTAB. The structures of these surfactants are shown in Figure 2.7.

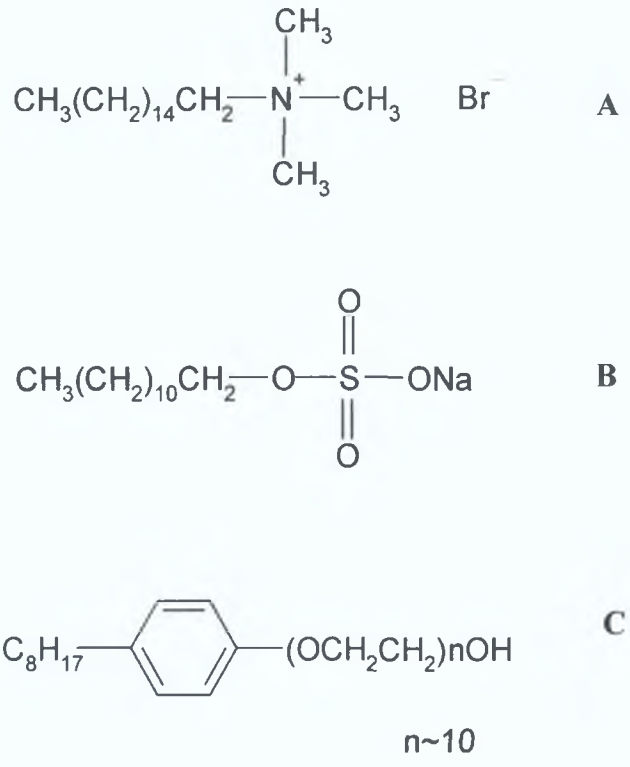

Figure 2.7: Structures of CTAB (A), SDS (B) and Triton X-100 (C).

The optimised hydrogen peroxide and 1,10-phenanthroline conditions of 5 % and 0.03 mM respectively, and a copper (II) concentration of 10 μg L^{-1} were used in this work and the concentration of each surfactant was kept constant at a concentration of 0.05 mM. It was found that Triton X-100 (non-ionic: no net charge) and SDS (anionic: negative charge) did not increase the signal. The addition of the cationic surfactant CTAB (carrying a positive charge) was found to dramatically increase the chemiluminescence signal and also reduce some of the background noise in this work (Figure 2.8). This corresponds well with the work carried out by Yamada and Suzuki [9] on the effect of different surfactants.

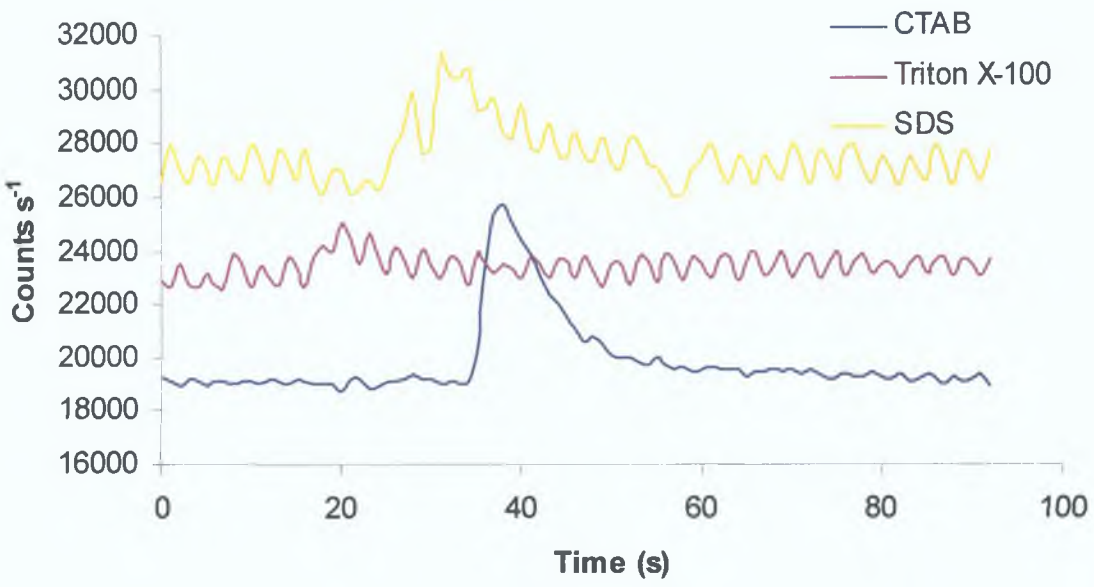

Figure 2.8: Comparison of the effect of three different surfactants CTAB, Triton X-100 and SDS on 10 μg L^{-1} copper (II) standard. Reagent conditions: 0.03 mM 1,10-phenanthroline, 0.05 mM surfactant, 0.075 M NaOH, 5 % H_2O_2.

The most effective surfactant in this case was found to be CTAB and this was used as the surfactant in all future work. Different concentrations of CTAB were investigated and it was found that a concentration of 0.05 mM CTAB reduced the noise without compromising the copper (II) signal (Figure 2.9). The signal to noise ratios for 0.05 mM and 0.10 mM CTAB were 19.9 and 6.3 respectively.

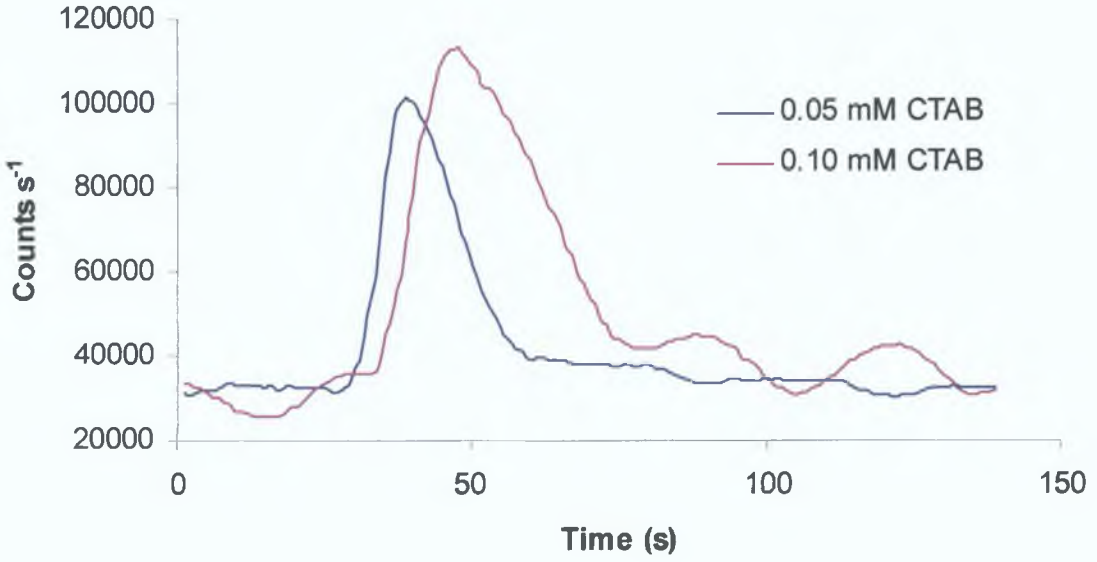

Figure 2.9: Comparison of CTAB concentration using a 250 μg L^{-1} copper (II) standard. Reagent conditions: 0.03 mM 1,10-phenanthroline, 0.075 M NaOH, 5 % H_2O_2.

Based upon this series of optimisation experiments, the optimum concentration of hydrogen peroxide was taken to be 5 % hydrogen peroxide. The optimum 1,10-phenanthroline concentration was 0.03 mM and the CTAB concentration, which was added to enhance chemiluminescence signal was chosen to be 0.05 mM. For all further work in this chapter, these optimum concentrations were used.

2.3.3 Background Chemiluminescence Emission and Baseline Noise

The mixing of reagent solutions through the manifold also generated a background emission, which remained stable throughout the analyses. The baseline noise was considerably reduced when Milli-Q water only was passed through the flow cell, due to the absence of the chemiluminescence reagents, showing that the reagents contributed to most of the background noise in the system. Optimisation of all the reagents resulted in reduced background chemiluminescence emission and baseline noise due to the reagent flow.

An increase in chemiluminescence emission with air temperature may occur due to the release of thermally generated electrons from the photocathode, which consequently increase the dark count current [19]. The emission or dark count rate doubles with every 4 to 6 ^{o}C. Cooling the PMT can reduce this, but was not investigated here as when the reagent conditions were optimised and the experiments were performed in a relatively stable room temperature environment (~ 22 ^{o}C), it was found there was no need to cool the PMT. Occasionally, some small air bubbles were noted in the waste line downstream of the detection cell, which were probably the by-products of the chemiluminescence reaction. These were not cause for concern and the reagents upstream of the flow cell were maintained by a smooth continuous flow.

2.3.4 Linearity Studies

Using the optimised conditions, determined in section 2.3.2, linearity studies were carried out. Once again, direct injection (without the itaconic acid column) was used for simplicity. The resultant peaks detected by the PMT during the copper (II)

calibration study are shown below in Figure 2.10. Three replicate injections (n = 3) were made for each copper (II) standard over the range 1 μg L^{-1} to 50 μg L^{-1}.

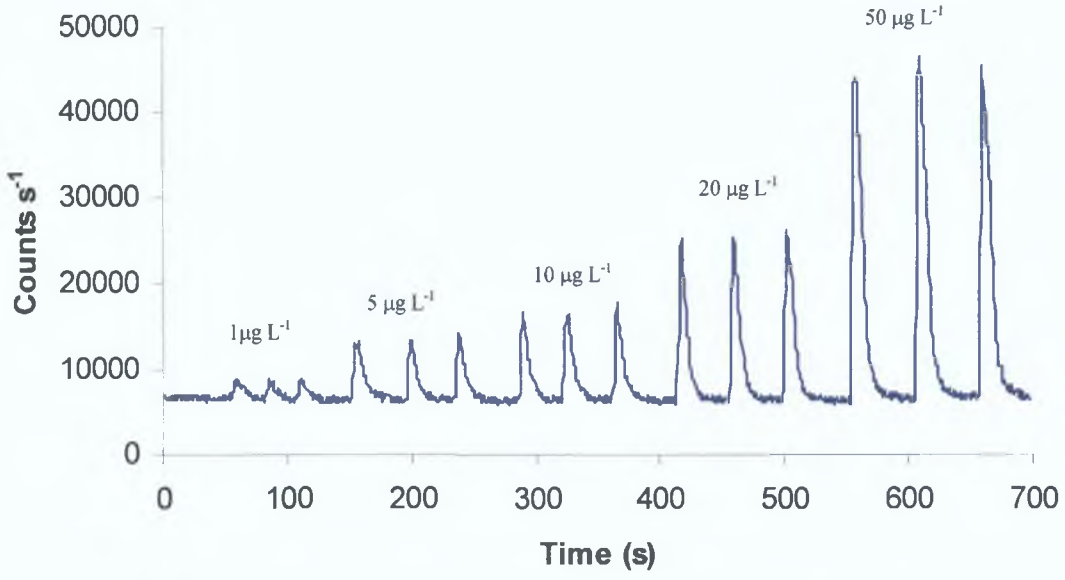

Figure 2.10: Linearity studies of copper (II) over the range of 1 to 50 μg L^{-1} (n = 3) using optimised reagent conditions of 5 % w/v H_2O_2, 0.03 mM 1,10-phenanthroline, 0.05 mM CTAB and 0.075 M NaOH.

A calibration graph of the chemiluminescence intensity (counts s^{-1}) versus the copper (II) concentration (μg L^{-1}) was obtained. The results were found to be linear over the concentration range 1 to 50 μg L^{-1} of copper (II) producing an excellent correlation coefficient, R^2 value of 0.9946 and it was found that copper (II) could be easily determined at levels as low as 1 μg L^{-1} (Figure 2.11) illustrating the high sensitivity of this technique. As three replicate injections were made for each copper standard, the error associated with each was calculated by the difference between the highest and lowest value for each standard. It was found that the difference was calculated to be < 4.8 %, which was deemed acceptable for these results.

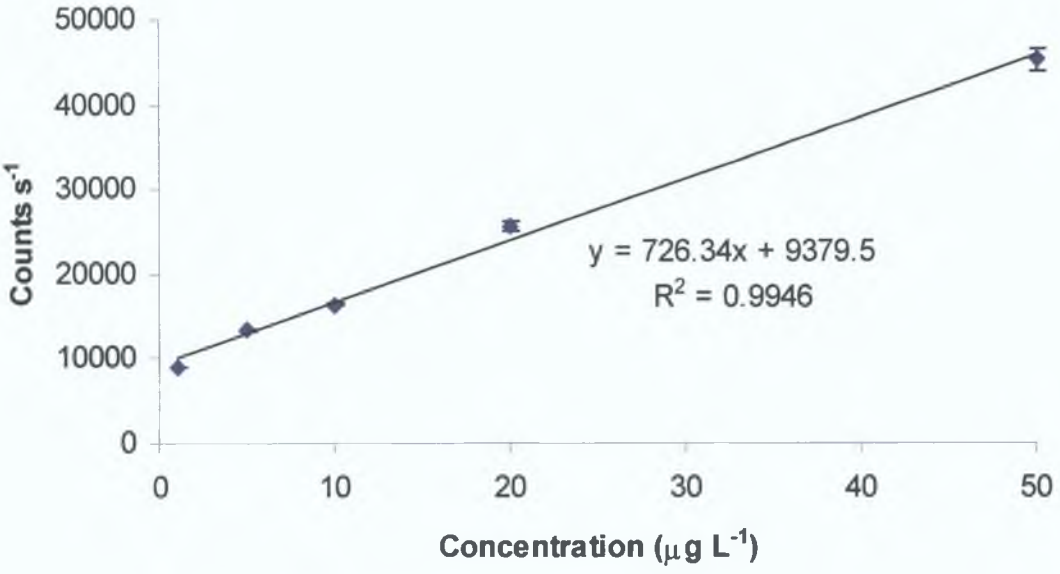

Figure 2.11: Copper (II) linearity studies (n = 3) over the concentration range 1 to 50 µg L^{-1}.

2.3.5 Selectivity Studies

Many chemiluminescence reactions are unselective with respect to the metal ions that catalyse them. However, as previous work has shown, the 1,10-phenanthroline chemiluminescence reaction for copper (II) is quite selective, with little or no response to excess concentrations (>10 mg L^{-1}) of alkali metals or chromium (III) and chromium (VI), manganese (II), nickel (II), cobalt (II), cadmium (II), lead (II), aluminium (II), iron (II) and iron (III) [9]. However, it has been reported that high concentrations of zinc (II), calcium (II) and magnesium (II) can cause minor interference at the above concentration. In order to verify this, a study of potential interferences was carried out to determine the tolerance for a range of metal ions.

A range of metals were investigated up to a concentration of 100 mg L^{-1} in order to investigate the enhancement or quenching effect of these metal ions on the 1,10-phenanthroline chemiluminescence reaction. Metal solutions for this study were prepared from 1,000 mg L^{-1} atomic absorption spectroscopy standard solutions stored in 1 % nitric acid. Various amounts of the potential interferences ranging from 6.25 mg L^{-1} to 100 mg L^{-1} were investigated. The experimental parameters used were the same as those derived by the simple optimisation described previously.

A total of eight metal ions were investigated here. These were injected over a range of concentrations to evaluate their effect on the chemiluminescence signal for a copper (II) standard. The signal due to the copper (II) standard only was considered to be 100 % and the effect of each metal was investigated and related to this figure. Table 2.1 shows the effect of metals over the concentration range of 6.25 mg L^{-1} to 100 mg L^{-1}, which were compared with that for the copper (II) standard only. As can be seen manganese (II), nickel (II), cadmium (II) and cobalt (II) showed little response over this concentration range, while some response was seen for calcium (II), magnesium (II), zinc (II) and lead (II) at these concentrations.

Table 2.1: Responses of a range of metals to the 1,10-phenanathroline chemiluminescence reaction.

Metal	Signal Intensity (0 mg L^{-1})	Signal Intensity (6.25 mg L^{-1})	Signal Intensity (12.5 mg L^{-1})	Signal Intensity (25 mg L^{-1})	Signal Intensity (50 mg L^{-1})	Signal Intensity (100 mg L^{-1})
Ca (II)	100	111	113	116	118	121
Mg (II)	100	98	99	100	111	141
Zn (II)	100	103	105	102	116	133
Mn (II)	100	98	99	101	100	102
Pb (II)	100	105	108	102	112	118
Ni (II)	100	97	99	101	102	99
Cd (II)	100	102	101	102	104	103
Co (II)	100	99	99	101	100	101

Generally, complex sample matrices such as seawater and brines can be difficult to process and analyse, causing problems with sensitivity, detection limits, accuracy and precision during an analysis, resulting in a need for preconcentration or separation of the analyte of interest. To further increase the selectivity of the developing method, a copper (II) selective PRP-X800 itaconic acid micro-column was investigated for separation purposes.

Itaconic acid contains two weak carboxylic acid groups (pKa_1 = 3.85, pKa_2 = 5.45) and is capable of acting as a weak cation exchanger and/or a strong chelating ion exchanger. The unusual selectivity of itaconic acid is due to the two carboxylate groups, which can selectively complex certain metal ions. Carboxylic acids can work as chelating ligands and retention occurs due to the coordination of the metal ion with two oxygen donator atoms. Chelating stationary phases containing carboxylic acid functional groups can be used for the determination of trace metal ions in complex sample matrices such as seawater, due to their strong preference for

complexing transition metals over alkali and alkaline earth metals. Previous work carried out on the itaconic acid stationary phase showed a strong selectivity towards copper (II) [10]. The stationary phase selectivity was determined for a number of ions and was found to increase in the order shown here:

$Li<Na<NH_4<K<Cs<Mg(II)<Ca(II)\leq Sr(II)<Mn(II)\leq Ba(II)<Cd(II)<Zn(II)<Co(II)$
$<<Pb(II)<<Cu(II)$

This unique selectivity of itaconic acid allows the separation of copper (II) from high concentrations of alkali and alkaline earth metals, and also lesser retained transition metals such as zinc (II), manganese (II) and cadmium (II).

In this work, copper (II) standards over the concentration range 1 μg L^{-1} to 1 mg L^{-1} were made up in a sample matrix containing 10 mg L^{-1} calcium (II) and 10 mg L^{-1} magnesium (II). The same flow system was used as described in section 2.2.1 with the exception of the PEEK sample loop, which was changed from 120 μL to 100 μL and the itaconic acid column was incorporated into the system between the sample injector and the first mixing T-piece. The reagent concentrations used were 5 % w/v hydrogen peroxide, 0.03 mM 1,10-phenanathroline, 0.05 mM CTAB and 0.075 M sodium hydroxide.

Prior to the analysis, the effect of pH on the retention of copper (II) by the itaconic acid column was investigated over the range of pH 3.0 to pH 5.0. At low pH values the itaconic acid is fully protonated and no metal complexes are formed. As the pH increases, dissociation of the itaconic acid begins to occur, as the dissociation constant $pKa_1 = 3.85$, therefore chelation can take place (complete dissociation of itaconic acid occurs at higher pH values as the second dissociation constant is $pKa_2 = 5.45$). It was found that at pH 4.0 there was complete retention of all the copper (II) by the column. An acetate buffer was used for this purpose. At this pH the calcium, magnesium and sodium ions present in the sample matrix were not retained by the column. This allows for the separation of trace quantities of copper (II) from complex sample matrices such as seawater samples.

2.3.6 Retention of Copper (II) on Micro-Column in the Presence of Excess Calcium (II) and Magnesium (II)

The effect of a number of different trace metal ions on the chemiluminescence reaction has already been looked at. In this section, the interference problems generated by a complex sample matrix are investigated. In order to apply the 1,10-phenanthroline chemiluminescence reaction for the determination of copper (II) in seawater or other complex matrices, it is necessary to introduce a preconcentration or matrix removal step because of the low concentrations of copper (II) in seawater, and because of the interference from the major matrix cations, calcium (II) and magnesium (II). Quantitative methods for the determination of elements at very low concentrations require satisfactory levels of accuracy and sensitivity, without contamination of the sample occurring, therefore care must be taken when choosing a technique for preconcentration purposes.

This study investigated the effect of calcium (II) and magnesium (II) present in excess with respect to copper (II) (present in trace quantities). After the optimum buffering pH was obtained, the analysis took place. A range of copper (II) standards from 1 to 1,000 μg L^{-1} were made up in a sample matrix of 10 mg L^{-1} calcium (II) and magnesium (II). Figure 2.12 shows the resultant peaks detected by the PMT for the copper (II) standards, which were separated from the complex sample matrix, of 10 mg L^{-1} calcium (II) and magnesium (II), by the PRP-X800 itaconic acid column. This was done by passing the copper (II) sample in the complex matrix through a buffered (pH 4.0) itaconic acid column. At this pH all of the copper (II) in the sample was retained by the column while the calcium (II) and magnesium (II) were unretained. A blank sample and Milli-Q water were also analysed. The analytical blank for a calibration is defined as the signal generated by a solution containing none of the added analyte of interest, but containing all of the other sample reagents, in this case 10 mg L^{-1} calcium and magnesium.

A 100 mM nitric acid eluent was then used to remove the copper (II) from the column. Care must be taken when using a strong acid solution for eluting metals from columns as it can be difficult to control the final reaction pH for the optimum

generation of chemiluminescence. In this case 100 mM nitric acid was deemed satisfactory and did not significantly interfere with the chemiluminescence reaction. The copper (II) was detected by the PMT as a result of the chemiluminescence reaction between the copper (II) and 1,10-phenanthroline. The signals produced for 1 mg L^{-1} and for 100 μg L^{-1} copper (II), were in excess of 280,000 counts s^{-1} and 195,000 counts s^{-1} respectively.

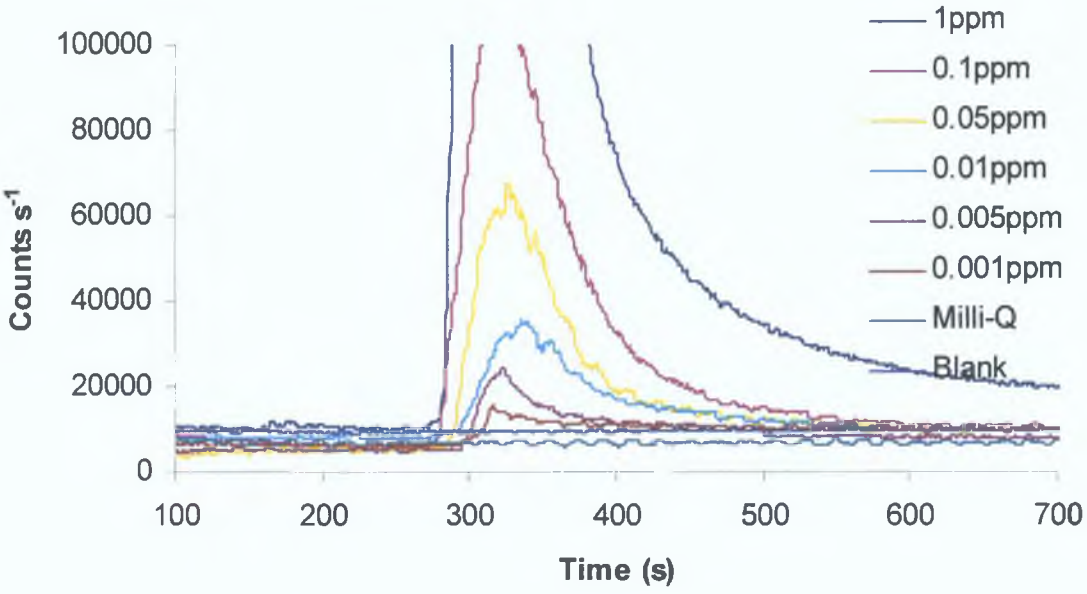

Figure 2.12: Resultant peaks generated for copper (II) standards over the concentration range of 1 μg L^{-1} to 1 mg L^{-1}, separated from sample matrix of 10 mg L^{-1} magnesium and 10 mg L^{-1} calcium using the PRP-X800 itaconic acid column. Reagent conditions: 0.03 mM 1,10-phenanthroline, 0.05 mM CTAB, 0.075 M NaOH, 5 % H_2O_2.

The results obtained for the copper (II) standards made up in a 10 mg L^{-1} calcium (II) and magnesium (II) matrix were similar to those obtained for copper (II) standards made up in Milli-Q water over the same concentration range of 1 μg L^{-1} to 1 mg L^{-1} (Figure 2.13), showing there was 100 % separation and recovery of the copper (II) from the sample matrix. This shows how the itaconic acid column could be used to increase the selectivity of the flow injection chemiluminescence manifold and selectively retain copper (II), removing the possible interference effects from sample matrices containing high levels of calcium and magnesium. From Figure 2.13 it is also interesting to note that Milli-Q water itself gave a small response equivalent to < 1 μg L^{-1} copper (II) when analysed directly, which was eliminated after treatment with the micro-column. This would indicate that some potentially interfering species

(other than copper (II)) in the Milli-Q water itself was causing a slight positive signal within the blank.

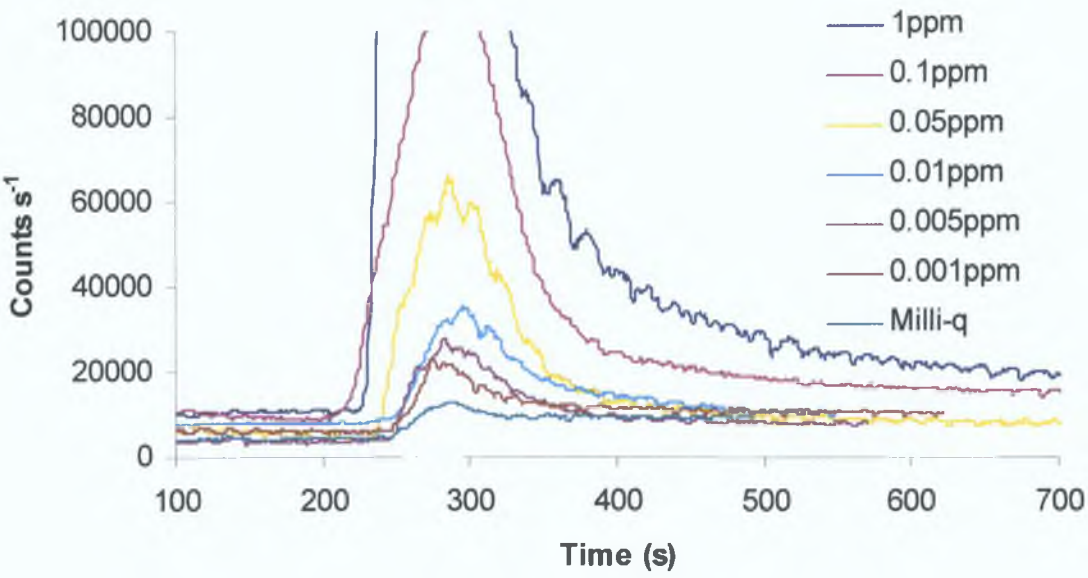

Figure 2.13: Resultant peaks generated for copper (II) standards in Milli-Q water over the concentration range of 1 μg L^{-1} to 1 mg L^{-1}. Reagent conditions: 0.03 mM 1,10-phenanthroline, 0.05 mM CTAB, 0.075 M NaOH, 5 % H_2O_2.

Table 2.2 compares the peak heights (counts s^{-1}) obtained for each of the standards analysed. It shows there was little difference between the results obtained for the copper (II) standards made up in a 10 mg L^{-1} calcium (II) and magnesium (II) matrix (when passed through the itaconic acid column to remove matrix effects) and those obtained for the copper (II) standards made up in Milli-Q water, verifying that the itaconic acid column could be successfully used for the separation and recovery of copper (II) from a complex sample matrix. Ideally, higher concentrations of calcium (II) and magnesium (II) should have been investigated during the course of this work to ensure copper (II) could be separated from a larger excess of metal ions e.g. >100 mg L^{-1} calcium (II) and magnesium (II), but due to time constraints this was not carried out.

Concentration ($\mu g\ L^{-1}$)	Peak Height of Signal-Blank (in Ca(II) and Mg(II) matrix)	Peak Height of Signal-Blank (in Milli-Q water)
0	0	0
1	5,456	4,834
5	10,164	11,396
10	18,368	20,792
50	50,496	54,278
100	96,256	100,580
1000	249,548	256,144

Table 2.2: Comparison of peak heights obtained for copper (II) standards in calcium (II) and magnesium (II) matrix and copper (II) standards made in Milli-Q water.

2.4 CONCLUSION

This chapter has described the successful setup and development of a flow system designed for trace copper (II) determinations using chemiluminescence detection. The chemiluminescence reaction based on the copper (II) catalysed oxidation of 1,10-phenanthroline by hydrogen peroxide has been thoroughly investigated for detection purposes. A complete total analysis system (TAS) was developed based on a peristaltic pump, preconcentration/separation column, reaction coils and detection flow cell, and a photomultiplier tube. Data collection and interpretation of results were computer controlled using a laptop computer.

To summarise, these preliminary results show that by using this flow system with micellar enhanced chemiluminescence detection, a reproducible system could be used for the sensitive and selective determination of copper (II) in samples. Sufficient selectivity was achieved by removal of the interferences by the incorporation of the mini-chelating column of itaconic acid (on-line) and copper (II) could be easily determined at concentrations as low as 1 $\mu g\ L^{-1}$ in a complex sample matrix of calcium (II) and magnesium (II). In conjunction with its simplicity and rapidity, it could be concluded that copper (II) could be separated and preconcentrated from a range of complex sample matrices very successfully using this method.

2.5 REFERENCES

1. *Europa – Environment – Water quality in the EU – Drinking Water* 2003, Gateway to the European Union, Jacques Delors European Information Centre, 1400-026 Lisbon, Portugal, viewed 18 November 2004 <http://europa.eu.int/comm/environment/water/water-drink/index_en.html>
2. C. M. Sakamoto-Arnold, K.S. Johnson, *Anal. Chem.*, 59 (1987) 1789-1794.
3. Y. Fuster Mestre, L. Lahuerta Zamora, J. Martinez Calatayud, *Luminescence*, 16 (2001) 213-235.
4. M. Yamada, S. Suzuki, *Chem. Lett.*, (1982) 1747-1748.
5. B. Yan, P.J. Worsfold, *Anal. Chim. Acta*, 236 (1990) 287-292.
6. A. Safavi, M.R. Baezzat, *Anal. Lett.*, 33 (2000) 667-675.
7. K.H. Coale, K.S. Johnson, P.M. Stout, C.M. Sakamoto, *Anal. Chim. Acta*, 266 (1992) 345-351.
8. H. Zamzow, K.H. Coale, K.S. Johnson, C.M. Sakamoto, *Anal. Chim. Acta*, 377 (1998) 133-144.
9. M. Yamada, S. Suzuki, *Anal. Lett.*, 17 (1984) 251-263.
10. W. Bashir, E. Tyrrell, O. Feeney, B. Paull, *J. Chrom. A.*, 964 (2002) 113-122.
11. H.K. Chung, H.S. Bellamy, P.K. Dasgupta, *Talanta*, 39 (1992) 593-598.
12. G.J. de Jong, N. Lammers, F.J. Spruit, C. Dewaele, M. Verzele, *Anal. Chem.*, 59 (1987) 1458-1461.
13. R. Tijssen, *Anal. Chim. Acta*, 114 (1980) 71-89.
14. W. Sunda, S. Huntsman, *Mar. Chem.*, 36 (1991) 137-163.
15. O.S. Fedorova, S.E. Olkin, V.M. Berdnikov, *Zeit. Phys. Chemie (Leipzig)*, 263 (1982) 529-549.
16. Z. Cao, C. Lau, J. Lu, *Analyst*, 129 (2004) 1262-1266.
17. E. Pelizzetti, E. Pramauro, *Anal. Chim. Acta*, 169 (1985) 1 – 29.
18. A.R. Bowie, P.R. Fielden, R.D. Lowe, R. D. Snook, *Analyst*, 120 (1995) 2119-2127.
19. Users Manual for HC135-01 Bi-Alkai and HC135-02 Multi-Alkali Detectors, Hamamatsu Photonics.

CHAPTER THREE

MICROFLUIDIC STUDIES WITH CHEMILUMINESCENCE DETECTION

3.1 INTRODUCTION

In keeping with modern trends to miniaturise common laboratory devices, techniques and approaches, much work has taken place within the area of micro-fabricated fluidic devices. This approach seeks to integrate different operational units of an analytical process into a micro-fabricated device, which offers considerable practical potential in a chemical analysis. These microflow devices offer a number of advantages over conventionally sized systems such as increased portability and compact size, which in turn leads to a reduction in sample and reagent consumption and waste generation, and therefore drastically reduces the overall manufacturing and operating costs [1-3].

The use of chemiluminescence is a promising method of detection for microfluidic analytical systems due to its high sensitivity and the simplicity of the measurement technique. The low reagent consumption associated with microfluidic systems is an advantage when using chemiluminescence detection as the reactions are irreversible whilst in conventional flow systems there is a high consumption of reagents and large amounts of waste is produced. Micro-systems also improve efficiency with respect to response times and sample and data throughput. In addition to this, some studies are more difficult to carry out in larger devices, therefore smaller systems are preferential. The combination of chemiluminescence detection and microfluidic systems is proving to be very successful, although to date only a small number of different chemical and biological flow sensor systems have been developed [4-6].

Microfluidic chips are usually made from materials such as glass, silicon or plastics. Glass and silicon are well established within this area, although each material has its own advantages and disadvantages. Although most of the pioneering work in this area was performed using glass devices, the use of polymer materials is becoming more common [7]. A range of polymeric materials including poly(methylmethacrylate) (PMMA), polyethylene terephthalate (PET) or poly(dimethylsiloxane) (PDMS) have been used for the fabrication of plastic devices. There are a number of advantages that polymers have over glass and silicon including ease of manipulation, speed of manufacture, decreased fabrication costs and suitability for mass production allowing low cost, disposable devices to be

fabricated. Polymers also have a wide range of properties to suit the application and there are some fabrication technologies now available, such as hot embossing or injection moulding, that allow more complex structures to be fabricated, which cannot be fabricated from glass [8]. This recent progress in the development of fabrication methods for plastic microfluidic manifolds has added to the promising combination of microfluidic systems with chemiluminescence detection.

The previous chapter described how a working flow injection method with chemiluminescence detection was developed and optimised for the determination of copper (II) in water samples. This chapter describes how the manifold is further developed and incorporated within a microfluidic manifold, manufactured from PMMA. A number of different microfluidic manifolds were designed and manufactured using three different micro-fabrication techniques, namely hot embossing, laser ablation and direct micro-milling. The performance of the PMMA microfluidic manifolds fabricated has been investigated and in combination with chemiluminescence detection, these manifolds have been applied to the determination and monitoring of copper (II) in water samples. The aim of this study was to develop an analytical system, capable of low μg L^{-1} determinations of copper (II) in water samples, which could be applied to 'on-line' monitoring with minimal reagent consumption.

3.2 Experimental

3.2.1 Flow Manifold Design (Stage I)

Figure 3.1 shows the initial flow manifold design, which was fabricated using the in-house hot embossing system (detailed in section 3.2.2). The mixing ratio used is still the same as that used in the preliminary large-scale manifold described previously in chapter 2. The sample and 1,10-phenanthroline solution were first mixed in a 1:1 ratio in the mixing channel, followed by the introduction of the hydrogen peroxide solution prior to detection. The plastic manifold itself was composed of two PMMA plates of thickness 4 mm (the bottom plate containing the flow channels and the top plate as the cover plate). This manifold consisted of two inlets for the introduction

of the sample and 1,10-phenanthroline solutions, which were mixed together in the mixing channel. This channel was 1,000 mm in length and with an internal width of 1,000 μm and a depth of < 900 μm. This provided the mixing necessary for the reaction between the copper in the sample and the 1,10-phenanthroline to occur and replaced the 1,000 mm mixing coil in the preliminary manifold. There was another inlet at the end of the mixing channel immediately prior to the detection/reaction channel for the introduction of the hydrogen peroxide. The dimensions of the plastic chip were approximately 80 mm x 100 mm x 8 mm.

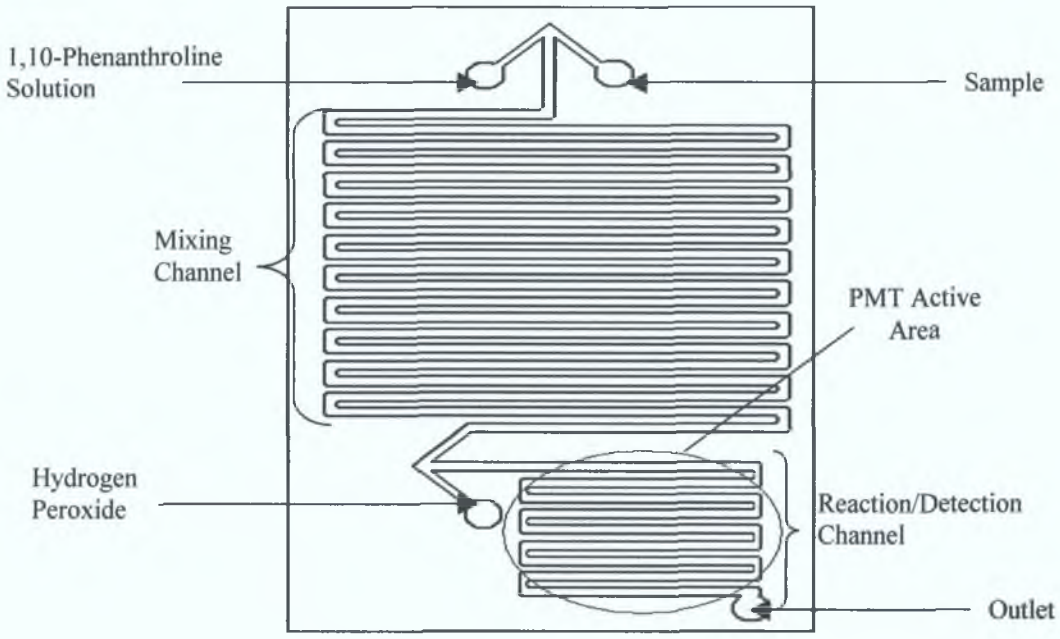

Figure 3.1: Diagram of plastic chip manifold made in PMMA comprising of a mixing channel 1,000 mm in length with an internal width and depth of 1,000 μm x < 900 μm and a detection channel 190 mm in length and 1,000 μm x < 900 μm in width and depth.

This manifold differed slightly from the large-scale setup described in chapter 2, where there was a short length of tubing (50 mm with a residence time of 0.72 s) before the detection cell, which resulted in a slight delay before the chemiluminescence emission was detected. In this plastic manifold, the chemiluminescence emission was detected instantly, with no time delay, as there was no excess length between the addition of the hydrogen peroxide solution to the copper-1,10-phenanthroline mixture, and the detection cell, resulting in a more

efficient detection. The actual detection/reaction channel was 190 mm in length and similar to the mixing channel, it was 1,000 μm in width and < 900 μm in depth. The PMT was positioned and secured directly on top of the detection channel area as shown in Figure 3.1.

The total volume of the detection flow cell was < 134 μL and a residence time < 45 s, when a flow rate of 180 μL min^{-1} was used. This detection channel was in place of the detection coil used in the previous chapter. Although this detection cell was shorter than the PE coil used in the previous work by approximately 50 μL, the residence time was calculated to be up to 8 times longer in this manifold, due to the lower flow rates used. Using this on-chip design, the need for T-piece connectors was removed. It is important to note that the exact depth of the channels could not be ascertained because when bonding of the top plate occurs the channel depth is significantly reduced, making it difficult to calculate exact volumes and residence times. The manifold described here offers an improvement on FIA system, discussed in chapter 2, which consisted of the separate mixing coils and spiralled reaction coil. Here all the processes are integrated onto one platform and the volumes of reagents and samples required as well as waste solutions for disposal, were reduced by at least a factor of 10.

3.2.2 Fabrication Process (Stage I)

In brief, the procedure involved in the fabrication of the plastic chip manifold is shown below in Figure 3.2. The advantage of using the hot embossing method is that the template could be used to repeatedly reproduce more plastic devices.

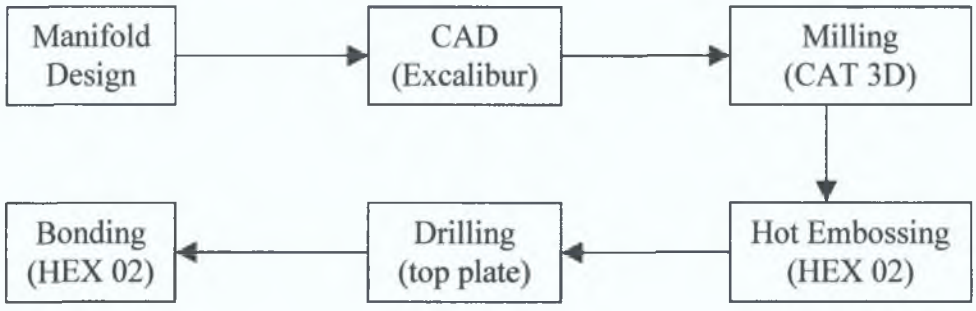

Figure 3.2: Flow diagram of fabrication process of the plastic chip manifold.

The manifold was initially designed using a Computer Aided Design (CAD) 3D Excalibur programme, as a 2D image. The software package then generated a 3D image of the design and the file could be edited to ensure the desired final substrate profile (Figure 3.3a). The choice of design, which uses straight parallel channels rather than the more conventional spiralled coil, was used due to ease of fabrication. The parallel portions of the channels were approximately 2 mm apart, which resulted in reducing the overall volume of solution in the detection flow cell onto which the PMT is incident. This caused a reduction in the intensity and subsequent sensitivity of the measurements. Following this, a brass master (Figure 3.3b) was fabricated by high precision milling and this was then used to hot emboss the PMMA to produce the channels in the plastic substrate (Figure 3.3c).

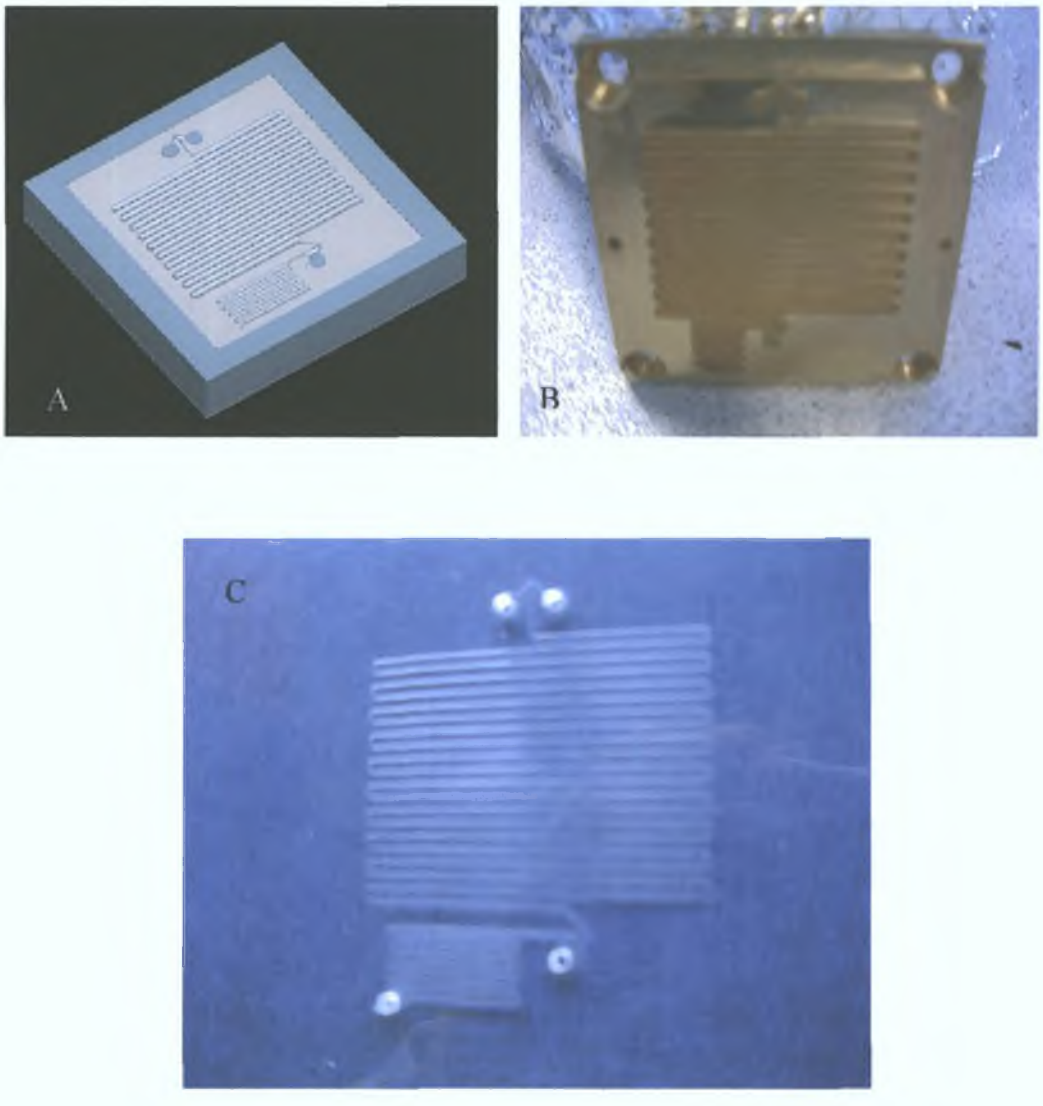

Figure 3.3: Plastic-chip Fabrication: CAD Excalibur design (A), Brass master (B), PMMA manifold (C).

In this work, a brass master of the appropriate inverse structure was fabricated by high precision in-house micro-milling. This was accomplished using a Datron 3-D M6 Micromachining Centre (Datron Technology Ltd., Milton Keynes, UK). This method allows high precision machining with miniature tools (down to 0.1 mm diameter) for the milling of moulds, which can then be used in an injection moulder or hot embosser to produce substrates. The resultant master was then used to hot emboss the PMMA flow manifolds using a Model HEX02 Hot Embosser (Jenoptik Mikrotechnik, GmbH, Jena, Germany).

The brass master was heated to 138 ^{o}C and a flat sheet of PMMA was heated to 125 ^{o}C, which is just above the glass transition temperature (T_g) of PMMA (105 ^{o}C). Using a controlled force (1000 N) the master was used to emboss the PMMA sheet of thickness 4 mm. This procedure typically took 15 minutes, during which time the images of the channels on the brass template were precisely replicated into the PMMA substrate. A flat top plate or cover plate of PMMA of equal width was then drilled to make the reagent entry and exit holes (1mm in diameter) and then was bonded to the embossed plate at 130 ^{o}C and 500 N resulting in a sealed plastic flow manifold (of total thickness 8 mm).

In order to obtain a tight bond, the surfaces of the top and bottom plate were both cleaned using ethanol and then both parts were immersed in isopropyl alcohol (IPA) for 10 minutes before bonding. The IPA was then wiped off with a lint free tissue in order to avoid particle contamination on the surface. Any liquid IPA in the structure must be avoided, since the channels could otherwise be clogged with softened excess material. The sealed chip was allowed to cool to room temperature under pressure to avoid stress cracks in the structure. This all took place in a Class 100 clean room, where rigorous clean protocols were followed.

When the bonding was complete, PEEK tubing of 0.8 mm I.D. was adhered to the inlet and outlet holes using an epoxy resin, for the sample and reagent pumping connections. In order to assess the effectiveness of the sealing of the top cover plate onto the hot embossed substrate, coloured dyes were introduced into the channels using a peristaltic pump at slightly higher flow rates than would be used during this work. Examination of the plastic flow device took place to ensure there was no

internal leakage (i.e. between the channels themselves) and there was no leakage from the tube fittings at the reagent inlets on the device. This study also investigated the ease of filling the channels and ensured there were no blockages within the device due to plastic fragments or dust particles. It was very important to check there was an effective seal between the two parts of the manifold and there were no leaks or blockages as these were shown to be problematic in previous attempts to fabricate the plastic device.

3.2.3 Experimental Setup and Instrumentation (Stage I)

The experimental setup was similar to the previous manifold described in chapter 2 with a few alterations (Figure 3.4). The need for a mixing coil, T-piece connections and coil detection flow cell were removed due to the introduction of the plastic flow manifold. It should be noted that the detection channel in this case was square in shape and the surface area of the detection channel did not match the surface area of the PMT as well as the coil flow cell did. In this work the itaconic acid column was also removed from the manifold to simplify the system as this work focused on the optimisation of reaction conditions and mixing. The total flow rate in this work was 180 μL min^{-1} (the flow rate of each reagent line was 60 μL min^{-1}). The flow rates in this case were dramatically reduced to those used in the previous work to avoid a build up of pressure in the reaction chamber, which would cause the flow channels to leak. The reduction in flow rates also resulted in an increase in the residence time in the detection channel. In addition, the six-port Rheodyne injection valve was fitted with a 3 μL PEEK sample loop for sample introduction in preference to the 120 μL loop used in the previous system which would introduce too much sample into this flow manifold.

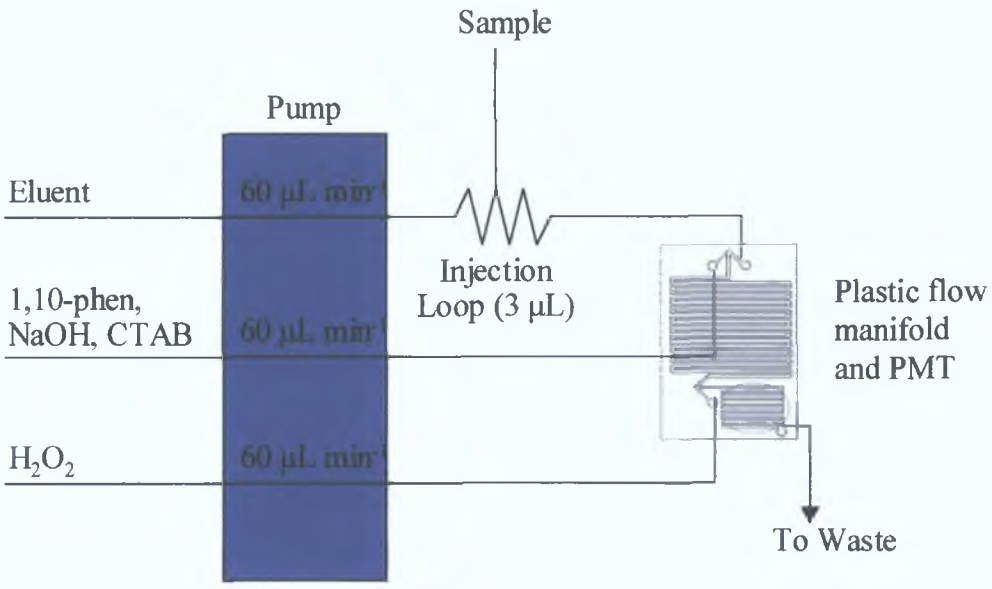

Figure 3.4: Block diagram of the reaction manifold (Stage I) used for the determination of copper (II) by flow injection analysis using plastic fluidic manifold. This manifold utilised a 3 µL injection loop, a total flow rate of 180 µL min^{-1} as described in the text.

3.2.4 Microfluidic Manifold Design and Fabrication (Stage II)

Following the initial studies on the larger setup (stage I), the system was further scaled down incorporating the use of three microfluidic peristaltic pumps and a smaller channelled manifold. The design of the microfluidic manifold was changed to suit the micro-system (stage II). As described in section 3.2.2, the manifold was fabricated using in house micro-milling equipment to produce a brass master, which was then used for hot embossing the PMMA substrate. In this design the mixing channel was reduced in length to 730 mm, while the reaction/detection channel was increased to 210 mm. In addition, the shape of the detection channel was changed, fitting exactly to the shape of the PMT window, to maximise the sensitivity. The channels themselves were significantly narrower than the channels of the larger chip, being 200 µm wide by approximately 200 µm in depth (although again due to bonding the ultimate depth of the channels was < 200 µm).

A T-junction was put in place of the third inlet for the possibility of using this inlet for the sample introduction whereby a smaller sample plug could be formed and introduced to the system (nanolitres/picolitres compared microlitres). It was found

later, that this idea was not possible as the chemiluminescence reaction only took place if the sample and 1,10-phenanthroline are first mixed together prior to the introduction of hydrogen peroxide. The actual plastic chip dimensions were reduced to 70 mm x 70 mm x 6 mm. The total thickness of the microfluidic device was also reduced as the top plate that was bonded to the embossed PMMA was changed from 4 mm in thickness to 2 mm in thickness.

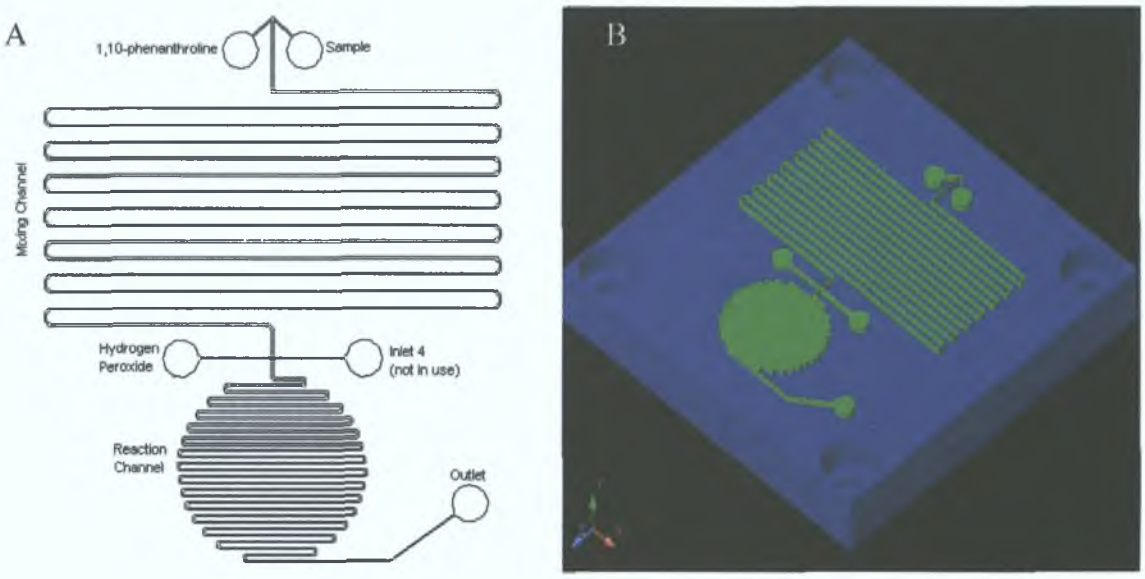

Figure 3.5: 2D image of new polymer flow manifold (A), CAD image of flow manifold (B).

3.2.5 Experimental Setup and Instrumentation (Stage II)

A schematic diagram of the new setup used in stage II is shown in Figure 3.6. Three micro-peristaltic pumps (manufactured by BVT Technologies, Euro-link Associates, Tyne & Wear, England) were used to drive the reagents through peristaltic tubing, which was connected to narrow bore, 0.127 mm I.D. PEEK tubing and into the microfluidic manifold. The total combined flow rate was 76 μL min^{-1}. To simplify the system, the Rheodyne injector and sample loop were removed from this setup completely. The sample itself was pumped continuously through the system and the need for a sample carrier was therefore also removed. This resulted in a continuous detector response rather than the previous transient signal. For the introduction of new sample and standard solutions, the sample pump was stopped whilst the solutions were changed. It was found that this manual procedure did not introduce

air into the system, although for future on-line work a low pressure-switching valve could be easily incorporated into the system for this purpose.

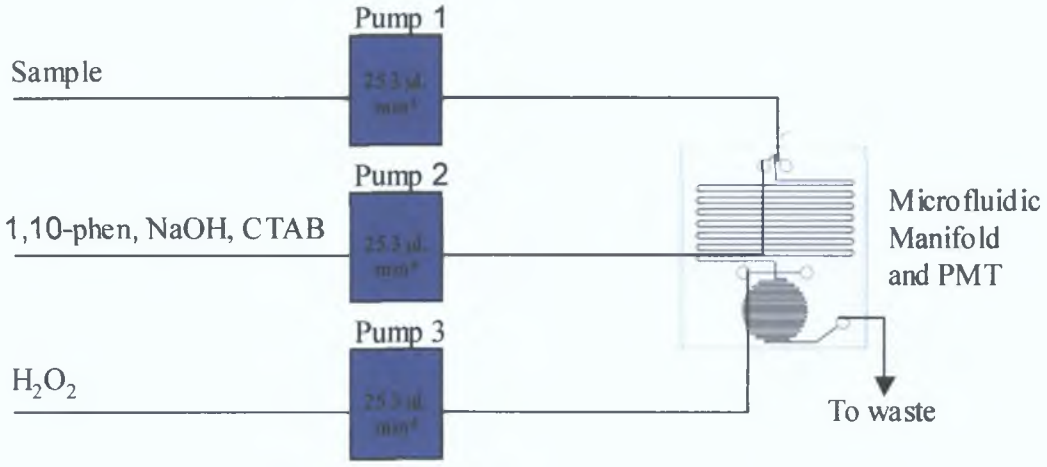

Figure 3.6: Schematic of new flow system (Stage II) incorporating three micro-peristaltic pumps and new flow manifold. Total flow rate: 0.076 mL min^{-1}.

The actual dimensions of the apparatus inside the light tight box are given below (Figure 3.7). The minimum height is 181 mm and the minimum width by depth is 70 by 70 mm.

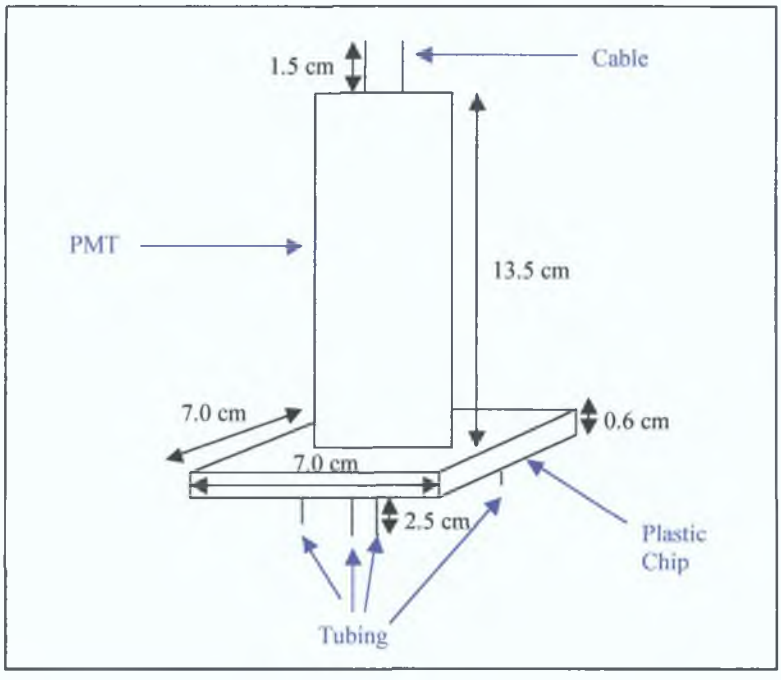

Figure 3.7: Diagram of PMT and plastic flow manifold inside light tight box.

Three single channel microfluidic peristaltic pumps were used in this system. These pumps have been designed for small portable devices. An example of one is shown in Figure 3.8. Each pump is manufactured in stainless steel and contains three roller heads. Each individual pump weighs 34 grams and is 60 mm in height. The base measurements are 16 x 16 mm. These pumps operate using a DC supply at 3 V and the maximum current is 0.5 A. The three pumps were connected together using a custom-made multi-pump control interface so they could be driven by one PC connection. When connected in this manner it was possible to set each flow rate independently for each pump in the range of 0.5 to 200 μL min^{-1} but in this work all the reagents were pumped at the same flow rate.

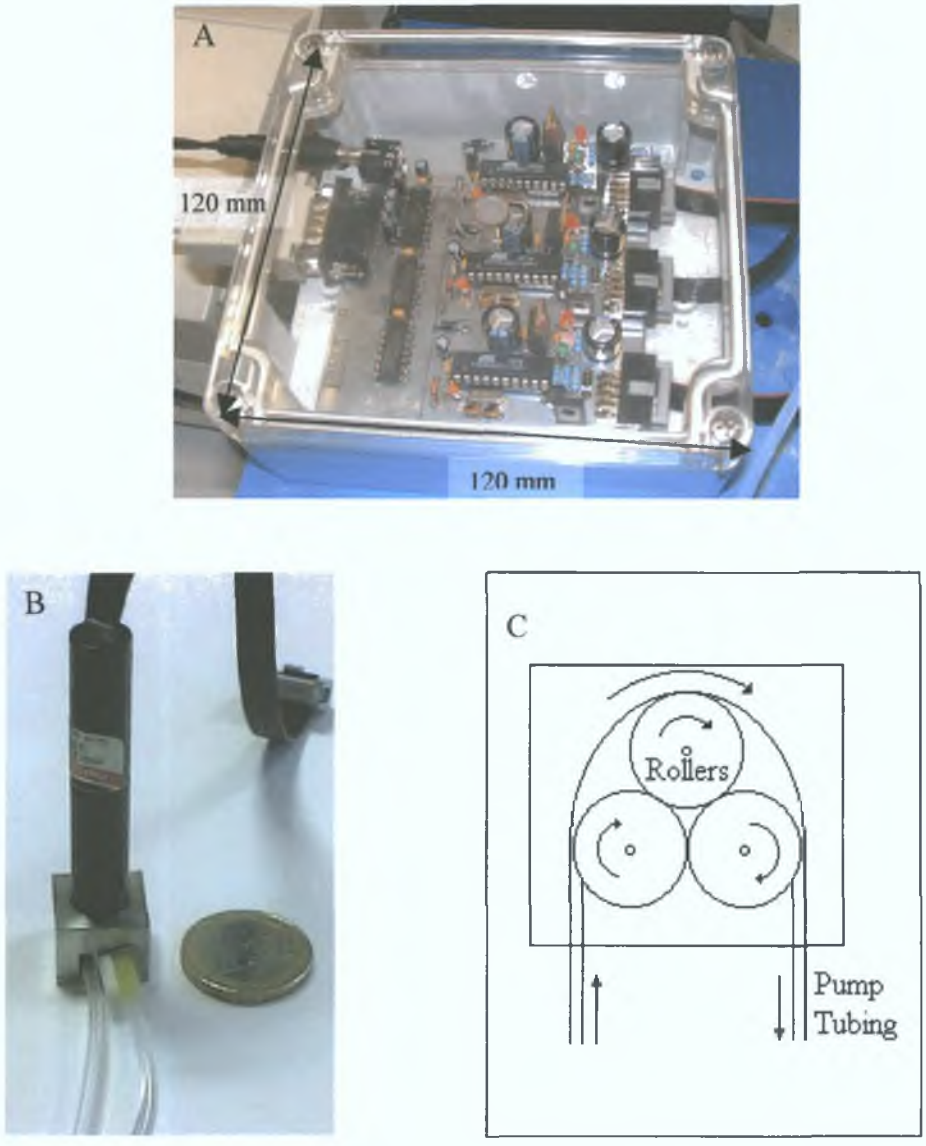

Figure 3.8: (A) depicts the electronics unit and interface of micro-peristaltic pumps used in this system, (B) micro-peristaltic pump, (C) schematic diagram of peristaltic pump.

Figure 3.9 illustrates the complete microfluidic setup as used in this work, including the micro-peristaltic pumps, electronics unit, PMT power supply and light tight box containing the PMT and plastic microfluidic manifold.

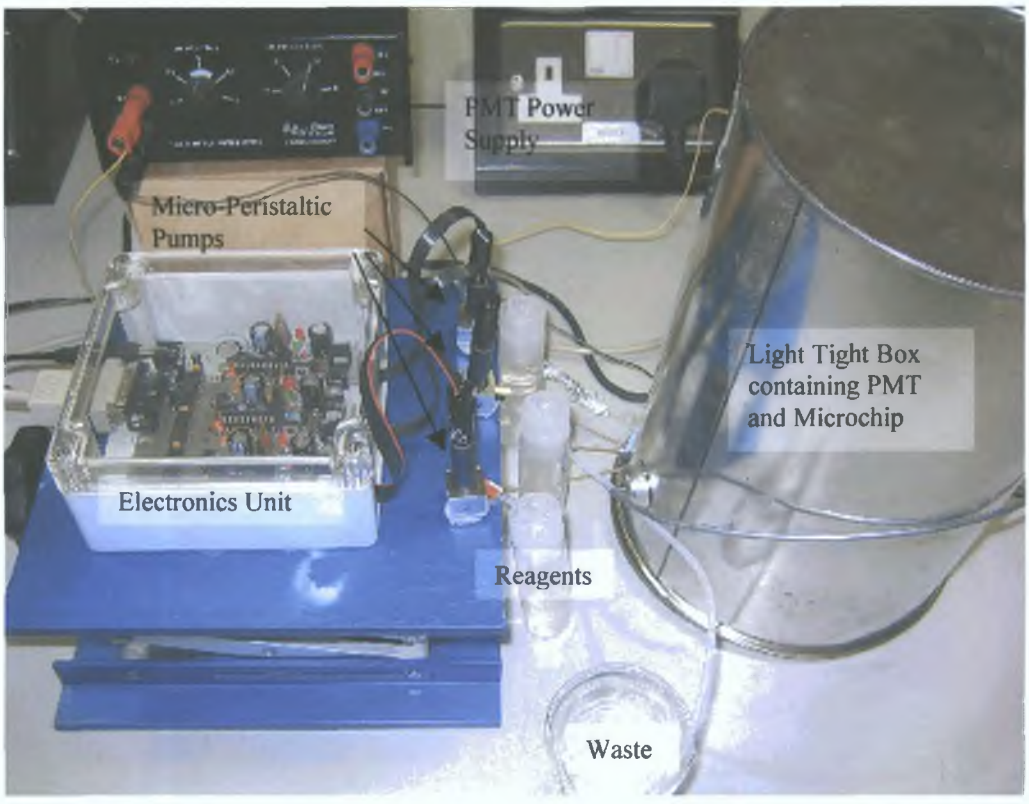

Figure 3.9: Experimental setup of microfluidic system (Stage II).

3.2.6 Reagents (Stages I and II)

All of the reagents and standards used in both stages of this work were the same as those described in the previous chapter (section 2.2.3). All of the solutions were degassed using sonication to ensure reagent dissolution and homogeneity. They were also all filtered through a 0.45 μm nylon membrane filter from Gelman Laboratories (Michigan, USA) prior to use. In microfluidic devices, gas bubbles, dust and other particles, found in solvents or arising from sample crystallisation can easily result in blockages within the device, requiring diligent care to be taken when making up all solutions.

3.3 Results and Discussion

PMMA was chosen for fabrication of the plastic manifold as it is the least hydrophobic of common plastics and has a softening temperature of 105 °C [9]. Prior to the fabrication of the PMMA micro-chip, the transparency of the PMMA was measured using a UV-VIS spectrophotometer (Varian Cary 50 UV-VIS spectrometer). Figure 3.10 shows that the transmittance of the PMMA sheet of 4 mm thickness was greater than 90 % over the wavelength of 400 nm, which illustrated that the polymer PMMA had very high transparency and was suitable for optical detection techniques.

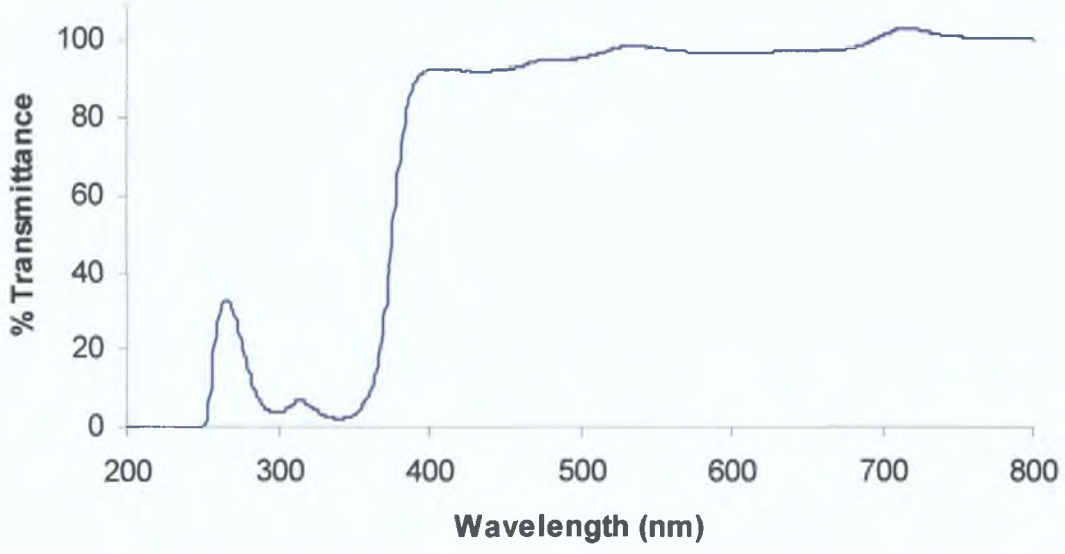

Figure 3.10: % Transmittance of PMMA plate with 4 mm thickness measured using a UV-VIS spectrometer.

The temperature and force profiles for the embossing experiment of the brass master and base plate are shown below in Figure 3.11. The process was carried out under vacuum conditions preventing undesirable deformations in the structure by reducing the high pressures caused by the presence of air. The initial variation in force was generated as the master and base plates came together in the embosser. Once the plates made contact, they were maintained at 1,000 N until the channels were fabricated.

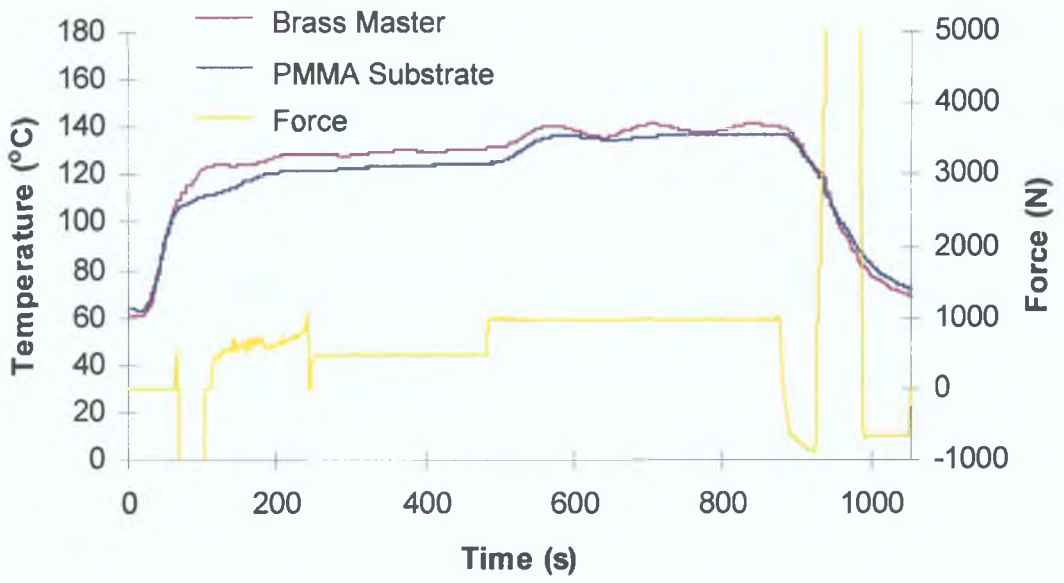

Figure 3.11: Example of profile of the change in temperature and force as a function of time for the hot embossing process.

The actual channel dimensions of the PMMA substrate were measured using a surface profiler (Dektak V 200-Si, Veeco Surface Metrology, Santa Barbara, CA). A profile of the base plate, containing the channels was taken before sealing and both the cover plate and base plate were profiled after the chip was dismantled. The cover plate was used as supplied and was a flat sheet of PMMA so no profile was recorded before sealing. It should be noted that when bonding took place the depth of the channels was reduced. It can be difficult to ascertain the exact depth of the channels after sealing, as the sealed chip needs to be dismantled. In one example from Stage II, where a chip was taken apart, it was found that the mixing channels were reduced from 100 μm in depth to 46 μm while the detection channels were reduced from 79 μm in depth before sealing to 30 μm after sealing. This corresponded to a reduction of 66 % in the mixing channel and 80 % in the detection channel after sealing. As a result of this care was taken to reduce as much as possible the amount of deformation to the channels. Note: attempts to reduce deformation can result in incomplete sealing leading to leakage when the reagents are introduced. In above example, the PMMA used for the cover plate was measured using callipers and found to be 5 % thicker than the specifications indicated by the supplier, therefore a recalculation for the embossing procedure using the actual measured thickness of the PMMA achieved satisfactory results.

3.3.1 Stage I – Initial Flow Studies and Miniaturisation

Initially, a 1 mg L^{-1} copper (II) standard was injected using the following conditions 0.03mM 1,10-phenanthroline, 0.075 M sodium hydroxide, 0.05 mM CTAB, 5 % hydrogen peroxide and 100 mM nitric acid, in order to investigate the repeatability of this preliminary system (stage I). These conditions were the same as those used in the large-scale study carried out in chapter 2 and were considered to be the optimum conditions in that study. The reaction peaks generated for a 1 mg L^{-1} copper (II) standard using these conditions are shown below in Figure 3.12. The repeat injection of the copper (II) standard solution using this system (where n = 6) gave an excellent RSD value of 2.2 % based on peak height.

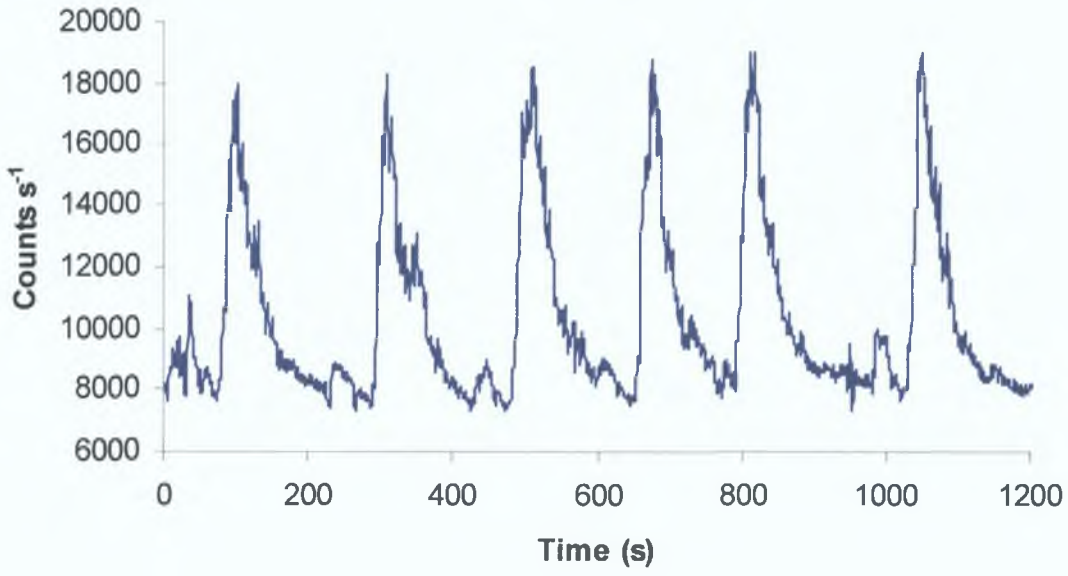

Figure 3.12: Reproducibility of 1 mg L^{-1} copper (II) standard where n = 6 (% RSD value = 2.2).

The standard deviation (s) was calculated for the replicate injections, which quantifies the dispersion of the dataset, using the equation given below:

$$\sqrt{\frac{\sum_{i=1}^{n}(x_i - \bar{x})^2}{n-1}} \qquad \text{(Equation 3.1)}$$

The relative standard deviation (RSD) was also calculated for each of the replicate injections to compare the precision. To calculate this, the standard deviation is normalised by dividing by the mean as shown in the following equation:

$$RSD = \frac{(100 \times s)}{\bar{x}} \qquad \text{(Equation 3.2)}$$

RSD values of ≤ 5.0 % are deemed acceptable for precise results. From the above results it was found that the reproducibility was acceptable and the relative standard deviation was found to be < 2.2 % for all of the replicate injections (n = 6).

3.3.2 Optimisation Studies (Stage I)

A series of experiments were then carried out to establish the optimum conditions for this stage I system, as it was important that the analysis was measured under the best conditions to avoid unnecessary poor precision and reduced sensitivity. The key variables for maximising the sensitivity of the chemiluminescence emission signal were considered to be the reagent concentration and flow rate of the reagents.

The two chemical variables optimised were the concentrations of 1,10-phenanthroline and surfactant CTAB. These variables were optimised simultaneously. The concentration of hydrogen peroxide and sodium hydroxide remained the same as before, 5 % w/v and 0.075 M respectively. The flow rates were then optimised to determine the best flow conditions for the copper (II) determinations with good sensitivity.

3.3.2.1 Optimisation of 1,10-Phenanthroline and CTAB Concentrations

The concentrations of 1,10 phenanthroline and CTAB were both optimised simultaneously in this study. The experimental space was defined by varying systematically both the concentrations of 1,10-phenanthroline and CTAB from 0.01 mM to 0.10 mM as shown in Figure 3.13. In all of the experiments, the following conditions were used: a total combined flow rate of 180 μL min^{-1}, a sample injection volume of 3 μL for a 1 mg L^{-1} copper (II) standard, 5 % hydrogen peroxide solution

and 0.075 M sodium hydroxide. By keeping all these parameters constant, the optimum concentrations of 1,10-phenanthroline and CTAB could be determined.

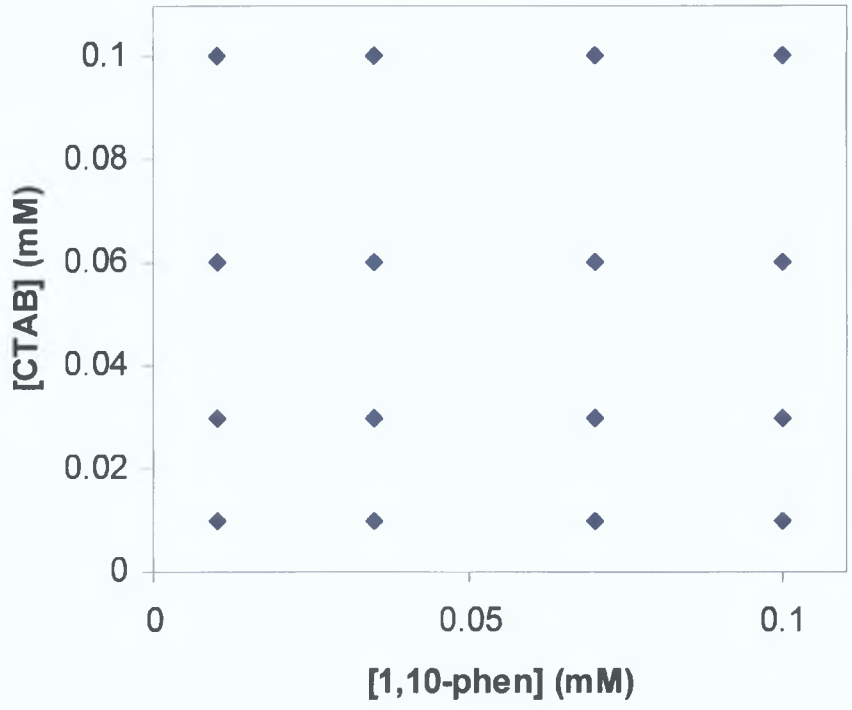

Figure 3.13: Schematic showing the test solutions within the chosen experimental search area used for optimisation of [CTAB] and [1,10-phenanthroline] using the following conditions: total flow rate of 180 μL min^{-1}, sample injection volume of 3 μL for a 1 mg L^{-1} copper (II) standard, 5 % H_2O_2 and 0.075 M NaOH.

A three-dimensional response surface plot (Sigma Plot Version 4.0) showing the combined effects of 1,10-phenanthroline and CTAB concentrations on the signal to noise ratio was constructed for the 1 mg L^{-1} copper (II) standard. The data was treated by calculation of each of the peak signal to baseline noise ratios, which were then plotted against the reagent concentrations. Each of the analyses were carried out in triplicate (n = 3). As can be seen from the Figure 3.14, the system performed quite well in the chosen concentration ranges. It was found that the highest signal to noise ratio was achieved when using 0.07 mM 1,10-phenanthroline and 0.06 mM CTAB. In this case the signal to noise ratio was found to be 27 when a 1 mg L^{-1} copper (II) standard was used.

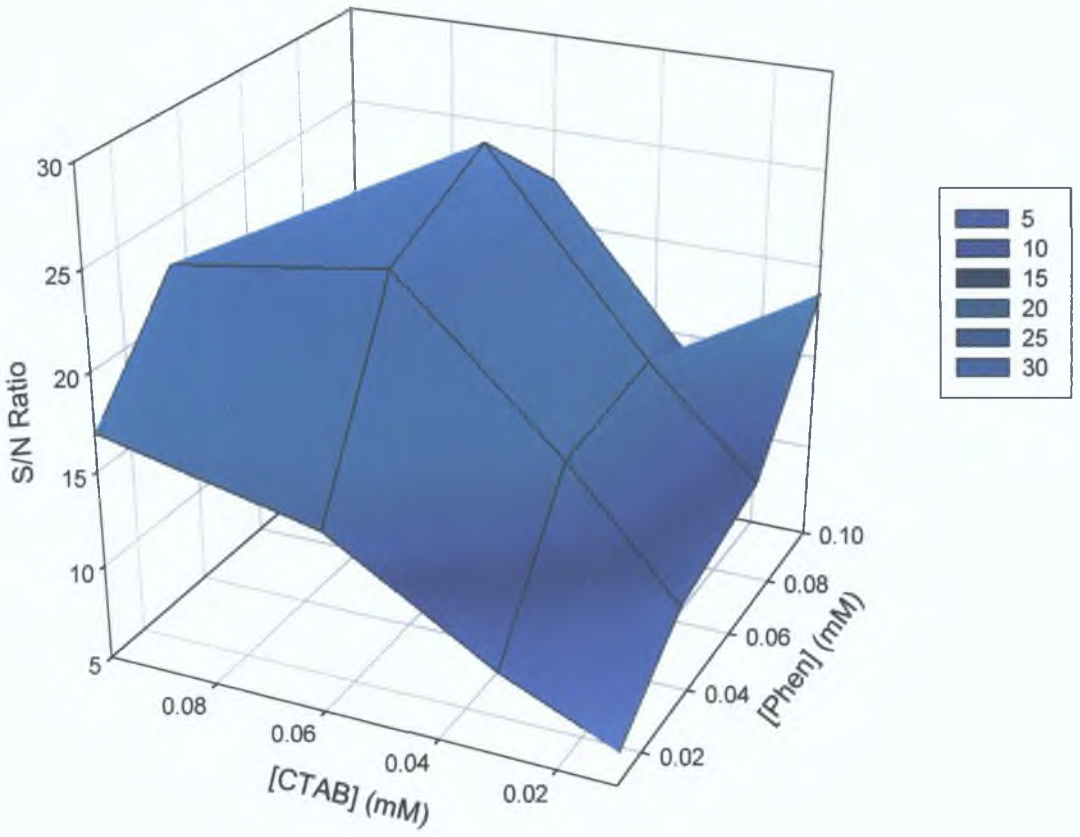

Figure 3.14: Response surface plot showing signal to noise ratio as a function of concentration of 1,10-phenanthroline and CTAB for a copper (II) standard of 1 mg L^{-1}. The optimum concentrations of 1,10-phenanthroline and CTAB were found to be 0.07 mM and 0.06 mM respectively, resulting in a S/N of 27.

At the lower concentrations of 1,10-phenanthroline, the formation of the 1,10-phenanthroline-copper (II) complex, which is an essential first step in the chemiluminescence reaction, was limited. At these lower concentrations, the 1,10-phenanthroline was more dispersed at the micelle interface, which resulted in a reduced chemiluminescence quantum yield. At higher concentrations (even higher concentrations than those investigated here), a rapid quenching of the signal can occur which is due to molecular aggregation which binds up the copper (II) or there may be a reduction in micelle stability. The quenching effect occurs by dissipation of the chemiluminescence emission via a non-radiative pathway such as molecular collisions rather than chemiluminescence.

3.3.2.1.1 Reproducibility and Linearity Studies

Using these optimised conditions, a calibration study was carried out. For this, a series of measurements were performed with copper (II) standard solutions ranging from 10 μg L^{-1} to 1,000 μg L^{-1} to investigate reproducibility and linearity. In each case three replicate copper (II) analyses took place (n = 3) between 10 and 1,000 μg L^{-1}. The peaks obtained can be seen in Figure 3.15. The reagent conditions used here were: 0.07 mM 1,10-phenanthroline, 0.06 mM CTAB, 0.075 M sodium hydroxide and 5 % hydrogen peroxide. The flow rate used for each line was 60 μL min^{-1}, with a combined total flow rate of 180 μL min^{-1}, resulting in a sampling rate of approximately 14 samples hr^{-1}.

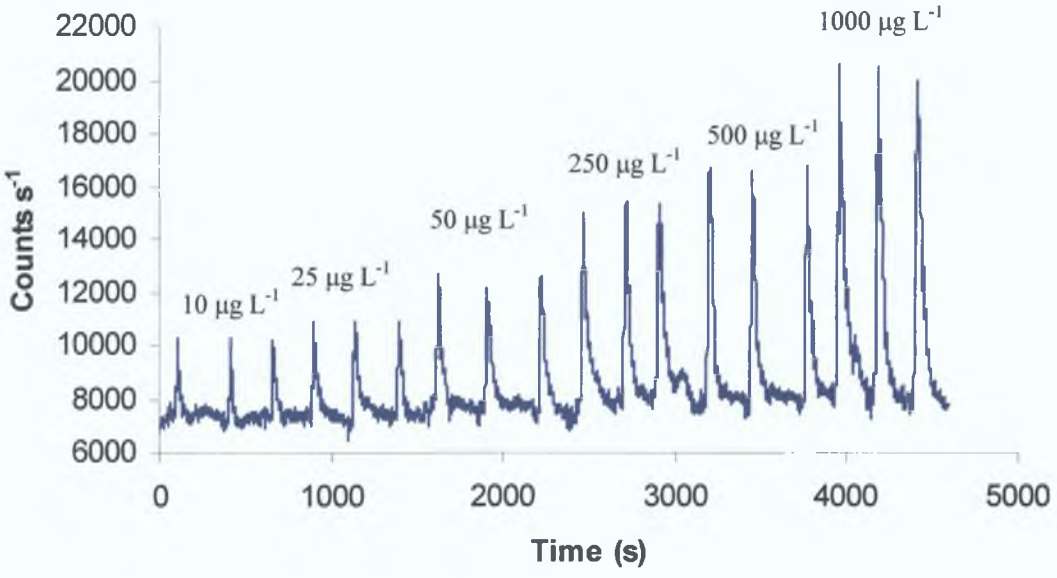

Figure 3.15: Reproducibility studies of copper (II) standards between 10 and 1,000 μg L^{-1}. Reagent conditions: 0.07 mM 1,10-phenanthroline, 0.06 mM CTAB, 0.075 M NaOH and 5 % H_2O_2.

A calibration graph was constructed of the chemiluminescence intensity (counts s^{-1}) versus copper (II) concentration (μg L^{-1}). The results were found to be linear (based on peak height) over the concentration range 50 μg L^{-1} to 1,000 μg L^{-1} as can be seen from Figure 3.16 and the resulting correlation coefficient, R^2 value, was 0.9962, representing acceptable linear reliability. Below 50 μg L^{-1} the resultant peaks were not linear.

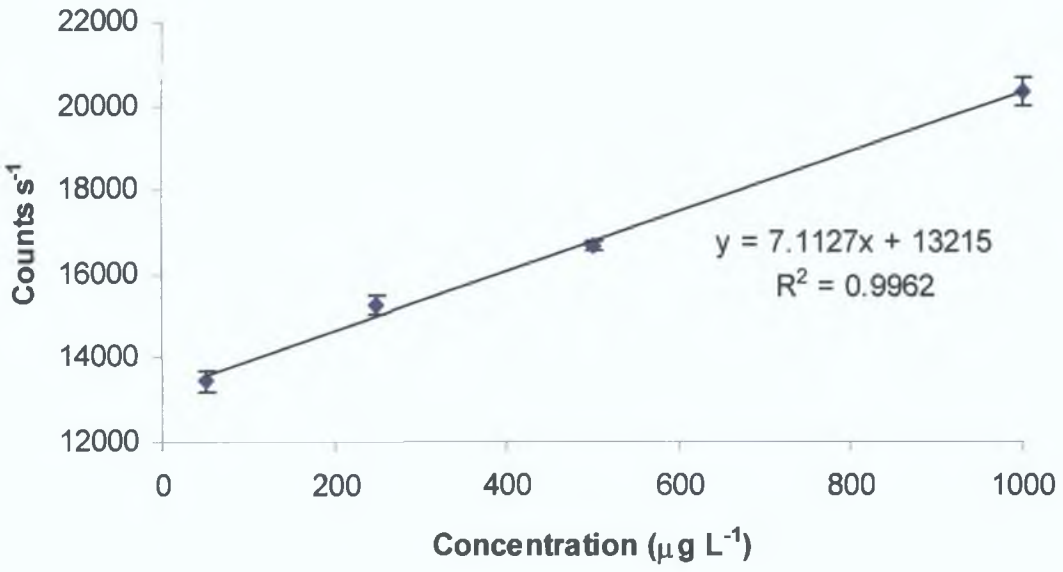

Figure 3.16: Copper (II) linearity studies (n=3) over the concentration range 50 to 1,000 µg L^{-1} where $R^2 = 0.9962$.

As three replicate injections were made for each copper standard, the error associated with each was calculated by the difference between the highest and lowest value for each standard. It was found that the difference was calculated to be < 3.4 %, which was deemed acceptable for these results. It should be noted that the linearity lower limit increased considerably (from 1 µg L^{-1} to 50 µg L^{-1}) when using the chip due to the reduced sample volume as the sample loop was changed from 120 µL, in the standard FIA system described in the previous chapter, to 3 µL in this system.

3.3.2.2 Optimisation of Flow Rates

The flow in a chemiluminescence detection system requires careful monitoring. The flow rate of this system was optimised using a 25 µg L^{-1} copper (II) standard. In the previous work on optimisation of reagents and reproducibility, the total flow rate used was 180 µL min^{-1}. The effect of flow rates, of the carrier and reagent streams, on the signal was investigated between 23 and 256 µL min^{-1} (Figure 3.17 (a) to (e)). Although, the flow rates for each stream can be controlled individually, equal flow rates for all lines were used. It was found that at lower flow rates, the signals produced were bigger and broader. Additionally the background noise also

increased. The reagent conditions used in this work were 0.07 mM 1,10-phenanthroline, 0.06 mM CTAB, 0.075 M sodium hydroxide and 5 % hydrogen peroxide. The optimum total flow rate was chosen to be 44 μL min^{-1} (e).

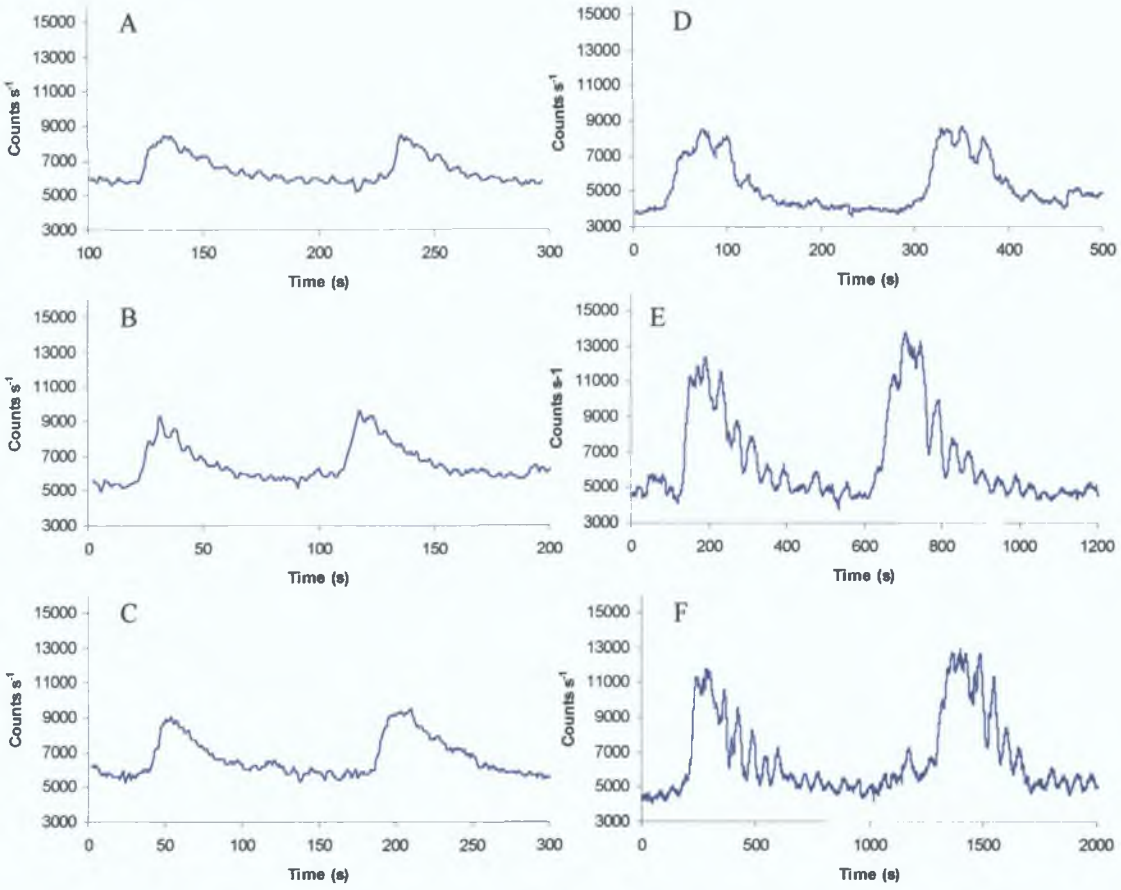

Figure 3.17: Optimisation of flow rates using a 25 μg L^{-1} copper (II) standard (n = 2) (A) 256 μL min^{-1}, (B) 193 μL min^{-1}, (C) 135 μL min^{-1}, (D) 70 μL min^{-1}, (E) 44 μL min^{-1}, (F) 23 μL min^{-1}. Reagent conditions: 0.07 mM 1,10-phenanthroline, 0.06 mM CTAB, 0.075 M NaOH and 5 % H_2O_2.

3.3.3 Further Optimisation Studies

3.3.1 Investigation of Mixing Process

Two important factors in any chemiluminescence determination are the mixing of the reagents and the detection cell (as discussed in section 2.3.1). The reagents must mix satisfactorily in order to obtain the maximum light emission. Poor mixing can result in a large consumption of reagents and a loss of sensitivity. The detection cell

controls the light that reaches the detector as well as the length and magnitude of the signal.

In an attempt to improve method linearity and further miniaturise the manifold, the dimensions of the mixing channel and reaction channels were investigated. Coloured dyes were used in place of the reagents to investigate the laminar flow within the channels and to investigate the mixing process, in order to reduce the length of the mixing chamber. Two dyes were pumped into the mixing chamber and Figure 3.18 shows that complete mixing of the two streams occurred after approximately 700 mm. It was decided, therefore, the length could be reduced by nearly one third of the initial length (approximately 1,000 mm to 700 mm).

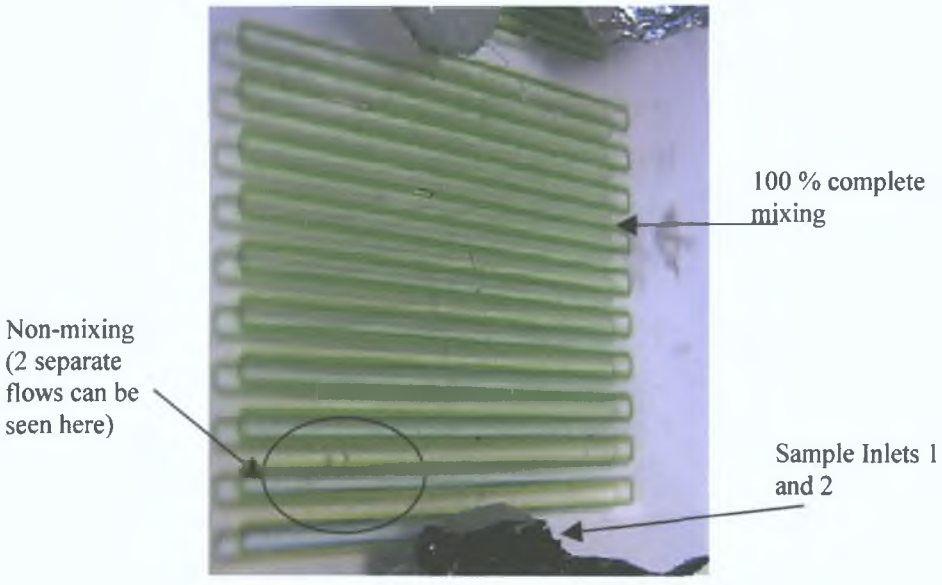

Figure 3.18: Mixing of coloured dyes to show where 100 % mixing occurs in the channels.

3.3.2 Optimisation of Detection Flow Cell

An investigation on the length of the reaction/detection channel was also carried out, to determine the optimal length. The chamber was divided into four equal parts, each containing two channels (Figure 3.19). Using a 100 μg L^{-1} copper (II) standard, the detection channel was increasingly masked from the PMT detector to ascertain the effect of shortening the reaction channel by 25, 50 and 75 % (equivalent to 143, 95 and 48 mm respectively). The resulting signals for the 100 μg L^{-1} standard can be seen in Figure 3.20.

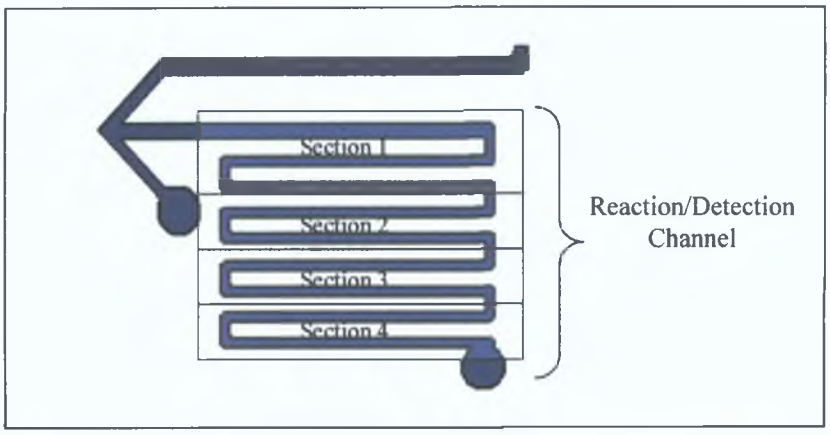

Figure 3.19: Diagram of reaction/detection channel divided into 4 sections.

During this experiment it was found that masking the last 25 % (section 4 as shown in Figure 3.19) of the reaction/detection channel, the chemiluminescence signal for the copper (II) standard decreased by more than half. It was also found that masking the last 75 % of the channel and leaving part 1 uncovered led to the signal being almost totally lost. This meant that although the chemiluminescence reaction was thought to occur almost instantaneously, maximum emission took place in the latter part of the detector channel due to a short time delay to facilitate mixing of the hydrogen peroxide and the sample/reagent flow. As a result, the length of the reaction channel could not be decreased and was subsequently increased.

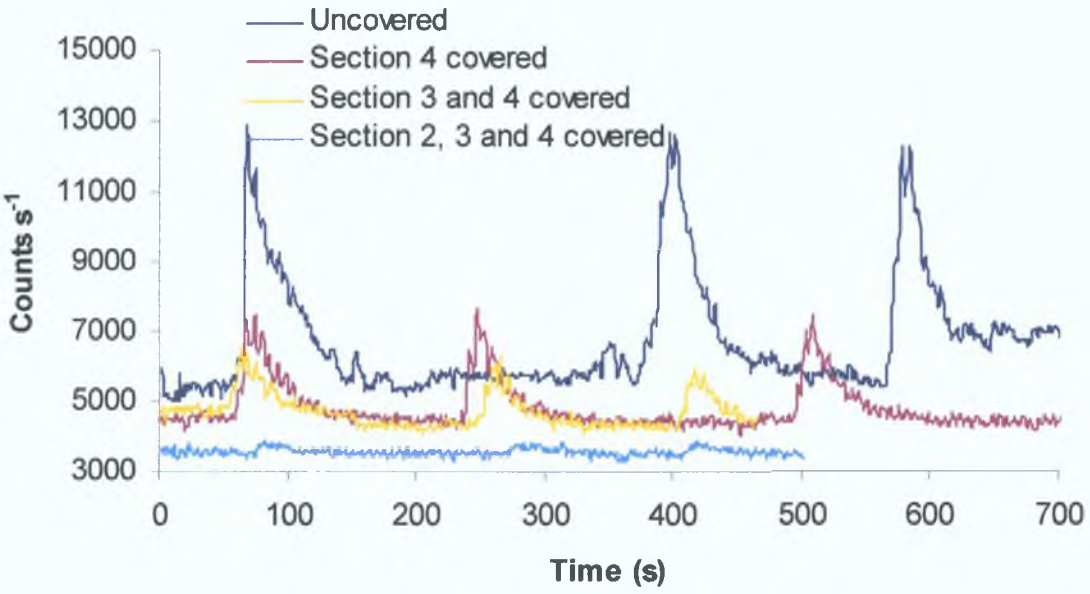

Figure 3.20: Investigation of length of detection channel using a 100 μg L^{-1} copper (II) standard. Reagent conditions: 0.07 mM 1,10-phenanthroline, 0.06 mM CTAB, 0.075 M NaOH and 5 % H_2O_2.

3.3.4 Stage II – Further Miniaturisation

A new flow manifold (stage II) was designed as a result of the preceding work whereby the length of the mixing channel was reduced from 1,000 mm in length to 730 mm in length. The shape of the detection/reaction channel was optimised and instead of being square in shape, it was round to maximise the use of the photosensitive area of the PMT generating the opportunity for more photons to be detected. The reaction/detection flow cell was increased to 210 mm in length. This resulted in a larger surface area for detection purposes, which fitted exactly to the shape of the PMT window, providing a more sensitive detection. By increasing this volume, the dwell time of the luminescent product was increased allowing the PMT to collect more light. The channels themselves were significantly narrower than the channels of the larger chip, being 200 μm wide by < 200 μm deep (as mentioned before, the ultimate depth of the channels was significantly less than 200 μm, due to bonding). These smaller diameter channels reduced dispersion of the transported sample zone, which in turn reduced the broadening of the reaction peaks. In this chip design, the parallel channels of the detection channel were fabricated closer together, each channel was < 1 mm apart compared to 2 mm in the previous design used in stage I.

The microfluidic manifold was connected to the peristaltic pump via micro-bore PEEK tubing (0.127 mm I.D.). The use of micro-bore tubing considerably reduced the amount of sample and reagent consumption in comparison to tubing used in the previous work (0.800 mm I.D.). It also minimised dispersion of the sample and reduced analyses times as the reagents flowed quicker through the system.

On testing this second iteration, the pressure required to pump the reagents and samples through the system was greater than expected. It was originally thought that the channels may have become blocked by fragments from the micro-machining or glue from fixing the delivery tubing, so another manifold was prepared as before paying careful attention to cleaning of the base plate, but similar high pressures were required again. As mentioned previously, it was found that the PMMA used for the cover plate was 5 % thicker than the specifications indicated by the supplier and as a

result of this the embossing process was altered achieving complete and uniform sealing of the device and reducing deformation of the channels. However, it should be noted that the exact channel depth in the bonded manifold could not be ascertained as mentioned before.

3.3.5 Pumping System and Flow Rates (Stage II)

As well as controlling the flow rate by the PC via the control interface, the flow is also dependent on the tubing diameter as shown in Figure 3.21. A range of pump tubing of varying internal diameters was used for this. The flow rates for the pump tubing were linear over the range of pump speeds used. It was decided to use pump tubing of 0.508 mm I.D. and the optimum total flow rate was found to be 0.076 mL min^{-1}. The reduction of the flow rates allows more time for the PMT to collect light from the chemiluminescence reaction in the detection channel. This reduction in flow rate also decreased the amount of reagent and sample used and also the waste generated, by a factor of almost three on the previous system. These pumps were regularly calibrated to ensure accurate and reproducible flow rates.

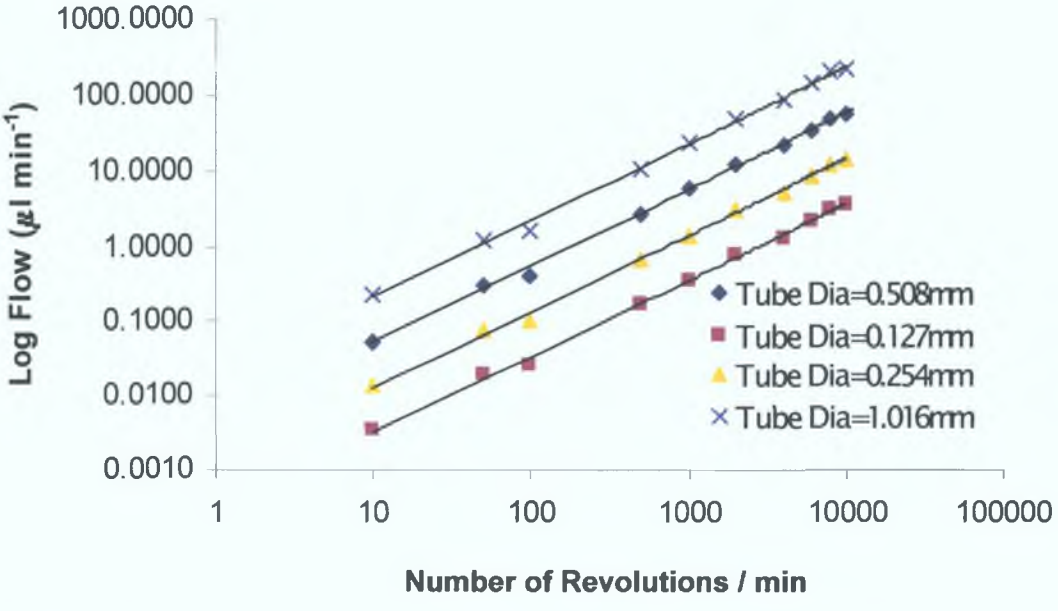

Figure 3.21: Standard pump calibration curves of flow rates for a range of tubing diameters.

The long-term stability of the flow was investigated and can be seen in Figure 3.22. The pump tubing was routinely replaced after 500 hours usage to ensure accurate flow rate.

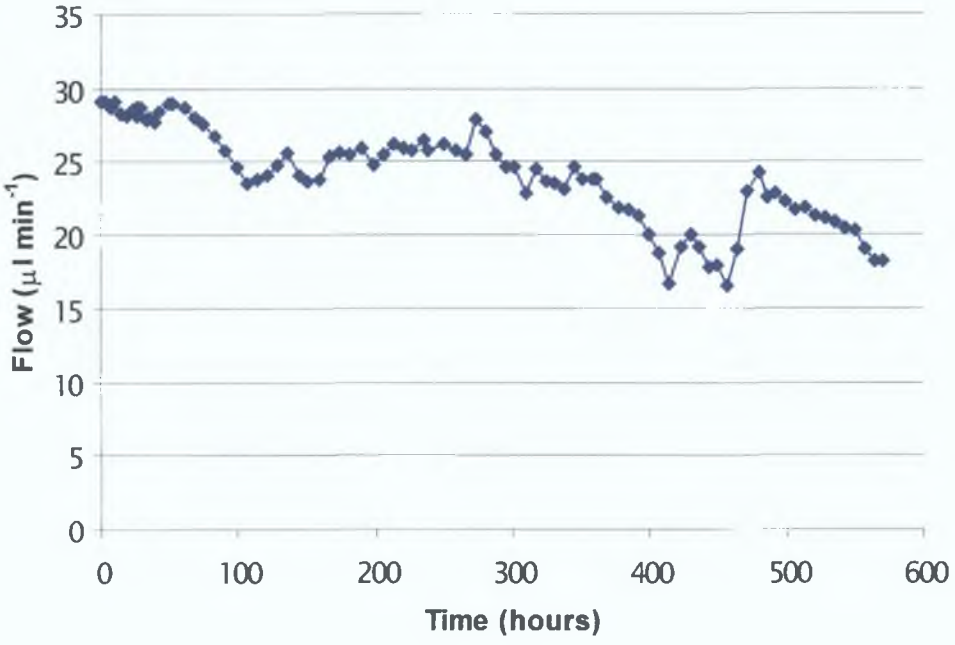

Figure 3.22: Long term stability of pump flow.

3.3.6 Optimisation Studies (Stage II)

3.3.6.1 Optimisation of Reagents

The concentration of CTAB and 1,10-phenanthroline were re-optimised to ensure the analysis was still being measured under the best conditions. The experimental space was defined as before by varying systematically both the concentrations of 1,10-phenanthroline and CTAB from 0.01 mM to 0.10 mM as shown in Figure 3.23. In all of the experiments a 30 µg L^{-1} copper (II) standard which was continuously pumped through the flow system and the following conditions were applied: a total flow rate of 76 µL min^{-1}, 5 % hydrogen peroxide solution and 0.075 M sodium hydroxide.

Note: By continuously pumping the sample through the system the chemiluminescence emission signal can be continuously monitored. During fast chemiluminescence reactions, where imprecise measurements can arise due to irreproducible mixing of the sample and reagents, the continuous monitoring of the signal can improve the precision, in comparison to measurement due to peak height or area.

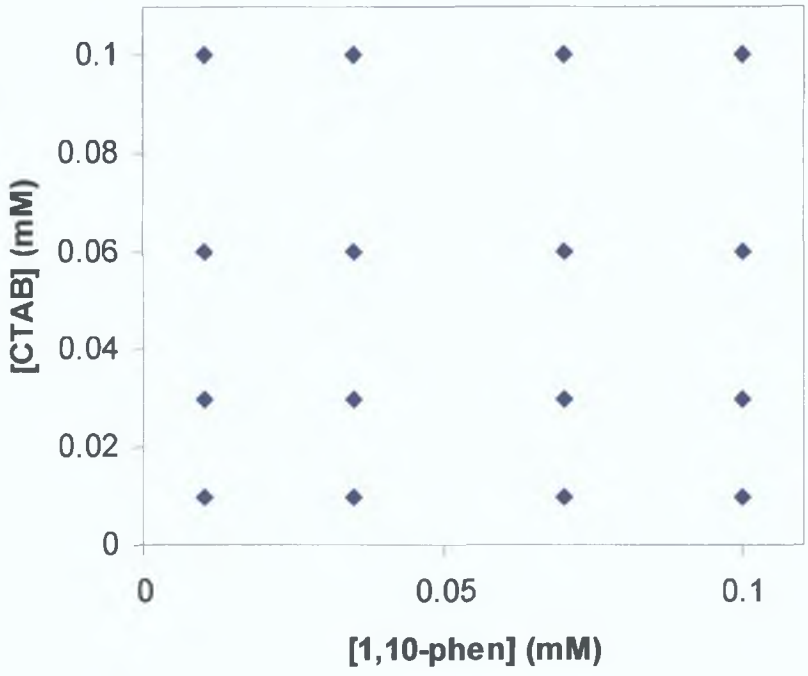

Figure 3.23: Experimental area used for re-optimisation of [CTAB] and [1,10-phenanthroline] using the following conditions: total flow rate of 76 μL min^{-1}, a 30 μg L^{-1} copper (II) standard which was continuously pumped through the flow system, 5 % H_2O_2 and 0.075 M NaOH.

A second three-dimensional response surface plot was constructed for the 30 μg L^{-1} copper (II) standard as before showing the combined effects of 1,10-phenanthroline and CTAB concentrations on the signal to noise ratio. As can be seen from the Figure 3.24, the highest signal to noise ratio was achieved when using 0.07 mM 1,10-phenanthroline and 0.10 mM CTAB, in this case the signal to noise ratio was found to be 34.

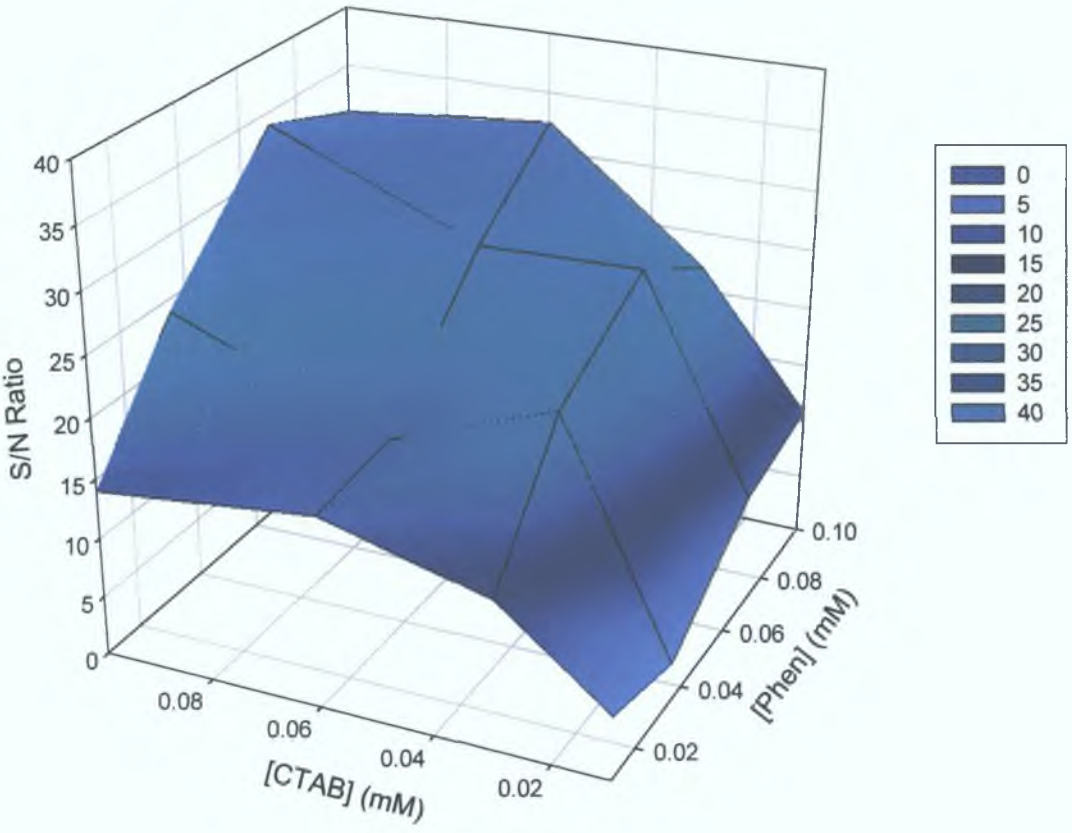

Figure 3.24: The response surface plot shows the optimum conditions of 1,10-phenanthroline and CTAB for a copper (II) standard of 30 μg L^{-1}. The optimum concentrations of 1,10-phenanthroline and CTAB were found to be 0.07 mM and 0.10 mM respectively, resulting in a S/N of 34.

In an attempt to improve the signal to noise ratio and further improve concentration sensitivity, the underside of the detection channel was sputter-deposited with a thin layer of gold, to act as a mirror in order to reflect any of the light lost from the chemiluminescence reaction from the underside of the chip during detection. It was found that after re-optimisation of the reagents, the results obtained were similar to those produced for the uncoated chip and the signal to noise ratio did not actually improve, therefore there was no need in future work to gold coat the underside of the plastic manifold.

3.3.6.2 Optimisation of Flow Rates

The flow rates used in microfluidic systems need to be very low, therefore micro-peristaltic pumps with precise low flow rates were used. While each reagent line was controlled by a separate micro-pump, all the reagents were pumped at the same

flow rate. Total flow rates of 0.086, 0.076 and 0.064 mL min^{-1} for the three reagent lines were investigated (Figure 3.25). The reagent conditions used in this work were 0.07 mM 1,10-phenanthroline, 0.10 mM CTAB, 0.075 M sodium hydroxide and 5 % hydrogen peroxide. Results showed that the analytical signals increased on decreasing flow rates. It was decided that although lower flow rates (less than 0.076 mL min^{-1}) produced higher signals as the dwell time was increased, the results at the lower flow rates were much noisier. Therefore the optimum combined total flow rate was taken to be 0.076 mL min^{-1}. It should also be noted that at lower flow rates mixing by diffusion and analysis times also increase.

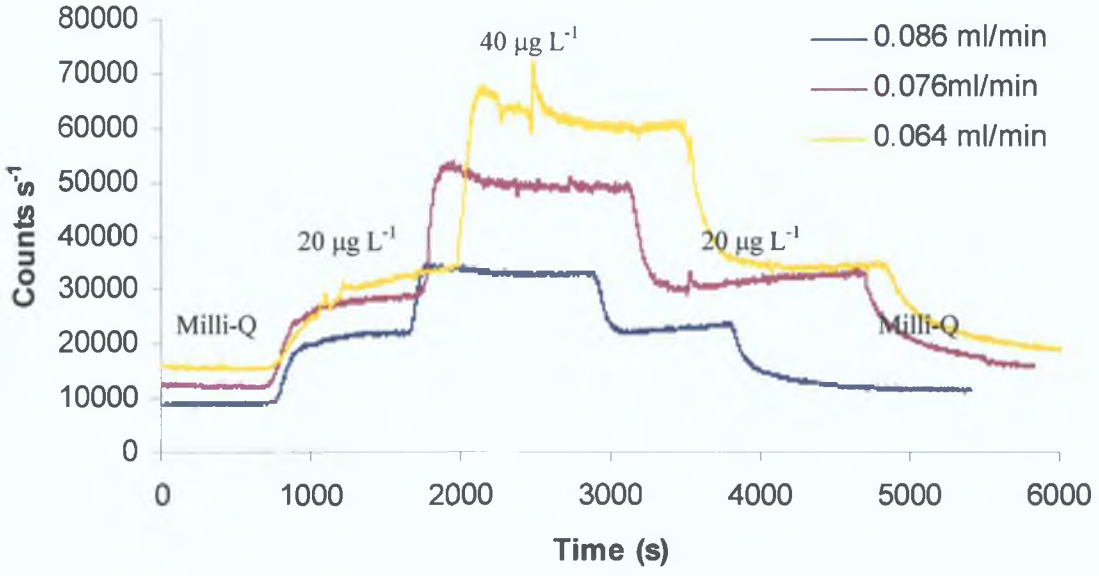

Figure 3.25: Optimisation of flow rates using stepwise graph from 0 to 40 µg L^{-1} copper (II). Reagent conditions: 0.07 mM 1,10-phenanthroline, 0.10 mM CTAB, 0.075 M NaOH and 5 % H_2O_2.

3.3.7 Calibration Study (Stage II)

Using the optimised conditions, a series of measurements were made with concentrations of copper (II) ranging from 10 to 50 µg L^{-1}. The reagent conditions used were the same as before. A stepwise graph was produced over this concentration range and can be seen in Figure 3.26. Each copper (II) standard was continuously pumped through the system.

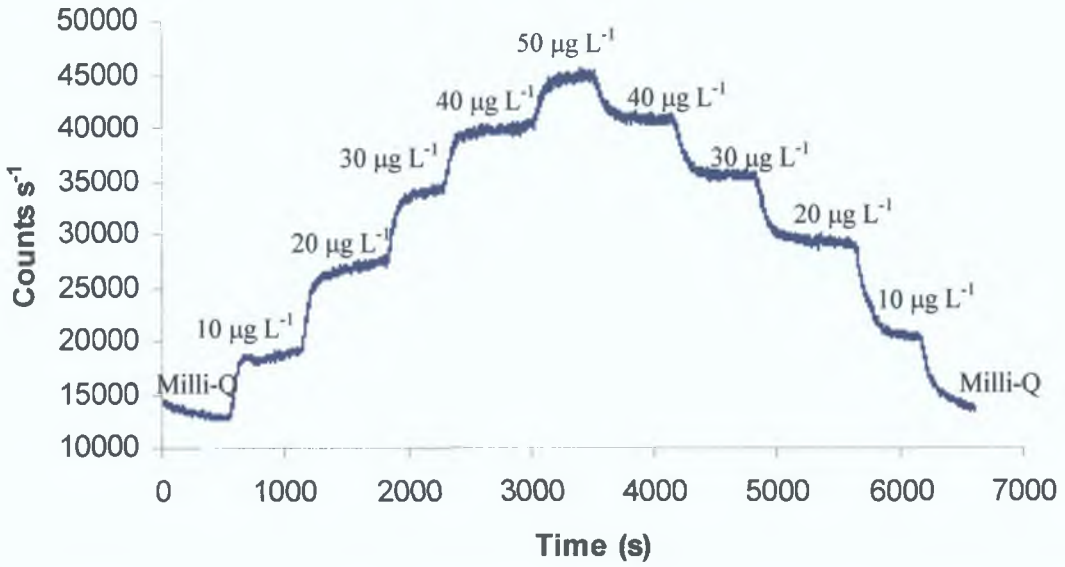

Figure 3.26: Stepwise graph of copper (II) standards between 10 and 50 µg L^{-1}. Reagent conditions: 0.07 mM 1,10-phenanthroline, 0.10 mM CTAB, 0.075 M NaOH and 5 % H_2O_2.

The resulting peak signals were plotted as a function of concentration versus chemiluminescence intensity (counts s^{-1}) and the results were found to produce a good linear correlation ($R^2 = 0.9931$) within this given concentration range as can be seen in Figure 3.27. Copper (II) was readily determined at levels as low as 10 µg L^{-1} (S/N = 7), with the S/N ratio above the norm of 3 suggesting that upon further work, a lower limit of detection could possibly be obtained. As two replicate injections were made for each standard, the error associated with each was calculated by the difference between the two values and was calculated to be < 4.8 %.

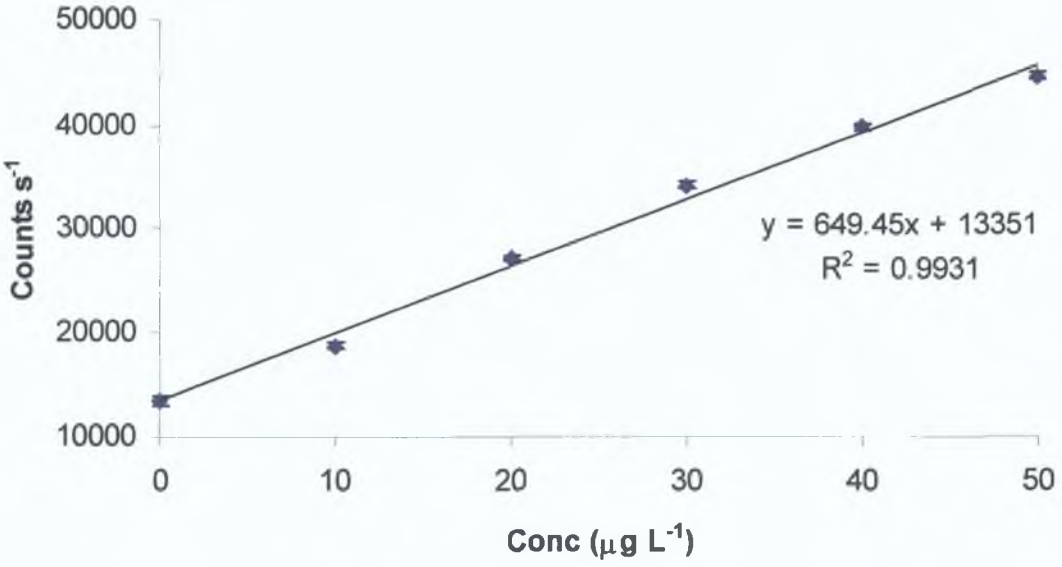

Figure 3.27: Standard calibration curve for copper (II) standards over the concentration range 10 to 50 µg L^{-1} where $R^2 = 0.9931$.

3.3.8 Real Samples (Stage II)

The on-line analysis of drinking water was undertaken, using the microfluidic manifold and conditions described above. The drinking water from a laboratory tap was continuously fed via an in-line filter to the sample inlet of the manifold. Within the sample line a switching valve was placed which allowed the tap water to either by-pass or be passed through the PRP-X800 itaconic acid micro-column (pre-buffered to pH 4.0) detailed in chapter 2, allowing verification that the detector response was due to copper (II) only. The results of the experiment outlined in Figure 3.28 show the concentration of copper (II) found within the laboratory tap supply was approximately 80 μg L^{-1} (much less than the 2 mg L^{-1} limit specified by the World Health Organisation (WHO) and the European Water Quality Directive [10]). On-line passage of the water through the itaconic acid column completely removed the chemiluminescence signal, indicating that the sample matrix was not causing significant interference in this application.

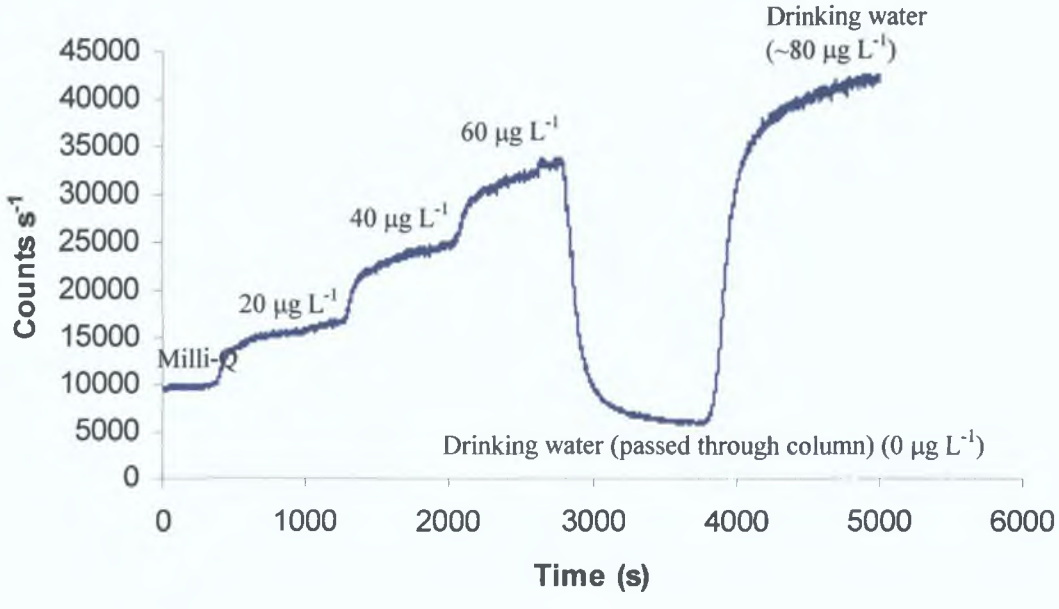

Figure 3.28: Comparison of drinking water samples passed through and not passed through the itaconic acid column. Reagent conditions: 0.07 mM 1,10-phenanthroline, 0.10 mM CTAB, 0.075 M NaOH and 5 % H_2O_2.

The use of direct analysis of drinking water removed the need for a preconcentration column and also the problems associated with it including pressure and pH effects and incomplete retention and recovery of the analyte.

3.3.9 Reproducibility and Linearity Studies (Stage II)

Reproducibility and linearity studies (n = 3) were carried out as shown in Figure 3.29. The conditions used in this work were the same as before. The total flow rate was 76 μl min^{-1} and the reagent concentrations were 5 % hydrogen peroxide, 0.07 mM 1,10-phenanthroline, 0.10 mM CTAB and 0.075 M sodium hydroxide. In this case, samples were directly analysed for 8 minutes with Milli-Q water between each sample run for 8 minutes.

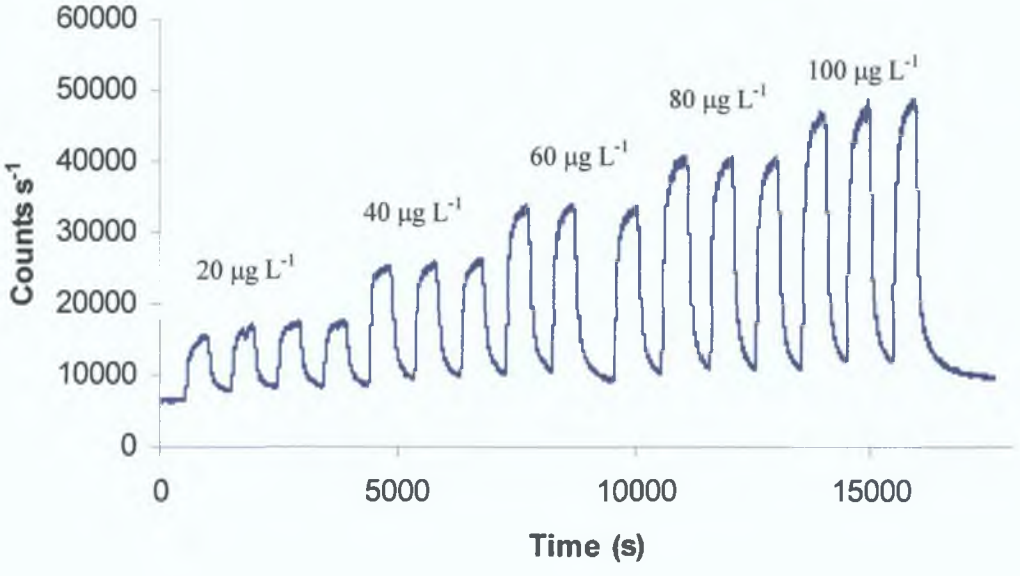

Figure 3.29: Reproducibility studies from 20 to 100 μg L^{-1} copper (II) standards.

These results were found to be linear (n = 3) over the concentration range 0 to 100 μg L^{-1} producing a R^2 value of 0.9975 and copper (II) could be easily determined at levels as low as 20 μg L^{-1} as can be seen from Figure 3.30. As three replicate injections were made for each copper standard, the error associated with each was calculated by the difference between the highest and lowest value for each standard. It was found that the difference was calculated to be < 2.5 %, which was deemed acceptable for these results.

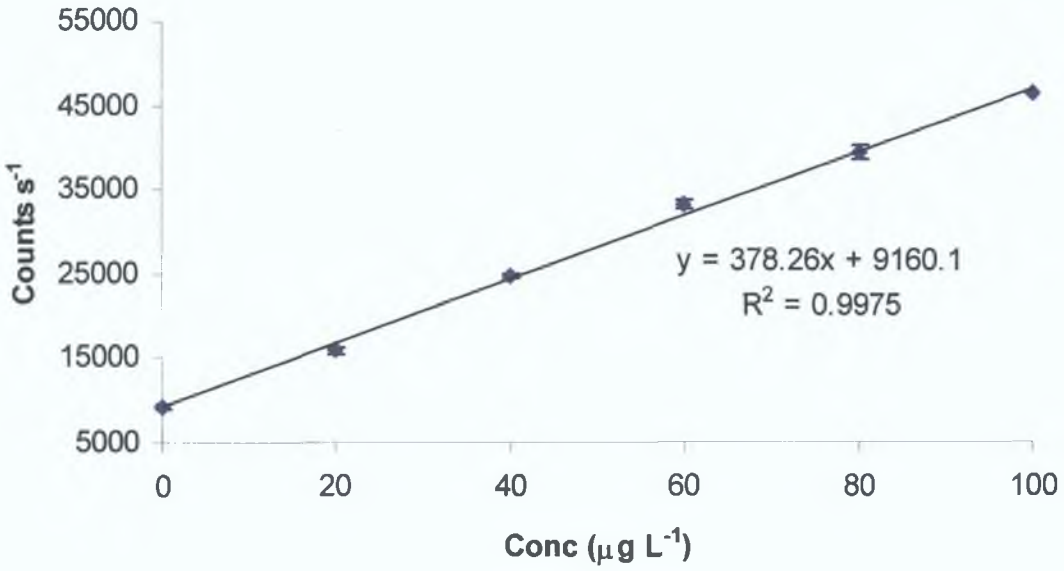

Figure 3.30: Copper (II) linearity studies over the concentration range 0 to 100 µg L^{-1} where R^2 = 0.9975.

3.3.10 Other Micro-Fabrication Techniques

It was decided to compare different micro-fabrication techniques with the hot embossing technique used previously. Two different techniques were investigated: micro-milling and laser ablation. Each technique produced different channel profiles and surface morphologies. For direct comparison of the manifolds produced by the new techniques, with the hot embossed manifold, detector response and linearity were determined on each manifold using identical reagent concentrations and flow rates.

3.3.10.1 Micro-milling

In this work, the micro-milling machine (Datron 3-D M6 Micromachining Centre), which was previously used to make the brass master for the hot embossing method, was used to make the microfluidic channels in the PMMA. The PMMA substrate was milled directly using the micro-miller. This method was much quicker than hot embossing as the brass master did not need to be fabricated and the actual process was quicker and simpler than the hot embossing technique. However, the surface of the channels were not as smooth as those produced by the hot embossing method and blockages could easily occur in these channels due to particles which could lodge in

between the channels. The channels were bonded and connected to micro-bore PEEK tubing as previously described for the hot embossing technique.

3.3.10.1.1 Micro-milled Microfluidic Manifold

Figure 3.31 shows the reaction peaks generated for 20 to 100 μg L^{-1} copper (II) standards using the milled chip. The reagent concentrations and flow rates were identical to those used in the hot embossed studies. The total flow rate was 76 μL min^{-1} and the reagent concentrations were 5 % hydrogen peroxide, 0.07 mM 1,10-phenanthroline, 0.10 mM CTAB and 0.075 M sodium hydroxide. In this case, samples were again analysed every 8 minutes with Milli-Q water between samples for 8 minutes. As seen by these results a certain degree of adsorbance of the reagents onto the channel walls can occur, which may be slowly washed off during the Milli-Q water washing step. In this case, there seemed to be slight baseline drift, but, as previous work has shown, the system does return to the starting baseline when allowed sufficient recovery time and although this may increase individual sample analysis time, for longer term on-line monitoring purposes this should not be a significant problem.

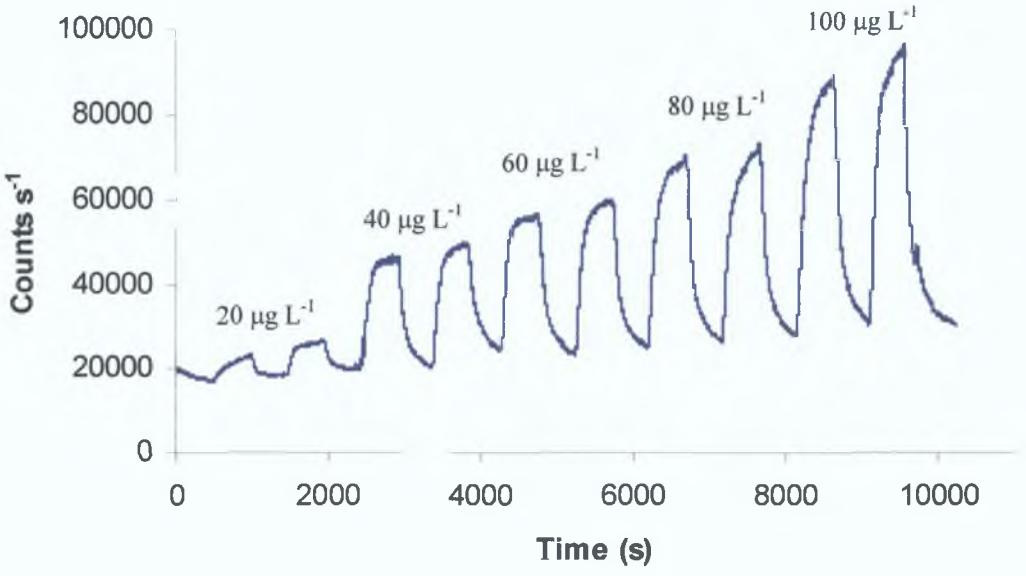

Figure 3.31: Reaction peaks generated for 20 to 100 μg L^{-1} copper (II) standards. Reagent conditions: 0.07 mM 1,10-phenanthroline, 0.10 mM CTAB, 0.075 M NaOH and 5 % H_2O_2.

The results were found to be linear over the concentration range 20 to 100 μg L^{-1} producing a R^2 value of 0.9884 and copper (II) could be easily determined at levels as low as 20 μg L^{-1} (Figure 3.32). As two replicate injections were made for each copper standard, the error associated with each was calculated by the difference between the two values for each standard. It was found that the difference was calculated to be < 5.2 %, which was deemed acceptable for these results.

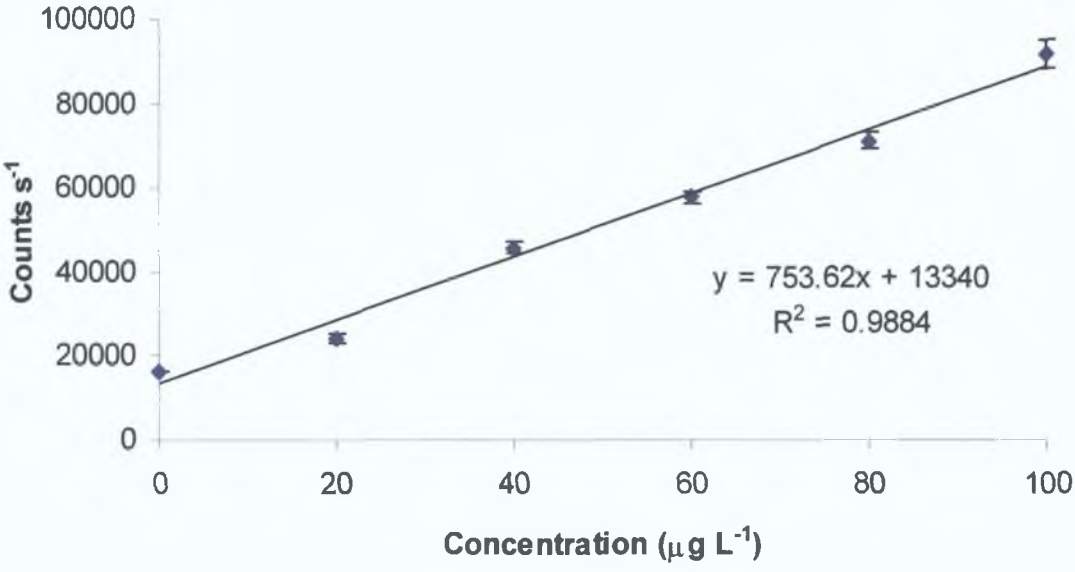

Figure 3.32: Copper (II) linearity studies (n = 2) over the concentration range 20 to 100 μg L^{-1}.

3.3.10.2 Laser Ablation

The process of laser ablation allows structures such as channels and through-holes to be produced, which means a complete plastic flow manifold could be fabricated by this method. In this work a KrF excimer laser (Optec Micromaster System), which emits laser photons at 248 nm, was used to make the microfluidic channels. The laser mask width was set to 250 μm, with a laser energy density of 1358 mJ cm^{-2} and a frequency of 50 Hz, resulting in a machining speed of 0.250 mm s^{-1}. The polymer substrate used was PMMA and the channels were sealed and connected to PEEK tubing as before. The dimensions of the mixing channel were 730 mm in length with an internal width and depth of 250 μm x 250 μm (triangular cross section). The reaction/detection channel was 210 mm in length and 250 μm x 250 μm in width and depth with a theoretical approximate internal volume of between 16 and 22 μL.

3.3.10.2.1 Laser Ablated Microfluidic Manifold

Figure 3.33 shows the reaction peaks generated for 25 to 100 μg L^{-1} copper (II) standards using the laser produced microfluidic manifold. The reagent concentrations and flow rates were identical to those used in the hot embossed and micro-milled studies. The total flow rate was 76 μL min^{-1} and the reagent concentrations were 5 % hydrogen peroxide, 0.07 mM 1,10-phenanthroline, 0.10 mM CTAB and 0.075 M sodium hydroxide. In this case, samples were once more analysed every 8 minutes with Milli-Q water between samples for 8 minutes.

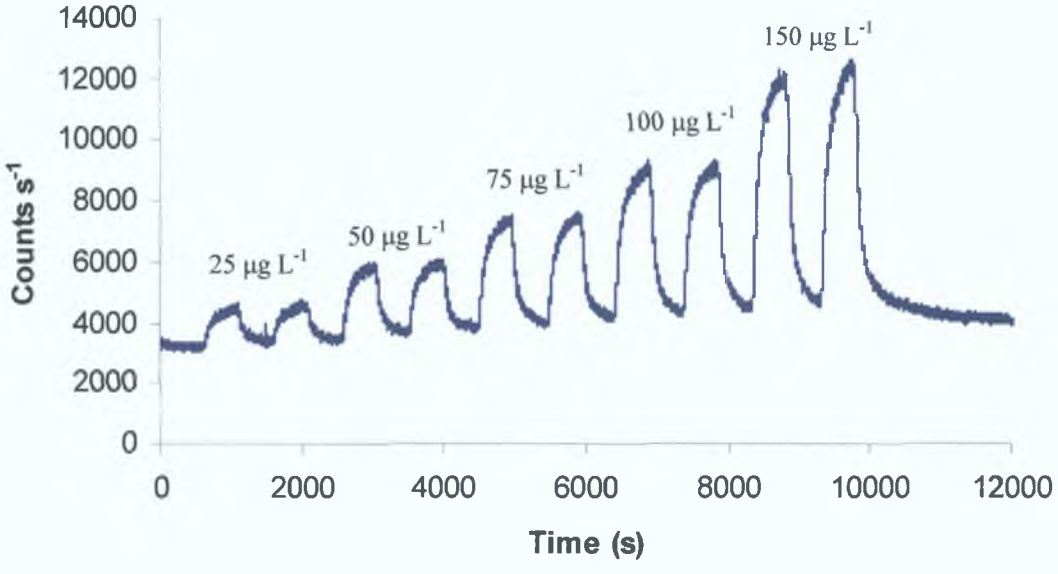

Figure 3.33: Reaction peaks generated for 25 to 150 μg L^{-1} copper (II) standards using laser produced plastic manifold. Reagent conditions: 0.07 mM 1,10-phenanthroline, 0.10 mM CTAB, 0.075 M NaOH and 5 % H_2O_2.

The results are linear (n = 2) over the concentration range 0 to 150 μg L^{-1} producing a R^2 value of 0.9979 and copper (II) could be easily determined at levels as low as 25 μg L^{-1} (Figure 3.34). As two replicate injections were made for each copper standard, the error associated with each was calculated by the difference between the two values for each standard. It was found that the difference was calculated to be < 4.6 %, which was deemed acceptable for these results.

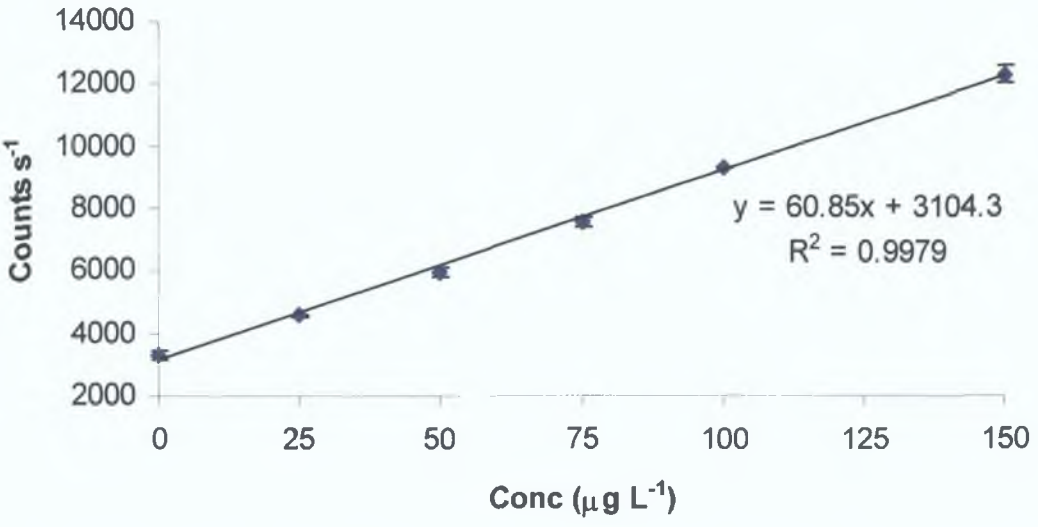

Figure 3.34: Copper (II) linearity studies (n = 2) over the concentration range 0 to 150 µg L^{-1} where $R^2 = 0.9979$.

Reproducibility studies were carried out using five replicate analyses of the 75 µg L^{-1} copper (II) standard (Figure 3.35). The reproducibility was good at this 75 µg L^{-1} level and the % RSD for peak height was found to be 3.4 % for five replicate injections.

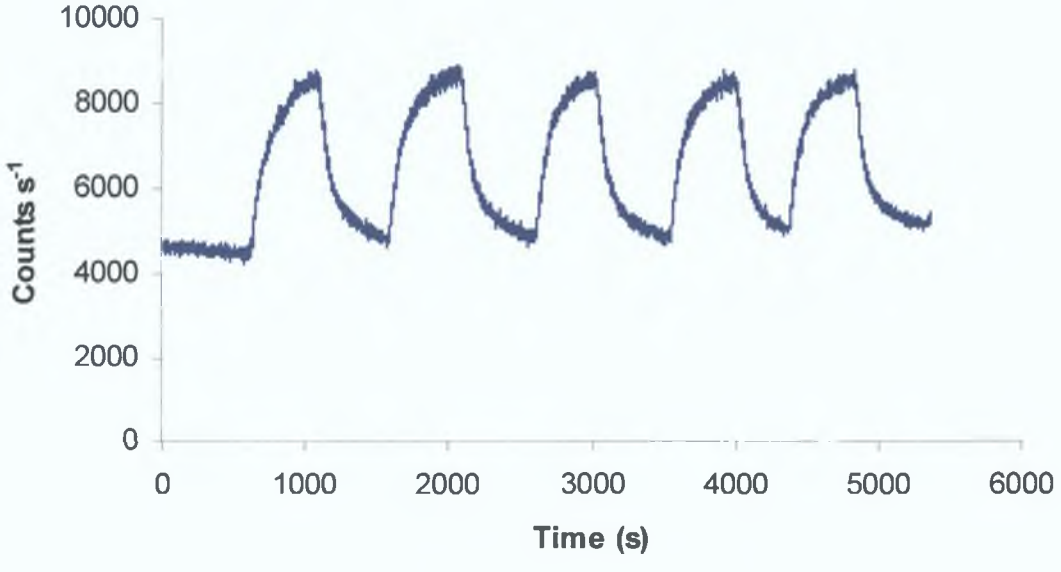

Figure 3.35: Reproducibility studies using 75 µg L^{-1} copper (II) standard (n = 5) RSD = 3.4%. Reagent conditions: 0.07 mM 1,10-phenanthroline, 0.10 mM CTAB, 0.075 M NaOH and 5 % H_2O_2.

3.3.10.2.2 Application to Certified Reference Material

The standardisation and certification of methods are achieved using certified reference material, to demonstrate the reliability of the trace level metal determination. In this case, the simplest way to assess the potential analytical use and the accuracy of the method was to analyse a reference material for which there are known concentrations of the analyte of interest. The proposed method was verified using an international certified Standard Reference Material (SRM) from the National Institute of Standards and Technology (NIST), which was analysed for copper (II). This sample SRM 1640 was composed of natural fresh water (river) collected from Clear Creek, CO, which had been filtered and acidified with 0.5 mol L^{-1} nitric acid. This sample was certified to contain 85.2 μg L^{-1} ± 1.2 μg L^{-1} copper (II). These samples have been rigorously analysed using a number of analytical techniques for many trace metals including copper (II). The acidified SRM sample was neutralised using sodium hydroxide and was diluted by 50 % with Milli-Q water, prior to the analysis. This sample was then analysed using the above mentioned laser ablated manifold. Firstly, a 50 and 100 μg L^{-1} copper (II) standard were analysed for 8 minutes with Milli-Q water between samples for 8 minutes. A 50 % dilution of the NIST standard was then analysed for 8 minutes as before. The resultant signals can be seen in Figure 3.36. Excellent agreement was found between the FI-CL values and the certified values for the NIST standard. The 50 % diluted sample was found to contain approximately 43 μg L^{-1} copper (II) which corresponds to the ~ 86 μg L^{-1} in the SRM, within ± 6 % (± 2.6 μg L^{-1}) of the true value, representing excellent accuracy for the microfluidic device when analysing a complex freshwater sample for trace amounts of copper (II).

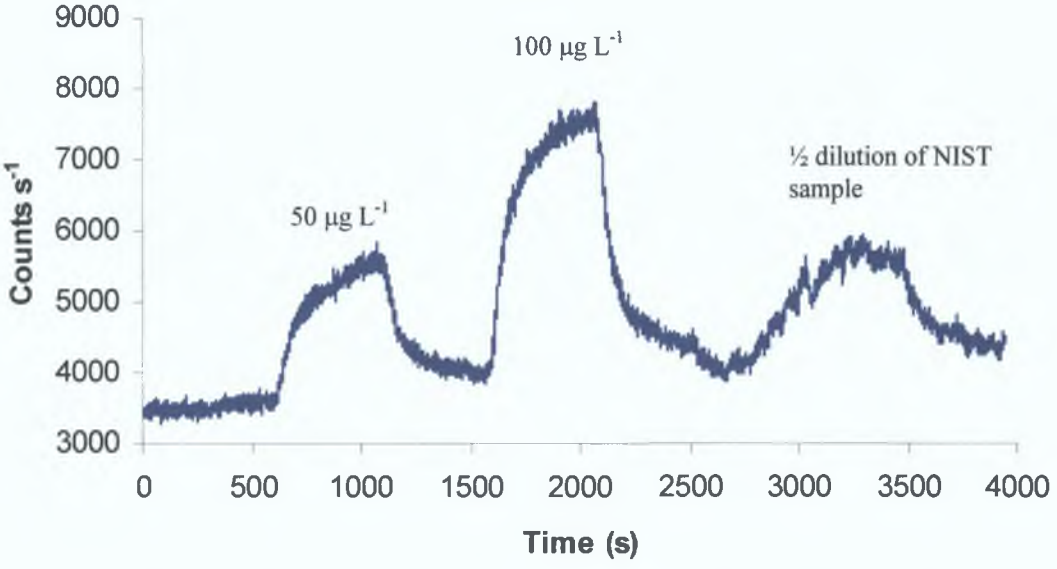

Figure 3.36: Analyses of 1 in 2 dilution of NIST standard, which contained approximately 43 µg L^{-1} copper (II). Reagent conditions: 0.07 mM 1,10-phenanthroline, 0.10 mM CTAB, 0.075 M NaOH and 5 % H_2O_2.

3.3.11 Comparison of Hot Embossed, Laser Ablated and Micro-milled Microfluidic Manifolds

To summarise, Figure 3.37 shows a comparison of the standard calibration results obtained from the hot embossed, laser ablated and micro-milled microfluidic manifolds for increasing copper (II) standard solutions. As can be seen from this, the directly micro-milled manifold resulted in the largest comparative unit response with a calibration slope of 753 counts s^{-1} approximately for each µg L^{-1} of copper (II) compared to approximately 378 counts s^{-1} for each µg L^{-1} of copper (II) for the hot embossed method. However, in the case of the micro-milled manifold, the background noise increased considerably.

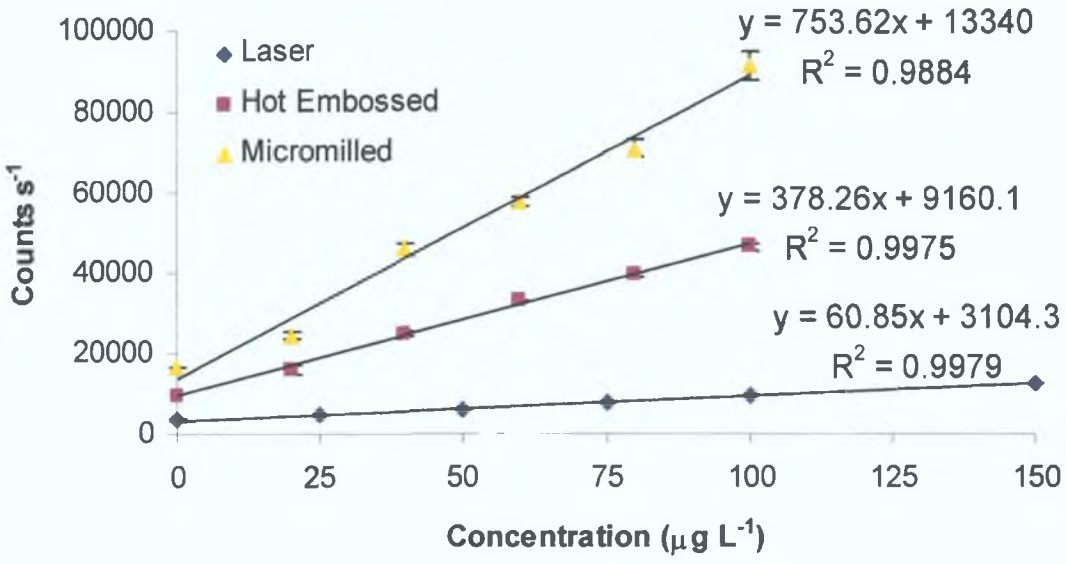

Figure 3.37: Comparison of standard calibration curves for copper (II) from the hot embossed, laser ablated and micro-milled microfluidic manifolds.

The laser ablated manifold was found to give the lowest unit response with the lowest calibration slope, only 61 compared to the above values. However the manifold also produced the most linear response over the greatest concentration range 0 – 150 µg L^{-1} (R^2 = 0.998, standards injected in duplicate). In addition to the above the laser ablated manifold also resulted in the lowest background noise, resulting in a linearity limit of approximately 20 µg L^{-1} copper (II). The reason for the lower response and noise with this manifold is simply related to the fact that the laser ablation process results in the shallow 'V' shaped channels which effectively reduces the channel volumes considerably (~ 50 %), compared to the alternative fabrication methods. To partially compensate for this profile the laser ablated channels were cut 250 µm wide by 250 µm deep, hence the reaction/detection channels of the ablated manifolds was calculated to be within the range 16 – 22 µL compared to 21 – 30 µL for the hot embossed manifold.

Table 3.1 shows the comparative analytical performance data determined for the three microfluidic manifolds, and those data obtained for standard flow injection analysis and the initial larger scale hot embossed manifold. The data shown represents that obtained under the specific reagent conditions used within this study only.

Table 3.1: Analytical performance data for developed methods.

Fabrication method	Flow rates (ml min^{-1} per reagent)	Linear range ($\mu g\ L^{-1}$)	R^2 value
Standard FIA	0.7	1 – 50	0.995
Hot Embossing 1000 x 900 μm*	0.06	50 – 1,000	0.996
Hot Embossing 200 x 200 μm*	0.025	0 – 100	0.998
Micro-Milling 200 x 200 μm*	0.025	0 – 100	0.983
Laser Ablation 250 x 250 μm*	0.025	0 – 150	0.998

* It is important to note that the exact depth of the channels could not be ascertained because when bonding of the top plate occurs the channel depth is reduced as discussed in 3.2.1.

3.4 Conclusion

This chapter describes the design and fabrication of microfluidic flow cells and the development of a manifold designed for the measurement of chemiluminescence in miniaturised systems. A number of different manifold designs and fabrication techniques were compared and contrasted, which were important in the overall design of the system. A complete miniaturised flow system was developed based on miniaturised peristaltic pumps, a microfluidic plastic manifold and a compact photomultiplier tube. Data collection was computer controlled using a laptop computer. The procedures were shown to be accurate by obtaining good agreement with certified values for a certified SRM sample.

3.5 References

1. A. Manz, J.C.T. Eijkel, *Pure Appl. Chem.*, 73(10) (2001) 1555-1561.
2. J.P. Kutter, *TrAC Trends in Anal. Chem.*, 19(6) (2000) 352-363.
3. J. Kuncova, *Lab-on-a-chip* 2000, Tampere University of Technology, Finland, viewed 27 October 2003 <http://www.ad.tut.fi/aci/courses/76527/Seminars2000/Lab-on-a-Chip.pdf>
4. Y. Lv, Z. Zhang, F. Chen, *Talanta*, 59 (2003), 571-576.

5. G.M. Greenway, L.J. Nelstrop, S.N. Port, *Anal. Chim. Acta*, 405 (2000) 43-50.
6. A.M. Jorgensen, K.B. Mogensen, J.P. Kutter, O. Geschke, *Sens. Actuators B*, 90 (2003) 15-21.
7. A. De Mello, *Lab on a chip*, 2 (2002) 31N-36N.
8. H. Becker, C. Gartner, *Electrophoresis*, 21 (2000) 12-26.
9. L. Martynova, L. Locascio, M. Gaitin, G.W. Kramer, R.G. Christensen, W.A. MacCrehan, *Anal. Chem.*, 69 (1997) 4783-4789.
10. *Europa – Environment – Water quality in the EU – Drinking Water* 2003, Gateway to the European Union, Jacques Delors European Information Centre, 1400-026 Lisbon, Portugal, viewed 18 November 2004 <http://europa.eu.int/comm/environment/water/water-drink/index_en.html>

CHAPTER FOUR

INTEGRATED ON-CHIP MICRO-COLUMN SEPARATION SYSTEM

4.1 INTRODUCTION

Many chemiluminescence reactions suffer from poor selectivity. For example, the oxidation of luminol in a basic aqueous solution is known to be catalysed by several trace metal ions (at nmol L^{-1} to sub-nmol L^{-1} levels), such as chromium (III), cobalt (II), copper (II), iron (II) and titanium (II) [1]. These interfering metal ions can alter the quantitative relationship between the luminescence produced and the analyte concentration, making analyte preconcentration or separation an important factor in the analysis.

Many of the earlier accounts (pre-1975) of trace metal determinations in complex matrices, such as seawater, were erroneous due to the application of inaccurate analytical procedures to the sample matrices, and resulted in metal concentrations that were many orders of magnitude higher than the true value [2]. Contamination during the sampling or analysis stages was often the main reason for these incorrect results. In a sample matrix like seawater, the high salt content provides sodium chloride (~ 0.5 M), calcium (~ 400 mg L^{-1}), magnesium (~ 800 mg L^{-1}) and other ions at high concentrations, that can interfere in the analysis of trace metal ions in the sample and can inhibit accurate measurement. As a result, some form of sample pre-treatment can often be required prior to the analysis to reduce the associated ion interference and to minimise ion suppression. The interfering agents can either be masked or completely removed from the sample before the analysis.

A number of techniques used for separation or preconcentration purposes, including solvent extraction, precipitation or evaporation techniques, can be time consuming and not easily automated. More stringent environmental concerns and controls are making the use and disposal of large amounts of organic solvents more difficult. The concept of solid phase extraction by use of chelating resins was first introduced in 1968 by Riley and Taylor [3]. The use of the Chelex-100 resin, containing an iminodiacetic acid (IDA) functional group, was employed for the preconcentration of trace metal ions from a seawater matrix. Similar methods have been used in recent years for matrix removal and preconcentration during trace metal ion determinations.

There are a number of advantages in combining a chelating stationary phase for preconcentration purposes with chemiluminescence detection. This approach provides systems with high sensitivities, which are useful for the determination of trace metal ions in complex sample matrices, with interference effects minimised. This approach also has advantages over alternative extraction and separation techniques, such as reduced solvent use, rapid analysis times and reduced contamination from trace level metal residues in the extra reagents used in alternative techniques. The use of on-line column preconcentration as part of a total analysis system (TAS) offers potential over and above conventional batch procedures. On-line columns offer greater efficiency than off-line procedures as a larger number of samples can be processed. In addition, sample consumption is much lower than conventional batch procedures, and the closed preconcentration system reduces the risk of contamination in comparison to the conventional system.

The search for inexpensive mass production of integrated chemical separation and preconcentration systems, with superior analytical performance using modern micro-fabrication technology, gave rise to much research activity over the past number of years. The separation of sample components generally represents an essential step in most trace metal analyses, but it is often the most difficult step in the analysis and can frequently be performed separately from the reaction and detection steps. There are a variety of examples of chip-based sample pre-treatments but there is no single universal approach available [4]. These pre-treatment procedures are individually tailored to the sample under investigation and the analytical method that will be used.

It was decided in the work presented here, to incorporate a stationary phase for separation/preconcentration purposes into the plastic chip device. The plan was to miniaturise and integrate all the components of a flow-through manifold into one unit. Characteristically, a total analysis system (and ultimately a μTAS) eliminates dependence on external laboratory analyses resulting in a totally complete and independent system. This meant that instead of the individual manifold components, such as the separation column, mixing channel and detection channel, all being joined by means of flexible tubing and connectors, the whole system of channels was

fabricated into the planar surface of a plate (in this case the PMMA substrate), which is significantly thick enough to accommodate the packed column and the system of microchannels, as well as the inlet and outlet holes for the connection of micro-bore tubing. These devices should be robust, capable of the analysis of very small sample volumes, avoid clogging of the microscopic features in the chip and be suitable for high-throughput analyses [5]. The use of two different stationary phases, one based on a polymeric monolith and the other based on chelating resins for on-chip preconcentration were investigated during the course of this work.

4.1.1 Monolithic Stationary Phases

A monolithic stationary phase is a continuous unitary porous structure that is made from in-situ polymerisation or consolidation inside column tubing [6]. Two types of monolithic stationary phases are commonly used; silica based monoliths and polymeric based monoliths. A monolithic column based on polymer materials contains a mixture of a monomer, cross-linker, initiator and one or two porogenic solvents. Polymerisation can occur when the mixture is heated or subjected to UV irradiation. A solvent is then pumped through to remove the porogens and other soluble compounds remaining on the column. The most commonly used polymers are polystyrene, polymethacrylate and polyacrylamide. The monolith structure and porosity are influenced by the porogen content in the reaction mixture, the quantity and quality of the initiator, the ratio of monomers/polymers and the temperature if the polymerisation is thermally induced.

4.1.2 Chelating Stationary Phases

The second type of stationary phase investigated during the course of this work was based on the incorporation of a particle type chelating stationary phase. Chelating resins can be used for the separation and preconcentration of metal ions at trace levels because of their selectivity. Basically, chelating resins are ion exchange resins, which contain different functional groups and can complex metal ions. The insertion of suitable functional groups into the polymeric matrix makes it capable of reacting with metal ions or metal species under certain conditions to form chelate rings, making these resins more selective than ordinary cation and anion exchange

resins. This means that the process can be applied to a multitude of different analyses including the determination of trace metal ions in a large variety of samples such as tap water, natural waters, biological and alloy samples [7]. The correct choice of chelating resin is critical to ensure successful extraction. There are a number of different requirements that are important in the selection of a chelating agent for a flow injection analysis chemiluminescence system:

1. The chelating agent should be selective for the target analyte.
2. There should be little swelling or contraction of the resin.
3. As many chemiluminescence reactions require a specific alkaline environment, the analyte should elute from the resin with a weakly acidic solution.

Three different commercially available chelating resins were investigated during the course of this work. The first, Duolite C-467 resin, is a macroporous, styrene divinylbenzene resin that contains an aminophosphonic functional group. The second, Chelex-100 which contains an iminodiacetic acid functional group attached by a $-CH_2-$ link to a styrene support. The final resin investigated was Duolite GT-73, which is a macroporous, polystyrene resin containing a thiol functional group. The structures of the three resins can be seen in Figure 4.1.

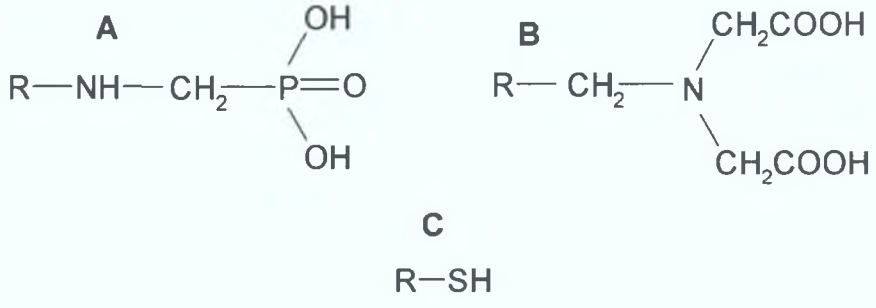

Figure 4.1: Structure of Duolite C-467 (A), Chelex-100 resin (B) and Duolite GT-73 (C).

Resins with aminophosphonic acid functional groups are a well-established group of chelating ion exchangers having an increased selectivity for toxic heavy metals, such as uranium, thorium and other trace metals from water samples [8]. The aminophosphonic acid chelating group is a potentially tridentate ligand (as it has two

bonding sites at the phosphonic acid group and one coordination site at the secondary nitrogen atom). However, it is more likely to act as a bidentate ligand at low pH values (chelation in this case occurs through the two oxygen atoms of the phosphonic acid group).

As mentioned earlier, Chelex-100 was originally described by Riley and Taylor in 1968 [3]. Resins with IDA functional groups are the most commonly used resins for chelation purposes in metal analyses due to the reasonably fast kinetics combined with the good selectivity of this particular functional group. Resins of this type are termed tridentate ligands as a result of the three donor atoms (one nitrogen and two oxygen atoms), which are available for chelation purposes. These resins show a high affinity towards transition metals along with the ability to provide good selectivity. The primary application of IDA-based resins has been for the determination of trace metals in seawater or polluted seawater samples due to its strong preference for complexing transition metals (polyvalent metals) over alkali and alkaline earth metals, which are present at high concentrations in seawater samples.

Resins containing a thiol (also termed mercapto/sulphydryl) functional group are classed as monodentate ligands and have one donor atom (a sulphur atom) available for chelation purposes. These resins have the unique ability to bind cationic and complexed forms of mercury [9]. Thiol-based resins also have a binding affinity for other soft acid cations such as silver (II), cadmium (II), copper (II) and lead (II). These resins show minimal interference from alkali and alkali earth metals, such as sodium, magnesium and calcium.

4.2 Experimental

4.2.1 Preparation of Monolithic Stationary Phases

The polymer-based monoliths used in this work were prepared using four volumes of a mixture of polystyrene (PS) and divinyl benzene (DVB) (50:50 v/v), which were both previously distilled under vacuum prior to use, and using azobisisobutyronitrile (AIBN) (1 wt % with respect to the monomers) as the initiator with six volumes of dodecanol as the porogenic solvent, in a similar method to that used by Wang *et al.*

[10]. All of the reagents used here were obtained from Sigma Aldrich Ltd., Dublin, Ireland.

The PS-DVB monoliths were prepared in short separation channels fabricated from PMMA. A series of channels were fabricated by micro-milling to produce a number of 5 mm holding channels (internal width of 1000 μm, depth ~ 1000 μm) in a sheet of PMMA. The micro-miller was used instead of the laser for this work as fabricating a channel of this depth was deemed to be too laser intensive. To laser produce a channel of these dimensions would require the laser to overlap, therefore a milled channel in this case was more easily produced and could be more accurately characterised than a laser fabricated one. An inlet and outlet channel of approximately 2 mm in length (250 μm width x 250 μm depth) was fabricated at either end of the monolithic holding channel by laser ablation. An inlet and outlet hole were drilled into the top-plate prior to bonding to which micro-bore PEEK tubing was later attached. The separation channels were then bonded to a top plate, as before using the hot embosser, to produce a closed channel device. The PS-DVB monolithic mixture was then injected into the closed channels and the radical polymerisation process was carried out in one of two different ways. The first method of polymerisation employed the use of temperature, whereby the device was placed in an oven at 70 ^{o}C for varying lengths of time up to 24 hours, while the second method involved the use of UV irradiation instead of temperature for the polymerisation of the PS-DVB monolith. The channels were exposed to the UV light for a range of times, varying from 10 seconds to 5 hours.

4.2.2 Preparation of Chelating Stationary Phases

The use of three different resins was investigated in this work, Duolite C-467, Duolite GT-73 and Chelex-100. All of the resins were obtained from Sigma Aldrich Ltd., Dublin, Ireland. These chelating resin beads had a mean diameter of 500 μm to 700 μm, which allowed them to be retained in the storage/holding chamber without the use of frits. The resins showed little sign of swelling or shrinkage (except in the case of Chelex-100, discussed in section 4.3.2.2.1), once they had been hydrated before use and were kept wetted throughout. There was very little back-pressure

from these columns as they were short in length and were not tightly packed which allowed a fairly even flow around the beads in the column.

Here a series of 26 micro-columns (holding chamber, containing chelating resin beads) were successfully fabricated by micro-milling and bonded into a single piece of PMMA (Figure 4.2). Each individual chamber was fabricated using the micro-miller, which was used to etch a channel of dimensions 1mm x 1mm x 15 mm into a base plate of PMMA. Following this, a flow channel of approximately 3 mm (250 μm x 250 μm) was fabricated at either end of the holding chamber, to allow flow through the micro-column and to create a weir-type structure to hold the resin particles in place. The hydrated chelating resin was then placed into the holding chamber before a top plate of PMMA was bonded to seal the chamber and flow channels. Once the base plate, containing the chambers was bonded to the top plate of PMMA, the chelating resin beads were retained within the enclosed holding chamber, allowing them to act as a chelating micro-column for preconcentration/separation purposes.

An inlet and outlet hole were drilled into the top-plate of PMMA, prior to bonding, to which micro-bore PEEK tubing was later attached. Similar to the fabrication of the holding channels for the monolithic columns, these chambers were fabricated by milling, as fabricating channels of these dimensions were deemed too laser intensive. As mentioned the chelating resin was hydrated with Milli-Q water before it was placed into the chamber, as problems due to swelling may arise during the re-hydration process if the resin was added in its dry form.

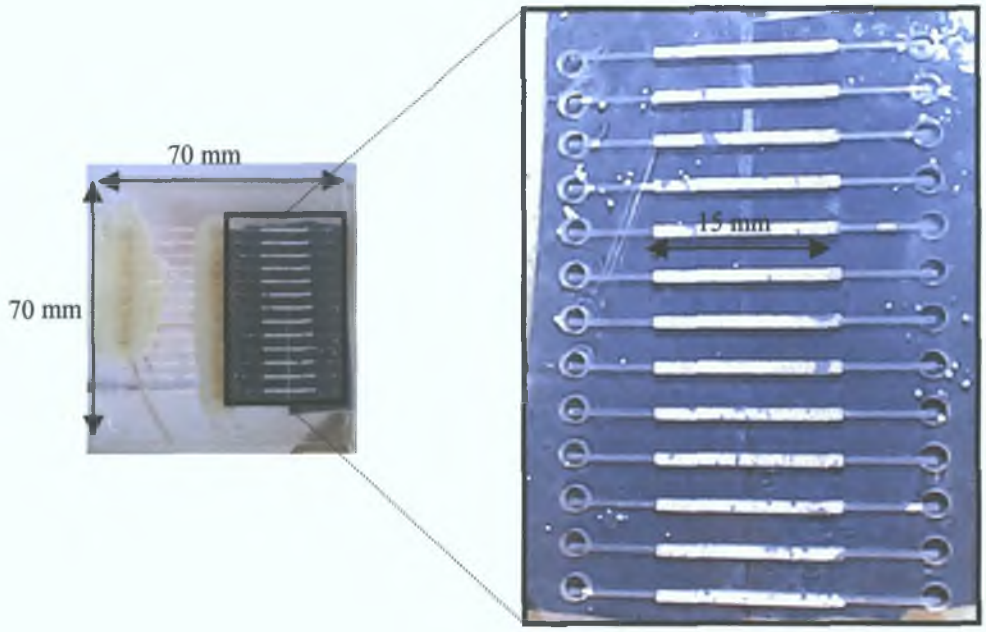

Figure 4.2: Series of 26 micro-columns containing chelating resin fabricated in PMMA sheet (70 mm x 70 mm)

The volume of the column was approximately 15 μL, and the column contained approximately 25 mg of resin. It should be noted that re-fabrication of these columns resulted in a slightly different volume as the size of each resin bead was not uniform. Figure 4.3 is used to illustrate schematically the micro-column holding chamber containing chelating resin particles.

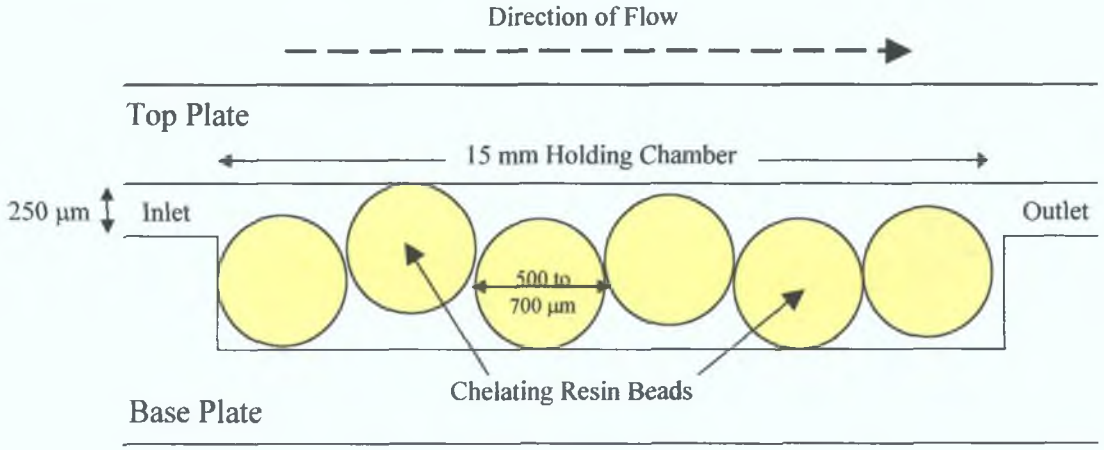

Figure 4.3: Cross-section of micro-column (holding chamber) containing the chelating resin beads.

4.2.2.1 Characterisation of Chelating Resins

The preconcentration/separation ability of each resin towards a number of different metal ions, over the pH range 2 to 5, was examined. This was carried out by investigating the amount of metal extraction (% sorption) by each resin, from the metal ion solution. The resin was added to an aliquot of pH adjusted metal solution, and the mixture was stirred continuously until the resin became saturated or had removed all of the metal ion from solution (termed batch mode). An aliquot of metal solution was analysed every 60 seconds during the batch extraction, by flame atomic absorption spectroscopy (FAAS), until all of the metal ion was extracted from solution or the capacity of the resin had been reached and no more metal extraction occured. The amount of metal extracted from solution by the resin (% sorption) was calculated using the following equation:

$$\% \text{ sorption} = [(A_0 - A_n)/A_0] \times 100 \qquad \text{(Equation 4.1)}$$

Where, A_0 is the absorbance value of metal solution at time = 0.

A_n is the absorbance value of metal solution at time = n (where n = 0,1,2,3....n min)

A Varian SpectrAA atomic absorption spectrometer was used for all metal measurements carried out during the characterisation study of the resins. Analyses were carried out under standard operating conditions of FAAS determinations (see Table 4.1). A standard single-slot nebuliser-burner head (air/acetylene burner head) was used for the flame determination of each metal and was operated at an air pressure of 60 psi and acetylene pressure of 15 psi. The nebuliser uptake rate was adjusted to give optimal response for conventional sample aspiration. All working standards were freshly prepared, prior to each analysis, as some metal solutions were not stable at low concentrations for more than a day. Standards were prepared by appropriate dilution of a 50 mg L^{-1} stock standard metal solution and were made up with Milli-Q water. Calibrations were performed using standard solutions and the instrument was optimised prior to every analysis.

Table 4.1: Table of optimum linear range and wavelength for each metal.

Metal	Optimum Wavelength (nm)	Operating Current (mA)	Optimum Linear Range (mg L^{-1})	Slit Width (nm)	Fuel/Oxidant
Copper	324.8	8	0.03-10	0.5	Acetylene/Air
Zinc	213.9	5	0.01-2	1.0	Acetylene/Air
Cadmium	228.8	4	0.02-3	0.5	Acetylene/Air
Nickel	232.0	10	0.1-20	0.2	Acetylene/Air
Lead	217.0	5	0.1-30	1.0	Acetylene/Air
Calcium	422.7	7	0.01-3	0.5	Acetylene/Air
Magnesium	285.2	4	0.003-1	0.5	Acetylene/Air
Iron	248.3	7	0.06-15	0.2	Acetylene/Air

4.2.2.2 Preliminary Chelating Resin Micro-Column Studies (Setup and Procedure using Fluorescence Detection)

Figure 4.4 shows a schematic of the manifold used for the preliminary investigations on the efficiency of the chelating micro-column. Two micro-peristaltic pumps (manufactured by BVT Technologies, Euro-link Associates, Tyne & Wear, England) were used to control the flow of the reagents. Each flow rate could be controlled independently, although the individual flow rates were both set at 30 μL min^{-1}. A Rheodyne rotary injection valve fitted with a 15 μL sample loop was used for the introduction of sample. The chelating resin micro-column was incorporated into the system after the sample loop, prior to the mixing T-piece, where the sample and reagent streams mixed before entering the detector cell. All the tubing used was micro-bore PEEK tubing (0.127 mm I.D.) with the exception of the peristaltic tubing (0.508 mm I.D. peristaltic tubing). A 10 mM sodium acetate buffer was used to buffer the micro-column and as the sample carrier stream for loading the sample onto the column. This line was then switched to a 25 mM nitric acid solution, which was used to elute the sample from the column for detection.

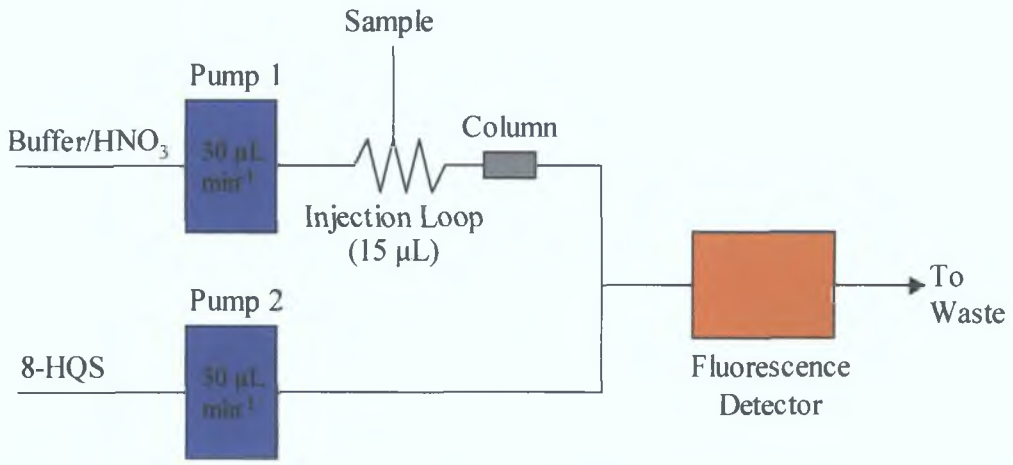

Figure 4.4: Schematic of flow manifold used for testing the efficiency of the chelating micro-column (using fluorescence detection).

In this preliminary work, *fluorescence detection was used which employed the use of 8-hydroxyquinoline 5-sulphonic acid (8-HQS) for detection purposes. A Millipore Waters 470 Scanning Fluorescence Detector (Milford, MA, USA) with a detector cell of 16 µL was used at an excitation wavelength of 360 nm and an emission wavelength of 500 nm (excitation and emission slits set at 18 nm). The fluorescence detector was connected to a data logger (Pico ADC-16), which was then connected to the PC through the RS232 serial port. This allowed the signal output from the detector to be continuously monitored throughout the analysis by the PC.

* In the course of this work, a leak in the flow system caused damage to the bi-alkali PMT, therefore the use of fluorescence detection was employed in this section of work. Instead of copper (II), zinc (II) was used during the analysis, as it is known to form a stable, fluorescent complex with 8-HQS.

A solution of 8-HQS (98 %), obtained from Sigma Aldrich Ltd. (Dublin, Ireland) was made up in an acetate buffer (buffered to pH 4.60). The concentration of 8-HQS was chosen to be 5 mM. As in previous work, all of the solutions were filtered through a 0.45 µm nylon membrane filters (Gelman Laboratories, Michigan, USA) and degassed using sonication to ensure reagent dissolution and homogeneity. They were also all made up using 'purified' Milli-Q water. The Milli-Q water (18 MΩ water obtained from a Milli-Q Plus system, Millipore, Milford, MA) was 'purified', in order to remove any other metal ions present in the water, using a chelating resin

(Duolite C-467), which was continuously stirred for 1 hour in the Milli-Q water. The Milli-Q water was then filtered and used to make up all the reagents and standards used in this study unless otherwise stated.

Initially the micro-column was buffered to pH 4.0, using a 10 mM sodium acetate buffer solution. This was a short step as the micro-column was small and did not require a long buffering time. Following this, a 15 μL aliquot of a zinc (II) standard was injected into the flowing buffer stream and loaded onto the column. The buffer was allowed to flow for a couple of minutes after sample injection to ensure that none of the sample was lodged in the interstitial pore spaces in the micro-column. The acetate buffer stream was then switched to the nitric acid stream (25 mM nitric acid solution), which subsequently eluted the zinc (II) from the column, before it mixed with the 8-HQS stream for detection by fluorescence.

4.2.2.3 Incorporation of Chelating Micro-Column into Flow Manifold (Setup and Procedure using Chemiluminescence Detection)

A new flow device was designed as shown in Figure 4.5, which incorporated a chelating micro-column holding chamber into the plastic flow device. The basic device design was similar to that described in chapter 3, with the addition of a large chamber (to act as the micro-column/resin holding chamber) directly before the mixing channel. As mentioned earlier in section 4.2.2, the holding channel itself was fabricated using the micro-miller, while the rest of the flow channels in the flow manifold were fabricated using laser ablation. The dimensions of the mixing channel were 730 mm in length by 250 μm in width and 250 μm in depth. The detection channel was 210 mm in length by 250 μm in width and 250 μm in depth. These laser produced manifolds resulted in the characteristic 'V shaped' channels as described previously in chapter 3.

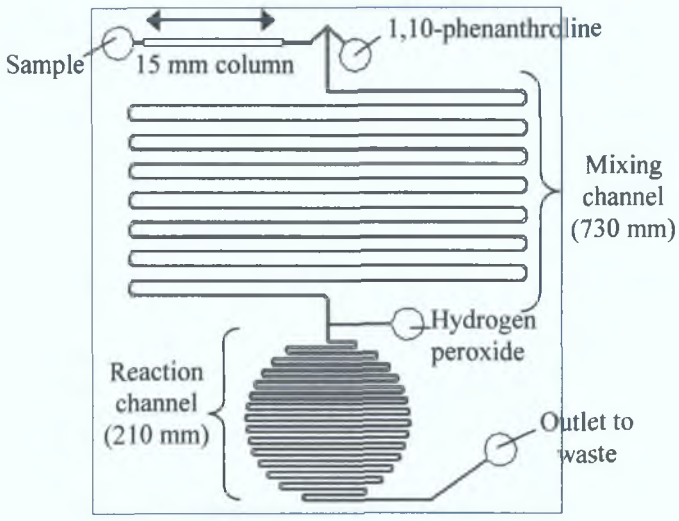

Figure 4.5: Design of flow manifold incorporating the column preconcentration system.

The experimental setup used was similar to previous flow setups. In this case, the three micro-peristaltic pumps were used for reagent delivery. The combined total flow rate used here was 102 μL min^{-1}, with each individual pump delivering a flow of 34 μL min^{-1}. It was found higher flow rates caused the manifold to leak. This manifold incorporated the use of a Rheodyne injection valve with a PEEK sample loop of 8 μL for sample introduction and a PMT was used for detection purposes**. The reagent conditions used in this work were 0.06 mM 1,10-phenanthroline, 1.3 mM CTAB, 0.075 M sodium hydroxide and 5 % hydrogen peroxide solution. The concentrations of 1,10-phenanthroline and CTAB are optimised in chapter 5. The micro-column was buffered using a 10 mM sodium acetate buffer (pH 4.7) and a 25 mM nitric acid solution was used for removing the copper (II) from the column. Figure 4.6 illustrates the flow manifold used in this setup.

**A new PMT, H9319-02 multi-alkali (Hamamatsu Photonics), was obtained during this section of work and it was found that the sensitivity of the system rose considerably. This version of PMT differed slightly from the HC135-01 version, as the earlier version had been discontinued by the manufacturer. This newer version provided a 22 mm diameter active detection area compared to 21 mm on the HC135-01 series. As well as this, the HC135-01 bi-alkali series covered the range from UV to 650 nm, while the H9319-02 multi-alkali covered the range beyond 650 nm and into the near infra-red (850 nm). Similar to the bi-alkali PMT, the multi-alkali PMT used a +5 volt power supply connected to the detector and a cable was used to connect the PMT directly to the PC through the serial port

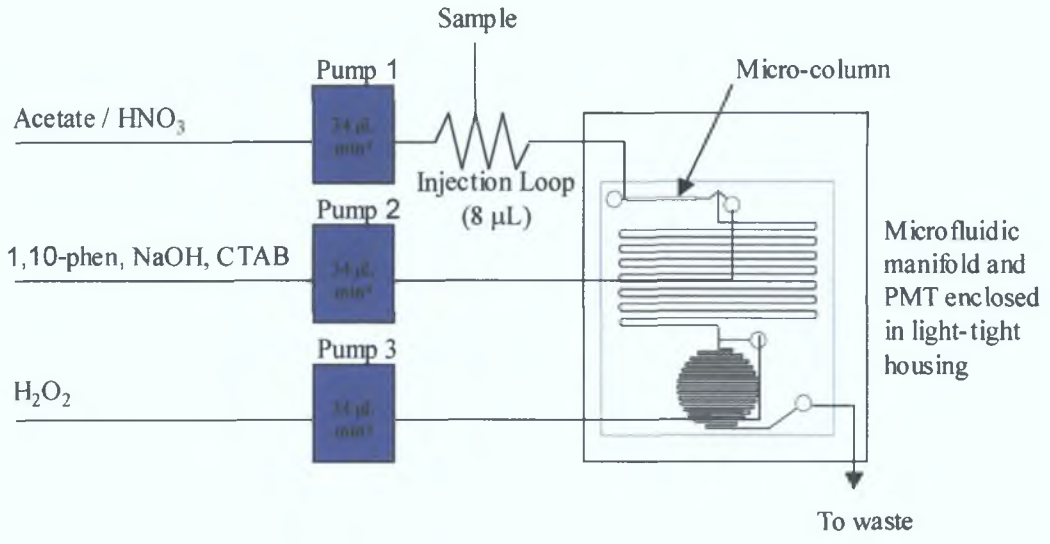

Figure 4.6: Diagram of the reaction manifold used for the determination of copper (II) by flow injection analysis using microfluidic manifold with micro-column. This manifold utilised a 8 µL injection loop, a total flow rate of 102 µL min^{-1} as described in the text.

A new housing was designed at this stage for the new PMT and plastic flow cell device. The manifold was contained within a custom built, light tight, steel box with a light seal and secure lid. This box was relatively inexpensive and contained the following features:

1. A light tight seal was secured between the box and the lid, while the two entry holes for the cables and tubing were covered with black masking tape and aluminium foil to ensure no stray light entered the system. The tubing entry holes were positioned at the base of the box to minimise the light that entered the system through the tubing.
2. Specific holders, fabricated for the PMT and plastic flow device, ensured they did not move about in the box and positioned the detection cell close to and in line with the PMT.
3. Unlike the old PMT housing, the actual PMT and flow device did not need to be wrapped in aluminium foil as the box was light tight and wrapping the manifold in aluminium foil did not reduce the dark count any further.

The external dimensions of the box were 250 mm x 250 mm x 100 mm and can be seen in Figure 4.7.

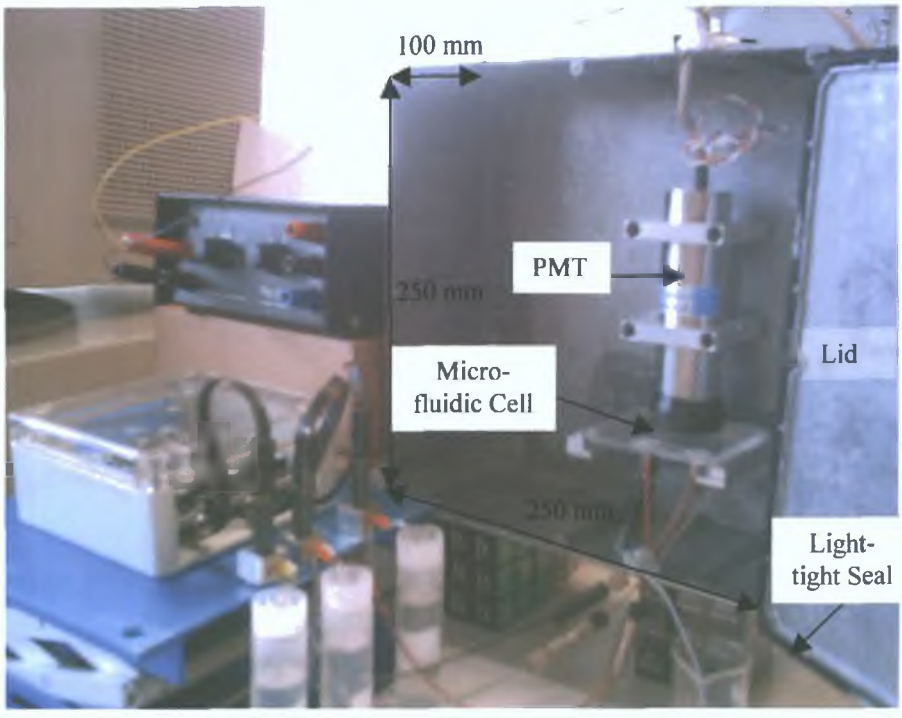

Figure 4.7: New light-tight housing for PMT and microfluidic manifold.

4.3 Results and Discussion

A number of problems can occur when trying to introduce a stationary phase into a microchannel flow system. Problems may arise in the fabrication and preparation of frits, which can be difficult to introduce into the microchannels, are prone to clogging or can act as catalysts for bubbles in the system. Further problems can arise due to the non-uniformity of packing at the walls and corners of rectangular channels and the difficulty of packing through the microchannels. Also, columns of such small dimensions can be easily blocked and the capacity of these columns is relatively small. The integration of a monolithic stationary phase and the incorporation of a number of different chelating resins into the plastic flow manifold were investigated during the course of this work.

4.3.1 Monolithic Stationary Phase

Introducing a stationary phase into the flow manifold involved the integration of a polymer-based monolithic column into the plastic flow device. This was thought to

be the simplest way of incorporating a separation phase into the system, as the support is attached to the wall of the channel and no frit preparation or integration is necessary. The porosity can also be easily controlled in order to form large pores resulting in a low back-pressure, thus allowing easy flow, even at low flow rates.

The monolithic stationary phase was prepared as described in section 4.2. Wang *et al.* [10] had previously used this method to prepare a continuous column in a stainless steel tube (50 mm x 8 mm I.D.) and found that the pore sizes that resulted ranged from 7 nm to > 3,000 nm. However, the volume of pores exceeding 500 nm represented almost 70 % of the total pore volume of the monolithic rod. They found that the total pore volume by this method was approximately 69 %, even though this value actually exceeded the amount of porogenic solvent added to the polymerisation mixture (60 %). This reflected the contribution due to volume shrinkage.

In the work carried out here, the PS-DVB monolithic mixture was injected into the closed channels and the radical polymerisation process was carried out by either temperature or UV irradiation. The use of temperature (for a period of 24 hours) for the polymerisation process was found to be unsuccessful as the PMMA manifold cracked due to the long exposure to heat. This process was repeated again but the second time the heating time was reduced to 5 hours. Once again, the PMMA cracked due to expansion of the channels. The same PS-DVB mixture was packed into a piece of polyethylene tubing and this was heated at 70 °C for 24 hours. In this case, the monolith was successfully polymerised and porous, but did not attach itself to walls of the tubing.

The use of UV irradiation instead of temperature for the polymerisation of the PS-DVB monolith was also investigated during the course of this work. The monolithic mixture was prepared and injected into the channels as before. The channels were exposed to the UV light for a range of times varying from 10 seconds to 5 hours. It was found that when the channel was exposed to UV light for a short length of time e.g. seconds, the polymerisation process did not take place, while exposure for times longer than a few hours resulted in the PMMA plate cracking once more.

As mentioned previously, the PS-DVB mixture polymerised in a piece of polyethylene tubing when the monolith was heated at 70 °C for 24 hours. In this case, the monolith was porous but did not bond itself to walls of the tubing making the monolith ineffective. This can be seen in Figure 4.8, which shows a segment of the monolith in the plastic tubing. One way to overcome this problem is to modify the plastic channel surface prior to the in-situ preparation of the monolith, as non-treated channels can form voids at the monolith-wall interface due to the shrinkage of the monolith during the polymerisation process. Work carried out by Stachowiak *et al.* [11] modified the polymer surface of a microdevice by grafting with ethylene diacrylate by UV light. In this case a thin layer of polymer with multiple double bonds was grafted onto the surface followed by the covalent attachment of a methacrylate monolith to the wall. This resulted in good bonding between the wall and the monolith ensuring there was no formation of voids at the monolith-wall interface. However, this was not investigated here as it was decided it would to be more practical to use packed columns and it was decided to investigate a different method of incorporating a stationary phase into the micro-system. As a result, no more work was carried out on these monolithic stationary phases in the course of this study.

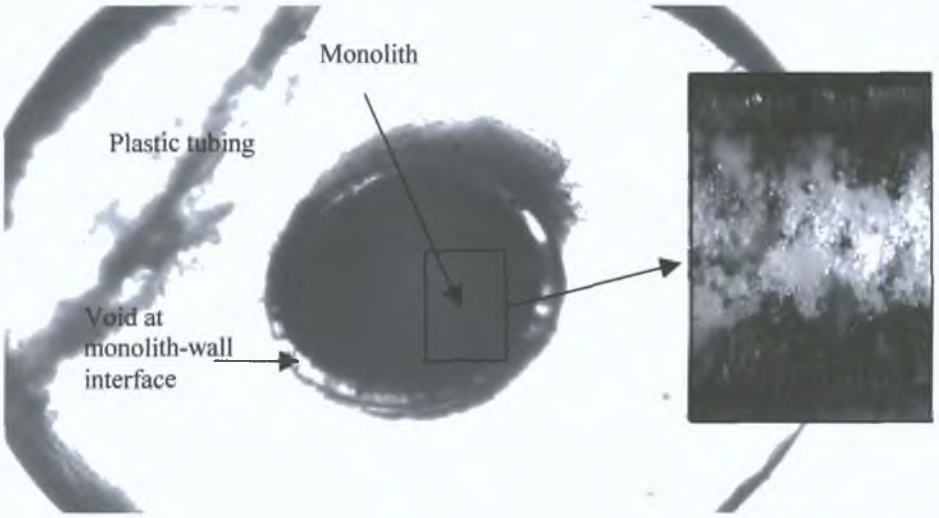

Figure 4.8: Section of polyethylene tubing containing PS-DVB monolith.

4.3.2 Chelating Stationary Phases

It was decided to create a packed bed of particles in a section of the microchannel, which was separate to the mixing and detection channels, to act as a micro-column, for preconcentration purposes, after the unsuccessful fabrication of the monolithic columns.

4.3.2.1 Characterisation Studies of Resins

The performance of the three chelating resins was firstly investigated for metal ion analysis. The investigation involved a comparative study of the three resins for the preconcentration and recovery of the following transition and heavy metal ions: copper (II), zinc (II), cadmium (II), nickel (II), lead (II), calcium (II) and magnesium (II).

Although resin selectivity is mainly due to the functional groups present, additional selectivity is possible by control of the pH. A change in pH can result in a change in the selectivity of the resin for different metal ions, due to the non-polar properties of the resin and the acidic-basic properties of most metal ions. The effect of the pH of the metals was evaluated by adjusting the pH over a range of pH 2.0 – 5.0. Buffering solutions of nitric acid (buffering range pH 2.0 – 3.0) and sodium acetate (buffering range pH 3.0 – 5.5) were used for this purpose. There were two reasons why this pH range was chosen. Firstly, at lower pH values, complexation and retention by the resin can be incomplete, while at higher values the performance of the chelating resins can rapidly decrease and be damaged [12]. Secondly, the pH of solution affects the solubility of metal ions in solution and at higher pH values, metals can form insoluble precipitates. The point of minimum solubility (optimum pH for precipitation) occurs at a different pH value for every metal e.g. copper hydroxide species (precipitate) can occur at pH 8.1 and cadmium hydroxide species can occur at pH 11.0 [13]. However at the chosen pH range of pH 2.0 to 5.0, none of the metal ions investigated here formed insoluble precipitates.

The preconcentration ability of the three resins towards each metal over the specified pH range was examined by the investigation of the % sorption of each metal by the

resins at individual pH values. This was carried out in batch mode as explained in section 4.2.2.1.

Figure 4.9 shows the sorption behaviour of the metals: copper (II), zinc (II), cadmium (II), nickel (II), lead (II), calcium (II) and magnesium (II) as a function of pH using the Chelex-100 resin.

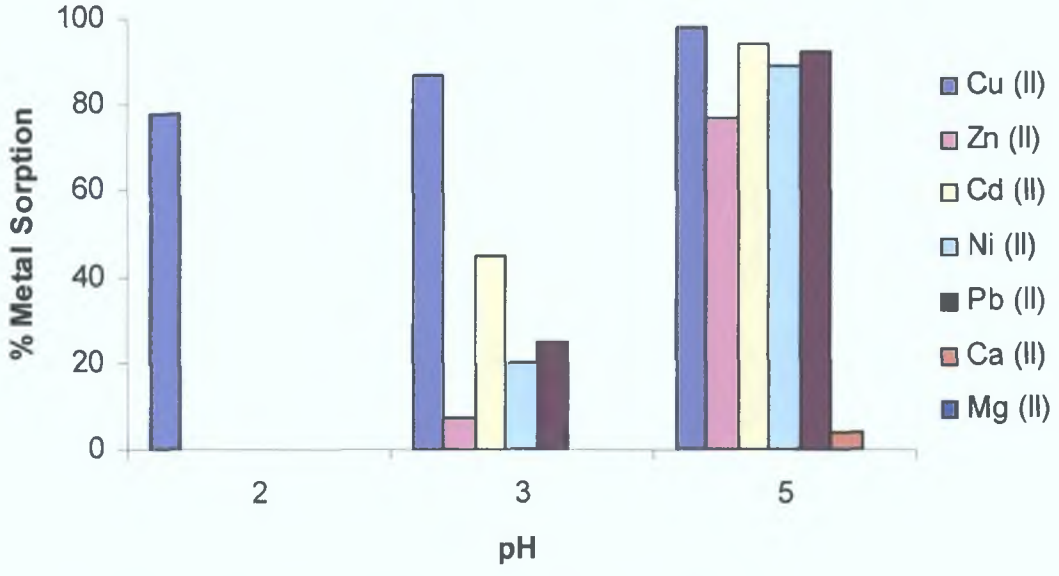

Figure 4.9: Effect of pH on sorption of metal ions by Chelex-100 resin.

At pH 2.0, there was no metal uptake by the resin except in the case of copper (II), where approximately 79 % metal sorption occurred. At the low pH values, the IDA is fully protonated and electrostatic repulsion prevents the formation of the complexes. Generally below pH 2.0, the resin acts as an ion exchanger and no chelation takes place, effective adsorption for this resin occurs in the pH range 4 – 14. As the pH increases, dissociation of IDA begins to occur (the dissociation constant for IDA is $pKa_1 = 2.98$) and chelation can take place (complete dissociation of IDA occurs at much higher pH values, as $pKa_2 = 9.89$). As the pH increased the amount of metal sorption increased also, particularly as the pH approached pH 5.0, where there was almost complete adsorption of copper (II), cadmium (II), nickel (II) and lead (II) with between 89 and 98 % sorption occurring.

It can also be seen from Figure 4.9 that the resin showed little or no affinity for calcium (II) and magnesium (II) at pH 5.0 and lower. There was no sorption of

magnesium (II) and approximately 4 % sorption of calcium (II) at this pH. This is due to the fact that IDA-based resins have a strong preference for complexing transition metals over alkali and alkaline earth cations, such as calcium (II) and magnesium (II). This property makes Chelex-100 very effective for seawater analysis as calcium (II) and magnesium (II) are present at high concentrations in seawater samples and will not be retained by the resin at pH 5.0, thus eliminating their interference effects during the analysis. In general, the adsorption of metal ions increases with increasing pH values, reaching a limiting value in each instance, followed by a decrease in adsorption beyond the limiting value. In all cases for Chelex-100, the limiting values were not exceeded; therefore no decrease in adsorption was seen.

An investigation was then carried out on the aminophosphonic acid based resin, similar to that which took place for the Chelex-100 resin. The relative affinity of this resin for various cations decreases in the order shown below:

Lead (II) > copper (II) > zinc (II) > magnesium (II) > calcium (II) > cadmium (II) > nickel (II) > cobalt (II) > strontium (II) > barium (II).

Figure 4.10 shows the sorption behaviour of the metals: copper (II), zinc (II), cadmium (II), nickel (II), lead (II), calcium (II) and magnesium (II) as a function of pH using the Duolite C-467 resin.

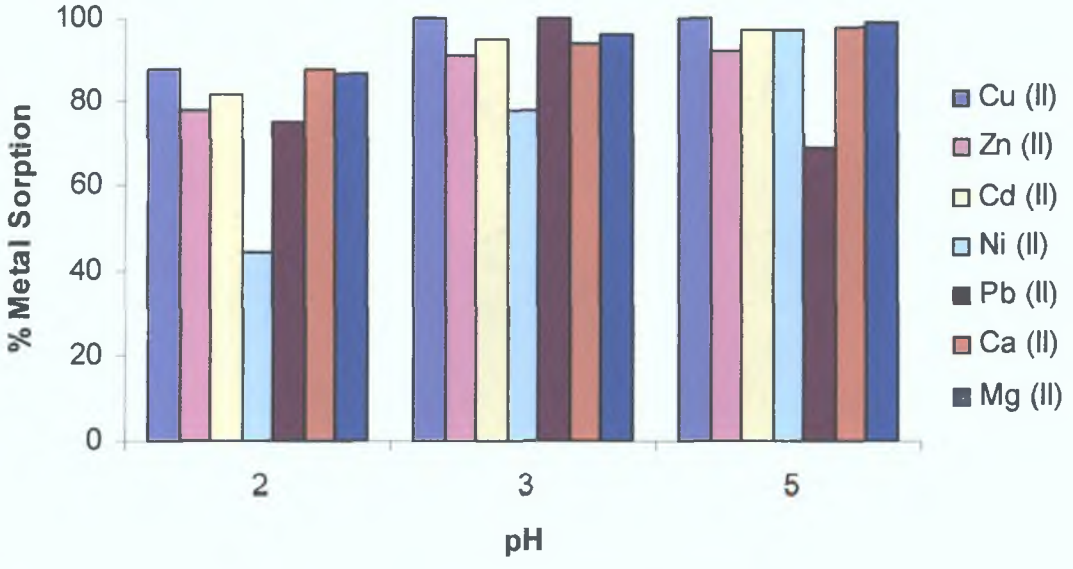

Figure 4.10: Effect of pH on sorption of metal ions by Duolite C-467 resin.

At pH 2.0, there was a 75 % or greater metal sorption observed for all metals except in the case of nickel (II), where approximately 44 % extraction was seen. This illustrates the affinity for this resin for most transition metals and alkaline earth metals even at low pH values. Similar to the results of the Chelex-100 resin, an increase in pH resulted in an increase in metal sorption, with between 92 % and 100 % metal sorption occurring at pH 5.0 for all the metal ions except in the case of lead (II). Metal sorption generally increases as pH increases because of a change in the coordination, from a bidentate ligand, where coordination occurs through the two oxygen atoms, to a tridentate ligand, where coordination takes place through the two oxygen atoms and the nitrogen atom, leading to an increase in the sorption of metal ion by the resin.

As mentioned earlier, the adsorption of metal ions by a resin generally increases with increasing pH value, reaching a certain pH (known as the limiting value) where maximum adsorption takes place, after which a decrease in adsorption is seen as the pH increases beyond the limiting value. It was found at pH 5.0 there was a decrease in the adsorption of lead (II), because the limiting value of lead (II) was reached (its limiting value occurred around pH 3.0, when 100 % sorption was observed). It can be also be seen that at pH 5.0 the resin showed a high affinity for calcium (II) and magnesium (II), with almost 100 % extraction of these metals taking place. These high extraction values make Duolite C-467 less ideal than Chelex-100 for seawater analysis as calcium (II) and magnesium (II) are present at high concentrations in seawater samples and therefore, will cause interference in the analysis of trace metal ions when Duolite C-467 is used for preconcentration purposes.

A similar investigation was then carried out on the thiol-based resin (Duolite GT-73), similar to that which took place for the other two resins. Figure 4.11 shows the sorption behaviour of the metals: copper (II), zinc (II), cadmium (II), nickel (II), lead (II), calcium (II) and magnesium (II) as a function of pH using the Duolite GT-73 resin.

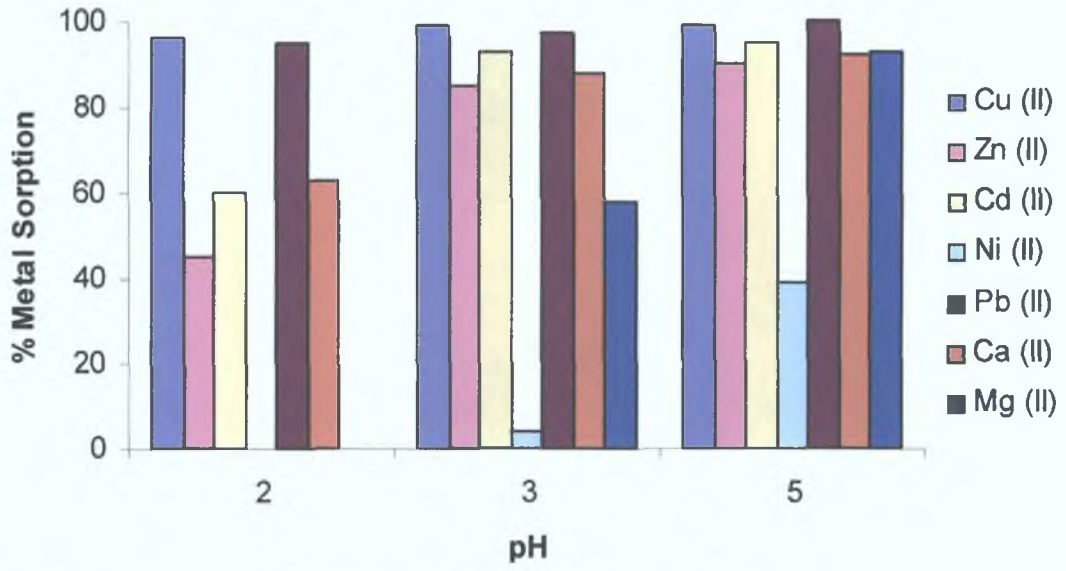

Figure 4.11: Effect of pH on sorption of metal ions by Duolite GT-73 resin.

At pH 2.0, there was nearly 100 % metal sorption observed for lead (II) and copper (II). There was also approximately half maximum sorption of calcium (II), cadmium (II) and zinc (II) at this pH with % extraction values of 63 %, 60 % and 45 % respectively for each of these metals. There was an increase in the % sorption for all of the metals analysed at pH 3.0. At this pH there was 85 % or greater extraction of copper (II), zinc (II), cadmium (II), lead (II) and calcium (II). There was a slight uptake (approximately 3 %) of nickel (II) at this pH compared to no sorption at pH 2.0. At pH 5.0 there was the highest sorption of all the metal ions with almost complete adsorption (between 92 and 100 % sorption occurring) of all the metals by the resin (except in the case of nickel (II)). This property would make Duolite GT-73 suitable for the analysis of samples for trace metals in a matrix with a high nickel (II) content.

4.3.2.2 Chelating Resin Micro-Columns

4.3.2.2.1 Incorporation of Chelex-100 into Micro-Column

Previous work by Rubí *et al.* [14] developed a micro-column packed with Chelex-100 for the preconcentration of iron (III) from fresh water and seawater samples. The dimensions in their case were considerably larger than those used in the work described here (55 mm x 2.5 mm I.D., compared to 15 mm x 1 mm I.D. in this work)

and they used a methacrylate cylinder loaded with the resin, which was stopped at either end using two pieces of filter paper. Olsen *et al.* [15] also developed a micro-column (50 mm x 2.0 mm I.D.) of Chelex-100 resin for preconcentration purposes and the column was made in a Perspex block, which was packed with the resin after the channel was fabricated, by injecting a slurry of the resin directly into the channel.

In the work described here, the Chelex-100 resin was incorporated into the microchannel prior to bonding as described in the previous section and the channel was bonded as before using hot embossing. However, a problem arose with this resin due to its higher tendency to swell compared with the Duolite resin. This resin is based on a relatively low cross-linked gel and the bed volume tends to change due to counter ion species or salt concentrations. The use of a more highly cross-linked macroporous support is more desirable as it is less susceptible to the volume change which can be observed in the Chelex-100 resin, particularly upon variation in pH. The Chelex-100 resin beads were also smaller in diameter than the Duolite C-467 beads, which resulted in restricted flow and increased pressure within the manifold and thus were no longer used.

4.3.2.2.2 Efficiency of Duolite C-467 Micro-Column (Fluorescence Detection)

As a result of the swelling problems associated with the low cross-linked Chelex-100 resin, an alternative series of micro-columns were fabricated incorporating the Duolite C-467. An investigation took place to ensure that the micro-column containing Duolite C-467 could efficiently separate or preconcentrate copper (II) from solution, even though this resin was not as selective as the Chelex-100 resin for copper (II). Although the micro-columns were small in size, which resulted in a lower column capacity in comparison to a larger column, this was thought not to be a problem in this work, as the low concentrations of copper ($\mu g\ L^{-1}$ levels) and small volumes of samples (μl range) used would not exceed the total capacity of this micro-column.

As fluorescence detection was used during this investigation, a fluorescence post column reagent (PCR) was required for detection purposes. Both 8-

hydroxyquinoline (8-HQ) and its more soluble derivative, 8-HQS have the ability to form stable complexes with a large range of metal ions. A large number of these complexes are fluorescent and have fast complexation kinetics and 8-HQS does not exhibit fluorescence in its uncomplexed form. As a result 8-HQS was therefore chosen as the PCR.

The experimental setup used here is described in section 4.2.2.2, whereby the sample was loaded onto the micro-column using an acetate buffer and eluted off using a nitric acid solution. It was found that zinc (II) was successfully retained by the column and then eluted off with the acid solution when this procedure was carried out. The reaction peaks generated for a range of zinc (II) standards over the concentration range of 0 to 1,000 μg L^{-1}, which were eluted from the column, are shown below in Figure 4.12. The experimental conditions used in this case were: total flow rate of 60 μL min^{-1} and a sample loop volume of 15 μL. The reagent concentrations were 5mM 8-HQS solution, 10 mM sodium acetate buffer solution, which buffered to approximately pH 4.0 and 25 mM nitric acid solution for the desorption of zinc (II) from the column.

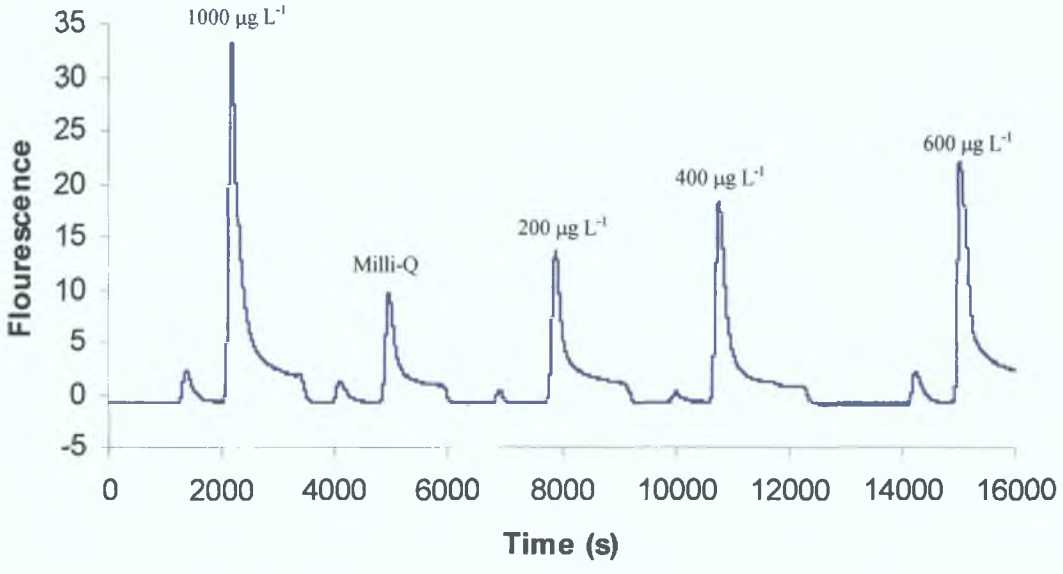

Figure 4.12: Reaction peaks generated for zinc (II) standards. Experimental conditions: 5mM 8-HQS solution, 10 mM sodium acetate buffer solution and 25 mM nitric acid solution. Total flow rate of 60 μL min^{-1} and sample loop volume of 15 μL.

A linear response of the calibration curve was observed over the concentration range 0 to 1,000 μg L^{-1} Zn (II), with a correlation coefficient of $R^2 = 0.9966$ as shown in Figure 4.13.

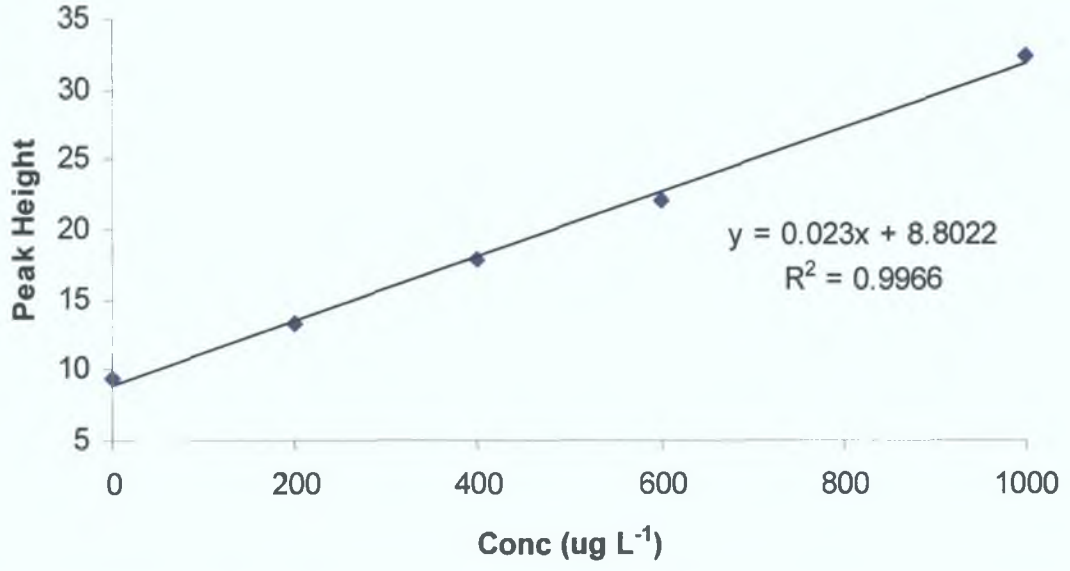

Figure 4.13: Standard calibration curve for zinc (II) over the concentration range 0 to 1,000 μg L^{-1} where $R^2 = 0.9966$.

It was then decided to join two of the micro-columns in series together to investigate the effect on recovery. However, it was found when a 15 μL sample of zinc (II) was introduced, there was no significant difference in recovery when two columns were used and the results obtained were similar to those obtained when a single column was used. This verified that there was no need to increase the size of the micro-column or the amount of resin for matrix removal.

4.3.2.2.3 Alternative Bonding Processes

The first iteration of the plastic manifold, incorporating the chelating resin micro-column, was bonded together using a flexible adhesive film of 100 μm polyester with 75 μm adhesive on both sides. This was used instead of heat bonding to seal the base plate of PMMA containing the etched channels and the cover plate together. This removed the need for heat during the bonding process as this method relied solely on pressure. Instead of using a 2 mm thick piece of PMMA, a thinner sheet of PMMA (125 μm in thickness) was used for the top cover, as no heat was required for bonding. However, this resulted in insufficient bonding and the channels were found

to leak into each other. This ultimately resulted in leakage between the base plate and top cover, rendering the device ineffective. This process was repeated with a longer bonding time under pressure, but this device was also unsuccessful. It was decided to return to the original form of bonding of the channels using the hot embosser, which resulted in adequate bonding of the channels.

4.3.2.2.4 Use of PMT Filters

As mentioned in the experimental section, the sensitivity of the new multi-alkali PMT increased compared to the old bi-alkali PMT. The background count generated by the reagents was significantly higher for the new PMT, in the region of 3,500,000 counts s^{-1} compared to 20,000 to 30,000 counts for the old PMT. As discussed in section 1.12, the PMT is very sensitive and high light intensities can damage the PMT. As a result of this, a filter was placed between the detection cell and the PMT window to reduce the background emission of the system. A black background was printed onto an acetate sheet and this sheet was cut into 22 mm in diameter disks. Two of these disks were deemed satisfactory to reduce the background counts and were inserted in between the detection cell and the PMT window. These brought the background noise down considerably as can be seen in Figure 4.14, which shows the reaction peaks generated for a range of copper (II) standards. Although the S/N decreased when the filters were used e.g. S/N = 163 for a 250 μg L^{-1} copper (II) standard when no filters were used, compared to S/N = 56 when 2 filters were used, the system was still deemed sensitive enough for this work, especially when the reagent conditions were optimised.

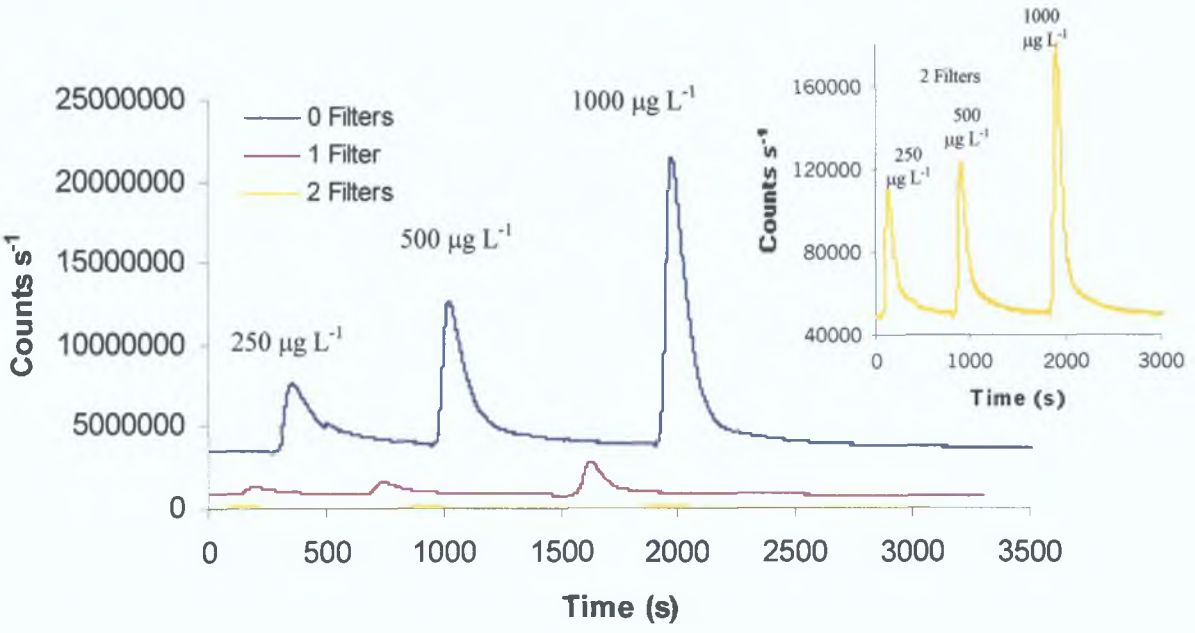

Figure 4.14: Effect of filters on the chemiluminescence signals produced for a range of copper (II) standards.

It can be seen from the above diagram that the original background count, when the reagents were flowing through the system, was approximately 3,500,000 counts s^{-1} when no filter was used, compared to 800,000 counts s^{-1} when a single filter was used and 48,000 counts s^{-1}, when two filters were used. All future work using the new PMT incorporated two filters into the system for reduction of background counts.

4.3.2.2.5 Application of Duolite C-467 Resin Micro-Column

Using the new microfluidic flow manifold incorporating the on-line chelating micro-column described in section 4.2.2.3, a range of copper (II) standards between 0 and 150 µg L^{-1} were analysed. An 8 µL volume of standard was loaded (and retained) on the micro-column and then successfully eluted using a weak acid solution. The reaction peaks generated for the eluted copper (II) standards can be seen in Figure 4.15.

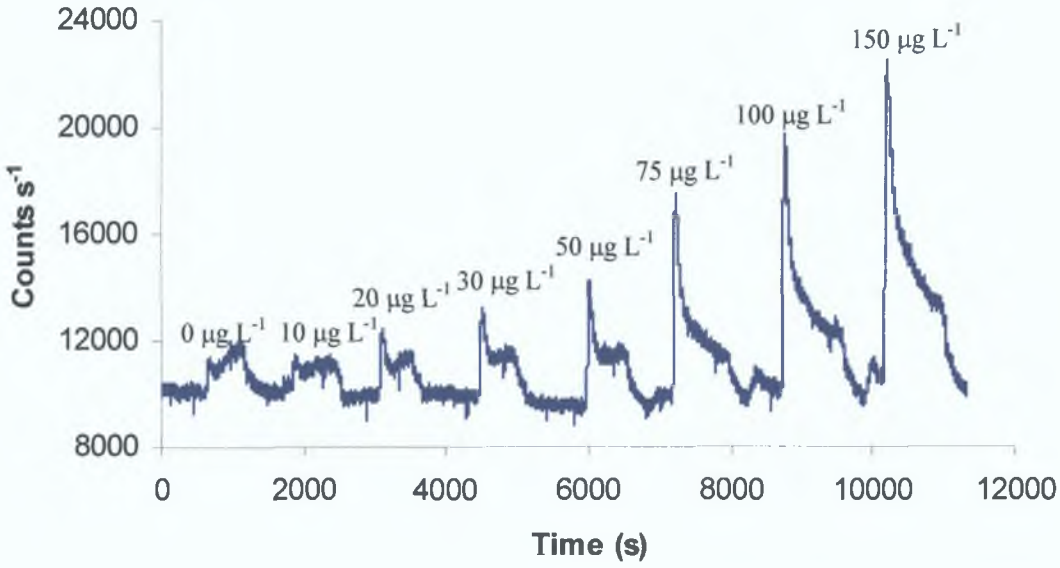

Figure 4.15: Reaction peaks generated for 0 to 150 µg L^{-1} copper (II) standards. Reagent conditions: 0.06 mM 1,10-phenanthroline, 1.3 mM CTAB, 0.075 M NaOH, 5 % H_2O_2, 10 mM sodium acetate buffer (pH 4.0) and 25 mM HNO_3.

These results were found to be linear over the concentration range 0 to 150 µg L^{-1} and a correlation co-efficient, R^2 value of 0.9858 was obtained, as shown in Figure 4.16.

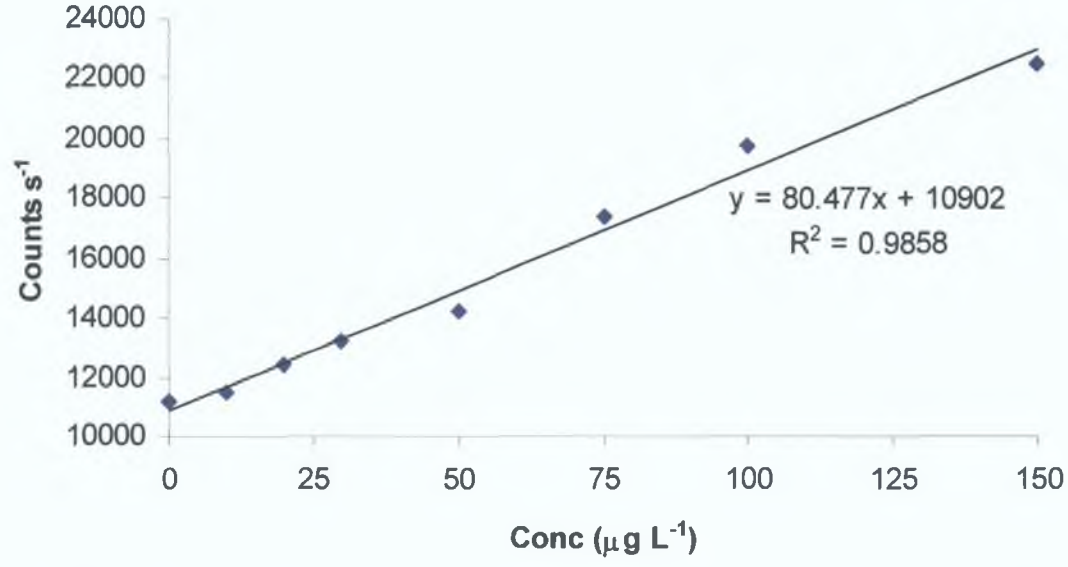

Figure 4.16: Copper (II) linearity studies over the concentration range 0 to 150 µg L^{-1}, $R^2 = 0.9858$.

Although this on-chip micro-column was capable of retention and elution of copper (II), there was one major disadvantage found with this system. The chelating resin was not completely resistant to physical degradation, which resulted in only a limited

operational lifetime for the column (and plastic flow manifold). In this work, a section of the mixing channel became blocked with a fine resin particle, which had become dislodged from the micro-column channel during the course of this work. A backwashing procedure was attempted to dislodge the debris from the channel but with no success. Unfortunately, no more work was carried out using this manifold and the system was not optimised for the determination of copper (II) or applied to any real samples or standard reference materials.

4.4 Conclusion

Two different methods of incorporating stationary phases into the microsystem were investigated for the separation and preconcentration of copper (II) in this work. The first method involved the integration of a monolithic micro-column, while the second employed the use of a chelating stationary phase contained within a micro-column within the microfluidic device. A polymeric based monolith was first investigated as it was thought to be the simplest way of incorporating a separation phase into the system as the support was attached to the wall of the channel and no frit preparation was necessary. It was found however that this was not the case as a number of unsuccessful attempts resulted in either cracking of the PMMA plastic manifold or the development of large voids at the monolith-wall interface.

The second method used for the integration of a separation phase involved the incorporation of a chelating stationary phase into the microflow manifold. A number of resins containing different functional groups were investigated for this use including Chelex-100, Duolite C-467 and Duolite GT-73. Characterisation studies were carried out on the three resins and it was found that the Chelex-100 resin, was the most suited resin for seawater analysis but showed signs of considerable swelling which resulted in blockages occurring and leakages within the microflow manifold. In comparison, the Duolite C-467 resin did not show as much signs of swelling and was successfully used for a short time for a calibration study of copper (II) between 0 and 150 $\mu g\ L^{-1}$ before some debris due to degradation of the resin resulted in a blockage of the device, which meant this system was not optimised or applied to any real samples.

4.5 References

1. A. R. Bowie, M.G. Sanders, P.J. Worsfold, *J. Biolumin. Chemilumin.*, 11 (1996) 61-90.
2. G. Benoit, K. Hunter, T. Rozan, *Anal. Chem.*, 69 (1997) 1006-1011.
3. J. Riley, D. Taylor, *Anal. Chim. Acta*, 40 (1968) 479-485.
4. J. Lichtenberg, N.F. de Rooij, E. Verpoorte, *Talanta*, 56 (2002) 233-266.
5. A. Manz, H. Becker, Microsystem Technology in Chemistry and Life Sciences, Springer Desktop Editions in Chemistry.
6. H. Zou, X. Huang, M. Ye, Q, Luo, *J. Chrom. A.*, 954 (2002) 5-32.
7. B.S. Garg, R.K. Sharma, N. Bhojak, S. Mittal, *Microchemical Journal*, 61 (1999) 94-114.
8. P. Nesterenko, M. Shaw, S. Hill, P. Jones, *Microchemical Journal*, 62 (1999) 58-69.
9. *SAMMS – Thiol-SAMMS* 2004, Pacific Northwest National Laboratory, P.O. Box 999, Richland, WA 99352, viewed 23 July 2004 <http://www.pnl.gov/etd/product/samms/thiol.htm>
10. Q.C. Wang, F. Svec, J.M.J. Fréchet, *Anal. Chem.*, 65 (1993) 2243-2248.
11. T.B. Stachowiak, T. Rohr, E.F. Hilder, D.S. Peterson, M. Yi, F. Svec, J.M.J. Fréchet, *Electrophoresis,* 24 (2003) 3689-3693.
12. V. Porta, C. Sarzanini, O. Abollino, E. Mentasti, E. Carlini, *JAAS*, 7 (1992) 19-22.
13. *WST –Precipitation by pH* 2003, Water Specialists Technologies LLC, 1515 Kastner Place, Sanford, Florida 32771, viewed 11 October 2005 <http://www.waterspecialists.biz/html/precipiation_by_ph_.html>
14. E. Rubí, R. Forteza, V. Cerdá, *Laboratory Robotics and Automation*, 8 (1996) 149-156.
15. S. Olsen, L.C.R. Pessenda, J. Ruzicka, E. H. Hansen, *Analyst*, 108 (1983) 905-917.

CHAPTER FIVE

APPLICATION OF CONVECTIVE-INTERACTION MEDIA® DISK MONOLITHIC COLUMNS

5.1 INTRODUCTION

A monolithic column is a continuous unitary porous structure that is made from in-situ polymerisation or consolidation inside column tubing [1]. The surface of the monolith can then be functionalised to achieve the desired binding properties. There are two types of monolithic stationary phases that are popular, namely silica based monoliths and polymeric based monoliths. The polymeric approach is generally more advantageous over the silica-based monoliths due to its simpler preparation process and easier pore size control.

The use of a monolithic column for separation or preconcentration purposes can overcome some of the limitations associated with resins or beads. One advantage of using a monolithic column is due to the fact that it is one continuous bed and the problems associated with debris due to degradation of resins, such as those described in chapter 4, can be avoided. As well as this, the low back-pressures and the high surface area, which are characteristic of monolithic stationary phases, make this method very suitable for on-line preconcentration within a microfluidic system.

The first useful monolithic stationary phase was developed in the early 1990's by Tennikova *et al.* [2]. This monolith was actually a methacrylate monolithic disk and was used for the separation of proteins. In 1993, Belenkii *et al.* studied the geometry of columns involved in the separation of proteins, resulting in the development of short separation columns [3]. These short columns increase the speed of separations, while keeping the back-pressures low. It was difficult and impractical to make these separation phases from resins or beads due to irregularities in the packing. Therefore the development of monolithic stationary phases in disk form was introduced. Generally, these are prepared in a flat or cylinder mould, which is then punched or sliced to obtain up to 3 mm thin disks, which can then be placed in a specially designed housing (usually a hollow cylinder).

The first Convective-Interaction Media® (CIM®) products became available in 1998 [4]. This medium was a short, continuous, homogenous methacrylate or styrene-divinylbenzene rigid polymer structure, cross-linked with three-dimensional interconnected channels with over 60 % porosity. The macrochannels were

approximately 1,500 nm in diameter, while the mesochannels were less than 100 nm in diameter. The larger channels resulted in the low back-pressure associated with CIM® products, while the mesochannels provided a large surface area for binding purposes.

In the work presented in this chapter, the use of modified CIM® disk monolithic columns was investigated for analyte preconcentration/matrix removal, whereby the monolithic disk has been coated with different chelating ligands. The coated disks were then incorporated into the flow system for the on-line preconcentration of copper (II). This system was then used in combination with chemiluminescence detection for the selective determination of copper (II) in a standard reference material and in real water samples including a coastal seawater sample and estuary water sample.

5.1.1 Chelating Ligands

The use of three different carboxylic acids was investigated for modifying the CIM® disk monolithic columns during this work: 2-pyridinecarboxylic acid (picolinic acid), 2,6-pyridinedicarboxylic acid (dipicolinic acid), and dodecyliminodiacetic acid. These carboxylic acids can work as chelating ligands and the structures of the acids can be seen below in Figure 5.1.

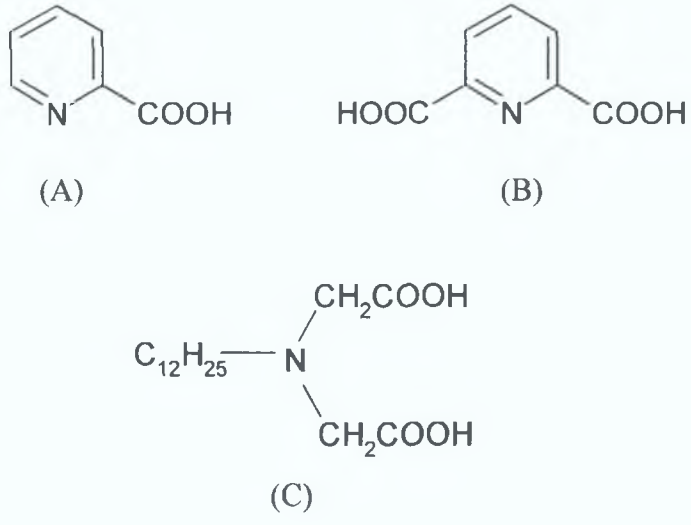

Figure 5.1: Structures of (A) picolinic acid (B) dipicolinic acid and (C) dodecyliminodiacetic acid.

Picolinic acid is a N,O chelator, whereby metal ions can complex with the nitrogen of the pyridine ring and the oxygen of the carboxyl group. Dipicolinic acid on the other hand has a second carboxyl group, meaning it has the potential of being a N,O,O chelator. Iminodiacetic acid also has the potential of being a N,O,O chelator due to the presence of a second carboxyl group. Chelating stationary phases containing carboxylic acid functional groups can be used for the determination of trace metal ions in complex sample matrices such as seawater samples due to their strong preference for complexing transition metals over alkali and alkaline earth metals [5].

These three carboxylic acids have all been successfully used in different systems for separation purposes due to their strong complexing ability for transition metals. Picolinic acid has been successfully used as an on-column chelating agent for the chromatographic separation of a range of transition metals including manganese (II), copper (II), nickel (II), cobalt (II), cadmium (II) and zinc (II), in industrial waste water [6]. Other applications of picolinate complexes have included the separation of lanthanides [7] and the determination of rare earth metals [8].

Much work has been carried out using iminodiacetic acid (IDA) based systems. A review by Nickson *et al.* illustrates the very successful application of the IDA chelating ligand for the separation of a range of transition metals from samples such as seawater, river water, brines and snow [9]. This separation is due to the fact that dicarboxylic acids show an even higher affinity towards transition metals than single carboxylic acid ligands, especially if a nitrogen atom is part of the ligand [5]. Other separation work involving the use of IDA includes the separation of trace alkaline earth metals in brines [10] and the separation of lanthanides [11].

Dipicolinic acid also has strong complexing ability and has been used for a number of analyses of transition and alkaline earth metals [12-14]. Dipicolinic acid has also been used as an eluent for the chromatographic determination of a number of transition metals, including cobalt (II), copper (II), zinc (II), cadmium (II) and lead (II) in waste-water samples [15]. In this work, an eluent containing dipicolinic acid was used to remove transition metal ions from an IDA-bonded silica column. It was found that the complexation of the metal ions with the dipicolinic acid in the eluent

was preferred to the complexation with the IDA on the column, even though dipicolinic acid and IDA molecules both have three centres involved in complexation i.e. the two carboxylate groups and the nitrogen atom, which are arranged similarly within the molecules. However, the IDA has a flexible structure, while the nitrogen present in the pyridine ring of the dipicolinic acid holds the two carboxylate groups rigidly, thus favouring the formation of metal complexes [5].

5.2 EXPERIMENTAL

5.2.1 Flow Injection Analysis System

A schematic of the flow injection analysis manifold used in this work is shown in Figure 5.2. Initially the setup used a six-port Rheodyne rotary injection valve, model 7125, (Rheodyne, Cotati, CA, USA) with a 65 μL sample loop (which was later changed to a 150 μL sample loop) and used a total flow rate of 0.56 mL min^{-1} (later optimised), which was controlled by a variable speed, 10 roller model peristaltic pump (Gilson Minipuls 312, Villiers, France). The detection flow cell used consisted of a 650 mm of 0.6 mm I.D. of transparent, flexible polyethylene (PE) tubing which was tightly spiralled in a coil to a diameter of 25.4 mm, total volume 184 μL and fixed onto the adhesive surface of a piece of tape. This cell was secured to the front of the PMT in a similar way to that described in chapter 2, using strong black plastic insulating tape, so that the spiral flow cell faced the PMT window. The PMT used in this work for detection purposes was the H9319-02 multi-alkali series (Hamamatsu Photonics). All tubing used in this system, except the peristaltic tubing (standard PVC peristaltic tubing) and detection flow cell tubing (PE tubing), was narrow bore PEEK tubing (0.127 mm I.D.) obtained from Alltech Associates Applied Science Ltd. (Lancashire, England).

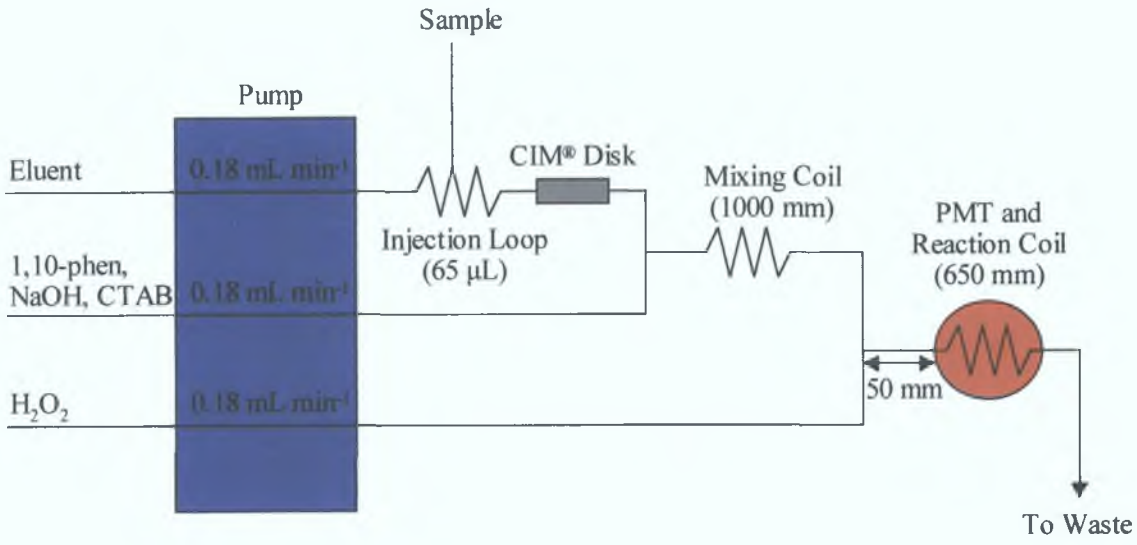

Figure 5.2: Schematic diagram of the reaction manifold used for the determination of copper (II) by the flow injection analysis system, incorporating the CIM® disk monolithic column and with a 65 µL injection loop and a total combined flow rate of 0.56 mL min^{-1} as described in the text.

A 65 µL sample volume was introduced into the flowing carrier stream, which passed through the CIM® disk monolithic column and was then mixed with the 1,10-phenanthroline solution at a T-piece merging connection. The sample and 1,10-phenanthroline solution were mixed together in a 1,000 mm mixing coil of PEEK tubing prior to meeting with the hydrogen peroxide solution through a second T-piece connection fitting. As described in chapter 2, the length of tubing between the second T-piece, where the sample and reagent streams merge, and the detection flow cell, where the chemiluminescence emission occurs, was kept as short as physically possible (approximately 50 mm) to ensure a rapid passage of solutions into the reaction cell since the chemiluminescence reaction occurs almost instantaneously and the light emission needs to be detected as soon as possible by the PMT.

The instrumentation used for the detection of calcium (II) and magnesium (II) in the synthetic seawater analysis discussed in section 5.3.6 is illustrated in Figure 5.3. It comprised of a Waters 501 HPLC pump module, which was used to deliver the nitric acid solution (1.0 mL min^{-1}). A manual sample Rheodyne injection valve fitted with a 16 µL sample injection loop was used for sample introduction. The analytical column was a 50 x 4 mm I.D. Dionex IonPac CG12A cation exchange column (Dionex, Sunnyvale, CA). A second pump was used for the introduction of the post

column reagent (PCR) at a flow rate of 1.0 mL min^{-1}, which was mixed with the post column eluent using a 0.3 m PEEK reaction coil (0.250 mm I.D.). A UV-VIS detector (Waters 486 Tunable Absorbance Detector) was used to monitor at 570 nm. The detector was connected to a data logger (Pico ADC-16), which was then connected to the PC through the RS232 serial port. This allowed the signal output from the detector to be continuously monitored throughout the analysis by the PC.

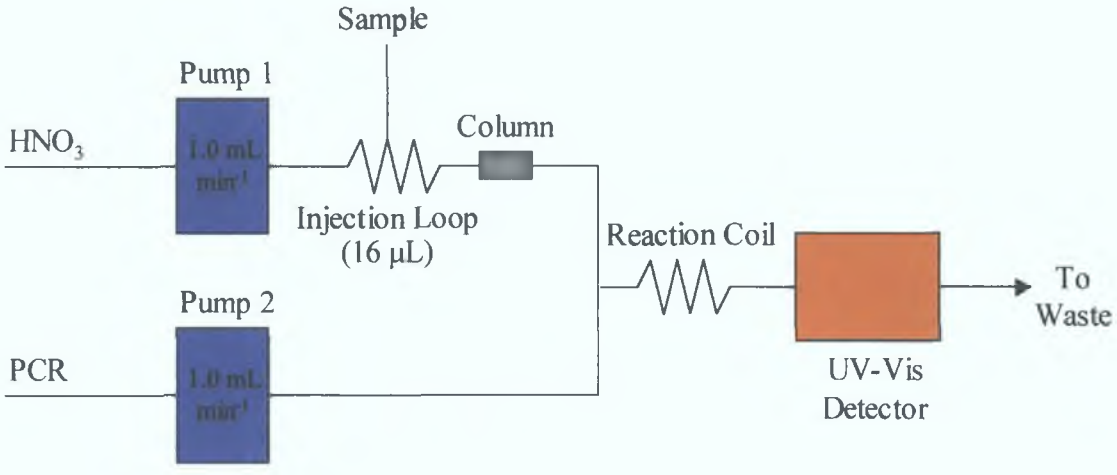

Figure 5.3: Schematic diagram of the reaction manifold used for the detection of calcium (II) and magnesium (II) in synthetic seawater analysis, incorporating a cation exchange column and with a 16 µL injection loop and a total combined flow rate of 2.0 mL min^{-1} as described in the text.

5.2.2 CIM® Disk Monolithic Column

CIM® disk monolithic columns, which are reversed-phase styrene-divinylbenzene co-polymer disks (RP-SDVB disk) (obtained from BIA Separations, Slovenia), are rigid, highly cross-linked monolithic polymer disks. These disks remain chemically and mechanically stable for several years. It is possible to accommodate up to four disks per housing and they can operate at a flow rate of up to 10 mL min^{-1} and a back-pressure of up to 50 Barr. They are stable within the pH range of pH 2.0 to 12.0 and at various ionic strengths but organic solvents, such as acetonitrile, should be avoided as they can seriously damage the column housing.

A CIM® disk monolithic column consists of a CIM® disk in a specially designed polyacetyl housing. The CIM® housing provides a low void volume and simple handling and can easily be fitted into a flow injection analysis system. The housing

dimensions are 30 mm in diameter and 65 mm in length. The CIM® disk itself consists of a CIM® matrix embedded in a non-porous, self-sealing fitting polyolefin ring, which acts as an impermeable sidewall and ensures only axial flow through the disk. It also prevents any sample or eluent leakage or by-pass taking place, ensuring that the sample is pumped through the entire volume of the matrix. As well as this the ring reinforces the disk and allows the disk to be firmly sealed between the cartridge-holder without excessive force on the monolith. The actual CIM® disk dimensions are 16 mm in diameter and 3 mm in thickness and has a volume of 0.34 mL.

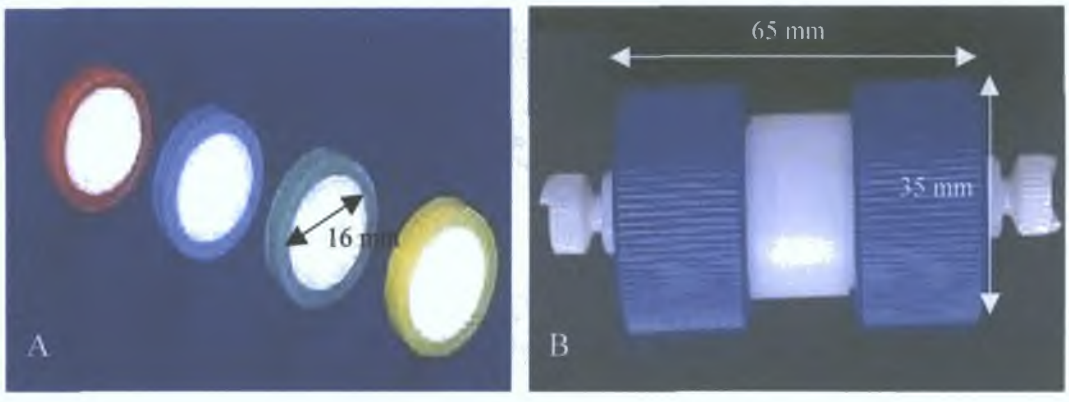

Figure 5.4: Range of CIM® disk monolithic columns (a), disk dimensions: 16 mm in diameter, 3 mm in thickness, active bed volume 0.34 mL. CIM® disk monolithic column (b), housing dimensions: 30 mm in diameter, 65 mm in length.

5.2.3 Reagents

All of the chemiluminescence reagents used in this system were the same as those described in the chapter 2, except that all used in this study were made up in ultra pure water obtained from Sigma Aldrich Ltd., Dublin, Ireland unless otherwise specified.

A synthetic seawater sample was made up containing approximately 0.5 M sodium chloride (10,800 mg L^{-1} sodium and 19,400 mg L^{-1} chloride approx.), 400 mg L^{-1} calcium (II) and 1,300 mg L^{-1} magnesium (II) (all obtained from Sigma Aldrich Ltd., Dublin, Ireland). Two real water samples were also used in this work, a coastal

seawater sample from Portmarnock Beach, Co. Dublin and an estuary water sample from Malahide Estuary, Co. Dublin.

The use of two different carboxylic acids, picolinic acid and dipicolinic acid (both obtained from Sigma Aldrich Ltd., Dublin, Ireland) were employed for the modification of the CIM® monolithic disks. In each case a 10 mM solution of the carboxylic acid in ultra pure water was prepared and used to coat the CIM® monolithic disk. All the solutions were degassed using sonication, prior to use, to ensure reagent dissolution and homogeneity and they were also all filtered through a 0.45 μm nylon membrane filter from Gelman Laboratories (Michigan, USA).

A CIM® disk was also modified using dodecyliminodiacetic acid, which was synthesised as follows: 4.77 g of chloracetic acid was dissolved in 2.50 mL of ethanol, the pH of which was adjusted to pH 9.5 with a sodium hydroxide solution. The chloroacetate was added to a solution containing 4.6 g of dodecylamine, which was dissolved in 5.0 mL of ethanol. This solution was heated and stirred for 4 hours and then boiled until a solid precipitate resulted. This product was then dissolved in a 70 mL aliquot of Milli-Q water. The sample was then boiled and cooled in an ice bath resulting in a pearl-like fine-grained precipitate, which was filtered and dried in an oven at 60 °C for 12 hours. A 10 mM solution of dodecyliminodiacetic acid was prepared and used for the modification of the CIM® monolithic disk. The dodecyliminodiacetic acid was insoluble in Milli-Q water, therefore the pH of the solution was increased from pH 2.6 to pH 11.3 using a 1.0 M sodium hydroxide solution, followed by heating and stirring on a hotplate. The solution was allowed to cool and the pH of the solution was then adjusted with glacial acetic acid to approximately pH 4.8. This solution was then filtered and made up with Milli-Q water. All the reagents used for the synthesis of dodecyliminodiacetic acid were obtained from Sigma Aldrich Ltd., Dublin, Ireland with the exception of the glacial acetic acid, which was obtained from Merck, Darmstadt, Germany.

For the analysis of calcium (II) and magnesium (II) in the synthetic seawater matrix, the two reagents used were 5 mM nitric acid solution and a post column reagent containing 0.4 mM *o*-cresolphthalein complexone (*o*-CPC), 0.25 M boric acid

adjusted to pH 10.5 using sodium hydroxide solution (monitored at 570 nm, using UV-VIS detector). All the reagents used here were obtained from Sigma Aldrich Ltd., Dublin, Ireland.

5.2.4 Modification of CIM® Disks

The CIM® disks were modified before use in the system by coating with picolinic acid, dipicolinic acid or dodecyliminodiacetic acid. This was done using approximately 25 mL of the 10 mM solution, which was made up and filtered through membrane filters as described earlier. The modifying solutions were pumped through the CIM® disk using a peristaltic pump. It was possible to re-use the disks afterwards, as the sorbed layer could be stripped from the disk by washing with a 1.0 M sodium hydroxide solution for 1 hour, followed by washing with 0.1 % trifluoroacetic acid (TFA) in isopropanol (IPA), allowing further modification of the disk by the same or a different compound. When the CIM® disk was removed from its housing it was cleaned and stored in a 50 % ethanol solution.

5.3 Results and Discussion

5.3.1 Initial Studies Using CIM® Disk Modified with Picolinic Acid

Initially, the reagents used in the flow system were chosen to be 5 % hydrogen peroxide solution and a combined solution of 0.03 mM 1,10-phenanthroline, 0.05 mM CTAB and 0.075 M sodium hydroxide. A 65 μL volume of copper (II) (ranging in concentration from 250 μg L^{-1} to 1,000 μg L^{-1}) was injected into a continuous flowing stream of ultra pure water (carrier solution) which was used to carry the sample to the picolinic acid modified CIM® disk. The total flow rate used here was 0.56 mL min^{-1}. A 25 mM nitric acid solution was then used to elute the retained copper (II) from the disk and the reaction peaks generated for a range of copper (II) standards using this initial flow system are shown in Figure 5.5.

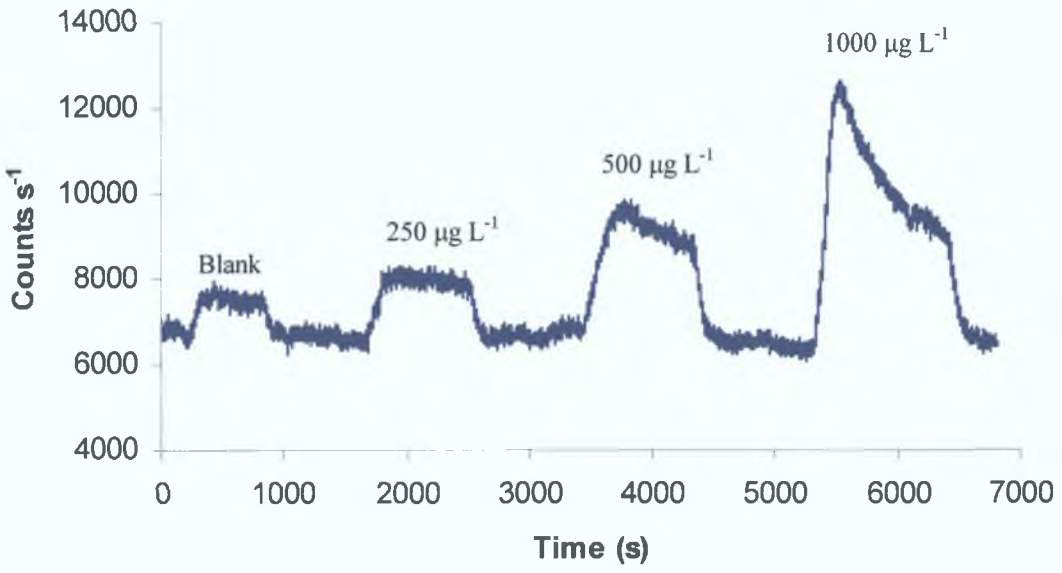

Figure 5.5: Reaction peaks generated for range copper (II) standards (0 to 1000 µg L^{-1}) on CIM® disk modified with picolinic acid. Reagent conditions: 0.03 mM 1,10-phenanthroline, 0.05 mM CTAB, 0.075 M NaOH, 5 % H_2O_2 and 25 mM HNO_3, at a combined flow rate of 0.56 mL min^{-1}.

Using the results obtained above, the signal produced for blank solution was then subtracted from each of the copper (II) standards and a calibration graph was then plotted of the chemiluminescence intensity of the signal minus the blank (based on counts s^{-1}) versus the copper (II) concentration (µg L^{-1}). Although these results were found to be linear over the concentration range 0 to 1,000 µg L^{-1} and resulted in a correlation coefficient of 0.9816 as shown in Figure 5.6, it can be seen that the system was not very sensitive. It was important therefore to carry out a series of optimisation studies in order to enhance the overall sensitivity of the system.

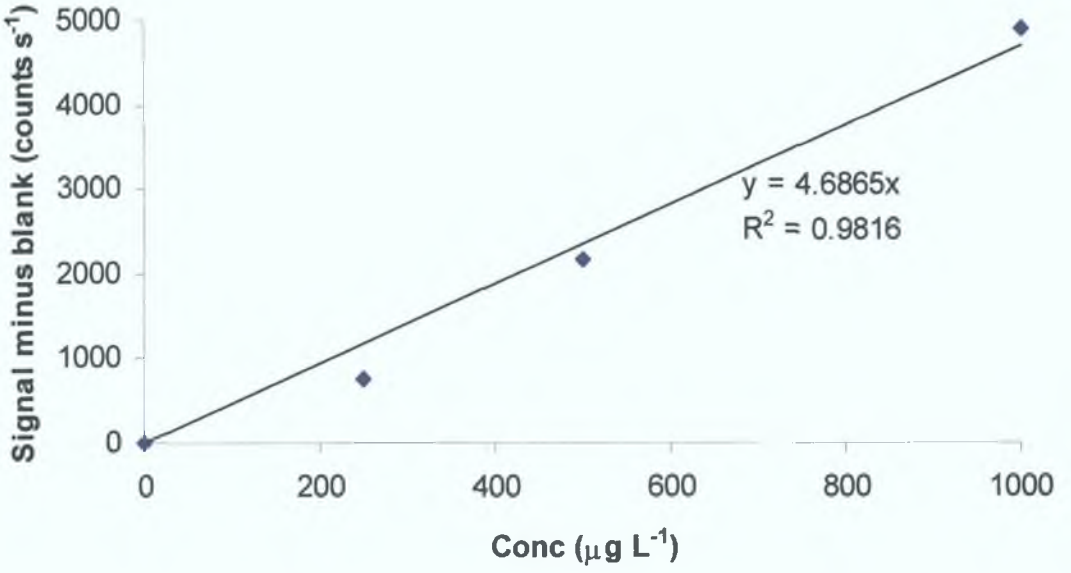

Figure 5.6: Copper (II) linearity studies over the concentration range 0 to 1,000 µg L^{-1} where R^2 = 0.9816 using picolinic acid modified CIM® disk.

5.3.2 Optimisation of Flow System

In this series of optimisation experiments, including the effect of sample loop size, flow rate and optimisation of reagent conditions, it should be noted that the manifold was used without the use of the CIM® modified disk in order to simplify the system. The optimisation procedure was quicker to carry out, as it was not necessary to wait for the copper (II) to be loaded on and then eluted off the CIM® disk. The set-up was also simpler, as there was no need to swap the carrier line between ultra pure water and the nitric acid solution (which were both required if the CIM® disk was used in order to load the sample onto the column and then to elute it off). In this case the carrier line of nitric acid solution was continuously pumped without the need for the ultra pure water line.

5.3.2.1 Effect of Sample Loop Size

Initially a 65 µL sample loop was used in the flow system, as described in section 5.2.1, with the exception of the CIM® modified disk which, as mentioned in section 5.3.2, was not used during the optimisation studies in order to simplify the system. The use of a 150 µL sample loop was investigated and the resultant peaks for a 500 µg L^{-1} copper (II) standard are compared with those obtained using the smaller

sample loop size, as shown in Figure 5.7. The reagent concentrations and flow rates were the same as those used in section 5.3.1 (without the use of the CIM® disk). It was found that by increasing the sample loop size the sensitivity was increased, which would also result in an increase in the limit of detection. For each sample loop investigation, a sample blank and a 500 μg L^{-1} copper (II) standard were analysed.

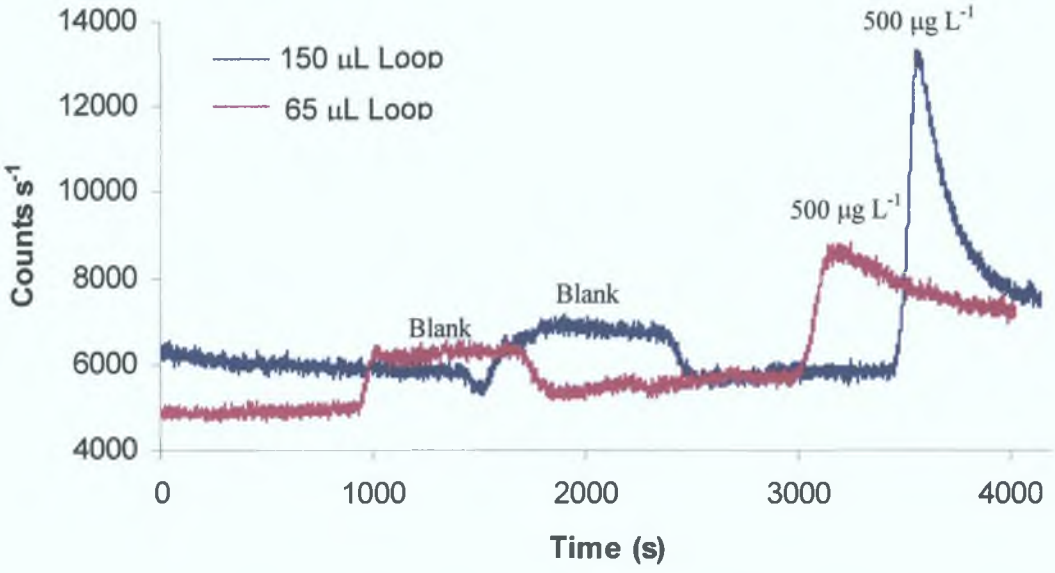

Figure 5.7: Comparison signals resulting from 65 μL and 150 μL sample loop. Reagent conditions: 0.03 mM 1,10-phenanthroline, 0.05 mM CTAB, 0.075 M NaOH, 5 % H_2O_2 and 25 mM HNO_3, at a combined flow rate of 0.56 mL min^{-1} (without the use of the CIM® modified disk).

5.3.2.2 Effect of Flow Rates

The flow rate is an important factor in a flow system as it affects the delivery of the reagents and hence the reaction time (i.e. the faster the flow rates, the quicker the reaction takes place). The flow rates therefore were varied on this system in order to investigate the effect on the resulting copper (II) chemiluminescence signal. These results can be seen in Figure 5.8, which compares the effect of three different flow rates on a blank signal and a 500 μg L^{-1} copper (II) standard. It was found that higher flow rates did not affect the sensitivity but reduced the analysis times. The period of chemiluminescence for the 500 μg L^{-1} copper (II) standard was approximately 470 s when the higher flow rate (1.14 ml min^{-1}) was used, compared to approximately 690 s when the lowest flow rate (0.53 ml min^{-1}) was used. The

reagent concentrations were the same as those used in the study on the effect of the sample loop size and a 150 µl sample loop was used for the introduction of sample. Once again, no CIM® disk was used in this work.

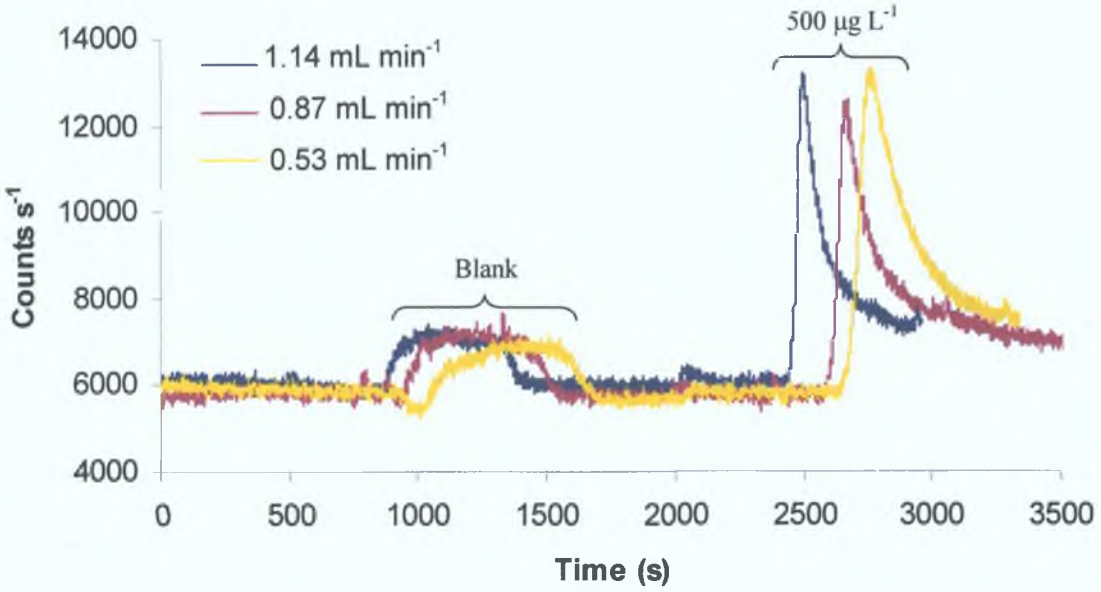

Figure 5.8: Comparison of flow rates using a sample blank and a 500 µg L^{-1} copper (II) standard. Reagent conditions: 0.03 mM 1,10-phenanthroline, 0.05 mM CTAB, 0.075 M NaOH, 5 % H_2O_2 and 25 mM HNO_3.

5.3.2.3 Effect of Nitric Acid Concentration

The concentration of nitric acid solution, for metal elution purposes, was investigated in this study as can be seen in Figure 5.9. Generally, the higher the acid concentration, the quicker elution occurs. As the copper-1,10-phenanthroline chemiluminescence reaction is pH dependent (optimum pH between pH 9.8 and pH 10.1), care must be taken to ensure the system pH does not vary too much. The concentration of acid used in this work, however, was in the low mM range and did not have a significant effect on the chemiluminescence reaction. The reagent concentrations were the same as those used in the study of the sample loop size and flow rate. A 150 µL sample loop was used for the introduction of sample (blank and 500 µg L^{-1} copper (II) standard) along with a total flow rate of 1.14 mL min^{-1}. The use of a CIM® disk was again not used in this study.

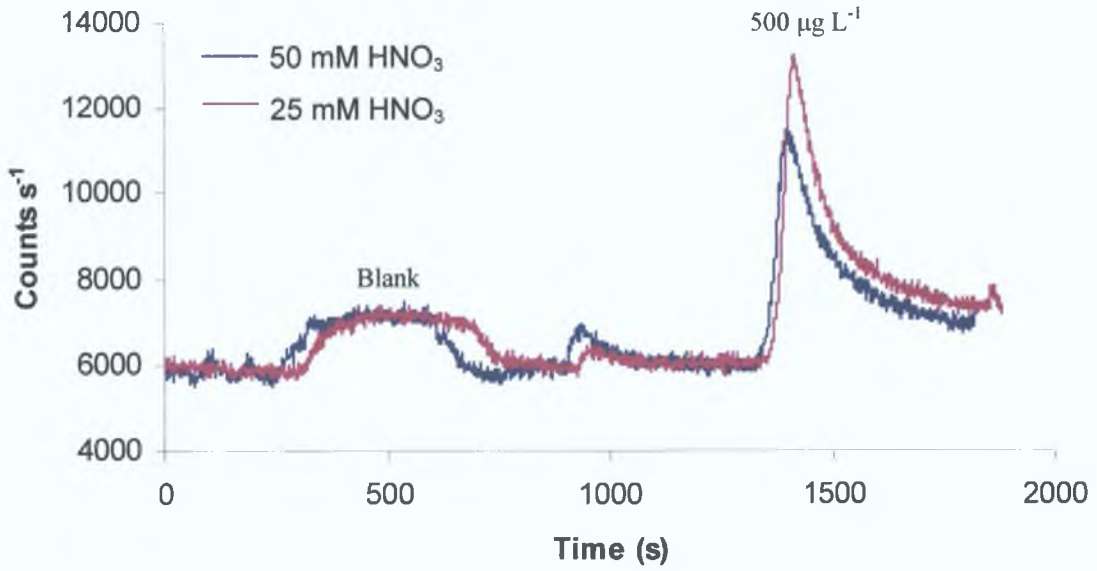

Figure 5.9: Comparison of nitric acid concentration. Experimental conditions: 0.03 mM 1,10-phenanthroline, 0.05 mM CTAB, 0.075 M NaOH and 5 % H_2O_2. Total flow rate 1.14 mL min^{-1} and sample loop size of 150 µL.

The concentration of the nitric acid solution was chosen to remain at 25 mM nitric acid, as this was found to produce a slightly higher signal for the 500 µg L^{-1} copper (II) standard than the 50 mM acid solution. This could be due to the fact that the higher concentration of acid had more of an impact on the overall pH of the system and therefore slightly reduced the resulting chemiluminescence signal.

5.3.2.4 Optimisation of 1,10-Phenanthroline and CTAB

Using the optimised sample loop, flow rate and nitric acid concentration, the 1,10-phenanthroline and CTAB concentrations were optimised. The experimental space was again defined by varying systematically both the concentrations of 1,10-phenanthroline and CTAB from 0.03 mM to 0.10 mM in the case of 1,10-phenanthroline and 0.05 mM to 2.00 mM for CTAB as shown in Figure 5.10.

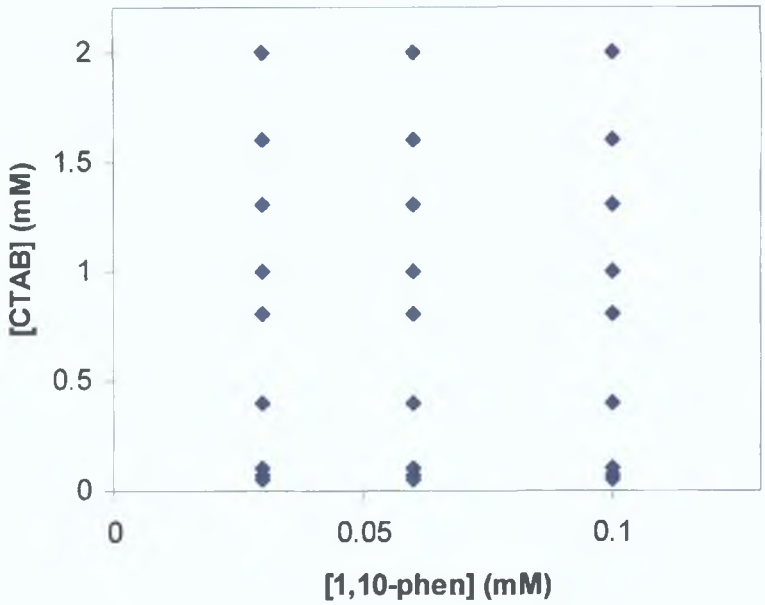

Figure 5.10: Experimental area used for optimisation of [CTAB] and [1,10-phenanthroline] using the following conditions: total flow rate of 1.14 mL min^{-1}, a 150 µL sample loop, 25 mM HNO_3, 5% H_2O_2 solution and 0.075 M NaOH.

A three-dimensional response surface plot was constructed for a 250 µg L^{-1} copper (II) standard showing the combined effects of 1,10-phenanthroline and CTAB concentrations on the signal to noise ratio. As can be seen from the Figure 5.11, the highest signal to noise ratio was achieved when using 0.06 mM 1,10-phenanthroline and 1.3 mM CTAB. In this case the signal to noise ratio was found to be approximately 172.

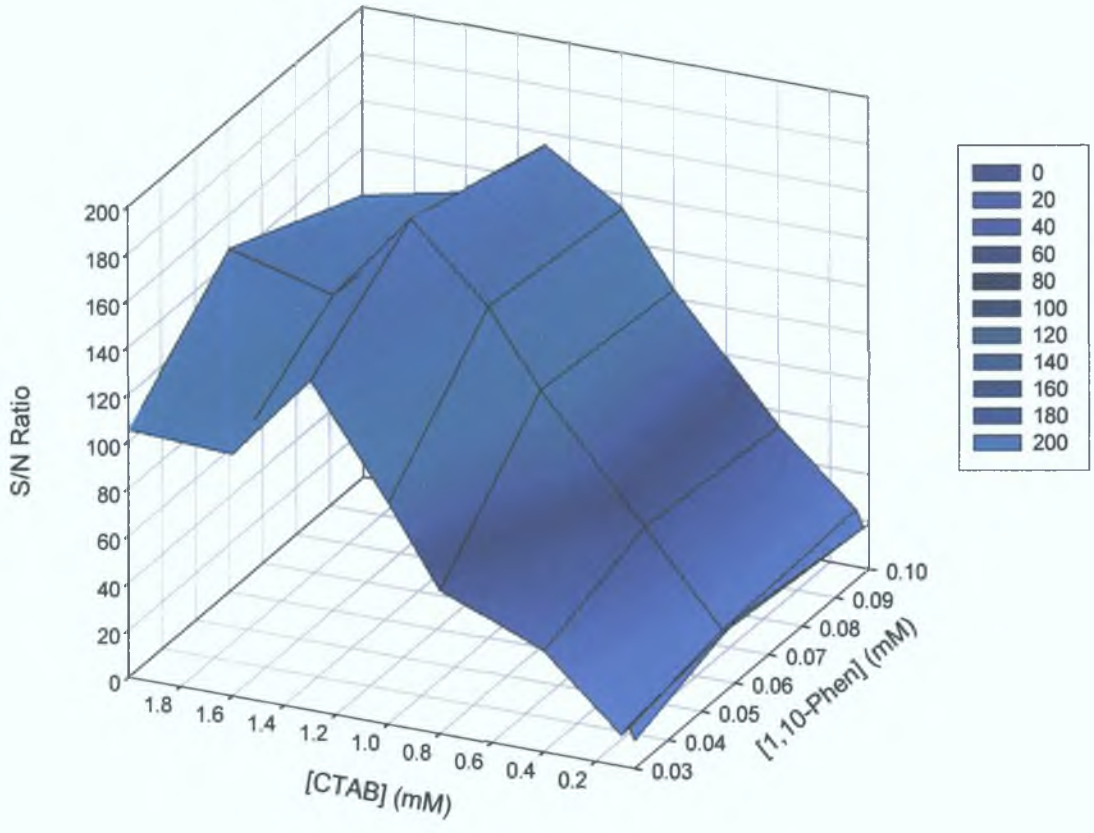

Figure 5.11: The response surface plot shows the optimum conditions of 1,10-phenanthroline and CTAB for a 250 μg L^{-1}copper (II) standard.

5.3.2.5 Optimisation of Hydrogen Peroxide Solution

The concentration of the hydrogen peroxide solution was then optimised using the previously optimised reagent and experimental conditions and a 250 μg L^{-1} copper (II) standard. The concentration of peroxide was varied from 2.5 % to 15.0 % hydrogen peroxide as can be seen in Figure 5.12. The optimum concentration was found to be 5.0 % peroxide solution, which had an RSD value of 3.6 % (where, n = 3).

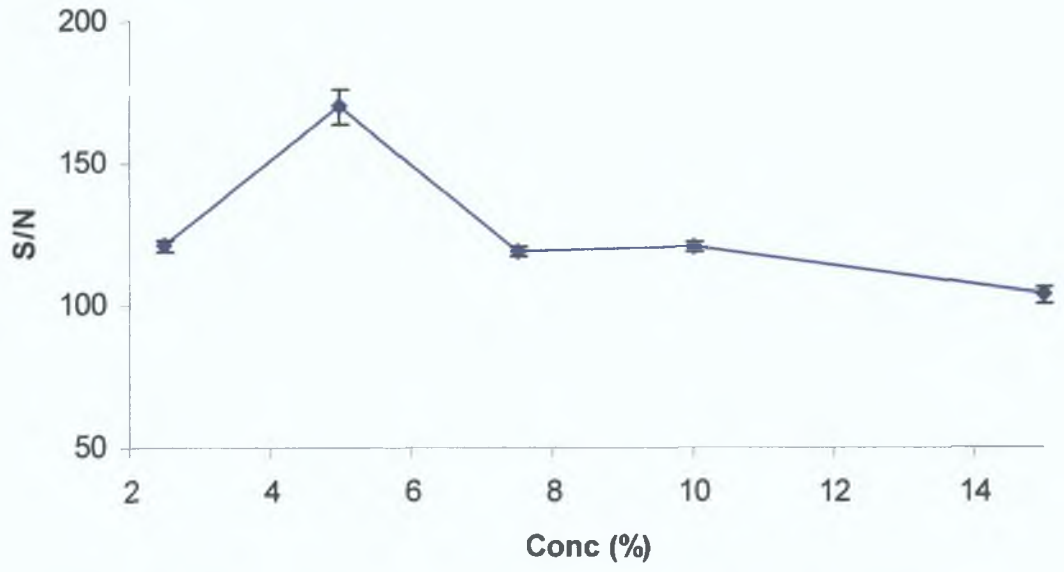

Figure 5.12: Optimisation of hydrogen peroxide solution, using a 250 μg L^{-1} copper (II) standard. Experimental conditions: 0.06 mM 1,10-phenanthroline, 1.3 mM CTAB, 0.075 M NaOH, 5 % H_2O_2 and 25 mM HNO_3. Total flow rate of 1.14 mL min^{-1} and sample loop size of 150 μL.

5.3.3 Reproducibility Studies

Using the optimised conditions obtained in section 5.3.2, a range of copper (II) standards varying in concentration from 0 to 500 μg L^{-1} were analysed in order to access the reproducibility of the optimised system. For simplicity, this system was again used without the inclusion of the CIM® modified disk. The optimised reagent conditions were: 0.06 mM 1,10-phenanthroline, 1.3 mM CTAB, 0.075 M sodium hydroxide, 5 % hydrogen peroxide solution and 25 mM nitric acid solution. A total flow rate of 1.14 mL min^{-1} and sample loop size of 150 μL were also used. The resultant peaks from this study can be seen in Figure 5.13.

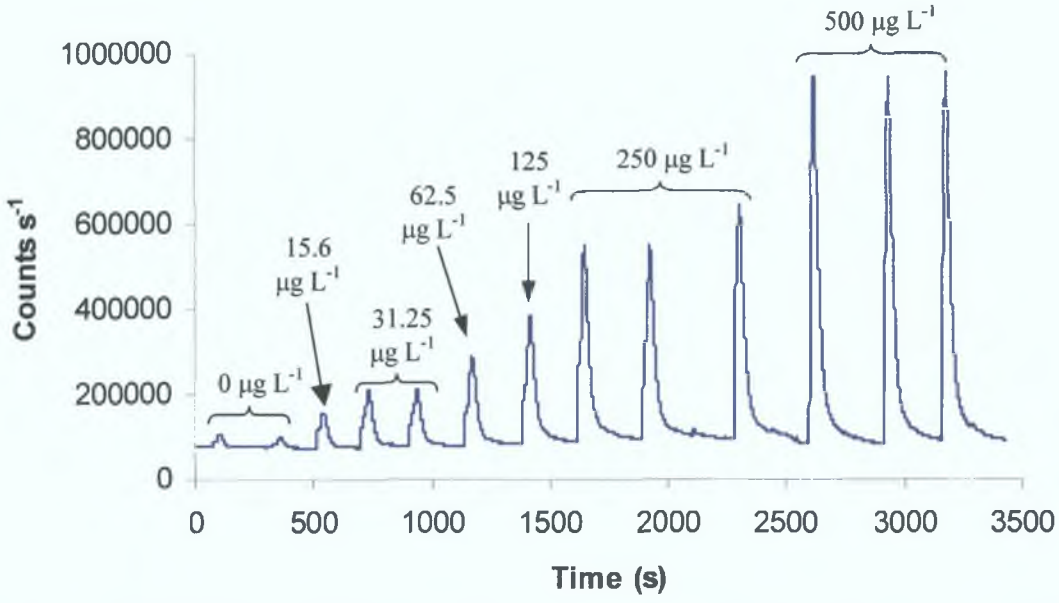

Figure 5.13: Reproducibility studies of copper (II) standards between 0 and 500 µg L^{-1}. Experimental conditions: 0.06 mM 1,10-phenanthroline, 1.3 mM CTAB, 0.075 M NaOH, 5 % H_2O_2 and 25 mM HNO_3. Total flow rate of 1.14 mL min^{-1} and sample loop size of 150 µL, without the incorporation of the CIM® modified disk.

Using the results obtained above, a calibration graph was plotted of the chemiluminescence intensity (based on counts s^{-1}) versus the copper (II) concentration (µg L^{-1}). The blank signal was subtracted from each of the copper (II) standard signals. This subtraction results in the removal of the effects of any interferences that may be present in the solutions. From these results it was found that there were two different areas of linearity. The first set of results were found to be linear over the concentration range 0 to 62.5 µg L^{-1}, with an R^2 value of 0.993 being obtained (Figure 5.14 (a)), while the second linear results were found over the concentration range 62.5 to 500 µg L^{-1} (R^2 = 0.999) (Figure 5.14 (b)).

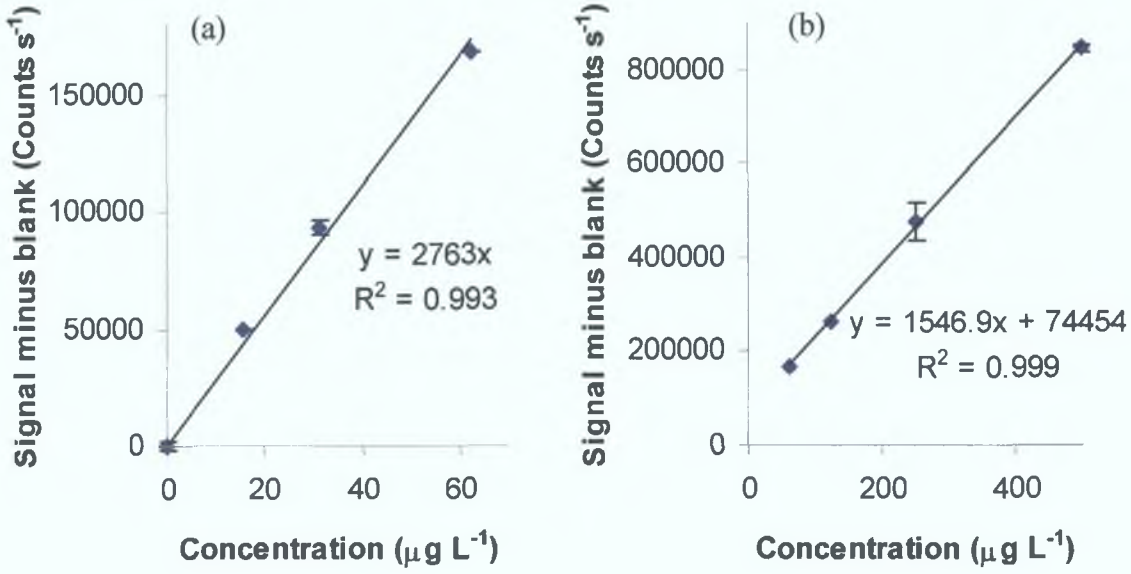

Figure 5.14: Copper (II) linearity studies over the concentration range (a) 0 to 62.5 µg L^{-1} and (b) 62.5 to 500 µg L^{-1}.

5.3.3.1 Calibration Study Using Picolinic Acid Modified CIM® Monolithic Disk

The picolinic acid modified CIM® disk was then incorporated back into the flow system as described in section 5.2.1 and using the same experimental conditions as before a range of copper (II) standards from 0 to 250 µg L^{-1} were injected into the system. The resulting chemiluminescence signals can be seen below in Figure 5.15. It should be noted in this section of work, the copper (II) standard was introduced into a flowing carrier stream of ultra pure water which allowed the sample to be loaded onto the CIM® disk. Following this the carrier line was changed over to the nitric acid solution to elute the copper (II) from the disk, which was subsequently detected using chemiluminescence.

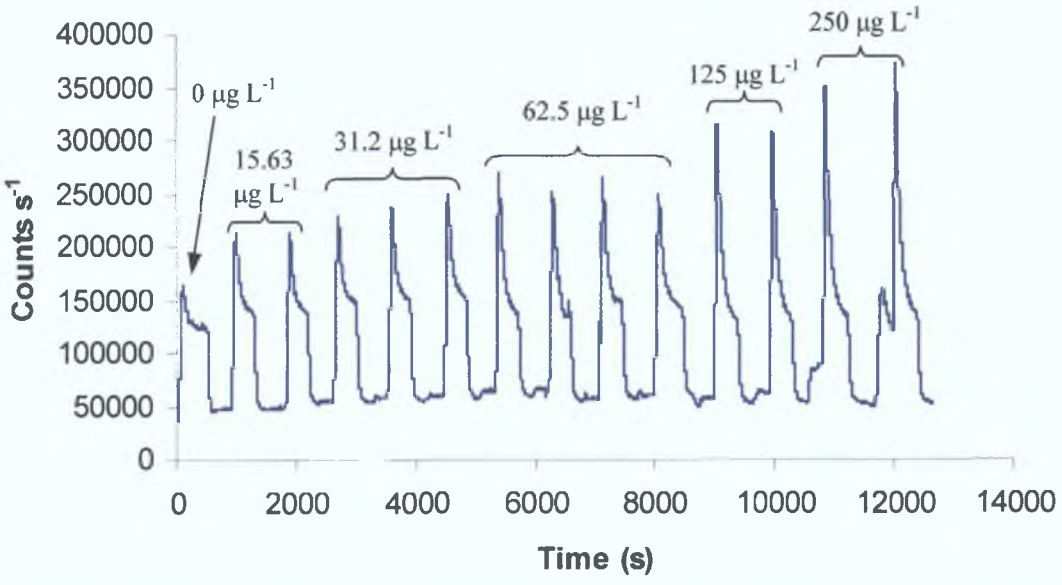

Figure 5.15: Reproducibility studies of copper (II) standards between 0 and 250 µg L^{-1} using picolinic acid coated CIM® disk. Experimental conditions: 0.06 mM 1,10-phenanthroline, 1.3 mM CTAB, 0.075 M NaOH, 5 % H_2O_2 and 25 mM HNO_3. Total flow rate of 1.14 mL min^{-1} and sample loop size of 150 µL.

As can be seen from Figure 5.15, there was a problem due to baseline shift when this system was used. This occurred when the carrier stream was changed from ultra-pure water to the eluent stream of nitric acid solution, which caused an increase in background chemiluminescence as a result of the change in the system pH, from approximately pH 10.0 to approximately pH 9.7. The background chemiluminescence changed from approximately 60,000 counts s^{-1}, when the pure water line was in use, to over 100,000 counts s^{-1} when the nitric acid line was in use. As mentioned previously, the optimum pH for this chemiluminescence reaction to occur is between pH 9.8 and pH 10.1, but it was found in this work, that even at lower pH values, an acceptable chemiluminescence response was obtained for a range of copper (II) standards.

The signal produced for 0 µg L^{-1} copper (II) (ultra pure water) was then subtracted from each of the copper (II) standard signals and the results were found to be linear over the concentration range 0 to 125 µg L^{-1}, based on peak height. The correlation coefficient was calculated to be 0.9812 over this concentration range (Figure 5.16 (a)). It was found that at concentrations above 125 µg L^{-1}, the graph began to curve

and deviate from linearity as the capacity of the modified CIM® disk monolithic column was reached (Figure 5.16 (b)).

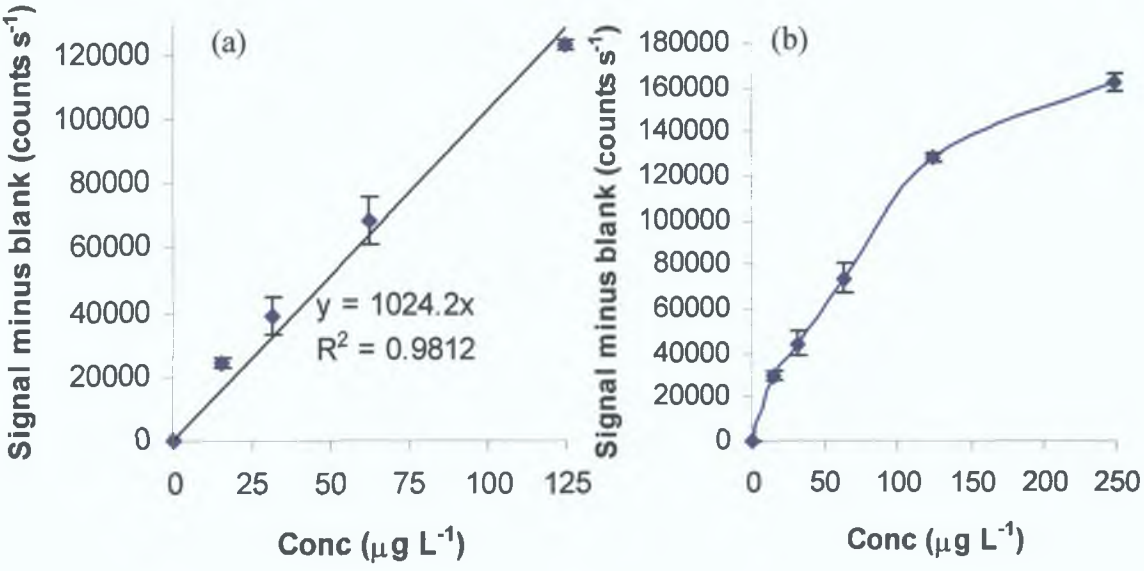

Figure 5.16: (a) Copper (II) linearity studies over the concentration range 0 to 250 µg L^{-1} based on chemiluminescence signal for copper (II) minus blank signal, where $R^2 = 0.9812$ (between 0 and 125 µg L^{-1}) using the picolinic acid coated CIM® disk, (b) calibration curve deviating from linearity over the concentration of 125 µg L^{-1} copper (II).

5.3.3.1.1 Application of Picolinic Acid Modified Disk to Certified Reference Material

The accuracy of this method was then verified using an international certified Standard Reference Material (SRM) from the National Institute of Standards and Technology (NIST), which was analysed for copper (II). This sample SRM 1640 was acidified with 0.5 mol L^{-1} nitric acid and was certified to contain 85.2 µg L^{-1} ± 1.2 µg L^{-1} copper (II). The sample was neutralised using a sodium hydroxide solution and was diluted by 50 % with ultra pure water. The resultant chemiluminescence signals for a sample blank and a 1 in 2 dilution of the NIST standard reference material can be seen in Figure 5.17.

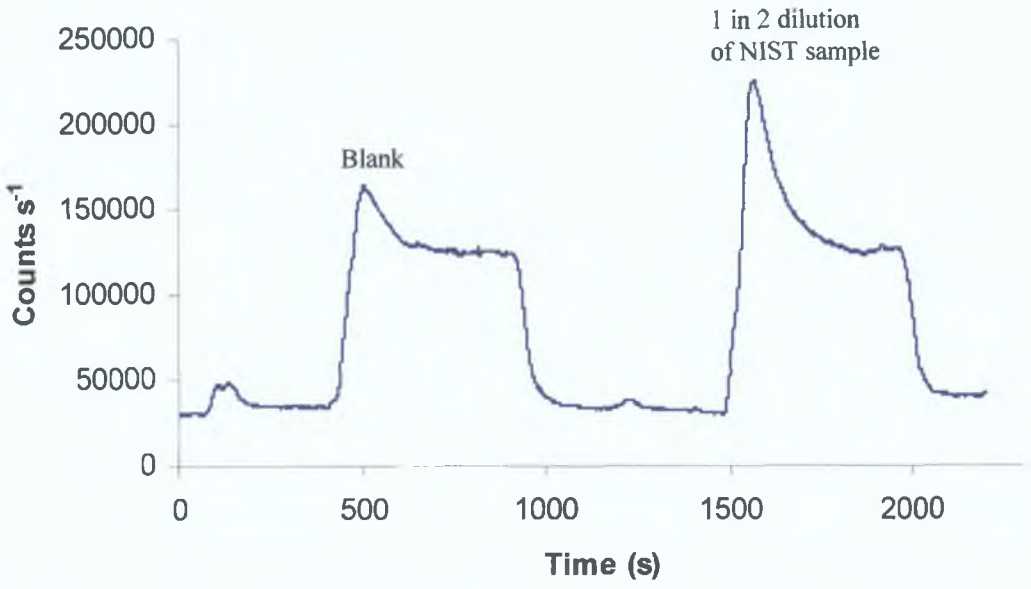

Figure 5.17: Analyses of 1 in 2 dilution of NIST standard which contained approximately 44 μg L^{-1} copper (II) using picolinic acid coated CIM® disk.

Based on peak heights, the signal for the 1 in 2 dilution of the NIST sample was calculated. The signal for the blank (ultra pure water matched to the pH of the diluted NIST sample) was subtracted from the sample which resulted in a figure of approximately 52,000 counts s^{-1}, which corresponded to approximately 44 μg L^{-1} for a 1 in 2 dilution and approximately 88 μg L^{-1} in the undiluted sample. This compared well to the certified value of 85.2 μg L^{-1}.

5.3.3.2 Calibration Study Using Dipicolinic Acid Modified CIM® Monolithic Disk

Using a similar procedure to that used for the picolinic acid coated CIM® disk, a similar study was carried out using the dipicolinic acid coated monolithic disk. The experimental conditions used were the same as those used in the previous section. The resultant chemiluminescence signals for a range of copper (II) standards from 0 to 250 μg L^{-1} are shown in Figure 5.18.

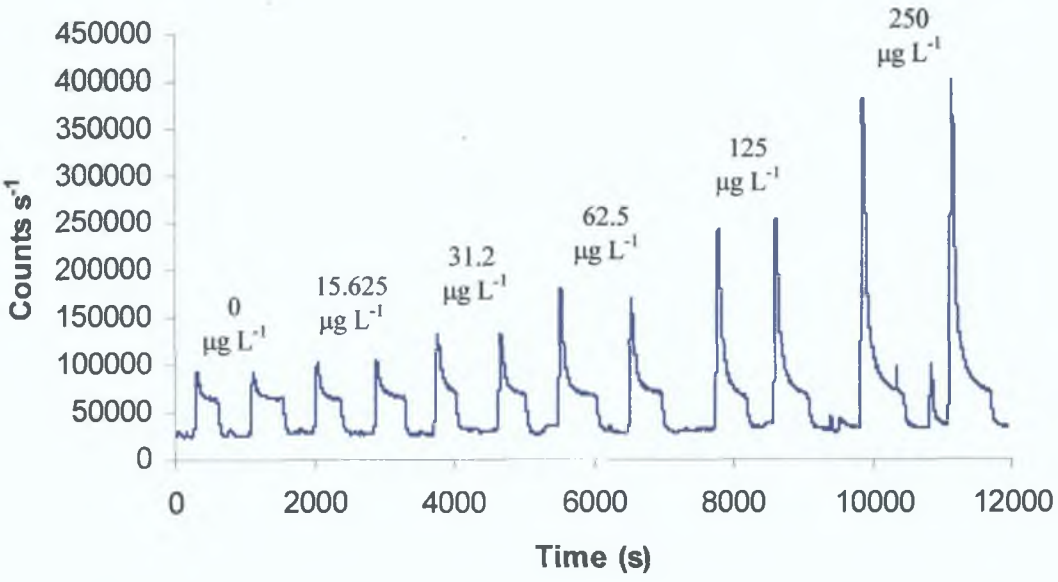

Figure 5.18: Reproducibility studies of copper (II) standards between 0 and 250 µg L^{-1} using dipicolinic acid coated CIM® disk. Experimental conditions: 0.06 mM 1,10-phenanthroline, 1.3 mM CTAB, 0.075 M NaOH, 5 % H_2O_2 and 25 mM HNO_3. Total flow rate of 1.14 mL min^{-1} and sample loop size of 150 µL.

The signal obtained for the 0 µg L^{-1} standard was then subtracted from each of the copper (II) standard signals as before and a calibration graph was plotted. These results were found to be linear over the concentration range 0 to 250 µg L^{-1} and an excellent correlation coefficient of 0.9980 was obtained over this concentration range, as can be seen from Figure 5.19.

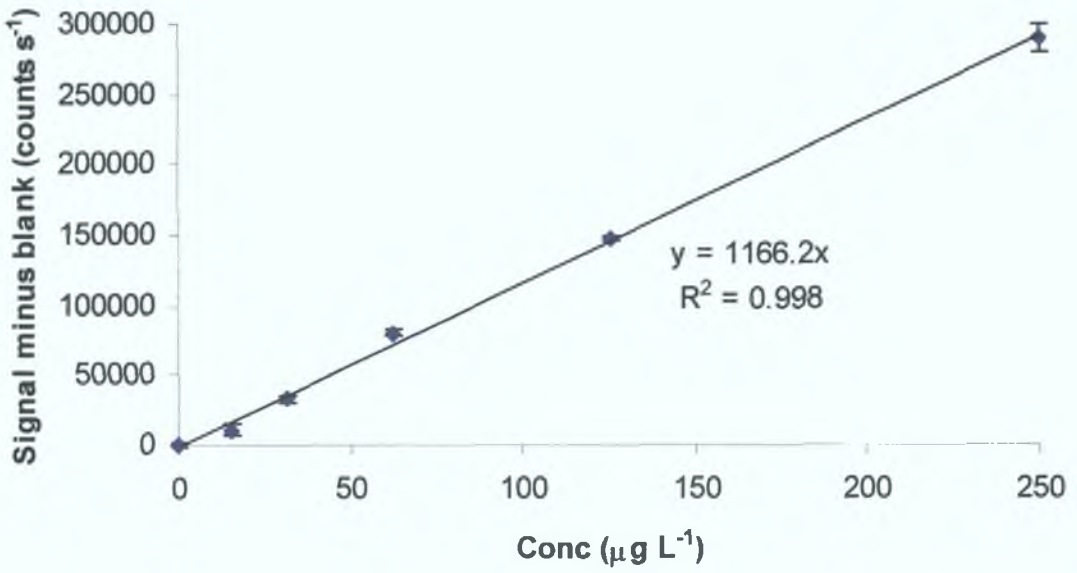

Figure 5.19: Copper (II) linearity studies over the concentration range 0 to 250 µg L^{-1} based on the chemiluminescence signal for the copper (II) standard minus the blank signal, where $R^2 = 0.9980$ for the dipicolinic acid coated CIM® disk.

When the results obtained for the dipicolinic acid modified CIM® disk are compared to those obtained for the picolinic acid modified disk, it can be seen that the linearity of the system has improved considerably for the dipicolinic acid system. The linear range for the dipicolinic acid modified disk ranges from 0 to 250 µg L^{-1}, with a R^2 value of 0.9980, compared to a linear range of 0 to 125 µg L^{-1} ($R^2 = 0.9812$) for the picolinic acid system. This improved linearity is due to the stronger complexing ability of the dipicolinic acid over the picolinic acid as discussed in section 5.1.1 of the introduction. The larger signal peaks obtained when the dipicolinic acid coated disk was used, represents a higher copper (II) recovery, which was also due to the stronger complexing ability of the dipicolinic acid.

5.3.3.2.1 Application of Dipicolinic Acid Modified Disk to Certified Reference Material

The accuracy of this method was then verified using the same international certified Standard Reference Material (SRM) as before, which was analysed for copper (II) (Figure 5.20). The sample was neutralised as before using sodium hydroxide and was diluted by 50 % with ultra pure water. The experimental conditions were the same as those used previously.

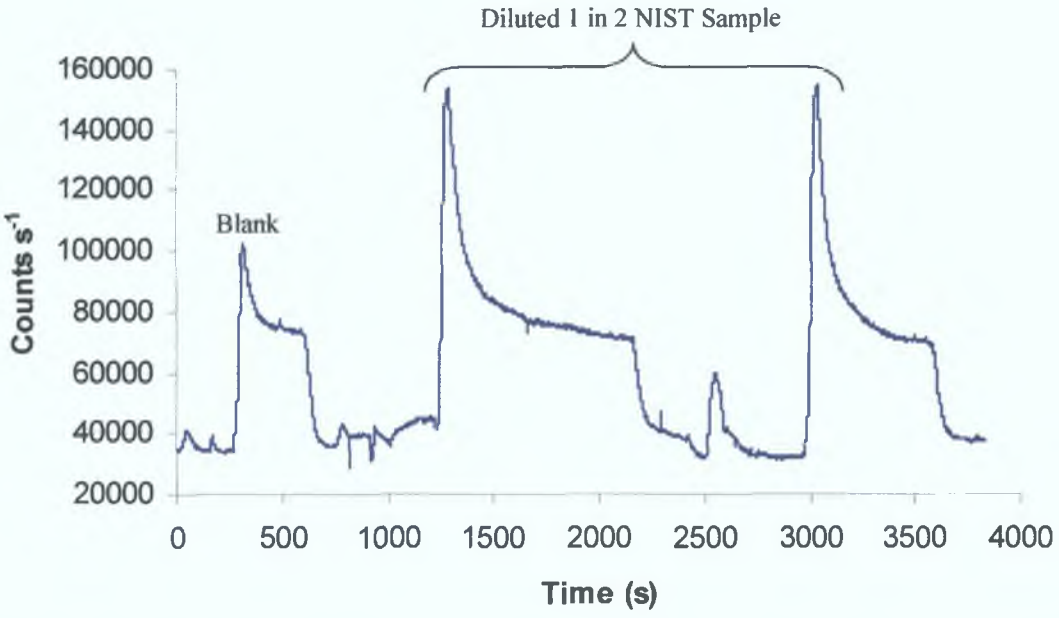

Figure 5.20: Analysis of 1 in 2 dilution of NIST standard (n = 2) which contained approximately 44 μg L^{-1} copper (II) using dipicolinic acid coated CIM® disk. Experimental conditions: 0.06 mM 1,10-phenanthroline, 1.3 mM CTAB, 0.075 M NaOH, 5 % H_2O_2 and 25 mM HNO_3. Total flow rate of 1.14 mL min^{-1} and sample loop size of 150 μL.

The signal for the blank (ultra pure water matched to the pH of the diluted NIST sample) was subtracted from the sample, in a similar way to that carried out in the picolinic acid study. This resulted in a figure of almost 50,600 counts s^{-1}, which corresponded to approximately 44 μg L^{-1} for a 1 in 2 dilution and approximately 88 μg L^{-1} in the undiluted sample. This again compared well to the certified value of 85.2 μg L^{-1} of the NIST sample.

5.3.3.3 Calibration Study Using Dodecyliminodiacetic Acid Modified CIM® Monolithic Disk

A CIM® disk was then coated with the dodecyliminodiacetic acid (C_{12}IDA) and a similar study to those carried out using the picolinic and dipicolinic acid modified CIM® disks was undertaken. A calibration was carried out and the resultant peaks for a range of copper (II) standards from 0 to 250 μg L^{-1} can be seen in Figure 5.21. The experimental conditions used here were similar to those used in the picolinic and dipicolinic acid studies.

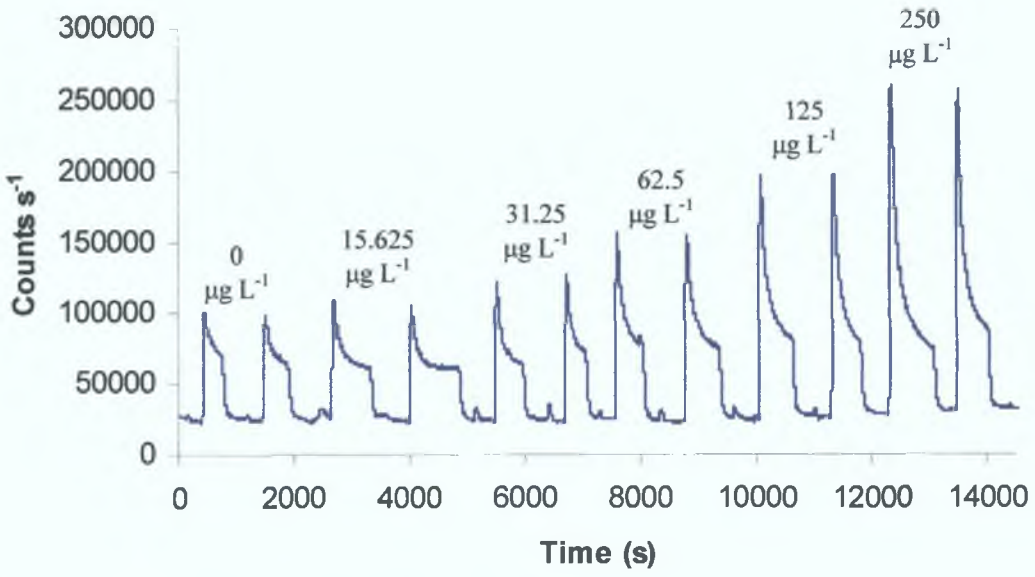

Figure 5.21: Reproducibility studies of copper (II) standards between 0 and 250 µg L^{-1} using dodecyliminodiacetic acid coated CIM® disk. Experimental conditions: 0.06 mM 1,10-phenanthroline, 1.3 mM CTAB, 0.075 M NaOH, 5 % H_2O_2 and 25 mM HNO_3. Total flow rate of 1.14 mL min^{-1} and sample loop size of 150 µL.

The signal due to the ultra pure water was then subtracted from each of the copper (II) standard signals and the results were found to be linear over the concentration range 0 to 125 µg L^{-1}, based on peak height. The correlation coefficient was calculated to be 0.9859 over this concentration range. Figure 5.22 shows the results of the copper (II) signals minus the blank signal. The % RSD for these results was calculated to be < 2.5 %. At concentrations above 125 µg L^{-1}, the graph appears to curve and begin to level off. Similar to the results obtained for the picolinic acid modified CIM® disk column, this curvature was due to the capacity of the column being reached.

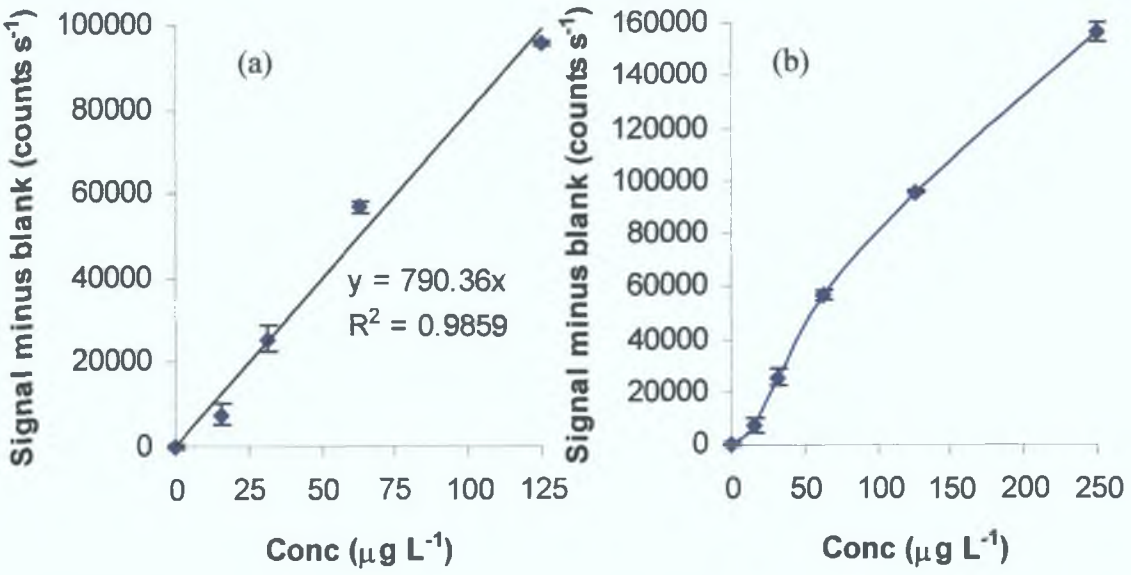

Figure 5.22: (a) Copper (II) linearity studies over the concentration range 0 to 250 µg L^{-1} based on chemiluminescence signal for copper (II) minus blank signal, where R^2 = 0.9859 (between 0 and 125 µg L^{-1}) using the dodecyliminodiacetic acid coated CIM® disk, (b) calibration curve deviating from linearity over the concentration of 125 µg L^{-1} copper (II).

The results obtained for the dodecyliminodiacetic acid modified CIM® disk were compared to those obtained for the dipicolinic acid modified disk. It was found that the linearity of the dodecyliminodiacetic acid system had decreased in comparison to the dipicolinic acid system. The linear range for the dipicolinic acid modified disk ranges from 0 to 250 µg L^{-1}, with a R^2 value of 0.9980 compared to a linear range of 0 to 125 µg L^{-1} (R^2 = 0.9859) for the dodecyliminodiacetic acid system. As before, this is due to the stronger complexing ability of the dipicolinic acid over the dodecyliminodiacetic acid as discussed in section 5.1.1 of the introduction.

5.3.3.3.1 Application of Dodecyliminodiacetic Acid Modified Disk to Certified Reference Material

The accuracy of this method was then verified using the same international certified Standard Reference Material (SRM) as before, which was analysed for copper (II). The sample was neutralised as before using sodium hydroxide and was diluted by 50 % with ultra pure water. The resultant chemiluminescence signals for a sample

blank and a 1 in 2 dilution of the NIST standard reference material (n = 2) can be seen in Figure 5.23.

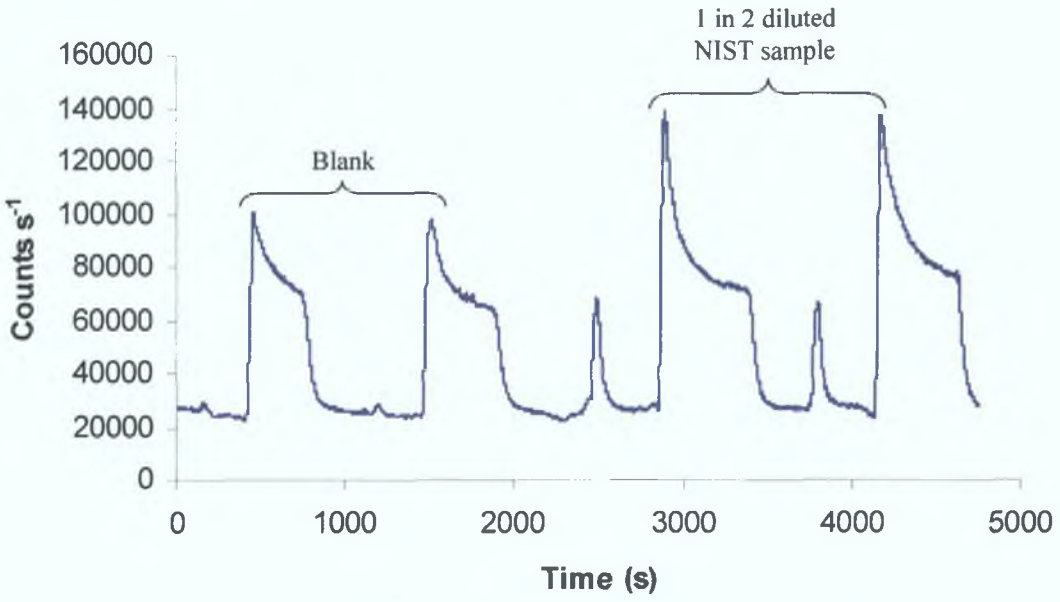

Figure 5.23: Analysis of 1 in 2 dilution of NIST standard which contained approximated 46 μg L^{-1} copper (II) using dodecyliminodiacetic acid coated CIM® disk.

As before, the signal for the blank (ultra pure water matched to the pH of the diluted NIST sample) was subtracted from the sample which resulted in a figure of approximately 38,000 counts s^{-1}, which corresponded to approximately 46 μg L^{-1} for a 1 in 2 dilution and approximately 92 μg L^{-1} in the undiluted sample.

5.3.3.4 Comparative Summary of the Carboxylic Acid Disk Modifiers

Table 5.1 shows the comparative analytical performance data determined for the three carboxylic acid CIM® monolithic disk modifying coatings. The data shown here represents that obtained under the specific conditions used within this study only. The best modifier in this case was chosen to be dipicolinic acid due to its largest linear range (up to 250 μg L^{-1} compared to 125 μg L^{-1} for the other two modifiers) and also because the best correlation coefficient was obtained for this carboxylic acid (R^2 = 0.9980).

Table 5.1: Analytical performance data for three carboxylic acid modifying coatings.

Modifying Ligand	Linear Range (μg L^{-1})	R^2 value
Picolinic acid	0 – 125	0.9812
Dipicolinic Acid	0 – 250	0.9980
Iminodiacetic Acid	0 – 125	0.9859

5.3.4 Re-optimisation of Nitric Acid Solution

It was decided to re-optimise the concentration of nitric acid solution which was required for removal of the copper (II) sample from the CIM® modified disk, as mentioned in optimisation section (section 5.3.2.3). In this work, the dipicolinic acid coated CIM® disk was used, as this modified disk achieved the best results, with a correlation coefficient of 0.9980 being obtained for the calibration over the linear concentration range of 0 to 250 μg L^{-1} copper (II) (section 5.3.3.2). The dipicolinic acid coated disk was used for subsequent processes described in the rest of this chapter.

The concentration of the nitric acid solution for elution purposes was varied from 2.5 mM to 25.0 mM, while all the rest of the experimental conditions remained the same as those used previously. A 50 μg L^{-1} copper (II) standard was used during this re-optimisation study. The resultant peak signals for this copper (II) standard are shown in Figure 5.24. The optimum concentration remained at 25 mM as it produced the highest resultant chemiluminescence signal. It was also found at some of the lower concentrations, that the copper (II) was slower to elute or in the case of the 2.5 mM nitric acid solution, the solution was found to be too weak to remove any of the bound copper (II) from the dipicolinic acid modified disk and as a result no elution occurred at all.

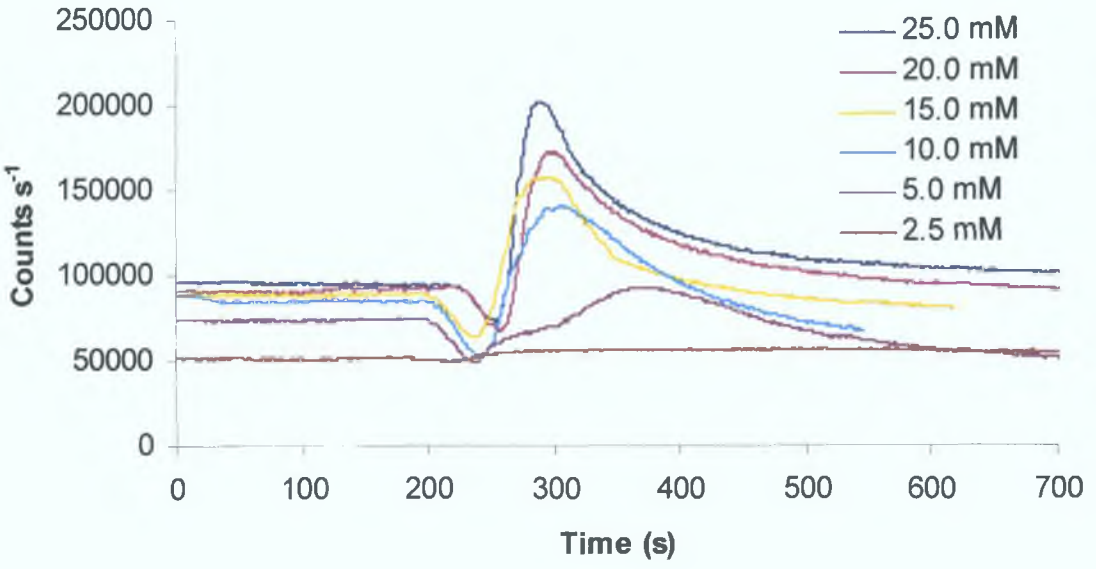

Figure 5.24: Resultant signals for 50 μg L^{-1} copper (II) standard in re-optimisation of HNO_3 solution. Experimental conditions: 0.06 mM 1,10-phenanthroline, 1.3 mM CTAB, 0.075 M NaOH, and 5 % H_2O_2. Total flow rate of 1.14 mL min^{-1} and sample loop size of 150 μL.

5.3.5 Effect of Increasing Number of CIM® Disks

As mentioned in section 5.2.2, it is possible to accommodate up to four CIM® disks per housing. It was decided to investigate the effect of increasing the number of CIM® disks, as up until now only one CIM® disk was incorporated into the housing. All the disks in this case were modified with dipicolinic acid prior to use. The experimental conditions used here were the same as those used before. In each case, the copper (II) standard (50 μg L^{-1}) was injected into the carrier stream of pure water at time = 0, then at time = 300 s the carrier line was switched to the nitric acid line for elution purposes. It was found that the retention of the copper (II) increased with the number of modified disks used in the system (Table 5.2). It was deemed satisfactory, however, to employ the use of a single CIM® disk for future work as the number of disks did not effect the sensitivity (as all the resultant peak heights were similar) and the overall sample throughput of the system could be improved as the copper (II) was eluted quicker when a single disk was used.

Table 5.2: Effect of increasing number of modified CIM® disks.

Number of Disks	Retention Time (s)	Approximate Peak Height (Counts s^{-1})
1	405	169,100
2	512	166,300
3	621	173,000

5.3.6 Synthetic Seawater Analysis

A synthetic seawater sample was made up containing 0.5 M sodium chloride, 1,300 mg L^{-1} magnesium (II) and 400 mg L^{-1} calcium (II) approximately. Aliquots of this sample were then spiked with varying concentrations of copper (II) and the resultant chemiluminescence signals can be seen in Figure 5.25. The experimental conditions were the same as those used previously and in this work a single dipicolinic acid modified CIM® disk was used.

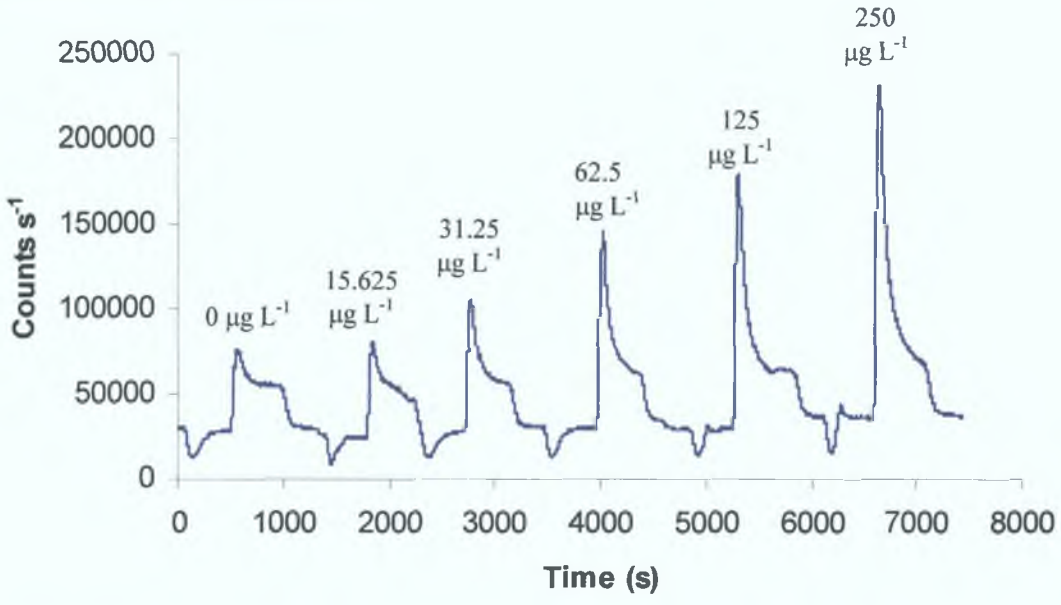

Figure 5.25: Reaction peaks generated for synthetic seawater sample spiked with copper (II). Experimental conditions: 0.06 mM 1,10-phenanthroline, 1.3 mM CTAB, 0.075 M NaOH, 5 % H_2O_2 and 25 mM HNO_3. Total flow rate of 1.14 mL min^{-1} and sample loop size of 150 µL.

It was then decided to pass the synthetic seawater sample through a Chelex-100 column, which was buffered to pH 5.0 in order to remove any copper (II) contaminants which may be present in the sample. Using the same procedure as before aliquots of this 'cleaned' synthetic seawater sample were spiked with varying concentrations of copper (II) and the resultant signals can be seen in Figure 5.26.

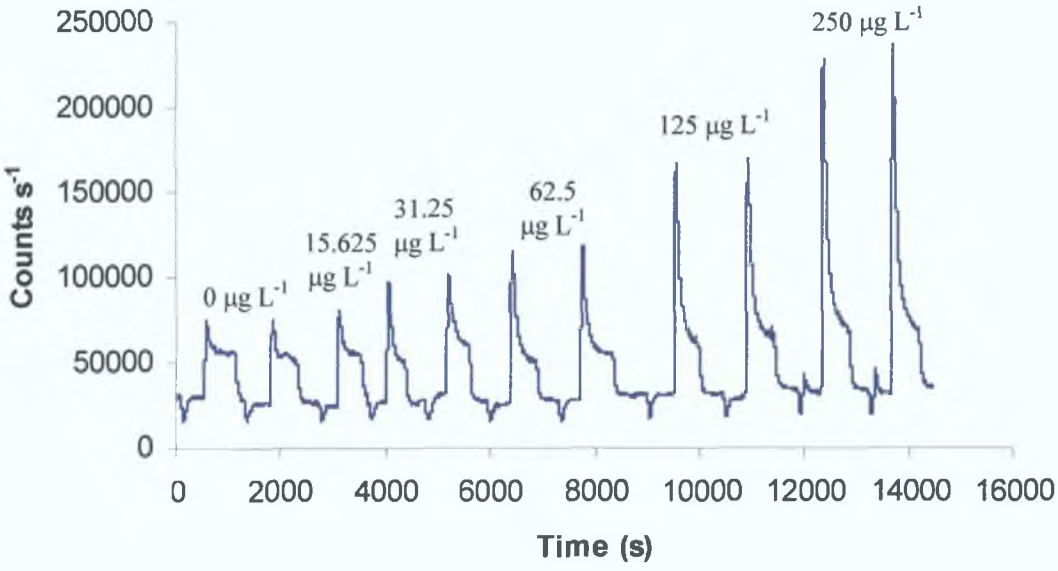

Figure 5.26: Reaction peaks generated for 'cleaned' synthetic seawater sample spiked with copper (II). Experimental conditions: 0.06 mM 1,10-phenanthroline, 1.3 mM CTAB, 0.075 M NaOH, 5 % H_2O_2 and 25 mM HNO_3. Total flow rate of 1.14 mL min^{-1} and sample loop size of 150 µL.

As can be seen from Figure 5.27, which compares the results of the 'cleaned' synthetic seawater with the 'un-cleaned' results, there was very little difference in the two results, showing there was little copper (II) contaminants present in the sample to begin with, and the chemiluminescence signal produced is only due to the copper (II) spiked into the sample. It should be noted that at concentrations above 125 µg L^{-1}, the graph began to curve and level off, and both sets of results were found to be linear over the range 0 to 125 µg L^{-1} copper (II).

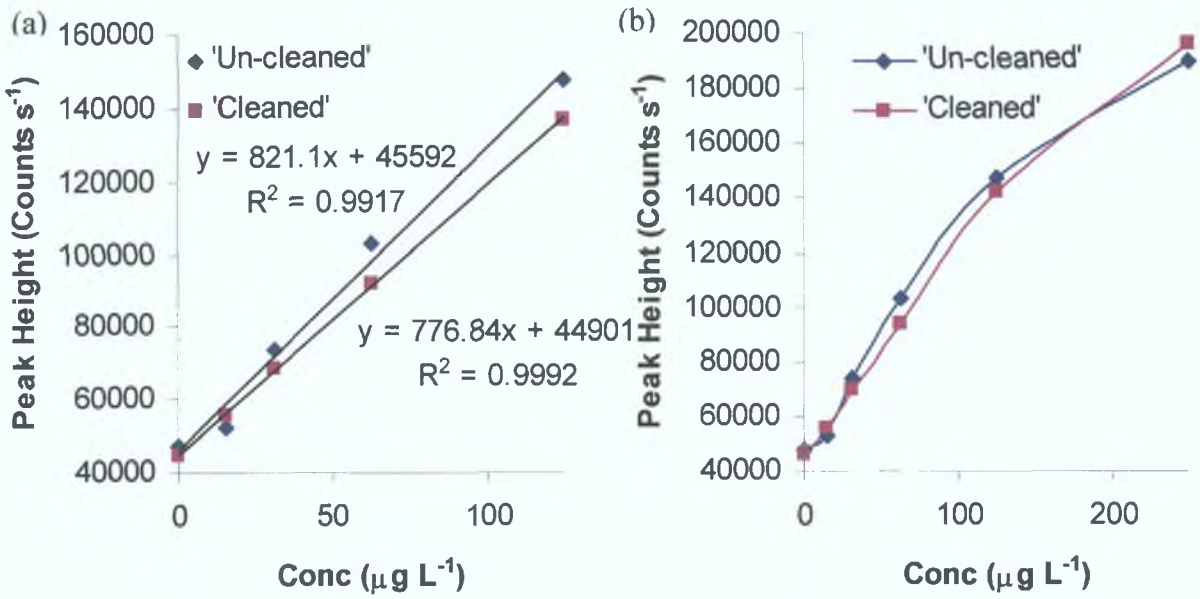

Figure 5.27: Comparison of 'cleaned' and 'un-cleaned' synthetic seawater standard additions, (a) standard calibrations where R^2 = 0.9992 and 0.9917 for 'cleaned' and 'un-cleaned' samples respectively (between 0 and 125 µg L^{-1}), (b) calibration curves deviating from linearity over the concentration of 125 µg L^{-1} copper (II).

To verify that the calcium (II) and magnesium (II) present in the synthetic seawater sample were all un-retained by the CIM® disk, the outlet solution was analysed by VIS detection using a post column reagent of *o*-CPC at 570 nm. Figure 5.28 shows the calcium (II) and magnesium (II) detected using VIS detection overlaid on the chemiluminescence signal produced for a 250 µg L^{-1} copper (II) standard made up in synthetic seawater. As can be seen from this Figure the signals measured for the calcium (II) and magnesium (II) correspond well to the negative peak on the copper (II) chemiluminescence signal verifying that the calcium (II) and magnesium (II) present in the seawater matrix are both un-retained by the CIM® disk.

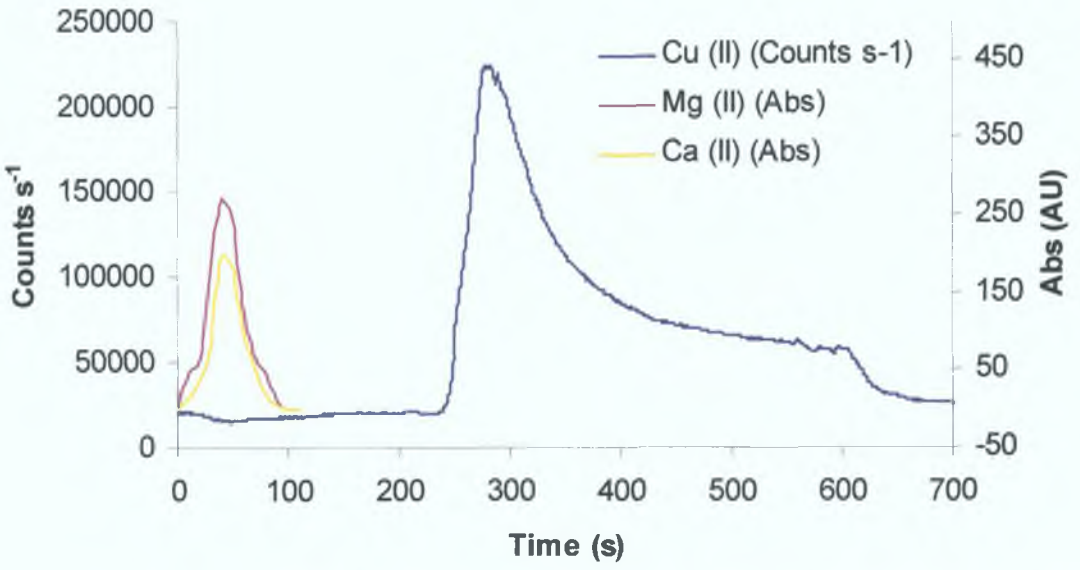

Figure 5.28: Overlay of calcium (II) and magnesium (II) signals detected by VIS detection and the chemiluminescence signal produced for a 250 μg L^{-1} copper (II) standard made up in synthetic seawater. Experimental conditions: Total flow rate of 1.14 mL min^{-1} and sample loop size of 150 μL. Chemiluminescence reagents: 0.06 mM 1,10-phenanthroline, 1.3 mM CTAB, 0.075 M NaOH, 5 % H_2O_2 and 25 mM HNO_3. VIS reagents: 5 mM HNO_3 and 0.4 mm *o*-CPC with 0.25 M boric acid, detected at 570 nm.

5.3.7 Real Sample Analyses

Ideally, calibration standards should approximate the composition of the samples to be analysed not only in respect of the analyte concentration but also with regard to the concentrations of the other species in the sample matrix, to minimise the effects of the various components of the sample [16]. For complex materials, it can be difficult to prepare standards that match the samples so the use of standard addition can overcome the matrix effects. In this case the developed method was used for the analysis of a coastal seawater sample and an estuary water sample. Both of the water samples were analysed in the same way. An aliquot of water was spiked with various concentrations of copper (II) and the sample was then analysed by the system. The experimental conditions were similar to those used previously.

Figure 5.29 shows the reaction peaks generated for the coastal seawater sample spiked with copper (II). A range of copper (II) standards were made up in the seawater sample over the concentration range 0 to 250 μg L^{-1}.

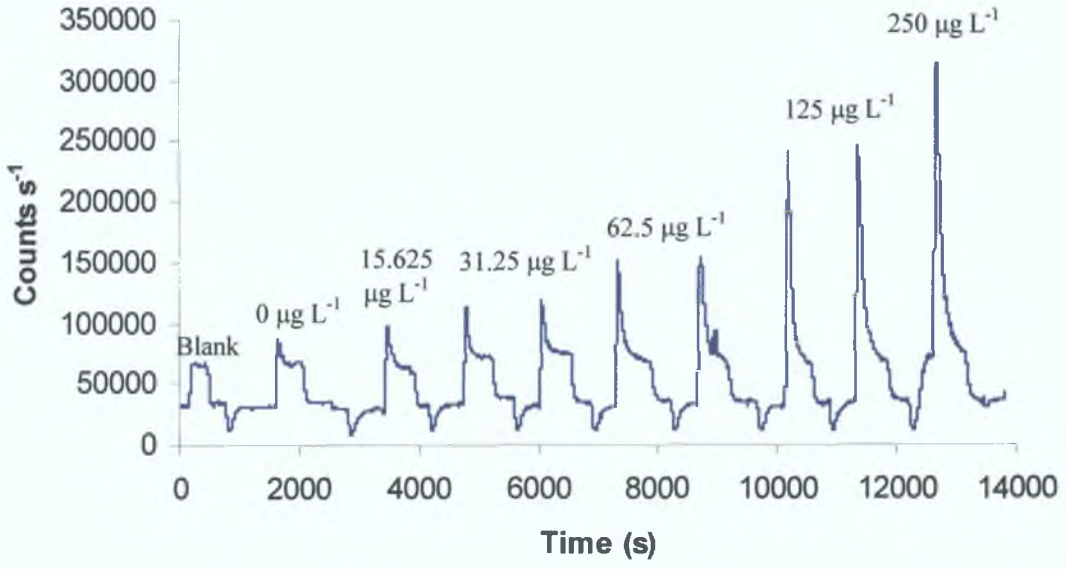

Figure 5.29: Reaction peaks generated for seawater samples spiked with varying concentrations of copper (II). Experimental conditions: 0.06 mM 1,10-phenanthroline, 1.3 mM CTAB, 0.075 M NaOH, 5 % H_2O_2 and 25 mM HNO_3. Total flow rate of 1.14 mL min^{-1} and sample loop size of 150 µL.

The blank signal was then subtracted from each of the standards in order to obtain an accurate result due to the copper (II) found in the sample. Figure 5.30 illustrates a section of the graph shown in Figure 5.29 (from 0 to 4,000 s), which shows the blank signal and two samples (unspiked sample containing 0 µg L^{-1} of copper (II) and spiked sample containing 15.625 µg L^{-1} of copper (II)). The pink line shows how the blank signal was subtracted from the 0 µg L^{-1} and 15.625 µg L^{-1} copper (II) spiked sample, to obtain a result for copper (II) only. A similar procedure was carried out for each of the other standards analysed in this study.

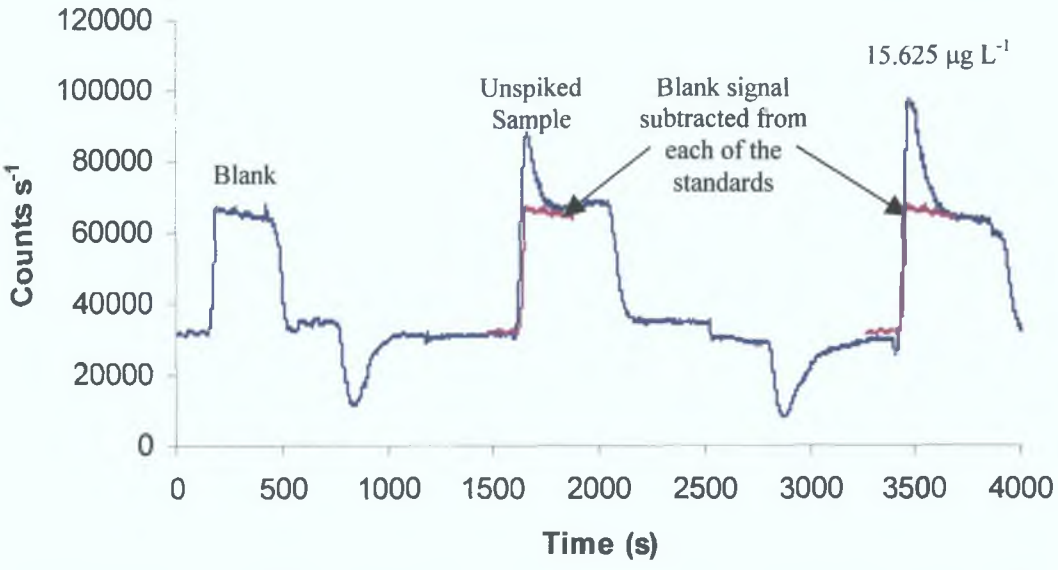

Figure 5.30: Subtraction of blank signal from copper (II) standards carried out during the seawater analysis.

A standard addition calibration graph was then obtained using the above results (standard minus blank signal) as shown in Figure 5.31. It was found that the results were linear over the concentration range 0 to 125 µg L^{-1} (R^2 = 0.9933) and at concentrations above this the graph deviated from linearity and began to level off due to overloading of the seawater matrix. Where two replicate injections were made for each copper standard, the error associated with each was calculated by the difference between the two values for each standard. It was found that the difference was calculated to be < 2.5 %, which was deemed acceptable for these results. As presented earlier, a similar analysis was carried out as shown in Figure 5.19, except that the copper (II) standards were made in pure water instead of a seawater sample matrix. In the case of the copper (II) standards made up in pure water, the results were found to be linear over the concentration range 0 to 250 µg L^{-1}, showing the seawater matrix is the cause of the deviation mentioned above.

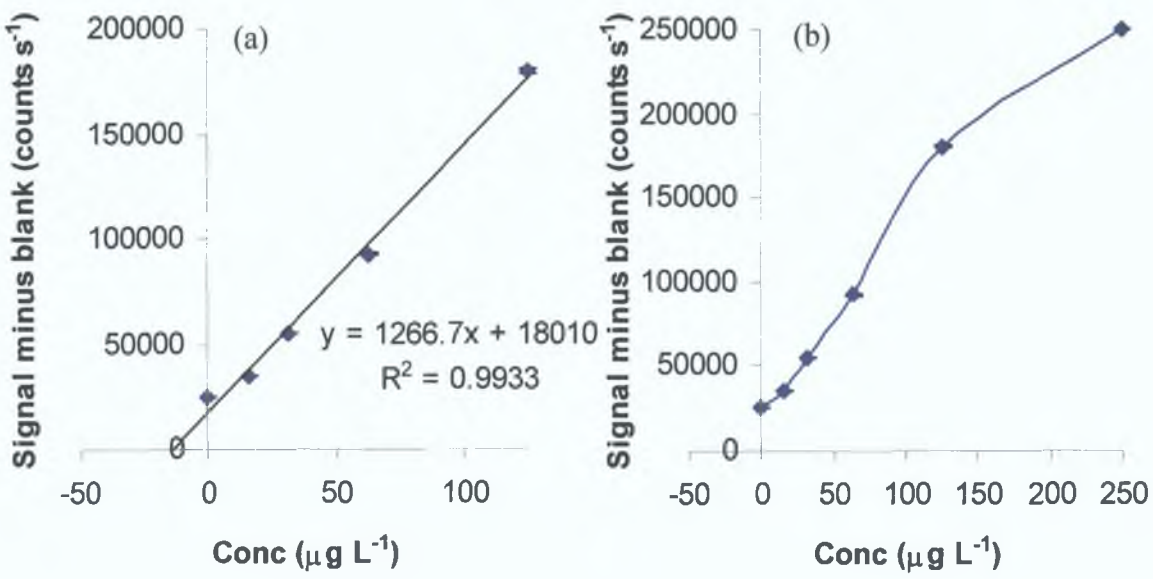

Figure 5.31: (a) Standard addition graph for seawater sample spiked with copper (II), R^2 = 0.9933 over the concentration range 0 to 150 µg L^{-1} copper (II), (b) calibration curve deviating from linearity over the concentration of 125 µg L^{-1} copper (II).

From the results shown in Figure 5.31, the amount of copper (II) present in the coastal seawater sample was calculated to be 14 µg L^{-1} using the equation of the line y = 1266.7x + 18010.

In similar work to the standard addition carried out on the seawater sample, the same procedure was carried out on an estuary water sample. Once again, an aliquot of the water sample was spiked with various concentrations of copper (II) and the sample was then analysed by the chemiluminescence system. The experimental conditions were similar to those used in the seawater analysis. Figure 5.32 illustrates the reaction peaks generated for the estuary water sample spiked with varying concentrations of copper (II).

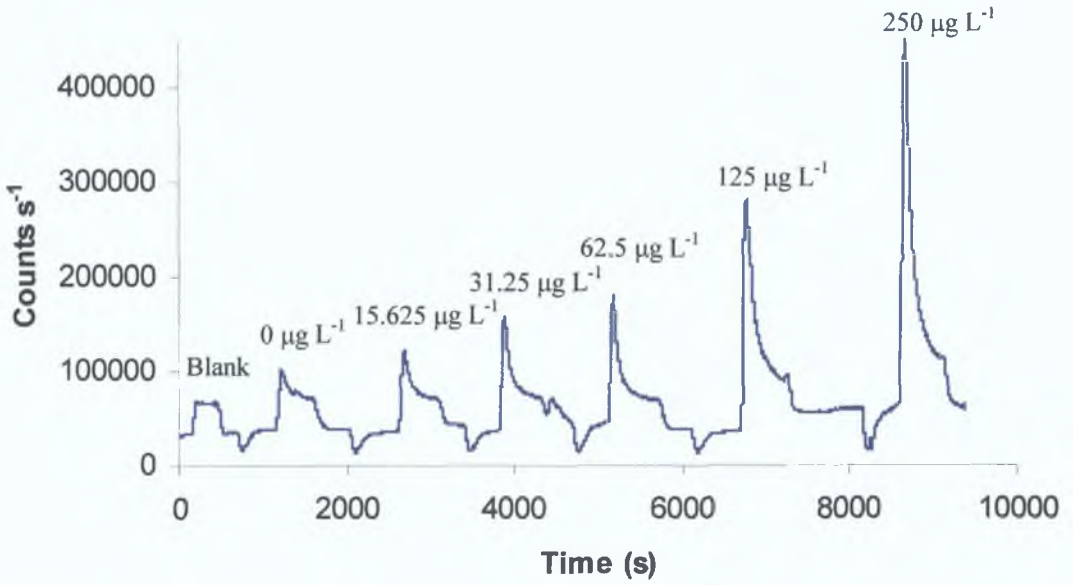

Figure 5.32: Reaction peaks generated for estuary water samples spiked with varying concentrations of copper (II). Experimental conditions: 0.06 mM 1,10-phenanthroline, 1.3 mM CTAB, 0.075 M NaOH, 5 % H_2O_2 and 25 mM HNO_3. Total flow rate of 1.14 mL min^{-1} and sample loop size of 150 µL.

A standard addition calibration graph was then obtained in a similar way to that obtained in the seawater standard addition. The blank signal was subtracted from each of the standards in order to obtain an accurate result due to copper (II) in the sample. It was found that the results were linear over the concentration range 0 to 250 µg L^{-1} (R^2 = 0.9973) as can be seen in Figure 5.33. It can be seen from this that the graph did not curve like the seawater results did, due to the fact that there was less calcium (II) and magnesium (II) present in the estuary water sample resulting in less overloading occurring. From these results the amount of copper (II) present in the estuary water sample was calculated to be 25 µg L^{-1} using the equation of the line y = 1430.6x + 35066.

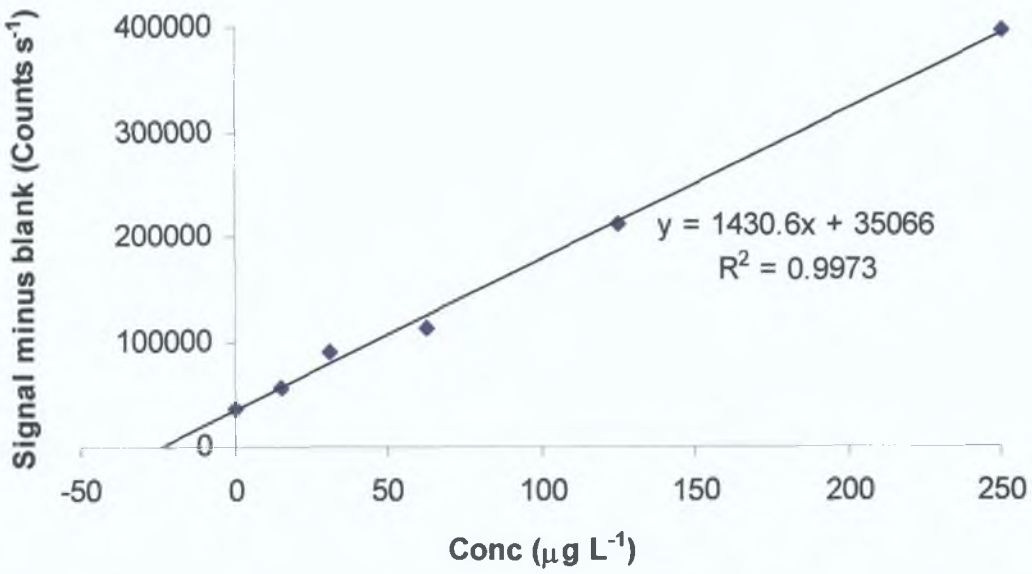

Figure 5.33: Standard addition graph for estuary water sample spiked with copper (II), $R^2 = 0.9973$.

5.3.8 Improving Overall Efficiency of Flow System

It was decided to try to improve the overall efficiency of the current working method. This included the re-optimisation of the sample injection loop size and the flow rates in order to improve the sample throughput and possible enhancement of sensitivity.

5.3.8.1 Re-optimisation of Sample Loop Size

A range of sample loops varying in size from 150 µL to 2,000 µL were investigated in this study. As can be seen from Figure 5.34, it was found that increasing the sample loop size resulted in an increase in the sensitivity. A range of copper (II) standards were made up in synthetic seawater and used during this analysis. The experimental conditions were the same as those used earlier. The optimum sample loop size was chosen to be 220 µL as this loop resulted in the best correlation coefficient ($R^2 = 0.9913$) over the concentration range 0 to 125 µg L^{-1} copper (II), although all of the sample loops were found to give acceptable results.

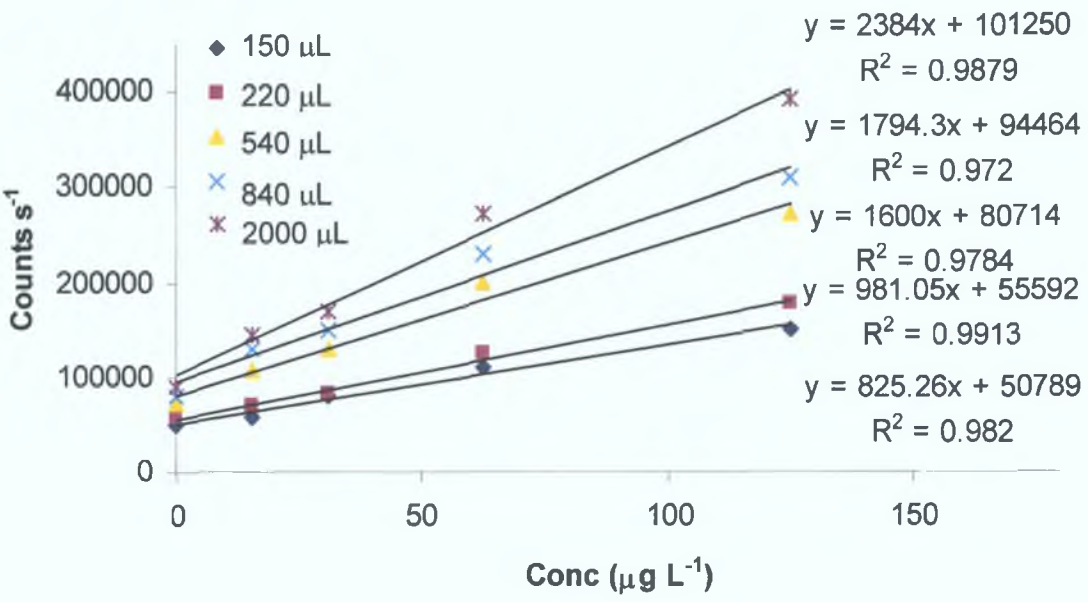

Figure 5.34: Comparison of effect of sample loop size. Experimental conditions: 0.06 mM 1,10-phenanthroline, 1.3 mM CTAB, 0.075 M NaOH, 5 % H_2O_2 and 25 mM HNO_3. Total flow rate of 1.14 mL min^{-1}.

5.3.8.2 Re-optimisation of Flow Rates

The flow rate was re-optimised in order to enhance the sample throughput by the system. Flow rates varying from 1.14 mL min^{-1} to 1.66 mL min^{-1} were investigated. The experimental conditions were the same as before with the exception of the sample loop size, which was changed from a 150 µL loop to a 220 µL loop. Figure 5.35 shows the resultant signals for a 125 µg L^{-1} copper (II) standard in synthetic seawater matrix. It should be noted here that there was very little change in sensitivity i.e. there was no major change in peak height when the different flow rates were used. At the higher flow rates, the chemiluminescence reaction itself was initiated quicker and the actual time for the reaction to take place was also reduced when the higher flow rates were used, resulting in a higher throughput. The optimum flow rate was taken to be 1.43 mL min^{-1} because it was found at higher flow rates the back-pressure was too high, resulting in leaks. A flow rate of 1.43 mL min^{-1} was deemed satisfactory to produce a higher throughput than a flow rate of 1.14 mL min^{-1} by reducing the time for a single analysis by nearly 50 %.

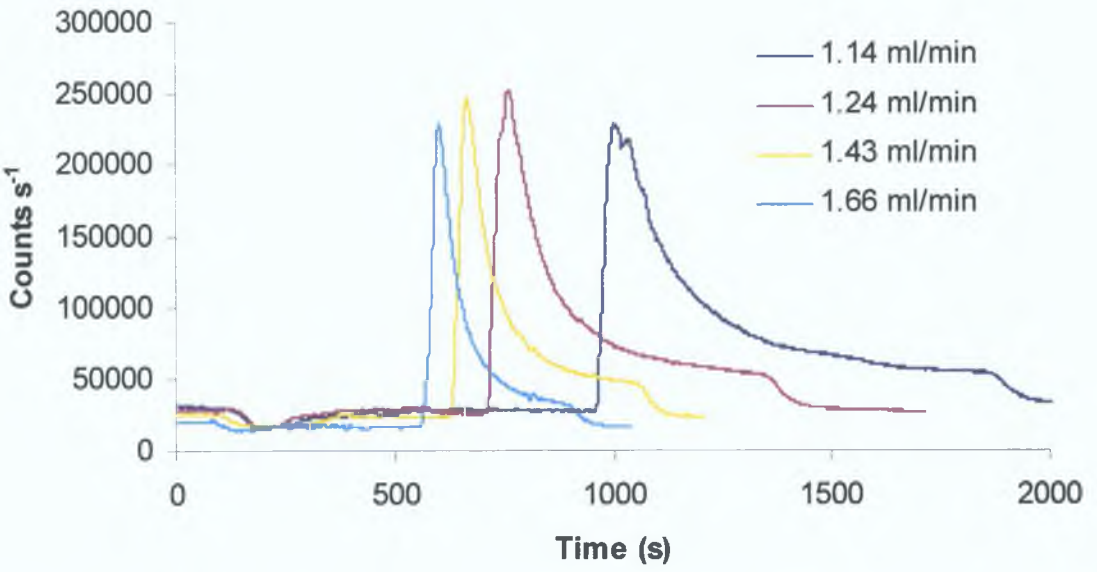

Figure 5.35: Comparison of flow rates. Experimental conditions: 0.06 mM 1,10-phenanthroline, 1.3 mM CTAB, 0.075 M NaOH, 5 % H_2O_2 and 25 mM HNO_3. Sample loop size of 220 µL.

5.3.8.3 Application of Enhanced System To Real Samples

Using the enhanced flow system with larger sample loop size and higher flow rates, the system was re-applied to the coastal seawater sample. In a similar procedure to that described in section 5.3.7, an aliquot of Portmarnock coastal seawater sample was again spiked with various concentrations of copper (II) and the sample was then re-analysed by the enhanced system. The experimental conditions were the same as those used in the previous seawater analysis, with the exception of a larger sample loop volume and a higher flow rate. Figure 5.36 shows the reaction peaks generated for the seawater sample spiked with copper (II) over the concentration range 0 to 250 µg L^{-1}. When these results are compared to those shown in Figure 5.29, the sample throughput has nearly doubled, showing an improvement on the previous system.

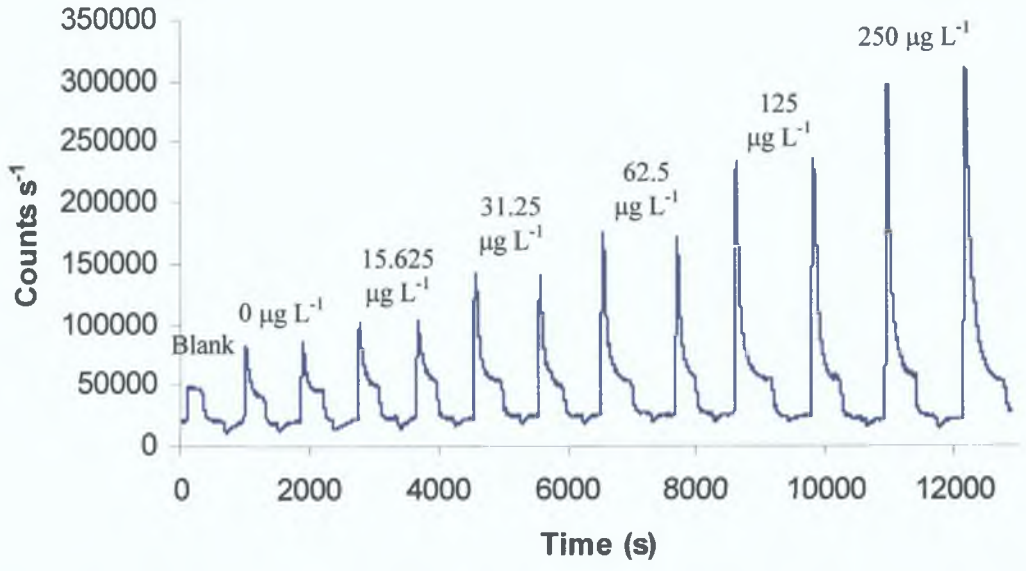

Figure 5.36: Reaction peaks generated for seawater samples spiked with varying concentrations of copper (II). Experimental conditions: 0.06 mM 1,10-phenanthroline, 1.3 mM CTAB, 0.075 M NaOH, 5 % H_2O_2 and 25 mM HNO_3. Total flow rate of 1.43 mL min^{-1} and sample loop size of 220 µL.

A standard addition calibration graph was then obtained using the above results as shown in Figure 5.37. The blank signal was once again subtracted from each of the standards in order to obtain an accurate result due to copper (II) in the sample. It was found that the results were linear over the range 0 to 62.5 µg L^{-1} (R^2 = 0.986) and at concentrations above this the graph curved and began to level off in a similar way to that described in the previous coastal seawater analysis discussed in section 5.3.7. As two replicate injections were made for each copper standard, the error associated with each was calculated by the difference between the two values for each standard. It was found that the difference was calculated to be < 4.9 %, which was deemed acceptable for these results. From the results obtained here, the amount of copper (II) present in the seawater sample was calculated to be 15 µg L^{-1} using the equation of the line y = 1486.6x + 21950.

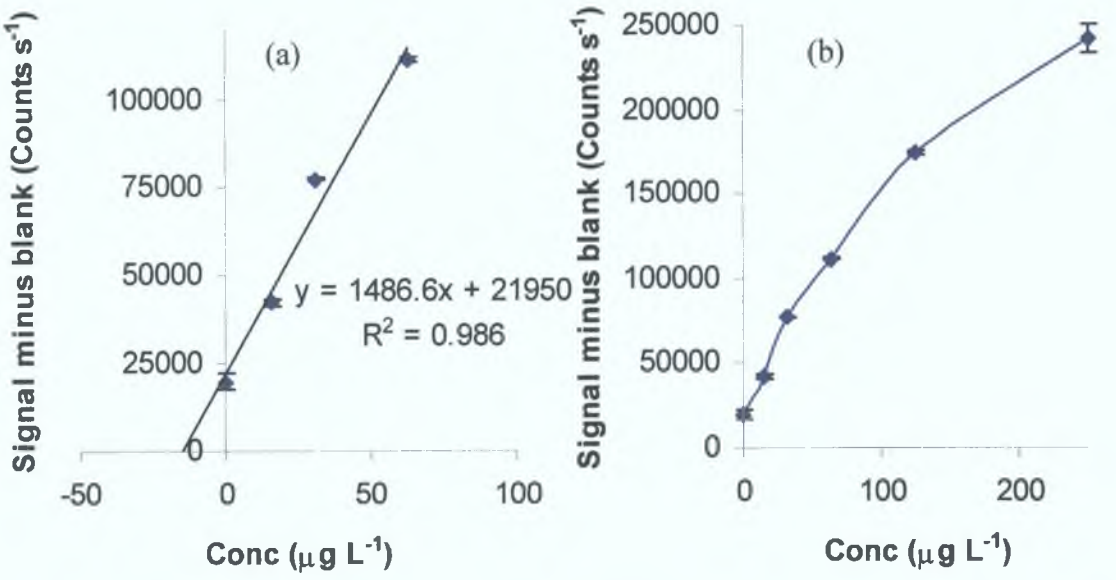

Figure 5.37: (a) Standard addition graph for seawater sample spiked with copper (II) using enhanced system, (b) calibration curve deviating from linearity over the concentration of 62.5 µg L^{-1} copper (II).

5.4 Conclusion

A different analytical procedure using a chelation exchange separation support based on Convective-Interaction Media® (CIM®) was developed here for the preconcentration/separation of copper (II) in samples. This approach was successfully incorporated into a flow injection analysis system using chemiluminescence detection for the determination of ultra trace amounts of copper (II) based on the oxidative destruction of the copper-1,10-phenanthroline complex by hydrogen peroxide at an alkaline pH. These CIM® disk monolithic columns were modified using picolinic acid, dipicolinic acid and iminodiacetic acid and the efficiency of the three acids were compared and contrasted for the separation of copper (II). The combination of the modified CIM® disk monolithic column with the 1,10-phenanthroline reaction, allows the determination of copper (II) even more selectively than the 1,10-phenanthroline reaction on its own.

The dipicolinic acid coated disk was chosen to be the best of the three modified disks, due to its stronger complexing ability over both picolinic acid and iminodiacetic acid. Studies showed that the linear range for copper (II) when the dipicolinic acid coated disk was used, ranged from 0 to 250 µg L^{-1}, in comparison to 0 to 125 µg L^{-1} for the other two carboxylic acids. This system was successfully

applied to a certified SRM sample and the results for the copper (II) analysis were found to be accurate by obtaining good agreement with the certified values. The procedure was also used successfully for the determination of copper (II) in a number of real samples including coastal seawater and estuary water samples.

5.5 References

1. H. Zou, X. Huang, M. Ye, Q. Luo, *J. Chrom. A*, 954 (2002) 5-32.
2. T.B. Tennikova, F. Svec, B.G. Belenkii, *J. Liq. Chrom.*, 13 (1990) 63-70.
3. B.G. Belenkii, A.M. Podkladenko, O.I. Kurenbin, V.G. Mat'tsev, D.G. Nasledov, S.A. Trushin, *J. Chrom. A,* 645 (1993) 1-15.
4. A. Strancar, M. Barut, A. Podgornik, P. Koselj, D. Josic, A. Buchacher, *LC-GC*, 11 (1998) 660-669.
5. G. Bonn, S. Reiffenstuhl, P. Jandik, *J. Chromatogr.*, 499 (1990) 669-676.
6. P.N. Nesterenko, G.Z. Amirova, T.A. Bol'shova, *Anal. Chim. Acta*, 285 (1994) 161-168.
7. N. Oztekin, F. Bedia Erim, *J. Chrom. A*, 924 (2001) 541-546.
8. Y.J. Park, B.H. Lee, W.H. Kim, Y.K. Do, *J. Colloid Interface Sci.*, 209 (1999) 268-270.
9. R.A. Nickson, S.J. Hill, P.J. Worsfold, *Anal. Proc. Inc. Anal. Comm.*, 32 (1995) 387-595.
10. W. Bashir, B. Paull, *J. Chrom. A*, 907 (2001) 191-200.
11. P.N. Nesterenko, P. Jones, *J. Chrom. A*, 804 (1998) 223-231.
12. S. Motellier, H. Pitsch, *J. Chrom. A*, 739 (1996) 119-130.
13. P. Janvion, S. Motellier, H. Pitsch, *J. Chrom. A*, 715 (1995) 105-115.
14. K. Ohta, K. Tanaka, B. Paull, P.R. Haddad, *J. Chrom. A*, 770 (1997) 219-227.
15. A.I. Elefterov, S.N. Nosal, P.N. Nesterenko, O.A. Shpigun, *Analyst*, 119 (1994) 1329-1331.
16. D.A. Skoog, D.M. West, F.J. Holler, Fundamentals of Analytical Chemistry (Seventh Edition), Saunders College Publishing.

Chapter Six

General Conclusions and Future Work

6.1 CONCLUSION

The work presented here outlines the development of a microfluidic based analytical system for copper (II) monitoring in environmental sample matrices. Initial work carried out successfully scaled down a standard flow injection analysis system into a microflow system incorporating the use of chemiluminescence detection for the determination of copper (II). A number of different plastic flow manifolds were designed and fabricated using a range of in-house micro-machining techniques including hot embossing, laser ablation and micro-milling. The chemistry of the copper (II)-1,10-phenanthroline chemiluminescence reaction has been thoroughly investigated and optimised during the course of this study. To further miniaturise the system, the use of micro-peristaltic pumps was assessed for reagent delivery and the pumps were successfully incorporated into the system.

A number of different novel on-line preconcentration/separation methods were also investigated during this work to allow the determination of copper (II) in complex sample matrices. These included the integration of monolithic columns and chelating resin columns into the flow system, as well as the use of modified CIM® monolithic disks. Of the three matrix removal techniques, the modified CIM® monolithic disks were found to work the best in the flow manifold. Unfortunately, the integration of micro-monolithic columns was unsuccessful due the development of voids at the monolith wall interface and cracking of the PMMA manifold. The use of a chelating resin micro-column was successfully fabricated, but was only used for a short time before degradation of the resin caused a blockage in the flow manifold rendering the device ineffective.

The study highlights a number of problems associated with microfluidic devices. It was found that blockages due to dust particles or plastic fragments were encountered in these small-scale devices if rigorous cleaning procedures were not adhered to during the fabrication process. Other blockages were occasionally found to occur during the analysis, as a result of gas bubbles or particles found in solvents, or arising from sample crystallisation, even when care was taken in making up all solutions for use within the microfluidic device. A reduction in sensitivity was also encountered in the miniaturised system, as smaller sample sizes lead to a reduced

signal for detection. In the case of the standard FIA system developed in chapter 2, the linear range for copper (II) was found to be 1 to 50 μg L^{-1}, compared to 20 to 100 μg L^{-1} for the hot embossed plastic flow manifold (200 μm x 200 μm) developed in chapter 3.

Although a number of difficulties were encountered through this work, it should be noted that many of the challenges in the area of micro-fabrication such as channel sealing and bonding, the application of leak-free fluid interconnects and the incorporation of chelating resins into a holding chamber of a microfluidic device – notable difficulties of micro-fabrication – have been successfully overcome.

To conclude, the microfluidic-based system, incorporating the use of on-line preconcentration and chemiluminescence detection, which was developed here, has resulted in a sensitive and selective technique for copper (II) monitoring in water samples. The use of an on-line matrix removal step eliminated the use of complex off-line sample pre-treatment techniques and also reduced the possibility of contamination and error due to minimal sample handling by the operator. It has been demonstrated in this work that this system could be used successfully for the analysis of real samples such as coastal seawater and estuary water samples, although further work is required to develop a robust and portable system that could be used for on-site analysis.

6.2 Suggestions for Future Work

As the area of microfluidics is a relatively new technique, it is only recently that groups have investigated the use of chemiluminescence techniques for detection purposes while using microflow systems. As with all emerging areas of analytical chemistry, there is an enormous amount of interest in the development and improvement of new techniques. Further areas of potential development include the following;

6.2.1 Further Investigation of Current Copper(II)-1,10-Phenanthroline Chemiluminescence Reaction

As discussed in chapter 1, a number of workers investigated the use of different masking agents that could be used to minimise matrix interferences. One such reagent is tetraethylenepentamine (TEPA), which is a strong complexing agent for copper and can minimise the effects of copper impurities present in the reagents. Future work could investigate the use of different masking agents to further enhance the system. Another variation on this chemiluminescence reaction uses alcohols instead of surfactants to enhance the chemiluminescence efficiency. Different complex matrices such as brines and saline samples could also be investigated

6.2.2 Study of Different Chemiluminescence Reactions

As discussed in chapter 1, there are a number of different chemiluminescence based analytical techniques for trace metal determinations in environmental samples, which have been developed in large scale systems but have yet to be exploited in smaller scale manifolds. One major advantage of using miniaturised devices is the decrease in the amount of sample and reagent consumption. Given that chemiluminescence reactions are non-reversible and some of the reagents are very expensive makes the use of a miniaturised system attractive for certain chemiluminescence reactions. The microfluidic system currently developed here for the determination of copper (II) could easily be adapted to different chemistries, resulting in the selective determinations of other trace metals.

6.2.3 Instrument and System Enhancement

The concept of a fully integrated analytical instrument became one of the main foci of this research. As a result of this further system improvement on the CIM® monolithic disk system described in chapter 5 could include the incorporation of a PMMA plastic flow manifold, similar to that designed in chapter 3, instead of the system of tubing, mixing coils, mixing T-pieces and PE spiral flow cell which was used. This may further improve the sensitivity of the system by removing the length of tubing before the flow cell, resulting in the immediate detection of the

chemiluminescence when it occurs. An improved microfluidic system would also include the use of the micro-peristaltic pumps, instead of the standard Gilson peristaltic pump in a move towards a more compact and portable system.

Although the use of the PMT has been successful and resulted in the development of a sensitive detection system, it requires an external power supply. In order to downsize the system and make it a more compact and portable system, the use of a battery operated PMT would be advantageous. Further investigation of detectors such as a photodiode (PD) to replace the PMT should also be considered.

APPENDIX 1

PAPERS PUBLISHED

ELSEVIER

Journal of Chromatography A, 964 (2002) 113–122

JOURNAL OF CHROMATOGRAPHY A

www.elsevier.com/locate/chroma

Retention of alkali, alkaline earth and transition metals on an itaconic acid cation-exchange column Eluent pH, ionic strength and temperature effects upon selectivity

Wasim Bashir, Eadaoin Tyrrell, Orlagh Feeney, Brett Paull*

National Centre for Sensor Research, School of Chemical Sciences, Dublin City University, Dublin 9, Ireland

Received 25 February 2002; received in revised form 26 April 2002; accepted 19 May 2002

Abstract

The unusual selectivity of a methylene succinic (itaconic) acid modified polymeric column was investigated for the separation of alkali, alkaline earth, transition and heavy metals employing non-chelating inorganic eluents. The retention of selected metal ions on the column was investigated with simple HNO_3 eluents and eluents prepared from KNO_3 and KCl salts of varying pH (adjusted using HNO_3). From these studies both the effect of eluent ionic strength and pH upon retention was evaluated for the itaconic acid stationary phase. The results obtained showed that despite slow exchange kinetics causing poor efficiencies, acceptable baseline separations of selected alkaline earth and transitions could be obtained under optimum conditions (the baseline separation of Mg(II), Ca(II), Mn(II), Cd(II), Zn(II) and Co(II) was possible using a 15 m*M* KNO_3–5 m*M* KCl eluent at pH 3.50 in under 25 min). The use of an simple ionic strength step gradient was shown that facilitated the addition of Pb(II) to the above group of metal ions. An investigation into the effect of temperature upon peak efficiency and retention showed increased column temperature could be used to improve the resolution of closely eluting metal ions such as Ca(II) and Sr(II) and Ca(II) and Mn(II).

Keywords: Stationary phases, LC; pH effects; Temperature effects; Ionic strength; Selectivity; Itaconic acid; Metal cations; Alkali metals; Alkaline earth metals; Transition metals

1. Introduction

The use of ion chromatography for the determination of alkali, alkaline earth and transition metal ions in water samples presents a useful alternative to atomic spectroscopic techniques and as such is often the method of choice in many analytical laboratories. With this in mind it is not surprising that a great deal of research effort has focused on the development of new stationary phases that can offer useful selectivities for these and other less common metal ions. Most of these recent developments in stationary phase technology for the separation and determination of metal ions using various modes of ion chromatography are detailed in recent review articles by Sarzanini and Mentasti [1] and Pohl and colleagues [2,3].

In its early stages ion chromatography was very much seen as purely being based upon the use of simple ion-exchangers as the stationary phase. For cations these were primarily either carboxylated or sulphonated resins or silica gels. However, the

*Corresponding author. Tel.: +353-1-700-5060; fax: +353-1-700-5503.

E-mail address: brett.paull@dcu.ie (B. Paull).

0021-9673/02/$ – see front matter
PII: S0021-9673(02)00652-0

selectivity exhibited by these cation-exchange phases was limited and so new phases with more than one type of ion-exchange group were developed, such as carboxylic/phosphonic acid functionalised columns (Ionpac CS12A), which showed improved selectivity for the simultaneous isocratic separation of alkali and alkaline earth metal ions.

More recently however, it has become clear that even greater selectivity, can be obtained through the inclusion of alternative retention mechanisms or solute interactions within the system, in particular stationary phase complexation or chelation has received much attention. For example, Ionpac CS15 contains crown ethers in addition to carboxylic/phosphonic acid groups, which acts to alter the selectivity of the column for those cations that can be complexed by the ligand. Alternative functional groups have also been investigated which possess the ability to retain the metal ion through both a simple ion-exchange mechanism and also through chelation/complexation. The extent to which either of these two retention mechanisms occurs is dependent upon eluent conditions such as pH, ionic strength and temperature. Examples of functional groups which have this chelation/ion-exchange capability are iminodiacetic acid (IDA), aminophosphonic acid and glutamic acid, all of which have been investigated regarding their application to the separation of alkali, alkaline earth and transition metal ions in earlier studies [4–8]. In each case unusual selectivities could be obtained due to what could be described as a dual retention mechanism. The use of such complexing stationary phases for the separation of metal ions in ion chromatography is the subject of a review by Jones and Nesterenko [9].

In this current study a methylene succinic acid (itaconic acid) functionalised polymeric stationary phase was evaluated for its selectivity for alkali, alkaline earth and common transition metal ions. To the authors' knowledge there has been no published studies into the selectivity of an itaconic acid resin for the above range of metal ions and so this selectivity was investigated here. As itaconic acid contains two carboxylate groups potential exists for complexation to play a role in retention, namely coordination of the metal ion with two oxygen donator atoms. The high degree of selectivity shown by the resin for certain transition metals over alkaline earth metals certainly indicates this to be the case. However, as shown in this study, eluent pH, ionic strength and manipulation of column temperature, can be used to control the degree of each retention mechanism occurring and thus achieve several useful separations of metal ions from each of the above groups.

2. Experimental

2.1. Instrumentation

A Dionex model GPM2 gradient pump module (Sunnyvale, CA, USA) was used to deliver the eluent (1.5 ml/min). A manual sample injection valve, model 7125 (Rheodyne, Cotati, CA, USA), fitted with a 250-μl injection loop was used for introduction of the samples. The analytical column was a 150×4.0 mm I.D. PRP-X800 cation-exchange column (particle size 7 μm) supplied by the Hamilton Company (Reno, NV, USA). A pressure-driven Dionex reagent delivery module was used for introduction of the postcolumn reagent (1.5 ml/min), which was mixed with the eluent postcolumn using a 0.5-m polyether ether ketone (PEEK) reaction coil (0.01 in. I.D; 1 in.=2.54 cm). A model SPD-6AV Shimadzu UV–vis detector (Kyoto, Japan) was used to monitor the resultant chromatograms at 510 or 570 nm (see below). These were recorded using Dionex AI450 chromatographic software. For the work on the effect of eluent temperature upon the retention of alkali metal ions a Dionex DX120 ion chromatograph was used employing indirect conductivity detection.

2.2. Reagents

The eluent and postcolumn reagent (PCR) were prepared using deionised water from a Millipore Milli-Q water purification system (Bedford, MA, USA). The postcolumn reagents used, 4-(2-pyridylazo) resorcinol (PAR) and *o*-cresolphthalein complexone (*o*-CPC), and sodium hydroxide were purchased from Sigma–Aldrich (Gillingham, UK) and used without further purification. Potassium nitrate was obtained from Merck (Darmstadt, Germany) and potassium chloride from Fluka (Buchs,

Switzerland). For the detection of transition metal ions the postcolumn reagent solution was 0.5 *M* ammonia, 0.4 m*M* PAR, adjusted to pH 10.5 (monitored at 510 nm). For the detection of alkaline earth metals this was 0.4 m*M* *o*-CPC, 0.25 *M* boric acid adjusted to pH 10.5 using NaOH (monitored at 570 nm). All standard solutions prepared were filtered through a 0.45-μm filter and degassed using sonication. Low level standard solutions were generally prepared freshly each day from stock solutions (1000 mg/l) stored in 1% nitric acid.

3. Results and discussion

3.1. Inorganic eluents

In this work the retention behaviour of alkali, alkaline earth and common transition and heavy metal ions on the itaconic acid stationary phase was evaluated using simple inorganic eluents. Initially, three eluents were investigated—HNO_3, KNO_3 and KCl. As itaconic acid contains two weak carboxylic acid groups (pK_{a1}=3.85, pK_{a2}=5.45 [10]), eluent pH will have a large affect upon metal ion retention due to the strong affinity of H^+ for the carboxylate groups. With simple dilute HNO_3 eluents the itaconic acid stationary phase exhibited similar selectivity to other dicarboxylate stationary phases, such as IDA [6,8]. With HNO_3 eluents the stationary phase selectivity was determined as follows; Li<Na<NH_4<K<Cs<Mg(II)<Ca(II)≤Sr(II)<Mn(II)≤Ba(II)<Cd(II)<Zn(II)<Co(II)≪Pb(II)≪Cu(II). For the alkali and alkaline earth metal ions the retention order shown was close to that expected if only ion-exchange were responsible for retention, as would be the case on a sulphonated cation-exchanger. However, for the transition and heavy metals investigated the selectivity was close to the reverse of that expected if only ion-exchange were taking place. In particular, the itaconic acid stationary phase showed strong selectivity towards Pb(II) and Cu(II) ions over the reminder of the above metals, with strongly acidic eluents (up to 50 m*M* HNO_3) being required for their elution from the column. Under such acidic conditions all the other metal ions tested were unretained, such that it was possible to selectivity separate and determine Cu(II) in samples containing a mixture of all of the above metal ions. Fig. 1a shows the strong affect of pH (HNO_3 eluent) upon retention of the alkaline earth and transition metal ions using the itaconic acid column. The retention slopes obtained for each of the metals injected were all very similar, ranging from −1.802 for Mn(II) to −1.978 for Cu(II). Fig. 1b demonstrates the unusual selectivity for Cu(II) with overlaid chromatograms of Ca(II), Pb(II) and Cu(II) standards, obtained using a 30 m*M* HNO_3 eluent. As can be seen from Fig. 1b it was evident that peak shapes rapidly became broad with relatively small increases in retention. This effect is often seen in chromatographic systems where more than one retention mechanism is taking place and is a strong indication of stationary phase chelation occurring, as complex formation/dissociation kinetics are general-

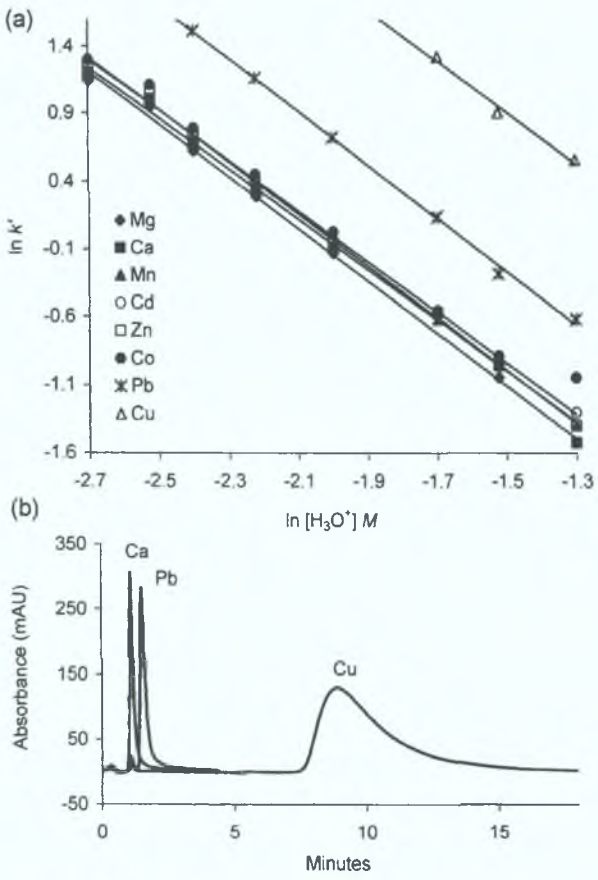

Fig. 1. (a) Effect of eluent pH on capacity factors (k') of alkaline earth and transition metals. (b) Overlaid chromatograms of Ca(II) (5 mg/l), Pb(II) (2 mg/l) and Cu(II) (2 mg/l) standards obtained using a 30 m*M* HNO_3 eluent. Detection using PCR with PAR.

ly much slower than the kinetics of simple ion-exchange [9]. The peak broadening shown was independent of standard concentration, with lower concentration standards being equally broad, this then eliminating column overload as a possible cause of the rather poor peak shape. In comparison with our previous work using dicarboxylate chelating ligands, namely IDA bonded 8-μm silica gels [6–8], it can be qualitatively stated that the efficiency of the itaconic acid resin was clearly poorer, this being an obvious disadvantage of the new polymer phase.

Where stationary phase complexation/chelation is contributing to retention it is expected that the effect of eluent ionic strength upon retention will be less than that seen if simple cation-exchange were the only retention mechanism. Therefore, the effect of eluent ionic strength upon retention was investigated here using varying ionic strength eluents prepared from nitrate and chloride potassium salts. The pH of all the eluents investigated was kept constant and slightly acidic at pH 3.3 to minimise error and ensure capacity factors were under 20 for the weakest eluents used. The effect of ionic strength was investigated over the range 0.02–1.0 *M* KNO_3 and KCl. The resultant log retention graphs are shown as Fig. 2a and b, respectively. As expected the selectivity of itaconic acid for K^+ is much lower than for H^+. Slopes obtained for the KNO_3 eluent ranged from −0.607 for Mg(II) to −0.948 for Zn(II). The eluents prepared using KCl proved to be the stronger eluents due to the added weak complexing ability of the chloride ions, here slopes ranged from −0.969 for Mg(II) to −1.346 for Co(II). Under all the eluent conditions tested Cu(II) was fully retained, even with the 1 *M* KCl eluent. The retention of Pb(II) was also considerable with retention times of >50 min when using a 0.1 *M* KCl eluent. Even with a 0.5 *M* KCl eluent (at pH 3.3) Pb(II) was retained for 8 min, illustrating the unusually selective properties of the itaconic acid functional group.

3.2. Metal separations

Using only dilute HNO_3 (0.6–2 m*M*) eluents separations of Mg(II), Ca(II), Mn(II), Cd(II), Zn(II) and Co(II) could be obtained using the itaconic acid column, with Pb(II) and Cu(II) totally retained. However, under these conditions run times were excessive (up to 30 min), as peak shapes were rather poor, particularly for the later eluting metal ions. More acidic eluents resulted in co-elution of the early eluting peaks of Mg(II), Ca(II) and Mn(II). Addition of either KNO_3 or KCl (20 m*M*) to the above eluents was investigated to see if peak shapes improved. As expected this led to a reduction in retention times and a slight improvement in peak shapes. In both cases the resolution of Mn(II) from the early eluting peaks of Mg(II) and Ca(II) was improved. However, the additions also caused the co-elution of Cd(II) and Zn(II) with the KNO_3 eluent and Zn(II) and Co(II) with the KCl eluent. Typical chromatograms obtained using the above eluents are shown in Fig. 3a–c. To facilitate the

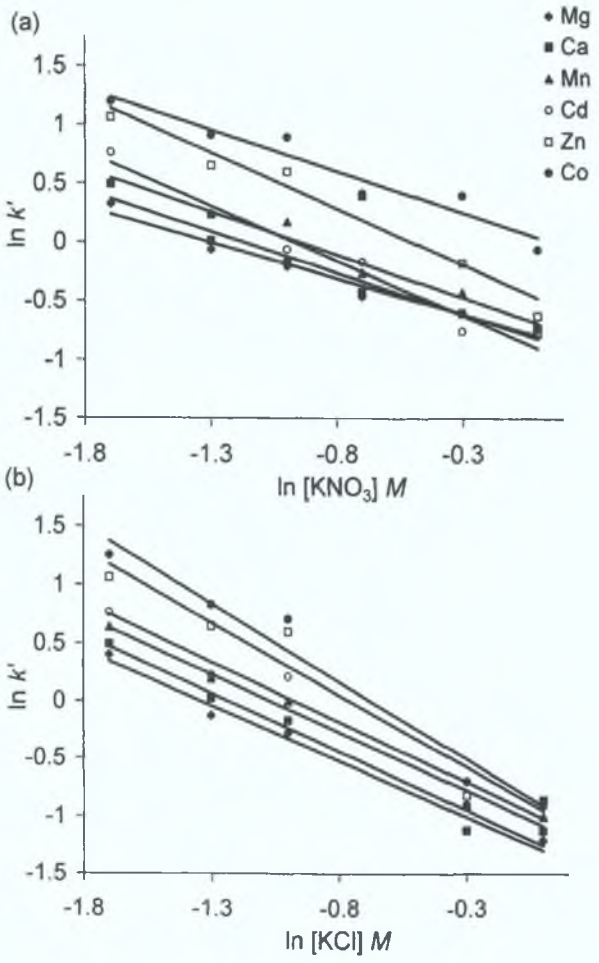

Fig. 2. Effect of eluent ionic strength on retention using a (a) KNO_3 eluent and (b) KCl eluent (pH adjusted to 3.3 using dilute HNO_3). Standard concentration 2 mg/l.

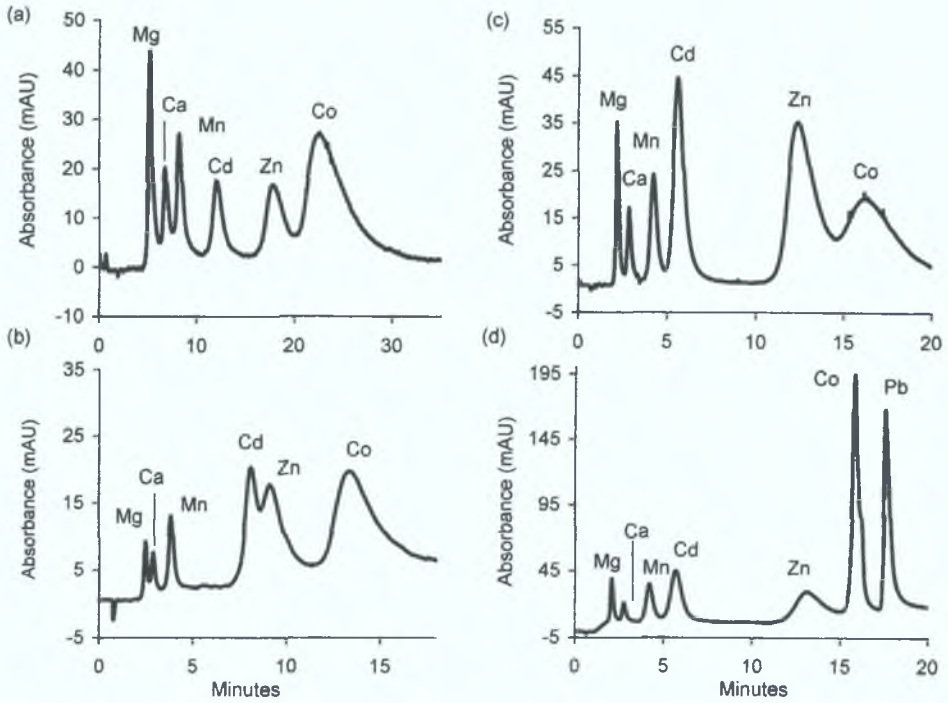

Fig. 3. Chromatograms showing the separation of Mg(II), Ca(II), Mn(II), Cd(II), Co(II) and Zn(II) using (a) a HNO_3 eluent (pH 2.7), (b) a 20 m*M* KNO_3 eluent (pH 3.3), (c) a 20 m*M* KCl eluent (pH 3.3) and (d) a 20 m*M* KCl eluent (pH 3.4) increased to 1 *M* KCl (pH 3.4) between 11 and 12 min. Detection using PCR with PAR. Standard concentrations between 0.5 and 5 mg/l.

elution of Pb(II) and Cu(II) from the column, both pH and ionic strength gradients were investigated. However, it was found that the high buffering capacity of the column due to the itaconic acid groups made using pH gradients difficult, resulting in poor reproducibility, attributed to long column re-equilibration times following each gradient run. The use of an ionic strength gradient whilst keeping the pH uniform proved more successful in terms of reproducibility and could be used to obtain a separation of Mg(II), Ca(II), Mn(II), Cd(II), Zn(II), Co(II) and Pb(II), although even when using a final eluent strength of 1 *M* KCl, Cu(II) was still retained. Fig. 3d shows the chromatogram obtained using a KCl gradient.

Finally, the use of mixed eluents was investigated under isocratic conditions. In an attempt to obtain the optimum resolution of the above metal ions in as short an overall run time as possible, eluents containing varying ratios of KNO_3 to KCl were prepared, keeping the total eluent concentration constant at 20 m*M*. The concentration of KCl had a significant effect upon the retention and resolution of the later eluting transition metal ions, but little effect upon the retention of Mg(II), Ca(II) and Mn(II). The optimum conditions found were 15 m*M* KNO_3, 5 m*M* KCl (pH 3.5), which resulted in the chromatogram shown in Fig. 4.

3.3. Temperature effects

The unusual selectivity exhibited by the itaconic acid column prompted an investigation into the effect of column temperature upon the retention of alkaline earth and transition metal ions. It has been shown in several previous studies that temperature can have a very different affect upon the retention of metal ions depending upon the exact mode of retention. Where only cation-exchange is responsible for retention, temperature is known to have only a small predominantly negative affect upon retention. Fortier and Fritz [11] first investigated this effect using a strong cation-exchange resin with a perchloric acid eluent. The results showed retention times of divalent metal ions decreased with an increase in system temperature. Much more recently, work by

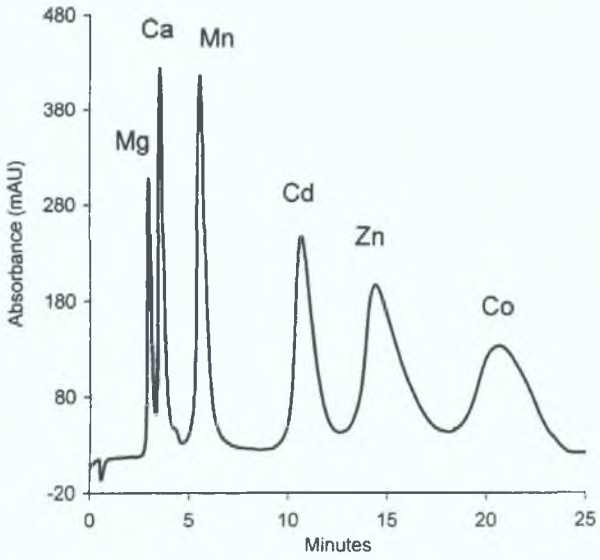

Fig. 4. Chromatogram showing the optimised separation of Mg(II), Ca(II), Mn(II), Cd(II), Zn(II) and Co(II) obtained using a mixed eluent of 15 m*M* KNO_3 and 5 m*M* KCl (pH 3.5). Standard composition: Mg(II), Ca(II), (10 mg/l) Cd(II), Co(II) (5 mg/l), Zn(II) (2 mg/l), Mn(II) (1 mg/l). Detection using PCR with PAR.

Rey and Pohl [12] and Hatsis and Lucy [13] showed similar trends when using a carboxylate/phosphonate stationary phase used with a methanesulphonic acid eluent. However, where retention of metal ions is the result of stationary phase complexation (or indeed a combination of both ion-exchange and stationary-phase complexation) the above negative effect of temperature is no longer seen. This has been illustrated recently in a number of studies on the separation of alkaline earth [6], transition metals [8] and the lanthanide metals [14] using iminodiacetic acid functionalised silica columns, where in each case under the eluent conditions studied, an increase in retention resulted from an increase in column temperature.

Fortier and Fritz [11] proposed the following equation to express the effect of column temperature upon retention ($\ln k'$) in ion-exchange;

$$\ln k' = -\Delta H^\circ/RT + \Delta S^\circ/R + \ln \phi \quad (1)$$

where ΔH° is the enthalpy of the sorption process, ΔS° is the change in entropy and ϕ is the phase ratio. Where the sorption process exhibits exothermic behaviour (negative values of ΔH°), the retention of the analyte ion will decrease with increasing column temperature, as shown recently by Hatsis and Lucy [13]. This will present itself graphically as a positive slope in a Van't Hoff plot ($\ln k'$ vs. $1/T$). However, studies on stationary phases capable of metal ion complexation have shown much higher values of ΔH°, particularly under eluent conditions which favour stationary-phase complexation over ion exchange (high ionic strength and increased pH) [4]. Under these conditions, the sorption process exhibits endothermic behaviour, resulting in a negative slope in a Van't Hoff plot.

The plots shown in Fig. 5 depict the effect column temperature has upon retention of alkali, alkaline earth and transition metal ions using the itaconic acid stationary phase under various eluent conditions. Using simple 1- and 2-m*M* HNO_3 eluents, the column was first tested for retention of alkali metal ions through simple ion exchange. The results obtained were similar to those shown by Hatsis and Lucy [13] with all (bar lithium with 1 m*M* HNO_3 eluent) exhibiting a decrease in retention with increased column temperature when using either eluent. With the stronger 2 m*M* HNO_3 eluent it was possible to elute Ca(II) and Mg(II) from the itaconic acid column. With this low ionic strength eluent the effect of temperature upon retention of these alkaline earth metals was clearly different to the effect upon the alkali metals. Only a very slight decrease in retention of Mg(II) could be seen, with the retention of Ca(II) remaining unaffected by temperature.

However, as shown in Fig. 5b, when using an eluent of higher ionic strength and pH (20 m*M* KCl eluent adjusted to pH 3.5 using HNO_3), both Ca(II) and Mg(II) behave very differently, and now like the transitions metals shown, exhibit an increase in retention with an increase in column temperature. Under these conditions it would be expected that both ion exchange and complexation would be contributing to the retention of the alkaline earth and transition metals. As complete stability constant data sets for itaconic acid complexes of alkaline earth and transition metals are not readily available, it was not possible to predict the exact contribution to retention of stationary phase complexation. However, if itaconic acid behaves similarly to other dicarboxylate ligands, it should be expected that complexation was playing a greater role in the retention of the transi-

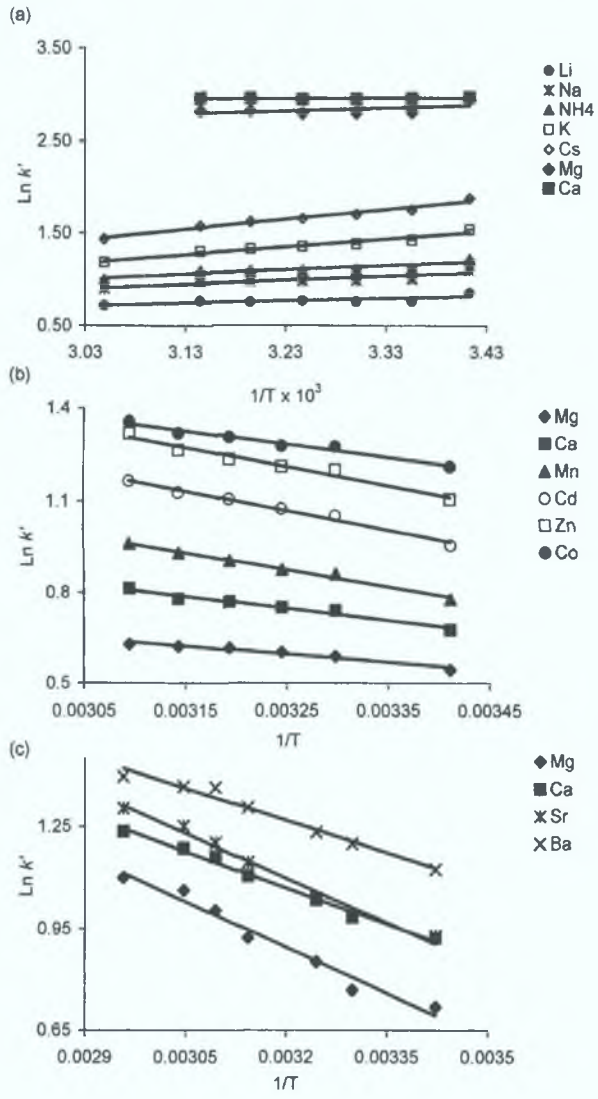

Fig. 5. Van't Hoff plots of metal retention vs column temperature. Eluent conditions: (a) 2 m*M* HNO_3, (b) 20 m*M* KCl (pH 3.5), (c) 100 m*M* KCl (pH 5.7).

tion metal ions than the alkaline earth metals. The slopes obtained from the data shown in Fig. 5b (listed in Table 1) support this assumption, with temperature having significantly less effect upon the retention of the alkaline earth metals compared to the transition metals.

This nonuniform response to temperature means column temperature can be used as an extra means to manipulate selectivity. For example, under the eluent condition used in Fig. 5b, the baseline resolution of Mn(II) from Ca(II) at room temperature was not possible. However, an increase in column temperature up to 50 °C caused a greater increase in the retention of Mn(II) relative to Mg(II) and Ca(II), resulting in their improved resolution (see Fig. 6).

From the above results it was predicted that if eluent conditions were such that ion-exchange interactions were minimised and complexation was the dominant retention mechanism, the effect of temperature upon the retention of alkaline earth metals would be much more pronounced. Therefore a 100-m*M* KCl eluent was prepared and adjusted to pH 5.7. The effect column temperature had upon the retention of alkaline earth metal ions using this eluent is shown as Fig. 5c. From the results obtained it is clear that under these conditions the effect of temperature is indeed more pronounced with consider-

Table 1
Slopes and correlation coefficients from Van't Hoff plots of alkali, alkaline earth and transition metals

	Slope	r^2
Eluent 1 m*M* HNO_3[a]		
Lithium	−0.1219	0.896
Sodium	0.1012	0.843
Ammonium	0.1213	0.837
Potassium	0.5033	0.997
Cesium	0.7155	0.998
Eluent 2 m*M* HNO_3[b]		
Magnesium	0.3356	0.319
Calcium	0.0485	0.326
Lithium	0.2517	0.596
Sodium	0.4290	0.832
Ammonium	0.4641	0.832
Potassium	0.8380	0.945
Cesium	1.0661	0.969
Eluent 20 m*M* KCl at pH 3.5[c]		
Magnesium	−0.265	0.952
Calcium	−0.395	0.967
Manganese	−0.553	0.988
Cadmium	−0.637	0.984
Zinc	−0.617	0.965
Cobalt	−0.427	0.970
Eluent 100 m*M* KCl at pH 5.7[d]		
Magnesium	−0.905	0.969
Calcium	−0.711	0.990
Strontium	−0.874	0.982
Barium	−0.628	0.974

[a] Temperature range 20–60 °C.
[b] Temperature range 20–60 °C.
[c] Temperature range 20–50 °C.
[d] Temperature range 19–65 °C.

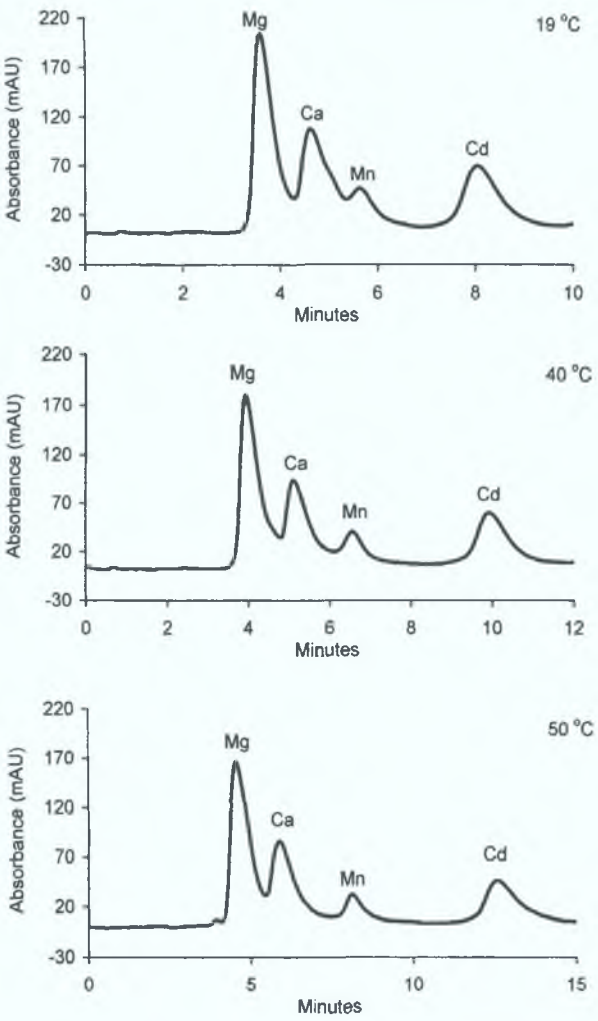

Fig. 6. Chromatograms showing the resolution of Mg(II), Ca(II), Mn(II) and Cd(II) at 19, 40 and 50 °C. Eluent conditions: 20 m*M* KCl (pH 3.5). Standard composition: Mg(II) (5 mg/l) Ca(II) (2 mg/l), Cd(II) (1 mg/l) and Mn(II) (0.2 mg/l). Detection using PCR with PAR.

able increases in retention for all four metals. The slopes obtained (see Table 1) are now even greater than even those obtained for the transition metal ions using the previous 20 m*M* KCl eluent. However, relative retention is not reflected in response to temperature, as Ba(II) being retained for the longest shows the least effect and Mg(II), which is the least retained of the four ions, shows the greatest effect. This may be a reflection upon the ion-exchange selectivity of the column. As the selectivity of most cation exchangers, including carboxylated resins, is Ba(II)>Sr(II)>Ca(II)>Mg(II), it could be that even with the 100-m*M* eluent, ion exchange was playing a minor role in the retention of Ba(II) and this was being reflected in resulting slope. For Mg(II), the opposite is true, with any ion-exchange interactions likely to have been predominantly suppressed, resulting in the ion showing the greatest response to temperature. However, this hypothesis does not explain the response of Sr(II), which is almost equal to that of Mg(II). Therefore, the only absolute conclusions that can be drawn from these observations are that clearly an increase in all four alkaline earth metal ions results from an increase in column temperature and that under these eluent conditions stationary phase complexation was likely to be the dominant retention mechanism.

As before, it was clear that nonuniform responses to changes in temperature could be used to improve resolution. At room temperature, the itaconic acid column showed poor resolution of Ca(II) and Sr(II) under most eluent conditions tested. However, as can be seen from the chromatograms shown in Fig. 7, under the eluent conditions described above, temperature could be used to resolve these two metal ions, without leading to the excessive retention of Ba(II).

3.4. Sample ionic strength

Finally, the unique selectivity of the itaconic acid phase was investigated in relation to the effect of sample ionic strength. If retention was predominantly due to complexation not ion exchange, sample ionic strength should have a less detrimental effect upon the separation of the alkaline earth metals. Therefore, two alkaline earth metal mixed standards were prepared. To each standard mix Li was added as a marker for the elution of alkali metals (Li is the only alkali metal to show significant detector response when using PCR with *o*-CPC). As mentioned above the alkali metals did not show an increased retention at elevated column temperatures and were only marginally retained with the 100 m*M* KCl eluent. To one of the standard mixes 0.1 *M* NaCl was added (2.3 g/l Na). The resulting chromatograms for the two mixed standards are shown overlaid in Fig. 8. Two observations can be made from the chromatograms obtained. Firstly, the usual loss in efficiency associated with high ionic strength samples can be seen with the peak for Li, with the peak shape

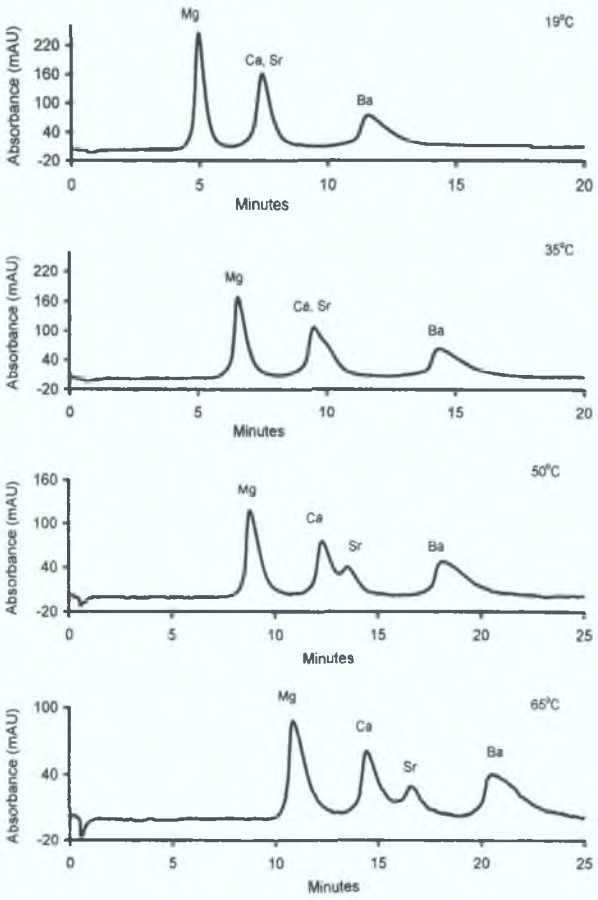

Fig. 7. Chromatograms showing the resolution of Mg(II), Ca(II), Sr(II) and Ba(II) at 19, 35, 50 and 65 °C. Eluent conditions: 100 m*M* KCl (pH 5.1). Standard composition: Ba (50 mg/l), Sr (10 mg/l), Mg(II) (5 mg/l) and Ca(II) (2 mg/l). Detection using PCR with *o*-CPC.

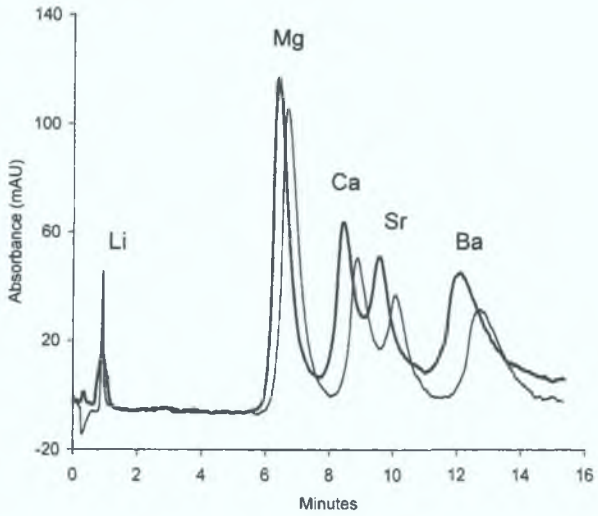

Fig. 8. Overlaid chromatograms of alkaline earth metal mixed standard solutions. Standard composition: (a) Li (70 mg/l), Ba (50 mg/l), Sr (10 mg/l), Mg(II) (4 mg/l) and Ca(II) (1 mg/l). (b) as (a) plus 2.3 g/l Na. Eluent conditions: as in Fig. 7. Column temperature: 65 °C; flow-rate: 2.5 ml/min. Detection using PCR with *o*-CPC.

dramatically poorer. Secondly, although a slight decrease in retention can be seen for the alkaline earth metals, their overall resolution and individual peak efficiencies were unaffected. This experiment illustrates a considerable advantage of the use of such complexing stationary phases in the analysis of real samples, which are often of high ionic strength, and shows how the itaconic acid phase is suitable for the determination of alkaline earth metals in samples containing excess concentrations of alkali metals.

4. Conclusions

The results have shown the itaconic acid phase exhibits unusual and useful selectivity for alkaline earth and transition/heavy metal ions resulting from a combination of both ion exchange and complexation interactions. Control of eluent pH was the most critical parameter in manipulating cation selectivity. Column temperature was shown to also affect selectivity, with an increase in column temperature causing an increase in the retention of all alkaline earth and transition/heavy metals tested, this being the opposite case to that expected if only ion exchange were taking place.

Acknowledgements

The authors would like to thank Dan Lee of Hamilton Company for the supply of the PRP-X800 itaconic acid cation column.

References

[1] C. Sarzanini, E.J. Mentasti, J. Chromatogr. A 789 (1997) 301.
[2] P.E. Jackson, C.A. Pohl, Trends Anal. Chem. 16 (1997) 393.

[3] C.A. Pohl, J.R. Stillian, P.E. Jackson, J. Chromatogr. A 789 (1997) 29.
[4] A.I. Elefterov, M.G. Kolpachnikova, P.N. Nesterenko, O.A. Shpigun, J. Chromatogr. A 769 (1997) 179.
[5] P.N. Nesterenko, M.J. Shaw, S.J. Hill, P. Jones, Microchem. J. 62 (1999) 58.
[6] W. Bashir, B. Paull, J. Chromatogr. A 907 (2001) 191.
[7] W. Bashir, B. Paull, J. Chromatogr. A 910 (2001) 301.
[8] W. Bashir, B. Paull, J. Chromatogr. A 942 (2002) 73.
[9] P. Jones, P.N. Nesterenko, J. Chromatogr. A 789 (1997) 413.
[10] Y.J. Seok, K.S. Yang, S.O. Kang, Anal. Chim. Acta 306 (1995) 351.
[11] N.E. Fortier, J.S. Fritz, Talanta 34 (1987) 415.
[12] M.A. Rey, C.A. Pohl, J. Chromatogr. A 739 (1996) 87.
[13] P. Hatsis, C.A. Lucy, Analyst 126 (2001) 2113.
[14] P.N. Nesterenko, P. Jones, J. Chromatogr. A 804 (1998) 223.

Design of a micro-fluidic sensor for high sensitivity Copper (II) sensing applications

Ceri Gibson*, Patrick Byrne, David Gray, Brian MacCraith, Brett Paul, Eadaoin Tyrrell
National Centre for Sensor Research, Dublin City University, Glasnevin, Dublin 9, Ireland

ABSTRACT

An all-plastic micro-sensor system for remote measurement of copper (II) ions in the aqueous environment has been developed. The sensing structure was designed for ease of milling and fabricated in poly (methyl methacrylate) (PMMA) using a hot-embossing technique. Issues of sealing the structure were studied extensively and an efficient protocol has been established. The detection system comprises a compact photo-multiplier tube and integrated photon counting system. This method has advantages of low sample volume, (creating a minimal volume of waste), low exposure to contaminants due to the closed system, no moving parts and employs a robust polymer material which is resistant to the environment of intended use. The sensor operates on the principle of flow injection analysis and has been tested using a chemiluminescence (FIA-CL) reaction arising from the complexation of copper with 1,10-phenanthroline and subsequent oxidation by hydrogen peroxide.

Keywords: hot embosser, micro-fabrication, chemiluminescence, copper, sensing

1. INTRODUCTION

There is a great requirement for integrated miniaturised sensing techniques in the water and wastewater industry. The design of lab-on-a-chip style micro-fabricated devices offers the possibility of huge improvements to bench top laboratory analysis equipment in the case of unattended sensing in small or inaccessible locations such as outlet drains or treatment tanks. The sensor also offers portability for remote sensing of rivers and harbours. The need for lesser volumes of reagents greatly reduces the cost per measurement and equally allows more determinations to be performed before reagent reservoirs need to be replenished. The reduction in waste to be disposed of is also of utmost importance to environmental implications and has the additional benefit of being more cost effective, as charges are introduced for disposal of chemicals.

The evaluation of heavy metals in the marine environment is of particular importance due to their hazardous effects on the ecosystems depending on the dose and toxicity. Copper is essential for the normal metabolism of many living organisms; it is required for the formation and function of haemoglobin as deficiency can lead to anaemia. However many fish varieties are particularly susceptible to high copper concentrations. The World Health Organisation, WHO and the European Water Quality Directive recommends the concentration of copper in drinking water not to exceed 2ppm (31μM).[1] The level of tolerance in fish however is much lower. Cu^{1+} is estimated to account for up to 5-10% of total copper in surface seawaters[2]. It is however the Cu^{2+} species that is biologically available and harmful to organisms, although hydroxide complexes have also been implicated and copper complexes with a range of low molecular weight organic ligands are also biologically available. Dissolved copper concentrations in marine environments are very low, ranging from 3.3 to 40ppb (0.5 to 6nM) but free ionic copper may be toxic at activities as low as 0.1ppb (10^{-11}M). The Environmental Protection Agency, Ireland sets the imperative parametric value, I/PV to be 0.05mg/L Cu for A1 waters (public supply water source with least degree of treatment) with special lower I/PV values for Salmonid water of between 0.005 and 0.112ppm Cu depending on the hardness of the water[3].

Original determinations of copper in sea water required complicated solvent extraction followed by quantification using graphite-furnace atomic absorption spectrophotometry, (GFAAS) which required clean room facilities[4]. Current methods for analysing copper content in solution include atomic absorption spectroscopy, (AAS), inductively coupled plasma emission spectroscopy (ICP-ES), photometric methods and in particular electrochemical methods such as anodic

* email: ceri.gibson@dcu.ie; tel: + 353 (0)1 7008512; fax: +353 (0) 1 7008221

Opto-Ireland 2002: Optics and Photonics Technologies and Applications, Thomas J. Glynn, Editor, Proceedings of SPIE Vol. 4876 (2003) © 2003 SPIE · 0277-786X/03/$15.00

or cathodic stripping voltammetry. These techniques have the advantage of being highly sensitive but require protracted analysis times, use large sample volumes and require specialised equipment and laboratory facilities. The determination can be complicated by the instability of competing ligands during the equilibration step[5]. Mayr et al have recently developed a dual lifetime referenced optical sensor membrane, which solves some of these issues. [6]

In this work, we use a novel chemiluminescent system, first reported by Yamada and Suzuki[7] and adapted by Zamzow *et al.*[8] which is reported as being simple, fast, selective and precise. The method applies direct injection, Flow Injection Analysis Chemiluminescence, (FIA-CL) to the determination of copper. Chemiluminescent light emitted from the relaxed excited state of a copper complex which has been reacted with hydrogen peroxide is proportional to the copper ion concentration. This chemiluminescence was detected using a PMT incident on a spiral coil of Teflon™ tubing (i.d. = 0.8mm).

Our paper discusses how micro-fabrication on to a rigid polymer structure offers an improvement on the above method by neatly integrating all processes onto one platform and further reducing the volumes of both reagents required and waste solutions for disposal. The sensor design has been based on the requirements as outlined by Zamzow *et al*[8] to include a mixing channel and subsequent emission channel after the sample inlet. The platform has been fabricated using micro-milling and hot embossing technology as described in the methodology section. A number of platform iterations are described and our preliminary results for the detection of copper are reported. Ultimately it is envisioned that the itaconic acid will be coated onto the base plate thus incorporating the pre-concentration step into the micro-fabricated channels. The incorporation of sufficient reagent reservoirs and guaranteed release mechanisms will be considered after the proof of principle has been achieved.

2. METHODOLOGY

2.1 Structure fabrication

The design of the micro-fluidic optical sensing platform is shown in figure 1. The sensing structure has been fabricated using a hot embossing technique (Hex 02/T hot embossing system, from JENOPTIK Microtechnik, GmbH, Jena, Germany). A brass mould of the appropriate inverse structure was machined using the in-house micro-miller. (DATRON milling machine, CAT3D-M6 coupled to a high-speed digital CNC controller). This method allows high precision machining with miniature tools (down to 0.1mm diameter) for the milling of moulds with micro-size structures, which can then be used in an injection moulder or hot embosser to produce substrates. The structure was designed in ex-CAD as a 2D image. The software package then generates a 3D image and the post file can be edited to ensure the desired final substrate profile. The choice of design which uses straight parallel channels rather than the more conventional spiral of a coil was used due to the ease of fabrication. There will be implications on the profile of the reaction front and turbulent mixing due to this channel shape which will be considered and studied in depth once the generic platform has been proven. A flat poly-methylmethacrylate, (PMMA) sheet was placed in the hot embosser and the brass mould was used to stamp out the micro-fluidic channels. This was then sealed using a thinner flat top plate also of PMMA. The procedure was continually reviewed to facilitate easy removal of the brass mould and to guarantee a uniformly sealed chip with minimum deformation of either the cover plate or base plate. Actual channel dimensions were measured using a surface profiler (Dektak V 200-Si, Veeco Surface Metrology, Santa Barbara, CA). A profile of the base plate was taken before sealing and both the cover plate and base plate were profiled after the chip had been used and pulled apart.

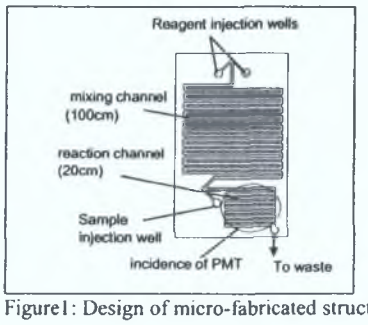

Figure1: Design of micro-fabricated structure.

The process is carried out under vacuum conditions thus preventing undesirable deformations in the structure by reducing the high pressures caused by the presence of air. Figure 2 shows the interplay of the most important variables, force and temperature, throughout the process. The initial variation in force is generated as the top and bottom plates of the hot embosser slowly come together. Once they are just in contact with each other a touch force of 500N is maintained until the top and bottom plates are coincident in temperature. The force is then increased to 4000N and a further heat cycle is introduced to bring the plastic up to its transformation point, Tg. This force is maintained until the imprint of the channels is achieved. The hot embosser is then brought up to atmospheric pressure and the substrate is cooled to a safe handling temperature. The sealing of the unit follows the same general form except that a lower force of 1000N is all that is required for a shorter time period.

Variations in Tg, pressure and time to ensure coherent sealing can be calculated for different substrates depending on the material and the thickness. For example an increase in thickness of 1mm PMMA requires heating at constant pressure for an extra 14 seconds.

Figure 2: Process variables for the sealing of the top plate on to the micro-channel structure.

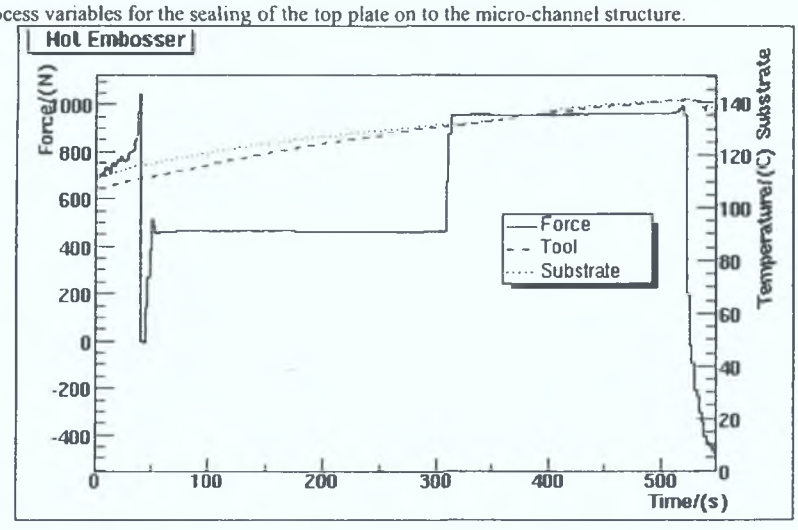

2.2 FIA system

A schematic of the complete experimental sensing system used for this project is shown in figure 3. A peristaltic pump (Gilson Minipuls 3, Scientific Ltd, Ireland) has been used to draw sample, carrier and reagents through polyaryletherketone, (PEEK) tubing into the sensor-chip. Sample/carrier and reagent flow rates were all set at 0.1mm min^{-1}. Cleaning of the lines is achieved with deionised water from the Milli-Q^{50} system between sample analyses. The injection loop has a volume of 120µl and a 1cm micro-column of itaconic acid (particle size ~ 20µm) is used to remove any interferents, such as large amounts of calcium and magnesium present in seawater samples for the low copper concentration samples.

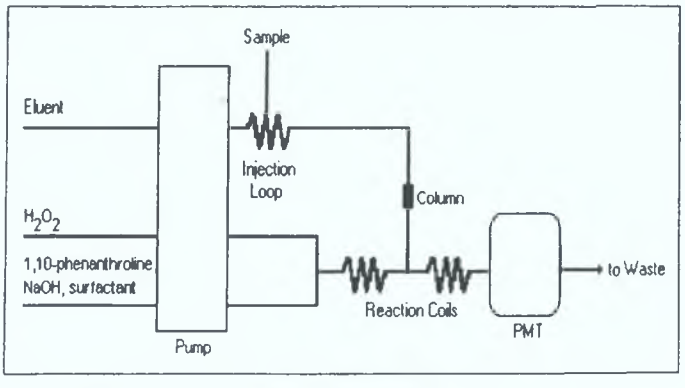

Figure 3: Complete experimental sensor system

During the initial verification of the chemiluminescent detection system the PMT was incident on a polytetrafluoroethylene, (Teflon™) coil, (i.d. 0.8mm, length 65cm). For subsequent measurements the PMT was placed incident on the emission channel of the micro-fluidic sensing platform. The mixing channel on the chip is approximately 100cm in length after which the sample is introduced and the reaction solution passes through an emission channel of length 20cm. During this time, luminescent light is emitted (emission peak maximum 445-450nm) which is detected by the Hamamatsu HC135-01bi-alkali assembly, (Hamamatsu, Middlesex, NJ) incorporating a PMT sensor module, embedded microcontroller and an RS-232-C interface positioned directly above the channel.

2.3 Reagents

The chemiluminescent reaction used for the copper sensing is detailed in figure 4 where * denotes the excited state which produces visible light on relaxation.

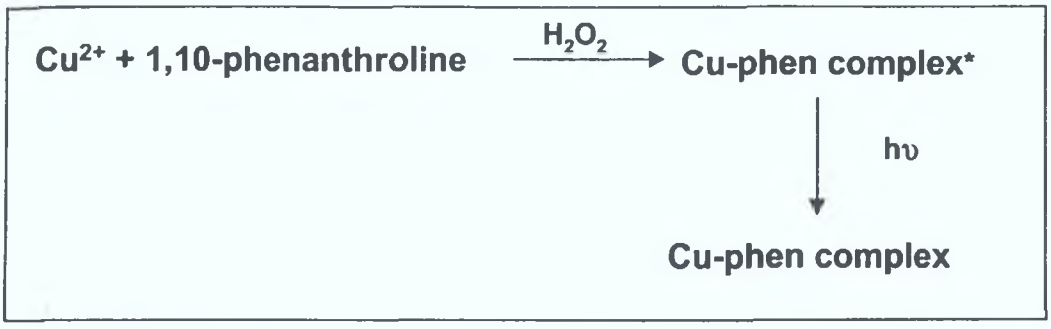

Figure 4: Chemiluminescent reaction

All reagents were ACS reagent grade and used as received except where stated otherwise. Hydrogen peroxide solution (Aldrich) was prepared daily, (27.5% wt vol solution in water). 1,10 phenanthroline (Aldrich) was further purified by recrystallisation in nitric acid and dried before use. Copper standard (Aldrich) 1000ppm in nitric acid (pH 4). Cetyltrimethylamonium bromide, CTAB (BDH, AnalaR, 99.0%). Water produced from a Milli-Q^{50} deionised system (Millipore) was used for reagent preparation and system flushing.

3. RESULTS AND DISCUSSION

3.1 Verification of literature method

The experimental system reported by Zamzow *et al* [8] was followed rigorously and the PMT was secured above a Teflon™ coil through which repeated doses of copper sample of increasing concentration were injected. This method involved the mixing of 1,10-phenantroline and hydrogen peroxide along a mixing coil (length = 100cm). The copper standard was injected into a 120µl loop and carried into the reaction flow by milli-Q^{50} water. All reagents and sample were passed along a 5cm length of tubing before the point at which the PMT was incident over the spiral coil to detect the chemiluminescent response as depicted in figure 3. Signal intensity and sensitivity equivalent to that reported have been achieved, the reaction peaks and a calibration graph are shown in figure 5.

The use of a surfactant to enhance sensitivity was also investigated. The addition of an anionic surfactant causes the formation of micelles which improve the sensitivity of the reaction to copper ions. The effect of incorporating cetyltrimethylammonium bromide, CTAB, Triton X-100 and didodecyl-dimethylammonium bromide, DDAB into the 1,10 phenanthroline solution were evaluated. CTAB was found to be the most effective surfactant and a concentration of 0.05mM CTAB further increased the signal to noise ratio without compromising the Cu^{2+} signal. The concentration of hydrogen peroxide and 1,10-phenanthroline were also optimised. It was found that reducing the hydrogen peroxide solution concentration from 10% to 5% increased the signal intensity. Using 0.03 mM phenanthroline solution significantly reduced the background noise.

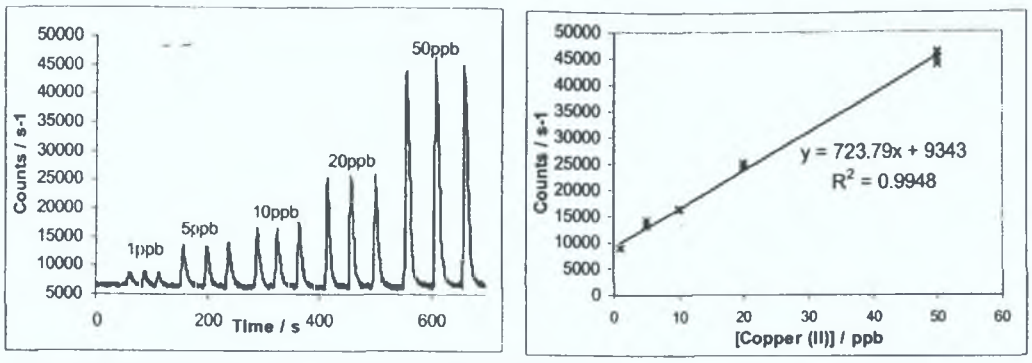

Figure 5: Reaction peaks and calibration graph for the analysis of copper using a coil. LoD 1ppb Cu(II)

3.2 Characterisation and Optimisation of the Sensing Platform

A first iteration micro-fluidic platform was manufactured with a channel cross section of 2mm^2. This allowed the flow of solutions through the system easily using the peristaltic pump. However, when tested with copper as discussed in section 3.3, (see figure 8,) broad signal peaks were produced which were noisy and would result in a low sensitivity system. In order to sharpen the signal response a new manifold with narrower channels was produced. Geometric factors that influence the peak profile include the flow rate of the sample, the cross-sectional area of the delivery tube or channel and the shape of the reactor itself. For a straight tube it has been shown that reducing the tube diameter yields sharper peak with greater intensity thus allowing a greater sensitivity range[9]. This second platform was achieved using a 2mm drill bit which removed material between the 0.2mm^2 raised structure of the brass stamp in order to produce 0.2mm^2 channels in the PMMA base plate. Smaller drill bits would be too brittle (fragile) to machine the area required for this chip. The use of the larger drill bit resulted in reduced machining time and a more robust final base plate. The parallel portions of the channels, however, are 2mm apart further reducing the volume of solution onto which the PMT is incident. This may reduce the intensity and therefore sensitivity of the measurement. The design will be revisited on review of data collected.

On testing this second iteration platform the pressure required to pump the solutions was greater than expected. It was originally thought that the channels might have been blocked either by burrs from the micro-machining or glue from fixing in the delivery tubing. Another platform was prepared following the same protocol paying careful attention to cleaning the base plate but the same high pressure was required. This sensing platform was dismantled and measured using the Dektak profilometer. The profiles illustrated in figure 6 depict the radical reduction on channel depth and the curvature of the whole plate.

The channel depths have been determined using the Dektak software, the average dimensions of which are shown in table 1. The cover plate is used as supplied and is a flat sheet of PMMA so no profile was recorded before sealing. After sealing the mixing and emission channels have been reduced by 66 and 80% respectively thus explaining the increased pressure required to pump the solutions through.

A calculation related to the thickness of the cover plate was carried out and the embossing process altered accordingly to reduce the deformation of the cover and base plate. This resulted in incomplete sealing of the platform leading to leakage when the fluids were introduced. The PMMA used for the cover was measured using callipers and found to be 5% thicker than the specifications indicated by the supplier. A further recalculation for the embossing procedure using the actual measured cover thickness achieved complete and uniform sealing of the sensing platform and this iteration is currently being used successfully to calibrate the system for copper detection.

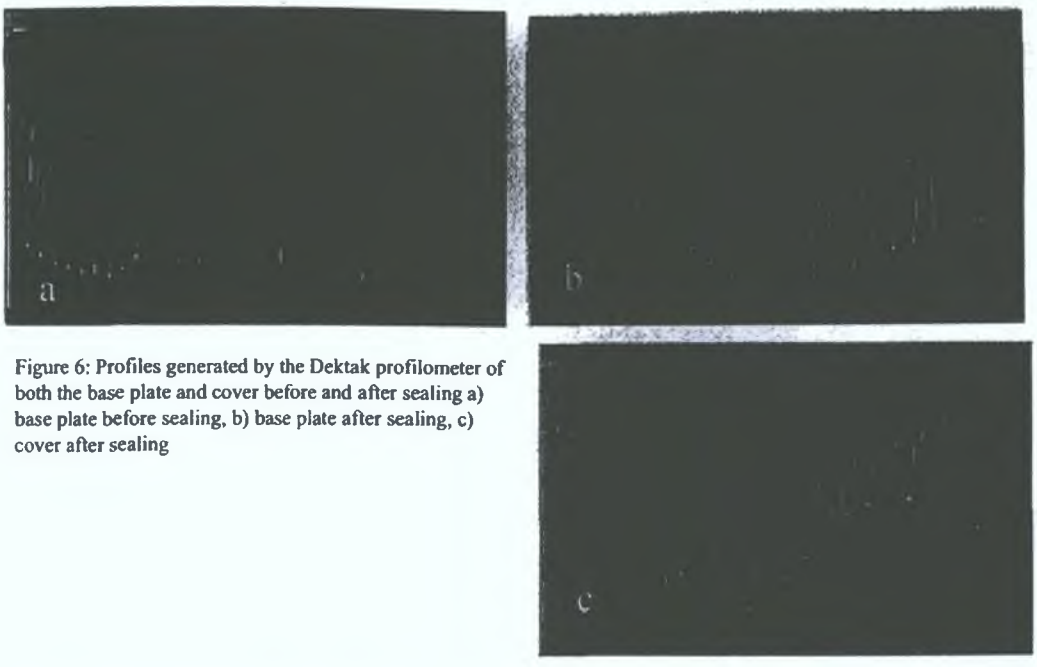

Figure 6: Profiles generated by the Dektak profilometer of both the base plate and cover before and after sealing a) base plate before sealing, b) base plate after sealing, c) cover after sealing

Table 1: Table of channel depths measured in microns using the Dektak profilometer.

	Mixing channels (μm)	Emission channels (μm)
Base plate before sealing	100	79
Base plate after sealing	46	30
Cover after sealing	13	13

3.3 Detection of copper

The first iteration micro-fluidic platform produced a peak for Cu^{2+} as shown in figure 7. The peak due to 1ppm copper is very broad at 94 seconds and has a peak maximum of approximately 2200 counts. This is low compared to the readings achieved using the coil set up, (see figure 5) which produced a sharp peak and a signal intensity of approaching 38 000 counts for just 50ppb.

A second iteration micro-fluidic device with smaller channels was successfully sealed as detailed in section 3.2 above and when incorporated into the experimental set up produced results as shown in figure 8. These peaks have a much shorter peak width of 12 seconds (baseline-to-baseline time, Δt) and a corresponding increase in peak height to approximately 125,000 photons per second. However the travel time, t_a, which is the time from injection of sample into main carrier stream from the injection loop until the peak is observed, varies by nearly one minute.

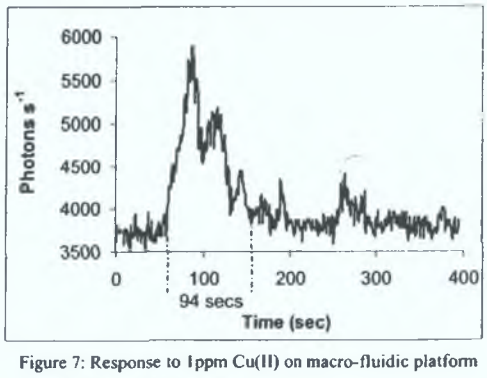

Figure 7: Response to 1ppm Cu(II) on macro-fluidic platform

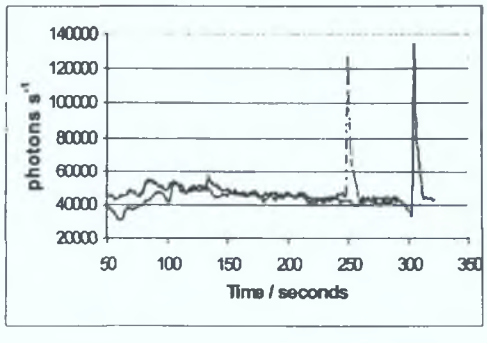

Figure 8: Response to 1ppm Cu (II) on micro-fluidic platform

Detailed analysis of the system revealed that the most likely explanation for this observation is that the sample plug was too large to allow complete reaction in the tubing as explained schematically in figure 9. Two short reaction zones exist at each interface between sample plug and reagents and this small volume generates a sharp peak. The length of the sample plug was in fact so elongated that the second peak is likely to be from the reaction zone at the end of the sample plug and not from a subsequent injection. This is a somewhat simplified explanation as, of course the reaction is short lived so the trailing reaction zone will be progressing through the sample plug with time and factors of diffusion and turbulence should also be considered. The injection loop was reduced from 120µl to 2µl and results achieved from this system are given in figure 10. Clearly these results, when compared to those of figure 5 have a longer Δt, lower peak intensity and a higher signal to noise ratio. The required sensitivity is, however, attainable and novel platform iterations are now in the process of being designed to further improve the integrated micro-fluidic device.

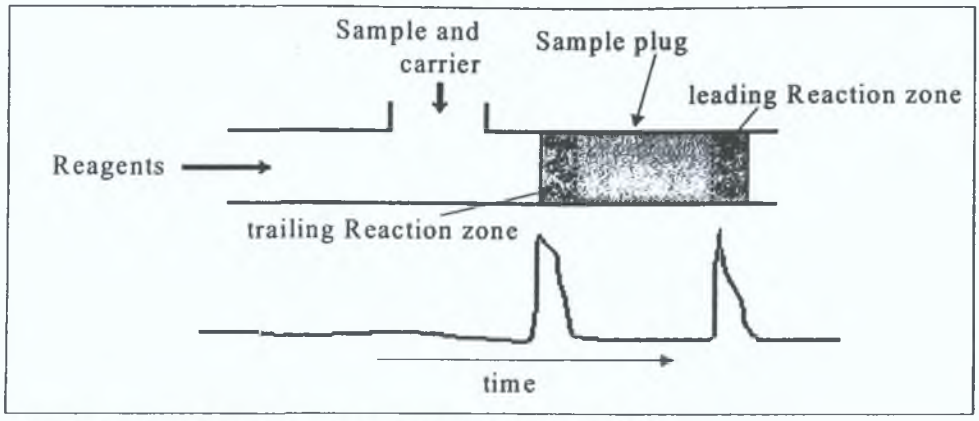

Figure 9: Schematic of reaction occuring in system using 120µl injection loop

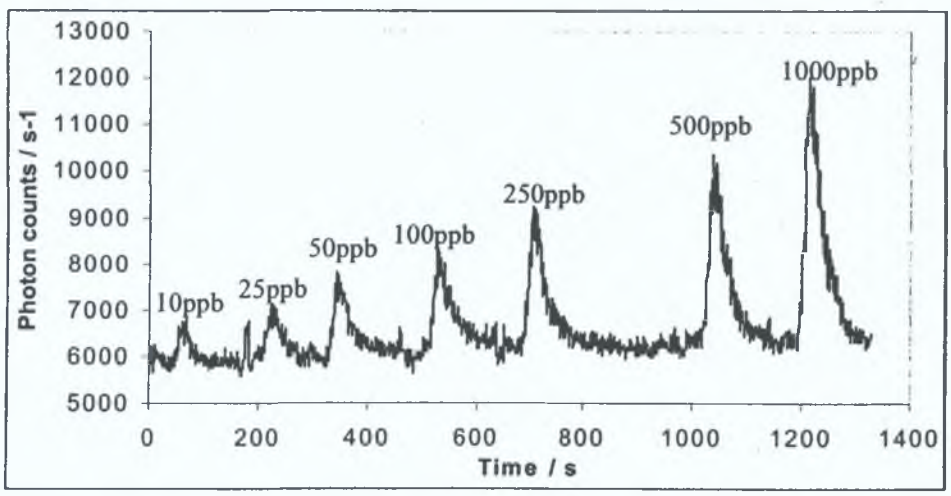

Figure 10: Reaction peaks from the current iteration of micro-fluidic sensing platform using a 2µl injection loop

4. CONCLUSIONS

This work has demonstrated the feasibility of in-house fabrication of a micro-fluidic structure using the technology of micro-milling and hot embossing. Preliminary results from aqueous copper (II) ion sensing indicate that the novel chemiluminescent sensing technique can be successfully incorporated into the micro-fluidic sensing structure. The detection range is already within the ppb range approaching that reported in the literature and improvements to the design of the platform are expected to reduce the limit of detection still further. Work is currently being carried out to characterise the reproducibility of chemiluminscence output for the current design. Issues concerning the channel geometry need to be investigated to ensure efficient mixing balanced with ease of manufacture and reproducibility of platform structure. Reagent reservoirs and solid-phase surfactant immobilisation on to the platform structure have yet to be achieved and inclusion of an on-board micro-pump is also required.

ACKNOWLEDGEMENTS

This work has been made possible through the HEA-PRTLI (Programme for Research in Third Level Institutes) grant, which realised the National Centre for Sensor Research and allowed purchase of the hot embosser and micro-miller.

REFERENCES

1. Water Quality Directive 98/83/EU, European Commission, Brussels, 1998
2. Pollution; Causes, effects and control. RSC publication 1990, ed. Roy M. Harrison
3. Parameters of Water Quality, Interpretation and Standards, EPA publication, Wexford, 2001
4. K.H.Coale, K.S. Johnson, P.M. Stout, C.M. Sakamoto, Analytica Chimica Acta, **266**, pp345-351, 1992
5. J.R.Donat, C.M.G. van den Berg, Mar. Chem. **38**, p **69**, 1992
6. T. Mayr, I. Klimant, O.S. Wofbeis, T. Werner, Analytica Chimica Acta, **462**, pp1-10, 2002
7. M. Yamada, S. Suzuki, "Micellar Enhanced Chemiluminescence of 1,10-phenanthroline for the determination of ultratraces of copper (II) by flow injection method," Anal. Lett. 17, pp 251-263, 1984
8. H. Zamzow, K.H. Coale, K.S. Johnson, C.M. Sakamoto, "*Determiniation of copper complexation in seawater using flow injection analysis with chemiluminescence detection*," Anal. Chim.Acta., **377**, pp 133-144, 1998
9. Flow Injection Analysis; Principles and Applications, M. Valcarcel, M.D. Luque de Castro, published by Ellis Horwood.

PAPER

www.rsc.org/loc

Development of a micro-fluidic manifold for copper monitoring utilising chemiluminescence detection

Éadaoin Tyrrell,[a] Ceri Gibson,[b] Brian D. MacCraith,[b] David Gray,[b] Pat Byrne,[b] Nigel Kent,[b] Conor Burke[b] and Brett Paull*[a]

[a] *National Centre for Sensor Research, School of Chemical Sciences, Dublin City University, Glasnevin, Dublin 9, Ireland. E-mail: Brett.Paull@dcu.ie; Fax: 00353 (0)1 7005503; Tel: 00353 (0)1 7005060*

[b] *National Centre for Sensor Research, School of Physical Sciences, Dublin City University, Glasnevin, Dublin 9, Ireland*

Received 16th January 2004, Accepted 31st March 2004
First published as an Advance Article on the web 26th April 2004

The progressive development of a micro-fluidic manifold for the chemiluminescent detection of copper in water samples, based on the measurement of light emitted from the Cu(II) catalysed oxidation of 1,10-phenanthroline by hydrogen peroxide, is reported. Micro-fluidic manifolds were designed and manufactured from polymethylmethacrylate (PMMA) using three micro-fabrication techniques, namely hot embossing, laser ablation and direct micro-milling. The final laser ablated design incorporated a reagent mixing channel of dimensions 7.3 cm in length and 250 × 250 μm in width and depth (triangular cross section), and a detection channel of 2.1 cm in length and 250 × 250 μm in width and depth (total approx. volume of between 16 to 22 μL). Optimised reagents conditions were found to be 0.07 mM 1,10-phenanthroline, containing 0.10 mM cetyltrimethylammonium bromide and 0.075 M sodium hydroxide (reagent 1 delivered at 0.025 mL min^{-1}) and 5% hydrogen peroxide (reagent 2 delivered at 0.025 mL min^{-1}). The sample stream was mixed with reagent 1 in the mixing channel and subsequently mixed with reagent 2 at the start of the detection channel. The laser ablated manifold was found to give a linear response (R^2 = 0.998) over the concentration ranges 0–150 μg L^{-1} and be reproducible (% RSD = 3.4 for five repeat injections of a 75 μg L^{-1} std). Detection limits for Cu(II) were found to be 20 μg L^{-1}. Selectivity was investigated using a copper selective mini-chelating column, which showed common cations found in drinking waters did not cause interference with the detection of Cu(II). Finally the optimised system was successfully used for trace Cu(II) determinations in a standard reference freshwater sample (SRM 1640).

Introduction

The determination of trace elements in environmental samples requires sensitive and selective analytical techniques. For measurements of trace concentrations of metals in various matrices there are a number of complex instrumental methods widely used, including graphite furnace atomic absorption spectroscopy (GF-AAS), inductively coupled plasma techniques with atomic emission spectroscopy (ICP-AES) or mass spectrometry (ICP-MS).[1] However, there are also many sensitive simpler alternatives to these complex techniques. The use of chemiluminescence for the determination of dissolved trace metals has become a popular choice over recent years as it requires only simple inexpensive instrumentation compared to the above methods and is often very sensitive and linear over a wide dynamic range. In addition, chemiluminescent techniques can be highly selective for certain species.[2] Chemiluminescence is commonly used in flow injection analysis (FIA) where it delivers low limits of detection, high precision and fast sample throughput.

Cu(II) is an important element for the metabolism of many living organisms, but, as with many other metals, at high concentrations it is toxic. Cu(II) compounds are commonly used in agriculture, for preservatives and for water treatment. The Environmental Protection Agency (EPA) has stated that drinking water should not contain more than 1.3 mg L^{-1} of Cu(II),[3] with levels above this producing astringent tastes. The recommended daily allowance (RDA) for adults is 1.1 mg per day.[4] Cu(II) can be determined sensitively using chemiluminescence. A number of different chemiluminescent methods have been proposed for the determination of Cu(II) in different sample matrices. Yamada and Suzuki determined trace amounts of Cu(II) using a chemiluminescent reaction based on a flavin mononucleotide–hydrogen peroxide–phosphate buffer system.[5] A second method, developed by Yan and Worsfold, determined Cu(II) by its catalytic effect upon the reaction between luminol (5-amino-2,3-dihydrophtalazine-1,4-dione) and hydrogen peroxide.[6] More recently, a method based on the quenching effect of Cu(II) on the chemiluminescent reaction of dichlorofluorescein with hydrogen peroxide was developed by Safavi and Baezzat, and subsequently applied to the determination of Cu(II) in blood samples.[7] Some methods have included an additional pre-treatment step prior to detection to improve selectivity. One such example used a micro-column of immobilised 8-hydroxyquinoline (8-HQ) for analyte preconcentration and removal of matrix interferences in seawater analysis,[8] although later work by Zamzow *et al.*[9] showed how the chemiluminescent reaction involved could, under certain conditions, be applied directly to the analysis of seawater without the use of such a column. The reaction involved was a well established reaction for Cu(II) determinations, based upon the formation of a complex between Cu(II) and 1,10-phenanthroline.[8–12] The chemiluminescent reaction, which emits between 445–450 nm, results from the oxidative destruction of the Cu(II)–1,10-phenanthroline complex by hydrogen peroxide at an alkaline pH, with increased sensitivity obtained through the addition of a cationic surfactant.[10]

Chemiluminescence is a promising method of detection for micro-fluidic analytical systems due to its high sensitivity and the simplicity of the measurement technique. The combination of chemiluminescence detection, with its simple instrumentation requirements, and micro-fluidic systems, with low reagent consumption and portability, is proving very successful, with a number of chemical and biological flow sensor systems having already been developed.[13–15] This promising combination is aided by recent progress in the development of fabrication methods for plastic micro-fluidic manifolds made from polymers such as poly(methylmethacrylate) (PMMA) or poly(dimethylsiloxane) (PDMS).[16]

In the work described here, the performance of PMMA micro-fluidic manifolds fabricated using a variety of micro-fabrication

DOI: 10.1039/b400805g

techniques has been investigated. In combination with chemiluminescence detection, these manifolds have been applied to the determination and monitoring of Cu(II) in water samples. The aim of the study was to develop an analytical system, capable of low μg L^{-1} determinations of Cu(II) in water samples, and which could be applied to 'on-line' monitoring with minimal reagent consumption.

Experimental

Preliminary Studies—stage I

Preliminary (stage I) studies took place using standard FIA instrumentation (see Fig. 1(a)) in order to optimise the chemistry of the system. A peristaltic pump (Gilson Minipuls 312, Villiers, France) was employed to deliver the sample and reagents through 0.8 mm id poly(ether ether ketone) (PEEK) tubing, at a total flow rate of 2.1 mL min^{-1}. The manifold included a manual sample injection valve, model 7125, (Rheodyne, Cotati, CA, USA) fitted with a 120 μL PEEK injection loop for the introduction of the samples. The injected sample and carrier stream merged with the 1,10-phenanthroline solution at a T-piece connection and were mixed in a 100 cm long mixing coil of PEEK tubing prior to meeting with the hydrogen peroxide solution through a second T-piece connector. The distance between the second T-piece and the detector flow cell was kept as short as possible (approximately 50 mm) as the chemiluminescence reaction occurred almost instantaneously. The flow cell itself consisted of 65 cm of 0.6 mm id transparent, flexible polyethylene (PE) tubing which was spiralled to a diameter of 25.4 mm and fixed to the window of a photomultiplier tube (PMT) (detailed below) and housed within a light tight box. Other details have been described previously by Coale *et al.*[8]

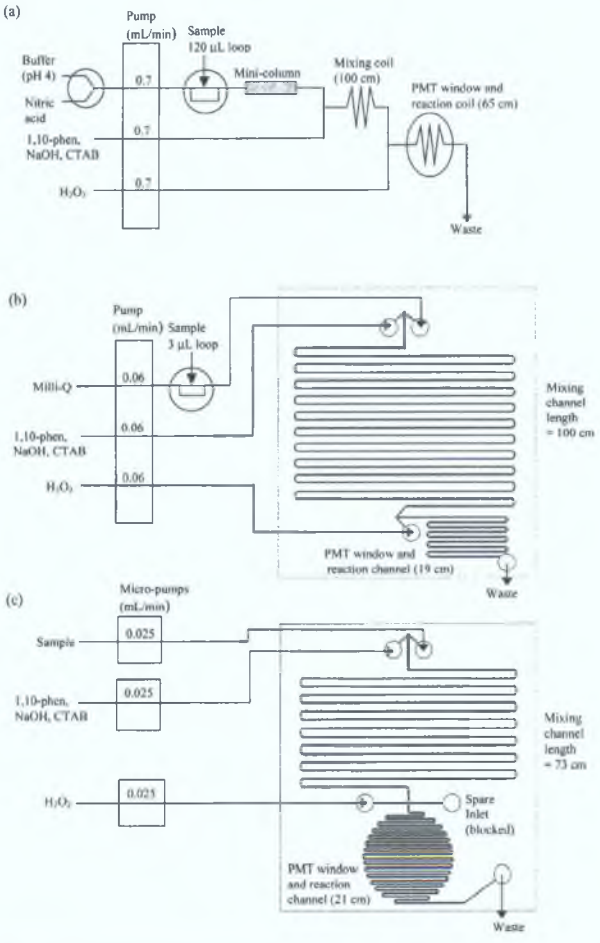

Fig. 1 Schematic diagrams and dimensions of the FIA and micro-fluidic manifolds developed. Chip dimensions = 7.0 × 7.0 × 0.8 cm.

Micro-column

A 0.8 cm long, 0.3 cm id micro-column packed with PRP-X800 itaconic acid functionalised 20 μm PS-DVB resin (Hamilton Company, Reno, NV, USA) was used for Cu(II) selectivity studies. The column was incorporated in the various manifolds prior to the introduction of the sample into the reagent streams. Back-pressure from the 0.8 cm column was sufficiently low not to affect performance of the peristaltic pumps used.

Reagents

In this study, all reagents were of analytical reagent grade and contained negligible concentrations of trace metals unless stated otherwise. Water obtained from a Milli-Q (Millipore) water purification system was used throughout this work. All the solutions were degassed using sonication and filtered through a 0.45 μm nylon membrane filter from Gelman Laboratories (Michigan, USA) prior to use. Under optimal final conditions the following reagents were prepared; Reagent 1; Deionised (Milli-Q) water containing 0.07 mM 1,10-phenanthroline made from a 12 mM stock solution, which was found to be stable for several days (obtained from BDH Laboratory Supplies, Poole, England and further purified by recrystalisation with nitric acid), 0.10 mM cetyltrimethylammonium bromide (CTAB) (BDH Laboratory Supplies, Poole, England) and 0.075 M sodium hydroxide (Sigma Aldrich Ltd., Dublin, Ireland). This solution was made up fresh each day. Reagent 2; A 5% w/v hydrogen peroxide (Sigma Aldrich Ltd., Dublin, Ireland) solution was prepared daily.

All Cu(II) standard solutions were prepared freshly each day from stock solutions (atomic absorption spectroscopy standard solution (Sigma Aldrich Ltd., Dublin, Ireland)) (1000 mg L^{-1}) stored in 1% nitric acid. Calcium chloride (obtained from Sigma Aldrich Ltd., Dublin, Ireland) and magnesium chloride (Sigma Aldrich Ltd., Dublin, Ireland) were used to make up a pseudo sample matrix to investigate selectivity. Other metals used for interference studies included zinc, manganese, lead, nickel, cadmium and cobalt. All of these were atomic absorption spectroscopy standard solutions stored in 1% nitric acid and were obtained from Sigma Aldrich Ltd., Dublin, Ireland. Normal precautions for trace metal analysis were taken including acid washing of all glassware and plastic containers.

Micro-fluidic manifold fabrication

The micro-fluidic manifolds were designed using CAD 3D Excalibur software. Following this, the manifold could be fabricated in one of three different ways; hot embossing from a micro-milled brass master, direct micro-milling into the PMMA chip or laser ablation. The first technique used a brass master that was fabricated by high precision micro-milling the channels of various dimensions. This was accomplished using a Datron 3-D M6 Micro-Machining Centre, (Datron Technology Ltd., Milton Keynes, UK). The resultant master was then used to hot emboss the PMMA chips using a Model Hex02 Hot Embosser (Jenoptik Mikrotechnik, Germany). In this case, the brass master was heated to 138 °C and the PMMA was heated to 125 °C, just above the glass transition temperature (T_g) of PMMA (105 °C). Using a controlled force (1000 N) the master was used to emboss the PMMA. This procedure typically took 15 min. A top plate of PMMA of equal width was then drilled to make the reagent inlet holes and this was bonded to the embossed plate at 130 °C and 500 N in a Class 1000 clean room.

The second technique used involved direct milling of the PMMA substrate. In this case, the micro-milling system was used to cut the micro-fluidic channels (200 × 200 μm) directly into the PMMA. Although direct micro-milling removed the additional hot embossing fabrication step, the surface of the channels was not as smooth

as that produced by the hot embossing method. The device was then bonded to a pre-drilled top plate as previously described above.

The third method of fabrication used in this study was laser ablation. A Excimer laser (Optec Micro-Master System, Optec S.A., Frameries, Belgium) was used to make the micro-fluidic channels in the PMMA (The laser mask size was set to 250 μm, with a laser energy density of 1358 mJ cm^{-2} and a frequency of 50 Hz, resulting in a machining speed of 0.250 mm s^{-1}). The manifold was bonded as before.

Micro-fluidic manifold and instrumentation—stage II

For the initial micro-fluidic manifolds (stage II) both reagents and sample carrier were again delivered using a standard peristaltic pump (Gilson Minipuls 312, Villiers, France) delivering the sample and reagents into the plastic manifold *via* connecting 0.8 mm inner diameter poly(ether ether ketone) (PEEK) tubing, glued into reagent inlet holes (1 mm diameter) on the underside of the plastic chips, at individual flow rates of 0.06 mL min^{-1} (0.18 mL min^{-1} total). The sample was introduced into the carrier stream using a manual sample injection valve, model 7125, (Rheodyne, Cotati, CA, USA) fitted with a 3 μL PEEK injection loop. The manifold itself had a mixing channel of 1000 mm in length, <900 μm in depth and 1000 μm in width, and a detection channel 190 mm in length and again <900 μm in depth and 1000 μm width. Chemiluminescence was continuously measured using a PMT (Hamamatsu Photonics HC135–01 series with R1924 bi-alkali tube). The PMT was approximately 135 mm in height and the window of the detector was 25.4 mm inner diameter. In this work, the chemiluminescence occurred between 445 and 450 nm, and the PMT spectral range was from 300 nm to 650 nm (absorbance of PMMA is negligible above 400 nm). The PMT operated in photon counting mode and the signal was recorded on a computer and data processed using Microsoft Excel. The PMT was placed over the detection channel and was secured tightly to prevent stray light from reaching the detector. The complete micro-fluidic manifold and PMT assembly was wrapped several times in aluminium foil to reduce the dark count rate and enclosed in a light tight box. Fig. 1(b) shows the schematic diagram of this initial system.

Micro-fluidic manifold and instrumentation—stage III

For the final micro-fluidic system (stage III) developed, three micro-peristaltic pumps with 0.51 mm id peristaltic tubing (manufactured by BVT Technologies, Euro-link Associates, Tyne & Wear, England) were used to drive the reagents and sample streams through the micro-fluidic manifold *via* connecting 0.13 mm id PEEK tubing, glued into reagent inlet holes (1 mm diameter) on the underside of the plastic chips. Each micro-pump weighed only 34 g and was 60 mm in height and only 16 × 16 mm at the base. These pumps were operated using a DC supply at 3 V and were connected together using a custom made interface driven by one PC connection. When connected in this manner it was possible to set each flow rate independently for each pump in the range of 0.5 to 200 μL min^{-1}. Under optimal conditions for this study, individual flows rates of 25 μL min^{-1} (75 μL min^{-1} total) were used.

The final version of the micro-fluidic manifold design is illustrated schematically as Fig. 1(c). The micro-fluidic manifold itself was manufactured from PMMA. A number of different designs and dimensions were investigated but the basic design consisted of two inlets for the sample and 1,10-phenanthroline solutions, which were subsequently mixed together in the mixing channel. This provided the mixing necessary for the reaction between the Cu(II) in the sample and the 1,10-phenanthroline to take place. A third inlet at the end of the mixing channel prior to the detection/reaction channel was used for the introduction of the hydrogen peroxide. At the end of the detection channel there was an outlet leading to waste. For the final laser ablated version of the micro-fluidic manifold the dimensions of the mixing channel were 730 mm in length with an internal width and depth of 250 μm × 250 μm (triangular cross-section), and 210 mm in length and 250 μm × 250 μm in width and depth for the reaction/detection channel. This meant the theoretical approximate internal volume of the reaction/detection channel was between 16 and 22 μL. Chemiluninescent detection was monitored with a PMT as with the stage II instrument described above.

Results and discussion

Preliminary studies—stage I

Initial studies took place using standard FIA in order to optimise the chemistry of the system and to ascertain the analytical performance characteristics that could be later compared to the micro-fluidic method. Using this system three of the reaction variables were optimised, the concentration of hydrogen peroxide, 1,10-phenanthroline and the concentration of surfactant.

Optimisation of hydrogen peroxide

Concentrations of 1,10-phenanthroline, CTAB and NaOH were kept constant at 0.06 mM, 0.1 mM and 0.075 M respectively, while the concentration of hydrogen peroxide was varied. From this work it was found that a 5% hydrogen peroxide solution resulted in a higher analytical signal for a Cu(II) standard than higher hydrogen peroxide concentrations, with little difference in background noise, even though in some of the literature a 10% hydrogen peroxide solution was used.[9] The actual signal to noise ratio for the 5% hydrogen peroxide was 13.2 compared to 8.4 for the 10% peroxide solution. The peroxide solution was prepared daily to avoid a decrease in sensitivity that resulted from reagent instability over time. No significant reductions in detector response when using a single hydrogen peroxide solution for a period of 12 h.

Optimisation of 1,10-phenanthroline

Using the optimised 5% hydrogen peroxide concentration, the concentration of 1,10-phenanthroline was then optimised. The concentrations of CTAB and sodium hydroxide again remained constant at 0.1 mM and 0.075 M, respectively. A 0.03 mM 1,10-phenanthroline solution was found to be optimal, producing a significant reduction in background noise compared to higher levels. The signal itself due to Cu(II) was also reduced but the signal to noise ratio for the 0.03 mM 1,10-phenanthroline solution was 27.63 compared to 8.86 for a 0.06 mM 1,10-phenanthroline solution. The 1,10-phenanthroline was also purified by recrystilisation with nitric acid as the Cu(II) signal was enhanced considerably (by approximately 40%) when the purified 1,10-phenanathroline was used and noise further decreased. Purified 1,10-phenanthroline was used in all future work.

Optimisation of surfactant

Previous work by Yamada and Suzuki[10] investigated the effect of different surfactants on the Cu(II)–1,10-phenanthroline chemiluminescent reaction. It was found that an increase in signal resulted from the addition of a cationic surfactant, while anionic and nonionic surfactants had no significant effect. In this work, several surfactants including Triton X-100, sodium dodecylsulfate (SDS) and CTAB were investigated. It was found that Triton X-100 (non-ionic) and SDS (anionic) did not increase the signal and the background noise was dramatically increased. The addition of low concentrations (<0.1 mM) of the cationic surfactant CTAB was found to dramatically reduce some of the background noise whilst not affecting the analytical signal for Cu(II). A concentration of 0.05 mM CTAB produced a signal to noise ratio of 19.9 compared to 6.4 for a 0.10 mM CTAB solution.

The optimal reaction pH was determined by Coale and co-workers to be between 9.8 and 10.1[8]. In this work, the reaction pH for Cu(II) analysis under optimised conditions was found to be 10.35. Using this system, Cu(II) could be easily determined at levels

as low as 1 μg L^{-1} and the response was linear (n = 5, standards injected in triplicate) over the concentration range 1 to 50 μg L^{-1}, producing a R^2 value of 0.995 (see Fig. 2(a)).

Selectivity studies

Previous work has shown the high selectivity of the Cu(II)–1,10-phenanthroline chemiluminescent reaction, which shows little or no response to excess concentrations (> 10 mg L^{-1}) of alkali metals or Cr(III) and (VI), Mn(II), Ni(II), Co(II), Cd(II), Pb(II), Al(III), and Fe(II) and Fe(III).[7,10] However, it has been reported that high concentrations of Zn(II), Ca(II) and Mg(II) can cause minor interference at the above concentration. To further increase the selectivity of the developing method, a Cu(II) selective itaconic acid functionalised resin (20 μm resin size) micro-column was investigated. Itaconic acid is a dicarboxylic acid capable of acting as a weak cation exchanger and/or a strong chelating ion exchanger, which within a 0.3 × 0.8 cm micro-column at pH 2 to pH 4 completely retained Cu(II) whilst showing no retention of alkali and alkaline earth metal ions, or Mn(II), Cd(II), Co(II), Zn(II), Pb(II) and Ni(II). By selectively removing Cu(II) from the sample matrix using the above micro-column on-line, followed by its subsequent elution, it was possible to remove the above potential interferences. To illustrate this, a complete set of Cu(II) standards over the range 1 μg L^{-1} to 1 mg L^{-1} were made up in a sample matrix containing 10 mg L^{-1} Ca(II) and 10 mg L^{-1} Mg(II) (typical concentrations found in drinking waters), whilst a second set was made up in Milli-Q water only. The standards containing Ca(II) and Mg(II) were each passed through the micro-column (column buffered to pH 4) and the Cu(II) was selectively retained. The Cu(II) was subsequently eluted with an equal volume of 100 mM nitric acid. Comparison of the eluted Cu(II) standards with those prepared and analysed directly in Milli-Q water would show how the column could be used for complete retention and elution of Cu(II) from samples containing high levels of Ca(II) and Mg(II).

Fig. 3(a) shows the resultant peaks for the Cu(II) standards, which were separated from the sample matrix containing Ca(II) and Mg(II) by the itaconic acid column. The results for Cu(II) standards made up in Milli-Q water over the same concentration range of 1 μg L^{-1} to 1 mg L^{-1} are show as Fig. 3(b). It can be seen that there was effectively 100% separation and recovery of the copper from the sample matrix using the itaconic acid micro-column. This means the micro-column could also be used for preconcentration of Cu(II) from complex sample matrices should the need arise. From Fig. 3 it is also interesting to note that Milli-Q water itself gave a small response equivalent to < 1 μg L^{-1} Cu(II) when analysed directly and that this response was eliminated after treatment with the micro-column. This would indicate that some potentially interfering species (other than Cu(II)) in the Milli-Q water itself was causing a slight positive signal within the blank.

Initial micro-fluidic work—stage II

The first micro-fluidic manifold in this study was manufactured in PMMA using the micro-milling and hot embossing facility. The first manifold fabricated had a mixing channel of 1000 mm in length, 900 μm in depth and 1000 μm in width. However, bonding the top plate to the lower design plate causes considerable reduction in the actual depth of the channels in the finished manifold, particularly with wide channels such as these, and so the exact channel depth in the bonded manifold could not be ascertained. This early design provided the same mixing channel length as the

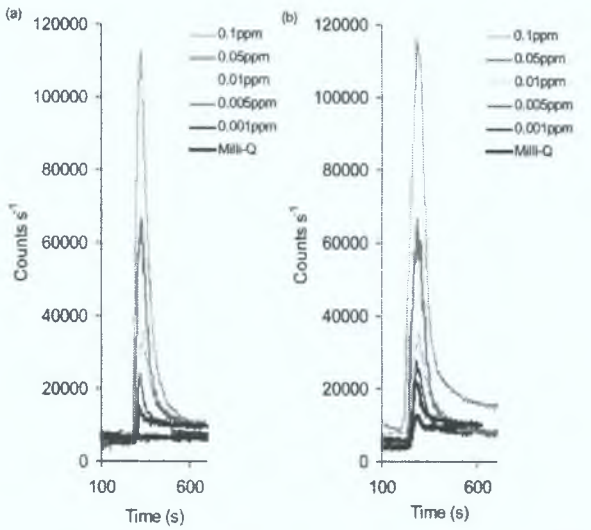

Fig. 3 Detector responses obtained for (a) Cu(II) standards prepared in a matrix of 10 mg L^{-1} Ca(II) and Mg(II) and passed through itaconic acid mini-chelating column followed by elution with 100 mM HNO_3, and (b) Cu(II) standards prepared in Milli-Q water only.

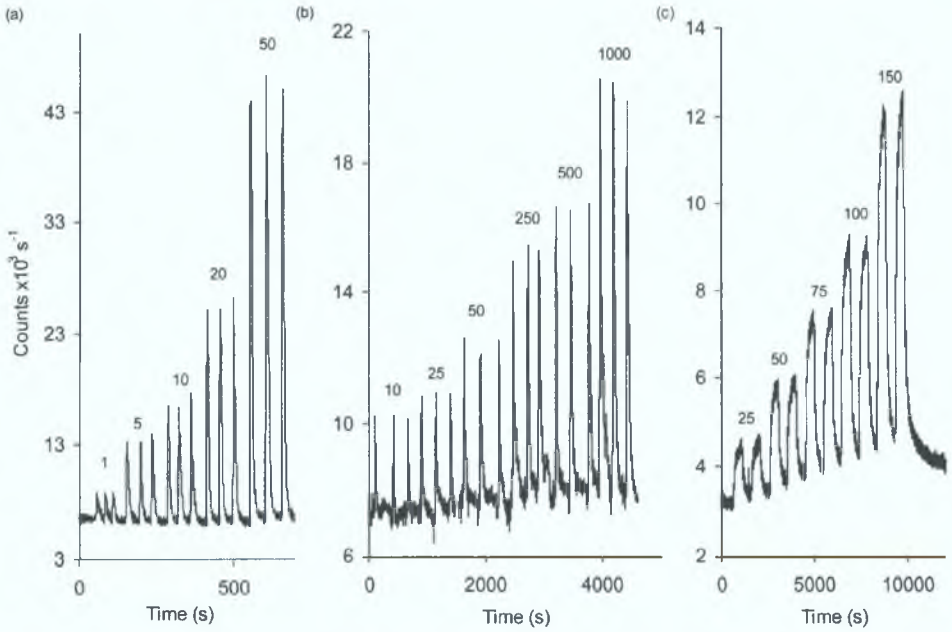

Fig. 2 Detector responses to Cu(II) standards obtained using (a) standard FIA manifold compared to (b) initial hot embossed design (1000 × 900 μm channels) and (c) laser ablated manifold (250 × 250 μm channels). Standard concentrations shown in μg L^{-1}.

standard FIA method and was found to be more than adequate for the required complete mixing of the Cu(II) in the sample and the 1,10-phenanthroline. The inlet for the introduction of the hydrogen peroxide was placed immediately prior to the detection/reaction channel as the chemiluminescent oxidation reaction was known to be almost instantaneous.

A series of experiments were again carried out in order to optimise the concentrations of 1,10-phenanthroline and CTAB under the new flow conditions. The experimental space was defined by varying systematically both the concentrations of 1,10-phenanthroline and CTAB from 0.01 mM to 0.10 mM. In all of the experiments, the following conditions were used; a total combined flow rate of 180 μL min^{-1}, sample injection volume of 3 μL, 5% hydrogen peroxide solution and 0.075 M sodium hydroxide. From this work the highest signal to noise ratio was achieved when using 0.07 mM 1,10-phenanthroline and 0.06 mM CTAB. Using these new conditions, linearity and response was again investigated, and the peaks obtained for a range of Cu(II) standards between 10 and 1000 μg L^{-1} can be seen in Fig. 2(b). As can be seen from the figure shown, linearity (if based upon peak height) was restricted to < 100 μg L^{-1} Cu(II). However, as can be seen, given the much reduced injection volume, analyte sensitivity was much improved, despite the large reduction in the size and volume of the reaction/detection coil. There was also very little change in background noise, giving a detection limit of approximately 6 μg L^{-1} (using 3 × baseline noise criterion). The repeat injection of a Cu(II) standard solution using this system (n = 6) gave a % RSD value of 2.2 based upon peak height.

Investigation of mixing process

In an attempt to improve method linearity and further miniaturise the manifold the impact of the dimensions of the mixing channel and reaction channels was investigated. Coloured dyes were used in place of the reagents to investigate the mixing process, in order to reduce the length of the mixing chamber. It was found that complete mixing of the two streams occurred after approximately 700 mm. It was decided, therefore, that the length could be decreased by nearly one third of the initial length (1000 mm to 700 mm). An investigation on the length of the reaction/detection channel was also carried out in order to determine the optimal length. Using a 100 μg L^{-1} Cu(II) standard, the detection channel was increasingly masked from the PMT detector to ascertain the effect of shortening the reaction channel by 25, 50 and 75% (equivalent to 143, 95 and 48 mm respectively). The resultant signals for the 100 μg L^{-1} standard can be seen in Fig. 4. During this experiment it was found that masking the last 25% of the reaction/detection channel, the chemiluminescent signal for the Cu(II) standard decreased (by more than half). It was also found that masking the last 75% of the channel led to the signal being totally lost. This meant that although the chemiluminescence reaction was thought to occur almost instantaneously, maximum emission took place in the latter part of the detector channel due to a short time delay to facilitate mixing of the hydrogen peroxide and the sample/reagent flow. As a result, the length of the reaction channel could not be decreased and was subsequently increased (see stage III below).

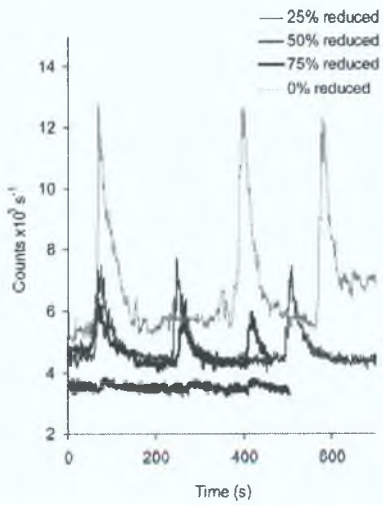

Fig. 4 Detector responses obtained for a 100 μg L^{-1} Cu(II) standard with increasingly reduced reaction/detection channel length (equivalent to 190, 143, 95 and 48 mm).

Further miniaturisation—stage III

Taking the above results into account, the design for the final (stage III) micro-fluidic manifold was finalised. As above, a manifold was prepared using micro-milling to produce a brass master, followed by hot embossing into PMMA. The final design, as shown in Fig. 1(c), utilised three individual micro-pumps to supply the reagent stream, hydrogen peroxide stream and sample stream. To further simplify the system, the sample injection valve was removed and the sample fed directly into the mixing channel itself. This would result in a continuous detector response rather than the previous transient signal. For introduction of new sample and standard solutions the sample pump was stopped whilst solutions were changed. It was found that this manual procedure did not introduce air into the system (as is evidenced by Fig. 5), although for future on-line work a low-pressure switching valve could be readily incorporated into the system for this purpose. The mixing channel was reduced in length to 700 mm, while the detection channel was increased to 210 mm. In addition, the shape of the detection channel was optimised (fitted exactly to shape of PMT window) to maximise sensitivity and reduce background noise. The channels themselves were significantly narrower than the channels of the larger chip, being 200 μm wide by 200 μm deep (although again due to bonding the ultimate depth of the channels was significantly < 200 μm). As in each previous case the reagent concentrations were re-optimised to suit the new manifold design. The highest signal to noise ratio was achieved when using 0.07 mM 1,10-phenanthroline and 0.1 mM CTAB, with other conditions set at a total combined flow rate of 76 μL min^{-1}, 5% hydrogen peroxide solution and 0.075 M sodium hydroxide.

Flow rates

The flow rates used in the stage III micro-fluidic system were each controlled by a separate micro-pump, however all the reagents were pumped at the same flow rate. Briefly, the effect of flow rate on response was investigated using individual flow rates of 0.029, 0.025 and 0.021 mL min^{-1} for each of the three streams (measuring in total 0.086, 0.076 and 0.064 mL min^{-1}). Results showed that the analytical signals were slightly increased by decreasing flow rates (see Fig. 5(a)). However, although the lowest flow rates (0.021 mL min^{-1} for each stream) produced the highest absolute signal, the background was also noisier, and therefore individual flow rates of 0.025 mL min^{-1} was found to be optimum.

Linearity

Using the optimised conditions, a series of measurements was performed with Cu(II) standard solutions ranging from 0 to 50 μg L^{-1}. A stepwise graph was produced over this concentration range and is shown as Fig. 5(b). The resulting signal heights were plotted as a function of concentration and the results were found to produce an excellent linear correlation within this given concentration range (R^2 = 0.993, n = 6, standards measured in duplicate). Using the micro-fluidic manifold, Cu(II) could be easily determined at concentrations as low as 10 μg L^{-1}, with the S/N ratio of 3.

Comparison of fabrication techniques

Three alternative micro-fabrication techniques were investigated, namely hot embossing into PMMA, direct micro-milling of the

channels into the PMMA itself and thirdly the use of laser ablation. Each of these techniques result in different channel profiles and surface morphologies. Laser ablation results in a characteristic shallow 'V' shaped channel and direct micro-milling into the PMMA results in a rougher surface than the hot embossed manifold. For direct comparison with the hot embossed manifold, detector response and linearity was determined on each manifold using identical reagent concentrations and flow rates. The directly micro-milled manifold resulted in the largest comparative unit response, with a calibration slope equal to ~751 counts s^{-1} for each μg L^{-1} of Cu(II) compared to ~378 counts s^{-1} for each μg L^{-1} Cu(II) for the above hot embossed manifold. However, background noise was also increased. The results using the directly micro-milled manifold were found to be linear up to 100 μg L^{-1} (R^2 = 0.983, n = 5, standards injected in duplicate).

The laser ablated manifold was found to give the lowest unit response with the lowest calibration slope, only 61 compared to the above values. However the manifold also produced the most linear response over the greatest concentration range 0–150 μg L^{-1} (R^2 = 0.998, n = 5, standards injected in duplicate, see Fig. 2(c)). In addition, the laser ablated manifold also gave the lowest background noise, resulting in a detection limit of approximately 20 μg L^{-1} Cu(II). The reason for the lower response and noise with this manifold is simply related to the fact that the laser ablation process results in the shallow 'V' shaped channels which effectively reduce the channel volumes considerably (~50%), compared to the alternative fabrication methods. To partially compensate for this profile the laser ablated channels were cut 250 μm wide by 250 μm deep, hence the reaction/detection channels of the ablated manifolds was calculated to be within the range 16–22 μL compared to 21–30 μL for the hot embossed manifold. Fig. 6(a) shows the comparative responses for each of the above micro-fluidic manifolds for increasing Cu(II) standard solutions (Milli-Q water was introduced between each standard reading). Fig. 6(b) shows the reproducibility of the laser ablated manifold with the repeated analysis (n = 5) of a 75 μg L^{-1} Cu(II) standard.

Sample carry over

Fig. 6 shows recovery time (time taken for a return to baseline signal following removal of the sample) for each of the micro-fluidic manifolds was in the order of 2–3 min. This indicates some degree of adsorbance of the reagents onto the channel walls, which may be slowly washed off during the Milli-Q washing step. However, as Figs. 5(b) and 6(a) show, the system does return to the starting baseline when allowed sufficient recovery time, and although this may increase individual sample analysis time, for

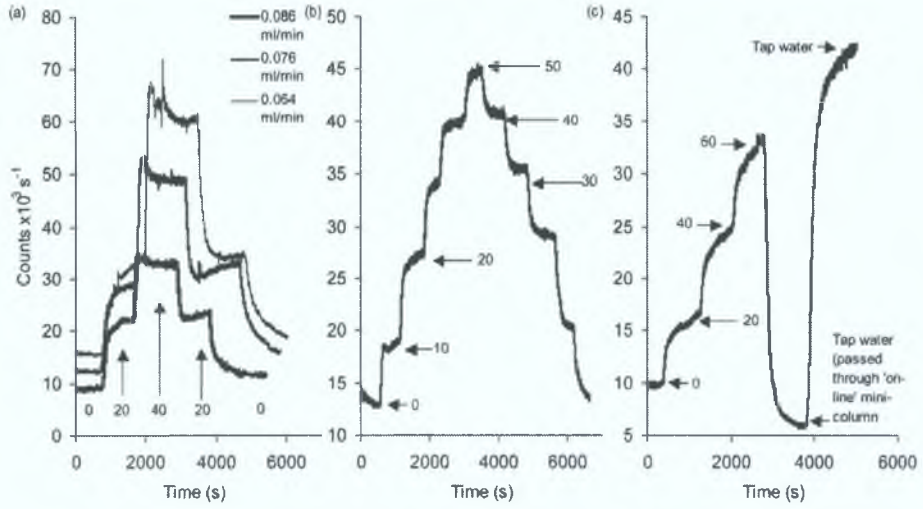

Fig. 5 Detector responses obtained using the hot embossed micro-fluidic manifold (200 × 200 μm channels). (a) Effect of flow rate upon response, (b) system linearity, and (c) on-line analysis of drinking water. All concentrations shown in μg L^{-1}.

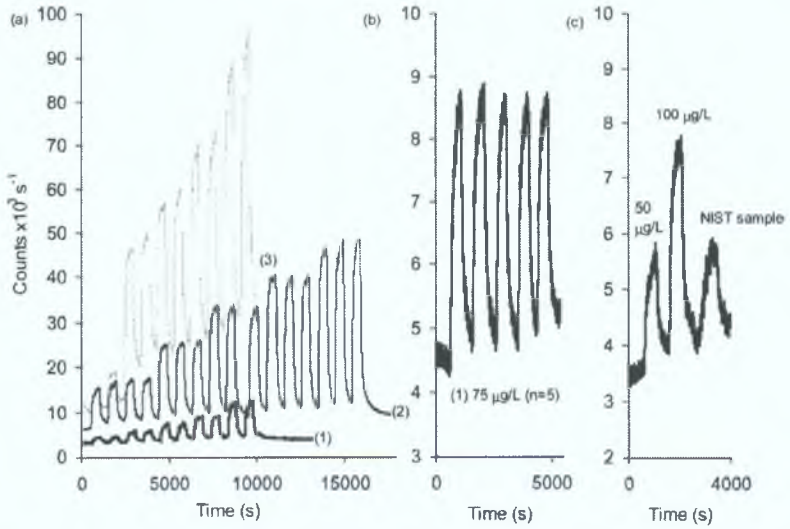

Fig. 6 (a) Comparison of detector response for three micro-fluidic manifolds, (1) laser ablated manifold (250 × 250 μm), (2) hot embossed manifold (200 × 200 μm), (3) direct micro-milled manifold (200 × 200 μm). (b) Repeat analysis of 75 μg L^{-1} Cu(II) standard using laser ablated manifold. (c) Analysis of SRM 1640 standard reference freshwater sample. Milli-Q water blanks run between each sample/standard analysis.

Table 1 Analytical performance data for developed methods

Fabrication method	Flow rates/ mL min^{-1} reagent	Linear range[a]/ μg L^{-1}	Slope	R^2 value	Reproducibility % RSD (no. replicates)	Approx. detection limit/μg L^{-1}
Standard FIA	0.7	1–50	726	0.995	1–2% (n = 3)	1
Hot embossing 1000 × 900 μm	0.06	< 100	—	—	2.2% (n = 6)	6
Hot embossing 200 × 200 μm	0.025	20–100	751	0.996	2–3% (n = 3)	10
Micro-milling 200 × 200 μm	0.025	40–100	378	0.983	4–5% (n = 2)	10
Laser ablation 250 × 250 μm	0.025	25–150	61	0.998	2–3.5% (n = 5)	20

[a] Data based upon peak height measurements.

longer term on-line monitoring purposes this should not be a significant problem.

Table 1 shows the comparative analytical performance data determined for the three micro-fluidic manifolds, and those data obtained for standard FIA and the initial larger scale hot embossed manifold. The data shown were obtained under the specific reagent conditions used within this study only.

Analysis of real samples on-line drinking water analysis

Using the hot embossed micro-fluidic manifold and conditions described above, the on-line analysis of drinking water was undertaken. The drinking water from a laboratory tap was continuously fed *via* an in-line filter to the sample inlet of the manifold. Within the sample line a switching valve was placed which allowed the tap water to either by-pass or be passed through the Cu(II) selective itaconic acid micro-column (pre-buffered to pH 4) detailed earlier, allowing verification that the detector response was due to Cu(II) only. The results of this experiment can be seen in Fig. 5(c). As can be seen, the concentration of Cu(II) found within the laboratory tap supply was approximately 80 μg L^{-1}. On-line passage of the tap water through the itaconic acid column completely removed the chemiluminescent signal, indicating that the sample matrix was not causing significant interference in this application.

Analysis of certified reference water sample

To check for method accuracy a standard reference material (SRM) from the National Institute of Standards and Technology (NIST) was analysed for Cu(II). The sample (SRM 1640) was composed of natural fresh water (river) had been filtered and acidified with 0.5 M nitric acid. This sample was certified to contain 85.2 μg L^{-1} ± 1.2 μg L^{-1} Cu(II). The sample was neutralised using sodium hydroxide and was diluted by 50% with Milli-Q water. This sample was then analysed using the laser ablated manifold. Firstly, 50 and 100 μg L^{-1} Cu(II) standards were analysed, with a Milli-Q water blank run between standards. The 50% dilution of the NIST standard was then analysed. The resultant signals can be seen in Fig. 6(c). This sample was found to contain approximately 40 μg L^{-1} Cu(II) which corresponds to ~80 μg L^{-1} in the SRM, within ±6% of the true value, representing excellent accuracy for a micro-fluidic device when analysing a complex freshwater sample for trace Cu(II).

Conclusions

The development of a micro-fluidic manifold and analytical method for Cu(II) determinations has been described. The results have shown that the standard FIA method can be effectively reduced to the micro-fluidic format whilst maintaining acceptable linearity, precision and accuracy and with appropriate detection methods such as chemiluminescence, also maintaining excellent sensitivity. The micro-fluidic system developed can be readily made portable or be used for on-line monitoring with as little as 3.0 mL h^{-1} total reagent consumption.

References

1 D. Harris, *Quantitative Chemical Analysis*, Freeman, New York, 5th edn, 1998.
2 C. M. Sakamoto-Arnold and K. S. Johnson, *Anal. Chem.*, 1987, **59**, 1789.
3 http://www.epa.gov/safewater/dwh/c-ioc/copper.html.
4 http://193.120.54.7/publications/reports/recommended_dietary_allowances_Ireland_1999.pdf.
5 M. Yamada and S. Suzuki, *Chem. Lett.*, 1982, 1747.
6 B. Yan and P. J. Worsfold, *Anal. Chim. Acta*, 1990, **236**, 287.
7 A. Safavi and M. R. Baezzat, *Anal. Lett.*, 2000, **33**, 667.
8 K. H. Coale, K. S. Johnson, P. M. Stout and C. M. Sakamoto, *Anal. Chim. Acta*, 1992, **266**, 345.
9 H. Zamzow, K. H. Coale, K. S. Johnson and C. M. Sakamoto, *Anal. Chim. Acta*, 1998, **377**, 133.
10 M. Yamada and S. Suzuki, *Anal. Lett.*, 1984, **17**, 251.
11 W. G. Sunda and S. A. Huntsman, *Mar. Chem.*, 1991, **36**, 137.
12 J. M. Lin and M. Yamada, *Analyst*, 2001, **126**, 810.
13 Y. Lv, Z. Zhang and F. Chen, *Talanta*, 2003, **59**, 571.
14 G. M. Greenway, L. J. Nelstrop and S. N. Port, *Anal. Chim. Acta*, 2000, **405**, 43.
15 A. M. Jorgensen, K. B. Mogensen, J. P. Kutter and O. Geschke, *Sens. Actuators, B*, 2003, **90**, 15.
16 A. de Mello, *Lab Chip*, 2002, **2**, 31.

APPENDIX 2

POSTERS PRESENTED

Development of a Microfluidic Based Sensor System for Copper Monitoring in Complex Environmental Sample Matrices

Éadaoin Tyrrell and Brett Paull
National Centre for Sensor Research
Dublin City University, Ireland.

Introduction

A microfluidic based sensor system for copper monitoring in complex environmental sample matrices is being developed.

The system will incorporate a copper selective itaconic acid (methylenesuccinic acid) modified polymeric micro-column, a polymeric microfluidic manifold and a photomultiplier tube (PMT).

The unique selectivity of the itaconic acid allows the separation of ultra trace amounts of copper from high concentrations of alkali and alkaline earth metals which may be present in the sample matrix.

A well known chemiluminescent reaction between copper and 1,10-phenanthroline is used for selective detection by the PMT.

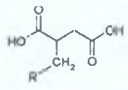

The structure of the itaconic acid resin is shown here, where R is the polymer to which itaconic acid is attached.

FIA Manifold

A method based on flow injection analysis with chemiluminescence detection (FIA-CL) has been developed for the analysis of copper in complex matrices. The setup is shown below. A peristaltic pump (Gilson) was used to draw eluent and reagents through 0.25 mm i.d. PEEK tubing. The itaconic acid chelating column is used to remove any interferents, such as large amounts of calcium and magnesium present in seawater samples.

A similar design will be used in the microfluidic system. Ultimately, the micro system will incorporate the itaconic acid resin into the micro channels, thus removing the need for a separate chelating column. Also, a photo diode array (PDA) will be used in place of the PMT for detection purposes to improve the overall sensitivity.

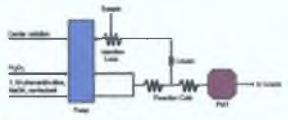

The manifold used a 120 µl injection loop, a flow rate of 0.7 ml/min and a 1 cm micro column of itaconic acid (particle size ~20 µm). A Hamamatsu PMT was used to detect photons produced by the oxidation reaction.

The micro column used in the system is shown here. It is employed for the preconcentration and separation of copper from the complex sample matrix.

The chemiluminescent reaction which takes place for detection is:

Cu^{2+} + 1,10-phenanthroline
↓
H_2O_2 → Cu-phen complex*
↓ hυ
Cu-phen complex

*represents excited state of complex

Optimisation

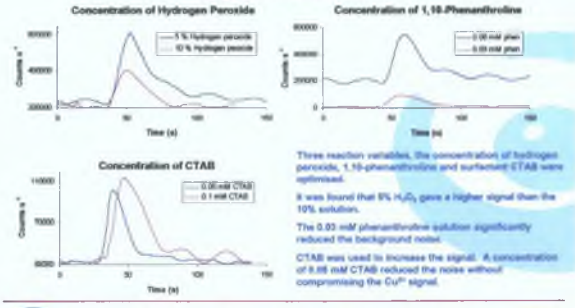

Three reaction variables, the concentration of hydrogen peroxide, 1,10-phenanthroline and surfactant CTAB were optimised.

It was found that 5% H_2O_2 gave a higher signal than the 10% solution.

The 0.03 mM phenanthroline solution significantly reduced the background noise.

CTAB was used to increase the signal. A concentration of 0.05 mM CTAB reduced the noise without compromising the Cu^{2+} signal.

Linearity Studies

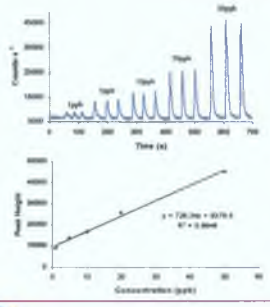

Shown left are the reaction peaks generated by the PMT during the copper analysis. Three replicate injections were analysed for each copper addition.

The results are linear (R^2= 0.9946) and copper could be readily determined at levels as low as 1 ppb.

Preconcentration and Separation of Copper in Water

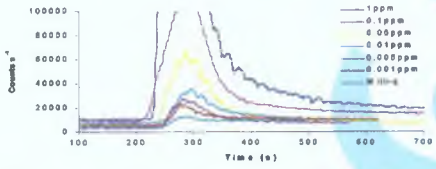

The itaconic acid column was used for the preconcentration of copper in deionised water. The linear concentration range was between 1 ppm and 1 ppb. The signal to noise ratio for these results were above the norm of 3, suggesting that upon further work a lower limit of detection could be reached.

Preconcentration and Separation of Copper in a Complex Matrix

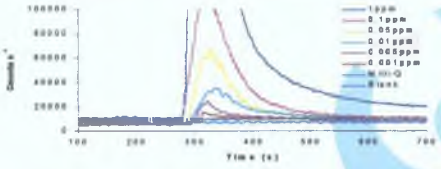

An itaconic acid column was used for the separation of copper from a sample matrix which contained 10 ppm calcium and magnesium. The column removed the interferences present and preconcentrated the copper sample. The results are comparable with those previously produced for copper in deionised water and with those reported in the literature.

Microfluid Manifold

Attached is a microfluidic manifold, manufactured in-house from polymethylmethacrylate (PMMA), similar to those to be used in this study.

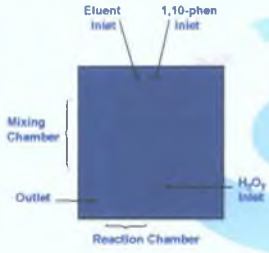

Future Work

- Applying current work with FIA manifold to microfluidic setup.
- Investigation of different microfluidic manifolds of various design and dimensions.
- Incorporating resin into microfluidic system, removing the need for a separate chelating column.
- Use of PDA in place of PMT detector for improved sensitivity.
- Study of different chemiluminescent reactions e.g. dichlorofluorescein and H_2O_2.
- Application of different resins e.g. APAS.
- Analysis of different complex matrices e.g. seawater, brines and saline samples.

Development of a Microfluidic Based Analytical System for Copper Monitoring in Environmental Sample Matrices

Éadaoin Tyrrell, Ceri Gibson†, Brian MacCraith†, David Gray†, Nigel Kent† and Brett Paull
National Centre for Sensor Research, School of Chemical Sciences, †School of Physical Sciences, Dublin City University, Ireland.
http://www.ncsr.ie/

Over the past number of years, as a result of the need for in-situ monitoring and reduced sample handling, as well as lower reagent consumption and reduced waste generation, a significant amount of work has taken place within the area of micro-total analysis systems (μTAS). Within the area of environmental analysis, micro-fluidic based analytical systems are a relatively recent advance. Work within the NCSR at DCU has begun on the development of a micro-fluidic based system for the monitoring of heavy metal ions in water samples. The work to date has focused on a system for copper determinations that incorporates a copper selective itaconic acid (methylenesuccinic acid) modified polymeric micro-column, a polymer micro-fluidic manifold and a photomultiplier tube (PMT) for chemiluminescence detection. The unique selectivity of itaconic acid allows the separation of copper from high concentrations of alkali and alkaline earth metals. In-house micro-machining and hot embossing facilities have allowed the rapid production of micro-fluidic manifolds, manufactured from PMMA, of various designs and dimensions. A well known chemiluminescent reaction between copper and 1,10-phenanthroline is used for selective detection. Ultimately, the chelating phase will be incorporated into the micro-fluidic system, thus removing the need for a separate chelating column and one individual system will provide all of the analysis on a single integrated micro-fluidic manifold.

A method based on micro flow injection analysis with chemiluminescence detection (FIA-CL) has been developed. A schematic diagram of the setup is shown below (fig. 1(a)). Three micro-peristaltic pumps (fig. 1(b)) (BVT) were used to draw the reagents through 0.127 mm i.d. PEEK tubing. Reagent flow rates were 0.030 ml/min. A Hamamatsu PMT was used to detect photons produced by the oxidation reaction.

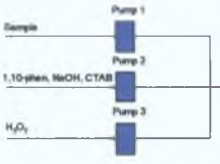

Fig. 1(a). Schematic of the FIA-CL system used for the copper monitoring.

Fig. 1(b). Micro-peristaltic pump

A brass master was milled and used to emboss poly(methylmethacrylate) (PMMA) to produce micrometer size channels in the plastic. The mixing channel was 730 mm in length, 200 μm in width and 100 μm in depth. The detection/reaction channel was 210 mm in length, 200 μm in width and 100 μm in depth. Figure 2 (a) shows the polymeric microfluidic manifold design (2D), while figure 2 (b) shows the CAD image (3D) used in this work.

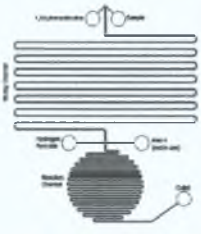

Fig. 2 (a). 2D image of polymer microfluidic manifold

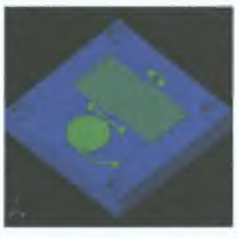

Fig. 2 (b). CAD image of microfluidic manifold

The following diagram outlines the process involved in the fabrication of the microchip (fig. 3).

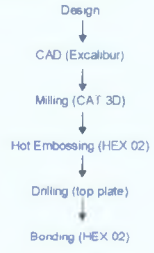

Fig. 3. Flow diagram of microfabrication process

The CL reaction, which emits between 445-450 nm, results from the oxidative destruction of 1,10-phenanthroline during the catalytic decomposition of hydrogen peroxide by the copper-1,10-phenanthroline complex and is illustrated below:

$$Cu^{2+} + \text{1,10-phenanthroline} \rightarrow H_2O_2 \rightarrow \text{Cu-phen complex}^* \xrightarrow{\downarrow h\upsilon} \text{Cu-phen complex}$$

*represents excited state of complex

Two reaction variables, the concentration of 1,10-phenantroline and cetyltrimethylammonium bromide (CTAB) were optimised. The addition of a cationic surfactant, such as CTAB, has been found to increase the CL signal and also reduce some of the background noise. The reagent concentrations producing the highest signal to noise ratio were found to be 0.07 mM 1,10-phenanthroline and 0.10 mM CTAB (graph 1).

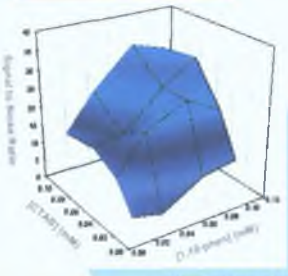

Graph 1: The response surface plot shows the optimum concentrations of 1,10-phenanthroline and CTAB

Using the optimised system, a step-wise graph was produced for copper standards between 0 and 50 μg/L (graph 2). The signal to noise ratio for these results were above the norm of 3 suggesting that upon further work, a lower limit of detection could be reached.

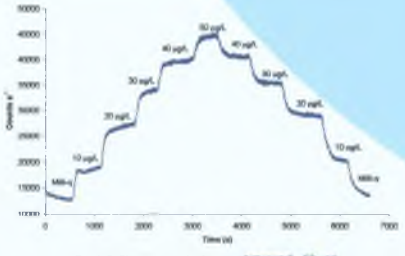

Graph 2: Stepwise graph of copper between 0 - 50 μg/L

The results are linear (R^2 = 0.9931) (graph 3) and copper could be readily determined at levels as low as 10 μg/L.

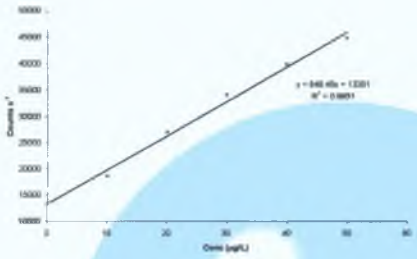

Graph 3: Copper linearity studies with R^2 = 0.9931

A chelating microcolumn (fig. 4 (a)) of itaconic acid is used for the preconcentration and separation of copper from complex sample matrices. The structure of the itaconic acid resin is shown here (fig. 4 (b)), where R is the polymer to which itaconic acid is attached.

Fig. 4 (a). Itaconic acid microcolumn

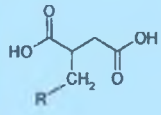

Fig. 4 (b). Structure of itaconic acid

Tapwater samples were analysed for copper. One sample was analysed immediately by the system while the other was passed through the itaconic acid column, in order to separate copper from the sample matrix. It was found that the aliquot passed through the column contained no copper and the sample matrix caused little or no interference. It could therefore be concluded that the signal from tap water was only due to the copper present in the sample (approximately 80 μg/L Cu(II)) (graph 4).

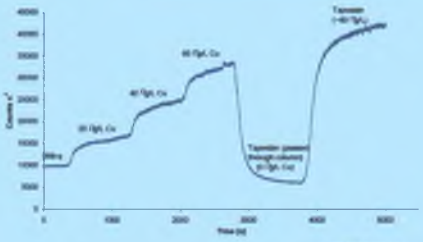

Graph 4: Comparison of tapwater samples passed through and not passed through the itaconic acid column

Future Work:

- Reduction of channel dimensions.
- Use of simple photo diode (PD) in place of PMT.
- Comparison of micro milled hot embossed chip with laser produced chips.
- Study of different CL reactions e.g. luminol and H_2O_2.
- Incorporating chelating resin into system.
- Analysis of different complex matrices.

NCSR
National Centre for Sensor Research

Development of a Microfluidic Based Analytical System for Copper Monitoring in Environmental Samples

Éadaoin Tyrrell, Ceri Gibson, Brian MacCraith, Nigel Kent and Brett Paull
National Centre for Sensor Research, School of Chemical Sciences, Dublin City University, Ire.
Email: Brett.Paull@dcu.ie
http://www.ncsr.ie/

Within the area of environmental analysis micro-fluidic based analytical systems are a relatively recent advance. A micro-fluidic based system has been developed for copper monitoring in water samples with sensitive and selective detection, based on the measurement of light emitted from the Cu(II) catalysed oxidation of 1,10-phenanthroline by hydrogen peroxide. Various micro-fluidic manifolds were designed and manufactured from polymethylmethacrylate (PMMA). A range of micro-fabrication techniques were investigated for the fabrication of the micro-fluidic manifolds including hot embossing, laser ablation and direct micro-milling. The final laser ablated design incorporated a reagent mixing channel of dimensions 7.3 cm in length and 250 x 250 μm in width and depth (triangular cross section), and a detection channel of 2.1 cm in length and 250 x 250 μm in width and depth (total approx. volume of between 16 to 22 μL). The concentrations of 1,10-phenanthroline, containing cetyltrimethylammonium bromide and sodium hydroxide (reagent 1 delivered at 0.025 mL/min) and hydrogen peroxide (reagent 2 delivered at 0.025 mL/min) were optimised. The sample stream was mixed with reagent 1 in the mixing channel and subsequently mixed with reagent 2 at the start of the detection channel. The laser ablated manifold was found to give a linear response (R^2 = 0.998) over the concentration ranges 0 – 150 μg/L and be reproducible (% RSD = 3.4 for five repeat injections of a 75 μg/L std). Detection limits for Cu(II) were found to be 20 μg/L. Selectivity was investigated using a copper selective mini-chelating column, which showed common cations found in drinking waters did not cause interference with the detection of Cu(II). Finally the optimised system was successfully used for trace Cu(II) determinations in a standard reference freshwater sample (SRM 1640).

Introduction

The performance of PMMA micro-fluidic manifolds fabricated using a variety of micro-fabrication techniques has been investigated, and applied in combination with chemiluminescence detection for the determination and monitoring of Cu(II) in water samples and could be applied to 'on-line' monitoring situations with minimal reagent consumption.

Micro-Fluidic Manifold and Instrumentation

The micro-fluidic manifold design is illustrated schematically as in Figure 1. Three micro-peristaltic pumps with 0.51 mm I.D. peristaltic tubing (BVT Technologies) were used to drive the reagent and sample streams through the micro-fluidic manifold via connecting 0.13 mm I.D. PEEK tubing. Each micro-pump weighed 34 grams and was 60 mm in height and 16 x 16 mm at the base. These pumps were operated using a DC supply at 3 V and are connected together using a custom made interface driven by one PC connection. Under optimal conditions for this study, individual flow rates of 25 μl/min were used.

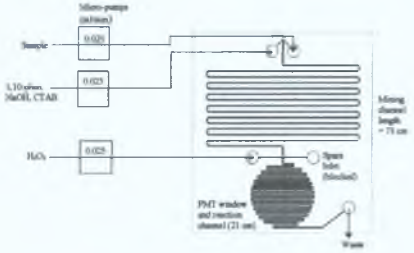

Figure 1. Schematic diagram and dimensions of the micro-fluidic manifold developed. Chip dimensions = 7.0 x 7.0 x 0.8 cm

The micro-fluidic manifold was manufactured from PMMA. A number of different designs and dimensions were investigated but the basic design consisted of two inlets for the sample and 1,10-phenanthroline solutions, which were subsequently mixed together in the mixing channel. There was a third inlet at the end of the mixing channel prior to the detection/reaction channel for the introduction of the hydrogen peroxide. At the end of the detection channel there was an outlet leading to waste.

The dimensions of the mixing channel were 730 mm in length with an internal width and depth of 250 μm x 250 μm (triangular cross-section), and 210 mm in length and 250 μm x 250 μm in width and depth for the reaction/detection channel. The theoretical approximate internal volume of the reaction/detection channel was between 16 and 22 μL.

Micro-Fluidic Manifold Fabrication

The micro-fluidic manifolds were designed using CAD 3D Excalibur software. Following this, the manifold could be fabricated in one of three different ways. The first technique involved hot embossing from a micro-milled brass master, designed as the inverse of the channel structure desired. The brass master was fabricated by high precision micro-milling the channels of various dimensions. The machined master was then used to hot emboss the design into PMMA chips.

The second technique used involved direct milling of the PMMA substrate. In this case, the micro-milling system was used to cut the micro-fluidic channels directly into the PMMA. Although direct micro-milling removed the additional hot embossing fabrication step, the corner sections of the channels were less smoothly rounded thank those produced by the hot embossing method and may increase the level of turbulent flow in the directly milled device.

The third method of fabrication used in this study was laser ablation. An Excimer laser was used to make the micro-fluidic channels in the PMMA. Bonding of all the fabricated designs were carried out using a top plate of PMMA of equal size, which was pre-drilled to make the required reagent inlet holes.

Table 1 shows the comparative analytical performance data determined for the three micro-fluidic manifolds. The data shown represents that obtained under the specific reagent conditions used within this study only.

Fabrication Method (Channel dimensions)	Linear Range (μg/L)	Slope	R^2 Value	Reproducibility % RSD (no. replicates)	Approx. Detection Limit (μg/L)
Hot Embossing (250 x 250 μm)	25 - 150	751	0.998	2 - 8 % (n = 5)	10
Micro-Milling (250 x 250 μm)	40 - 150	378	0.983	4 - 5 % (n = 2)	40
Laser Ablation (250 x 250 μm)	25 - 150	81	0.998	2 - 3.5 % (n = 5)	20

Table 1. Analytical performance data for developed methods.

Chemiluminescence Reaction

Chemiluminescence was continuously measured using a PMT (Hamamatsu Photonics HC135-01 series with R1924 bi-alkali tube). The PMT was approximately 135 mm in height and the window of the detector was 25.4 mm inner diameter. The PMT used was operational over the range 300 nm to 650 nm and operated in photon counting mode. The PMT was placed over the detection flow cell and was secured tightly to prevent stray light from reaching the detector.

The CL reaction, which emits between 445 -450 nm, results from the oxidative destruction of 1,10-phenanthroline during the catalytic decomposition of hydrogen peroxide by the copper-1,10-phenanthroline complex and is illustrated below:

Cu^{2+} + 1,10-phenanthroline
↓
H_2O_2 + Cu-phen complex*
↓ $h\upsilon$
Cu-phen complex

*hypothesised excited state of complex

Optimisation of Reagents

Two reaction variables, the concentration of 1,10-phenantroline and cetyltrimethylammonium bromide (CTAB) were optimised. The addition of a cationic surfactant, such as CTAB, has been found to increase the CL signal and also reduce some of the background noise. The reagent concentrations producing the highest signal to noise ratio were found to be 0.07 mM 1,10-phenanthroline and 0.10 mM CTAB (Figure 2).

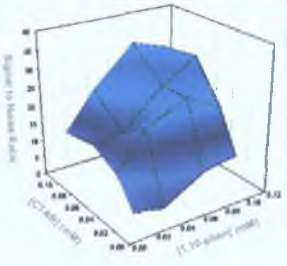

Figure 2. The response surface plot shows the optimum concentrations of 1,10-phenanthroline and CTAB.

Linearity

Using the optimised conditions, a series of measurements were performed with Cu(II) standard solutions ranging from 25 to 150 μg/L (Figure 3) using the laser ablated manifold. The resulting signal heights were plotted as a function of concentration and the results were found to produce an excellent linear correlation within this given concentration range (R^2 = 0.998, n = 5, standards measured in duplicate).

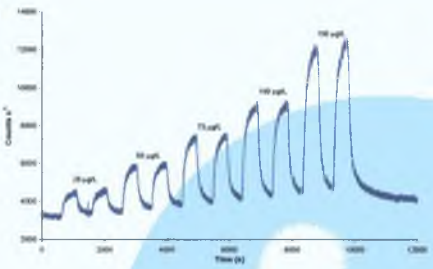

Figure 3. Reaction peaks generated for Cu (II) standard solutions from 25 to 150 μg/L (R^2 = 0.998).

Selectivity Studies and Analysis of Real Samples

The Cu(II)-1,10-phenanthroline chemiluminescent reaction is highly selective, with little or no response to excess concentrations (> 10 mg/L) of alkali metals, Cr(III), Cr(VI), Mn(II), Ni(II), Co(II), Cd(II), Pb(II), Al(III), Fe(II) or Fe(III). High concentrations of Zn(II), Ca(II) and Mg(II) can cause minor interference at the above concentration. Therefore, a Cu(II) selective itaconic acid functionalised resin (20 μm resin size) was used to further increase selectivity.

The on-line analysis of drinking water was undertaken. The drinking water from a laboratory tap was fed via an in-line filter to the sample inlet of the manifold. Within the sample line a switching valve was placed which allowed the tap water to either by-pass or be passed through the itaconic acid micro-column allowing verification that the detector response was due to Cu(II) only. The results can be seen in Figure 4a. As can be seen the concentration of Cu(II) found within the laboratory tap supply was approximately 80 μg/L. On-line passage of the tap water through the itaconic acid column completely removed the chemiluminescent signal, indicating that the sample matrix was not causing significant interference in this application.

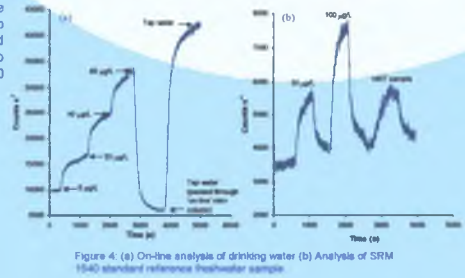

Figure 4: (a) On-line analysis of drinking water (b) Analysis of SRM 1640 standard reference freshwater sample

A standard reference material (SRM) from the National Institute of Standards and Technology (NIST) was analysed for Cu(II). The sample (SRM 1640) was composed of natural fresh water had been filtered and acidified with 0.5 mol L^{-1} nitric acid. This sample was known to contain 85.2 μg/L ± 1.2 μg/L Cu(II). The sample was neutralised using sodium hydroxide and was diluted by half. Firstly, 50 and 100 μg/L Cu(II) standards were analysed, with Milli-Q water blank run between standards. A 50 % dilution of the NIST standard was then analysed. The resultant signals can be seen in Figure 4b This sample was found to contain approximately 40 μg/L Cu(II) which corresponds to ~80 μg/L in the CRM, within ±6 % of the true value, representing excellent accuracy for a micro-fluidic device when analysing a complex freshwater sample for trace Cu(II).

Future Work

- Study of different CL reactions e.g. luminol and H_2O_2
- Incorporating chelating resin into system
- Application of different resins e.g. APAS
- Analysis of different complex matrices

NCSR
National Centre for Sensor Research

Development of a FIA System Incorporating a Micro-Chelating CIM® Monolithic Disk for Copper Monitoring in Environmental Sample Matrices

Éadaoin Tyrrell, Pavel Nesterenko and Brett Paull
National Centre for Sensor Research, School of Chemical Sciences, Dublin City University, Ire.
Email: Brett.Paull@dcu.ie
http://www.ncsr.ie/

The work presented here has focused on a system that incorporates a chelation exchange separation support, based on Convective-Interaction Media® (CIM®) which has been developed for the preconcentration/separation of copper (II) in saline environmental samples. These CIM® disk monolithic columns were coated with picolinic acid, dipicolinic acid and iminodiacetic acid and the efficiency of the three were compared and contrasted for the separation of copper (II) in complex matrices. This approach was successfully incorporated into a flow injection analysis system, using chemiluminescence detection for the determination of ultra trace amounts of copper (II), based on the copper-1,10-phenanthroline chemiluminescence reaction. The combination of the CIM® disk with the 1,10-phenanthroline reaction, allows the quantitative extraction and elution of copper (II) from saline samples, combined with the selectively of the 1,10-phenanthroline reaction. The developed method has been validated using saline certified reference materials and has also been applied to a number of real samples including coastal seawater and estuary water samples.

Introduction

The copper-1,10-phenanthroline chemiluminescence reaction is quite selective for the determination of copper (II) in samples. However, metal ions such as zinc (II), calcium (II) and magnesium (II) can cause interference at high concentrations (> 10 mg L^{-1}). An on-line preconcentration method to increase the selectivity of trace copper (II) determinations in complex sample matrices, using a chelation exchange support based on Convective-Interaction Media® (CIM®) monolithic disks is presented here.

Flow Manifold and Instrumentation

A schematic of the FIA manifold is illustrated in Fig. 1. A variable speed peristaltic pump was used to control the flow of reagents at a total flow rate of 1.14 ml min^{-1}. The detection flow cell consisted of a spiralled coil of polyethylene (PE) tubing (total volume 184 µl). A photomultiplier tube (PMT) (Hamamatsu Photonics H9319-02 series with multi-alkali tube) was used for detection purposes. The reagent conditions used were as follows: a carrier solution of ultra pure water or eluent of 25 mM nitric acid solution, a solution of 0.06 mM 1,10-phenanthroline, 1.3 mM CTAB, 0.075 M sodium hydroxide and a solution of 5 % hydrogen peroxide.

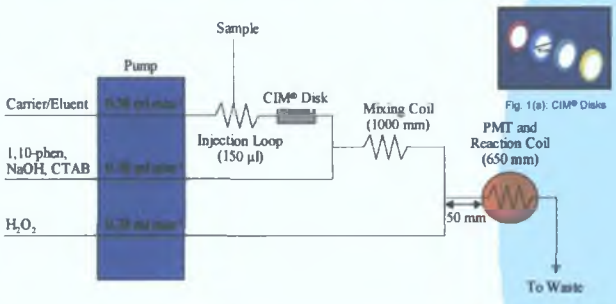

Fig. 1: Schematic diagram of the reaction manifold used for the determination of copper (II) by the FIA system, described in the text.

Fig. 1(a): CIM® Disks

Modification of CIM ® Disks

Three different carboxylic acids were used for modifying the CIM® disk monolithic columns during this work: 2-pyridinecarboxylic acid (picolinic acid), 2,6-pyridinedicarboxylic acid (dipicolinic acid), and dodecyliminodiacetic acid. These carboxylic acids can work as chelating ligands and the structures of the acids can be seen below in Fig. 2.

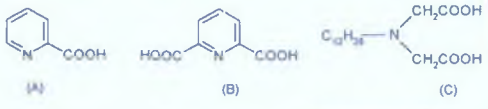

Fig. 2: Structures of (A) picolinic acid (B) dipicolinic acid and (C) dodecyliminodiacetic acid.

Table 1 shows the comparative analytical performance data which was determined for the three carboxylic acid CIM® monolithic disk modifying ligands. The data shown here represents that obtained under the specific conditions used within this study only.

Table 1: Analytical performance data for three carboxylic acid modifying coatings

Modifying Ligand	*Linear Range (µg L^{-1})*	*Slope*	*R^2 Value*	*Reproducibility % RSD*
Picolinic Acid	0 - 125	976	0.984	< 3.9 %
Dipicolinic Acid	0 - 250	1166	0.998	< 4.0 %
Iminodiacetic Acid	0 - 125	790	0.986	< 2.5 %

Chemiluminescence Reaction

The chemiluminescence was continuously measured using a PMT. The reaction, which emits between 445 -450 nm, results from the oxidative destruction of 1,10-phenanthroline during the catalytic decomposition of hydrogen peroxide by the copper-1,10-phenanthroline complex and is illustrated below.

Cu^{2+} + 1,10-phenanthroline
↓
H_2O_2 → Cu-1,10-phen complex*
↓ hυ
Cu-1,10-phen complex

*represents excited state of complex

Fig. 3 shows a series of measurements that were performed using the FIA-CL system incorporating the dipicolinic acid modified CIM® monolithic disk. A range of copper (II) standard solutions ranging from 0 to 250 µg L^{-1} were analysed. The resulting signal heights were plotted as a function of concentration and the results were found to produce an excellent linear correlation within this given concentration range (R^2 = 0.998).

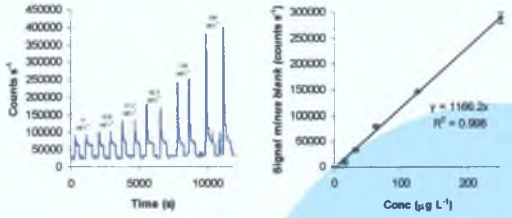

Fig. 3: (a) Range of copper (II) standards between 0 and 250 µg L^{-1} using dipicolinic acid coated CIM® disk, (b) copper (II) linearity studies.

Selectivity Studies

To verify that this method was selective for the determination of copper (II), an analysis of copper (II) made up in a synthetic seawater matrix containing 400 mg L^{-1} calcium (II) and 1,300 mg L^{-1} magnesium (II), was carried out.

Fig. 4 shows the calcium (II) and magnesium (II) detected using visible detection overlaid on the chemiluminescence signal produced for a 250 µg L^{-1} copper (II) standard made up in synthetic seawater. As can be seen from this Figure the signals measured for the calcium (II) and magnesium (II) correspond well to the negative peak on the copper (II) chemiluminescence signal verifying that the calcium (II) and magnesium (II) present in the seawater matrix are both un-retained by the CIM® disk.

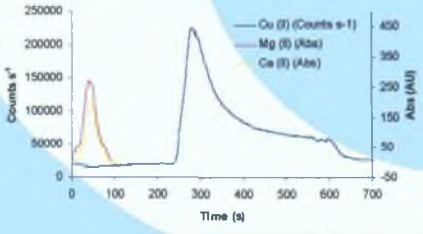

Fig. 4: Overlay of calcium (II) and magnesium (II) signals detected by visible detection and the chemiluminescence signal produced for a 250 µg L^{-1} copper (II) standard made up in synthetic seawater.

Analysis of Samples

This system was then successfully applied to a number of samples which were analysed by standard addition, including a standard reference material (SRM 1640), coastal seawater and estuary water sample. The SRM sample was analysed using this FIA-CL system and found to contain approximately 88 µg L^{-1} copper (II). This figure compared well to the certified value of 85.2 µg L^{-1} of copper (II) in the sample.

Fig. 5a shows how the blank signal was subtracted from each of the standards to obtain an accurate copper (II) result. The coastal seawater (Fig. 5b) sample was found to contain 18 µg L^{-1} of copper (II) by standard addition. The estuary water sample was analysed in a similar way and found to contain 24 µg L^{-1} of copper (II), which is well below the 2 mg L^{-1} limit recommended by the European Water Quality Directive.

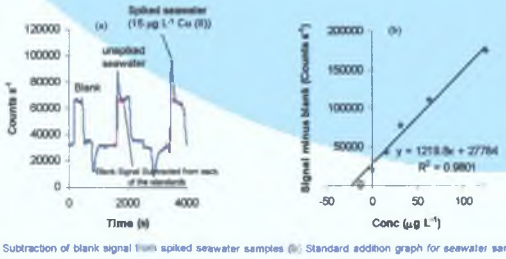

Fig. 6: (a) Subtraction of blank signal from spiked seawater samples (b) Standard addition graph for seawater sample spiked with copper (II).

NCSR
National Centre for Sensor Research